Synthesis and characterization of waterborne polyurethane and polyurethane-urea towards eco-friendly materials by cellulose nanocrystals and plant extracts incorporation

PhD Dissertation presented by

ARANTZAZU SANTAMARIA ECHART

Under the supervision of

Dr. ARANTXA ECEIZA
Dr. MARIA ANGELES CORCUERA

Donostia-San Sebastian, February 2017

Acknowledgments

Summary

In this work environmentally friendly anionic waterborne polyurethane and polyurethane-ureas dispersions were synthesized in order to prepare films by casting. The effect of molar composition was analyzed on the waterborne polyurethane dispersions as well as the properties of films. Furthermore, the evolution of films properties at room temperature over time was studied. In the case of polyurethane-ureas dispersions and films, diamine chain extender content, as well as the influence of its incorporation route in the synthesis process (in homogeneous or heterogeneous medium) was analyzed.

These waterborne polyurethane and polyurethane-urea dispersions were used for the preparation of new eco-friendly materials: dispersions and films containing nanoreinforcements or additives. Thereby, cellulose nanocrystals were isolated for the preparation of nanocomposites. The effect of matrix nature, cellulose nanocrystals contents as well as their incorporation route were analyzed in the final properties of the nanocomposites.

Moreover, electrospun nanocomposites mats were prepared from waterborne polyurethane-cellulose nanocrystals dispersions using poly (ethylene oxide) as polymer template. The effect of varying the nanoreinforcement content and incorporation route was analyzed in the morphology and surface behavior of mats.

In a second section, extracts containing bioactive compounds from two plants (*Salvia Officinalis L.* and *Melissa Officinalis L.*), were obtained by infusion for being incorporated to polyurethane-urea dispersions in order to confer antimicrobial properties. With this aim, three different incorporation routes were designed (after, during or before the dispersion formation) for the

incorporation of different extract contents. Polyurethane-urea dispersions containing plant extracts were characterized and films were prepared. The final properties of films were analyzed and antibacterial tests were carried out against Gram positive *Staphylococcus aureus* and Gram negative *Escherichia coli* and *Pseudomonas aeruginosa* bacteria.

Index

CHAPTER 3

CHAPTER 4

CHAPTER 5

CHAPTER 6

CHAPTER 7

7. Waterborne polyurethane-urea cellulose nanocrystals nanocomposites

CHAPTER 8

8. Electrospinning waterborne polyurethane nanocomposites loaded with cellulose nanocrystals by two incorporation routes

CHAPTER 9

9. Different incorporation routes of bioactive plant extracts in waterborne polyurethane-urea dispersions

CHAPTER 10

10. General conclusions, future works and publications   295

ANNEXES

CHAPTER 1

Introduction

1. INTRODUCTION

1.1 Motivation

The environmental awareness has been one of the reasons of increasing research and development of eco-friendly green synthesis routes for many different applications, such as the waterborne polymer systems. Thus, waterborne polyurethanes (WBPU) as well as waterborne polyurethane-ureas (WBPUU) have taken importance during last years. WBPU and WBPUU present the advantage of being synthesized by a solvent-free method which implies low organic compound levels and non-toxicity comparing with conventional solventborne polyurethanes and polyurethane-ureas. In this way, the synthesis of WBPU and WBPUU dispersions has been promoted by the addition of internal emulsifiers and obtaining stable water dispersions over months.

Furthermore, the possibility of dispersing hydrophilic reinforcements has focused attention in water dispersible entities such as environmentally friendly cellulose derivatives. Among them, cellulose nanocrystals (CNC) become a suitable candidate for the preparation of nanocomposite materials, considering their unique properties in the nanoscale dimension provided by their high length/diameter aspect ratio and high specific mechanical properties. In this way, the different CNC incorporation routes as well as CNC content to WBPU or WBPUU can open the opportunity of modulating the properties of the final material towards the desired application.

Moreover, the use of different processing techniques for obtaining WBPU and WBPUU based systems, results in the formation of different forms of the final material. In this way, electrospinning of dispersions provides the opportunity of

obtaining nanoreinforced fibers mats with high porosity and large surface area to volume ratio with tailored fiber diameters, which become an attractive alternative to conventional casted coatings in different applications.

Otherwise, the waterborne character of these systems facilitates the addition of water soluble additives in order to enhance a specific property of the WBPU and WBPUU. Thereby, the use of renewable sources for obtaining natural additives, focus the attention on extracts from plants. These extracts are composed by biologically active substances, which most of them can act as antibacterial agents besides presenting other features such as antifungal or antioxidant effects.

Therefore, in this work, different WBPU and WBPUU dispersions will be synthesized and loaded with isolated CNC as well as extracted plant extracts. The obtained dispersions were used in the preparation of films by casting or mats by electrospinning. In this way, WBPU and WBPUU based materials with tailored properties will be prepared.

1.2 Polyurethane and polyurethane-ureas

Polyurethanes and polyurethane-ureas are a versatile family of polymers which can be used in a wide range of applications such as biomedicine, textile, automotive, paintings, adhesives, coatings, … [1–3].

The characteristic functional group of polyurethanes is urethane group, which is formed by the addition reaction between isocyanate and hydroxyl groups. In the case of the polyurethane-ureas, besides urethane groups formation, urea groups are also formed, by the reaction of isocyanate with amine groups. Both reactions are specified in **Figure 1.1**.

R$_1$-NCO + R$_2$-OH ⟶ R$_1$-N-C-O-R$_2$
Isocyanate   Alcohol   Urethane

R$_1$-NCO + R$_2$-NH$_2$ ⟶ R$_1$-N-C-N-R$_2$
Isocyanate   Amine   Urea
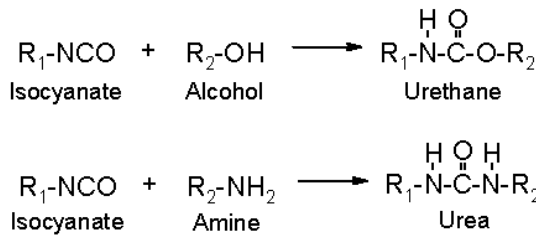
Figure 1.1 *Scheme of urethane and urea groups formation reaction*

Furthermore, one of the most remarkable differences between urethane and urea groups is related with their ability for hydrogen bonding formation, as can be observed in **Figure 1.2**.

R$_1$-N-C-O-R$_2$ R$_1$-N-C-N-R$_2$
    H   H   H

R$_1$-N-C-O-R$_2$ R$_1$-N-C-N-R$_2$
    H   H   H

Urethane single   Urea dual
hydrogen bonds   hydrogen bonds
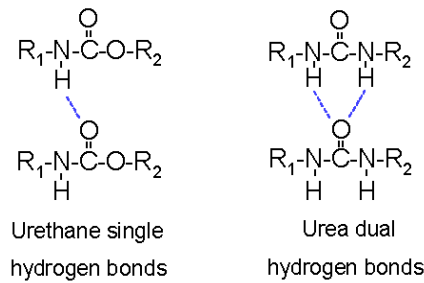
Figure 1.2 *Hydrogen bonding interactions between urethane or urea groups*

In the case of urethane groups, "single" intermolecular hydrogen bonds are formed, whereas ureas are able to generate "dual" hydrogen bonding interactions [4]. In this way, stronger interactions are formed when urea systems are used, resulting generally in stiffer films.

Polyurethanes and polyurethane-ureas are composed by two alternating blocks; the soft segment (SS) is usually formed by a polyol, and the hard segment (HS), generally consists on an isocyanate and a low molecular weight diol, used as

chain extender in the case of polyurethanes or diamine chain extender, when polyurethane-ureas are synthesized.

Both segments usually are thermodynamically incompatible, resulting in phase separation. Thus, a structure consisting on microdomains is obtained, which depending on the chemical composition can offer a broad range of properties [5,6]. In general, soft segment provides flexibility to the system, whereas hard segment will confer stiffness to the material. Nevertheless, attending to the composition and reactants nature, soft or/and hard segments can be arranged in either amorphous or crystalline ordered domains by the formation of hydrogen bonding interactions between segments. Microdomains and hydrogen bonding interactions scheme is shown in **Figure 1.3**.
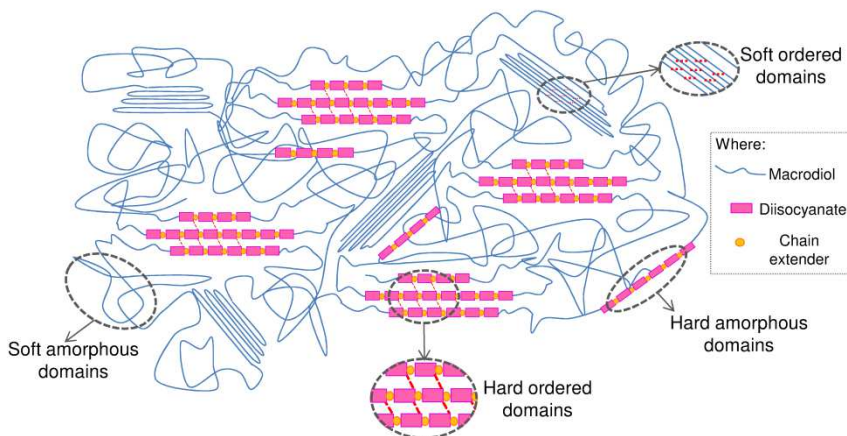
Figure 1.3 *A scheme of microdomains and hydrogen bonding interactions*

1.3 Waterborne polyurethane and polyurethane-ureas

Conventional polyurethane and polyurethane-ureas are solventborne systems, due to their hydrophobicity. The environmental awareness has promoted the development of waterborne polyurethane and polyurethane-urea systems which

can be achieved by the addition of an internal emulsifier [7], avoiding thus, the use of organic solvents and reducing the generation of volatile organic compounds.

The internal emulsifier, covalently bonded reagent, will form part of the polymeric chain [7], providing stability to the particles formed during the dispersion formation in the phase inversion step. In this way, a minimum of emulsifier is required for the formation of the stable dispersions, which will also depend on its nature as well as other factors such as precursors and hard/soft segments content [8–10]. Apart from environmental advantages, WBPU and WBPUU dispersions present other nice features exhibiting high solids content and high molecular weight, possessing low viscosity and non-flamability and film-forming ability at room temperature [11,12]. In addition, films with similar properties to conventional polyurethanes can be obtained, such as good chemical resistance, high flexibility, adhesion to many polymers and surfaces [13], among others.

Depending on reactant chemical structure and molar ratio, as well as, synthesis procedure and dispersion formation route, WBPU and WBPUU with different final properties can be synthesized.

1.3.1 Reactants

Waterborne polyurethane and polyurethane-ureas are formed by alternating soft and hard segments, composed by a polyol and by an isocyanate, chain extender and internal emulsifier, respectively.

- **Polyols**

Polyols are medium-high molecular weight macromolecules, comprised between 1000-8000 g mol^{-1}, containing hydroxyl groups. Polyols usually constitute the soft segment of the polyurethane or polyurethane-urea, conferring flexibility to the system. There are different types of polyols considering their molecular weight, functionality as well as nature. This fact offer the possibility of selecting the most appropriate polyol depending on the properties required in the final product. For instance, regarding molecular weight, different viscosities can be obtained during the synthesis process [14], or can affect the microstructure adopted by the SS in the film [15].

Considering the functionality of the polyol, different types of polyurethane and polyurethane-ureas films can be obtained. In the case of using difunctional polyol, named as macrodiols, with a functionality of 2, thermoplastic films are obtained, commonly used WBPU and WBPUU [16,17]. Nevertheless, higher functionality polyols can also be used, resulting in crosslinked WBPU and WBPUU thermosets systems [18]. Attending to the nature of macrodiols, polyethers, polyesters and polycarbonates are usually used in the synthesis of WBPU and WBPUU dispersions. Polyesters are suitable for applications of outstanding due to their resistance at light and ageing. Furthermore, polyesters present higher strength and oil resistance comparing with polyethers [8,19,20]. However, polyethers are preferable for improving water dispersion and obtaining more flexible materials. Polycarbonates, in general offers good hydrolysis and oil resistance and greater mechanical properties [19].

- **Isocyanates**

There are many types of isocyanates, but the most commonly used in the synthesis of WBPU and WBPUU dispersions are diisocyanates. Among them, different structures can be observed such as aromatic, aliphatic (cyclic or linear) [4], which will influence in the reactivity of the reaction process. For example, aromatic diisocyanates such as 2,4- or 2,6-toluene diisocyanate (TDI) or 4,4'-diphenyl methane diisocyanate (MDI) are not widely used in the synthesis of WBPU and WBPUU dispersions. Indeed, their higher reactivity with water and tendency to result in high viscosities, difficult the dispersion process [21]. Thereby, it is preferred the use of aliphatic cycloaliphatic diisocyanates, such as 5-isocyanate-1-(isocyanate methyl)-1,3,3-trimethyl cyclohexane (IPDI), 4,4'-dicyclohexyl methane diisocyanate (H$_{12}$MDI) and 1,6-hexamethylene diisocyanate (HDI). This type of diisocyanates improve the resistance against yellowing effect in films as well as thermal and hydrolytic attack comparing with aromatics diisocyanates [21,22]. Among them, IPDI is one of the most used in the synthesis of dispersions, since its low reactivity became the reaction process more controllable, resulting in more stable products [22]. Moreover, its asymmetrical structure that lead to less order structures, facilitates the diffusion of water towards hard segment domains during the dispersion step [21].

- **Chain extender**

Chain extenders are, generally difunctional, low molecular weight compounds [23,24]. Nevertheless, chain extenders with higher functionalities can be used, which would result in crosslinked WBPU or WBPUU dispersions. The main difference between WBPU and WBPUU dispersions is reflected in the type of chain extender employed in the synthesis process. In the case of WBPU, diol

compounds are used, whereas in WBPUU, diamines are employed. The use of diamines as chain extenders generally favors the cohesion forces between urea groups comparing with urethane linkages [4,25], leading to systems with higher mechanical strength.

- **Internal emulsifier**

There are different types of internal emulsifiers for the synthesis of WBPU and WBPUU dispersions. Attending to their nature, emulsifiers can be classified into nonionic or ionic, where ionics can be also divided into cationic or anionic, depending on the functional group that confers hydrophilicity to the system [26]. In the case of nonionic WBPU and WBPUU, the polymer contains an hydrophilic soft segment or side chain such as polyethylene oxide [13]. The use of nonionic WBPU and WBPUU dispersions is not such widespread because of the weaker hydrophilic character of these type of emulsifiers which difficult the dispersion in water. Nevertheless, nonionic dispersions are one of the more suitable WBPU and WBPUU for breathable coating applications [26].

Regarding ionic emulsifiers, anionic and cationic WBPU and WBPUU differ on the ionic center pendant in polymer backbone. These centers usually are acid or tertiary nitrogen groups which have to be neutralized or quaternized, respectively to form salts [1,13].

Between anionic emulsifiers, particularly 2,2-bis(hydroxymethyl) propionic acid (DMPA) and other compounds such as 2,2-bis(hydroxymethyl)butyric acid (DMBA) or sulfonated agents are commonly employed in the synthesis of anionic WBPU and WBPUU [27,28]. Instead, N-methyldiethanolamine (MDEA) is usually used as cationic emulsifier [27,29,30].

In general, anionic dispersions prevail over cationic systems but both are used in a wide range of applications such as adhesives, textiles, coatings, automotive topcoats or films for packaging [31].

- **Catalysts**

Regarding the reactivity of the WBPU and WBPUU reactants, usually catalysts are employed in order to accelerate the reaction between hydroxyl and isocyanate groups even at lower temperatures. Generally tertiary amines such as 1,4-diazabicyclo octane (DABCO), tryethylamine (TEA) or organo tin compounds, particularly dibutyltin dilaurate (DBTDL) and stannous octoate (SnOc) are employed [1]. Nevertheless, less harmful catalyst like zirconium based compounds have been promoted [21,32].

1.3.2 Polymerization process

The polymerization process can be carried out in one or two steps. In the case of two steps polymerization, the chemical structure of the polyurethane chains can be more accurately defined. **Figure 1.4** shows a general scheme of WBPU and WBPUU synthesis procedure by two steps polymerization.

First step

Second step

Chain extender

where:

with diol chain extender

with diamine chain extender
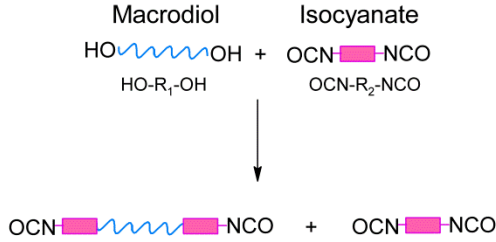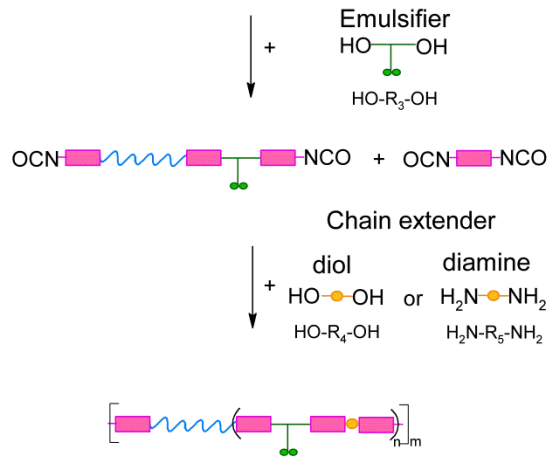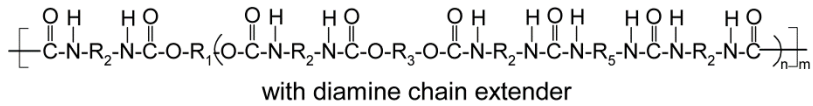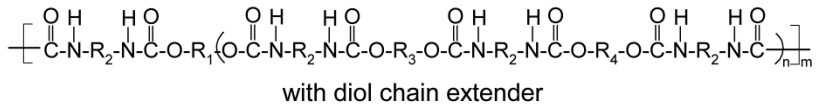
Figure 1.4 *WBPU and WBPUU polymerization synthesis procedure*

1.3.3 Dispersion formation

Once the polyurethane or polyurethane-urea chains are polymerized, the dispersion step is usually carried out. However, considering the nature of the chain extender and hence the reaction rate, the chain extension can be carried

out before water addition step, homogeneous medium, or after water addition step, heterogeneous medium.

Generally, diol chain extensions are performed before phase inversion step, thus avoiding side reactions due to their lower reactivity with isocyanates comparing with water. Instead, due to their higher reactivity, diamine chain extenders can be added either prior to water addition (before phase inversion), leading to the reaction in homogeneous medium or once the dispersion is formed (after phase inversion), completing the polyurethane-urea reaction in heterogeneous medium. This last method is the most used for chain extension with diamines.

Attending to the emulsifier nature, the stabilization mechanism of particles varies. In the case of nonionic emulsifiers, the mechanism for the dispersion formation is based in entropic repulsions. Hydrophilic segments of the chains located in the surface of the particles stretch into the water. In this way, when particles approach to each other, the mobility of these segments is restricted, leading to a reduction of entropy. Thus, spontaneous repulsion between particles is formed, resulting in the stabilizing of the dispersion.

Otherwise, the stabilization of ionic WBPU and WBPUU dispersions is based on the electrical double layer mechanism, adding previous to the dispersion step, a counterion. The counterion is the ion present in the system with the purpose of maintaining the electric neutrality of the ionic center [33]. **Figure 1.5** shows the particles formation mechanism of ionic WBPU and WBPUU dispersions.

When water is added, the ionic groups are located in the surface of the particles, surrounded by the counterions forming the electrical double layer [23,34] constituting the shell of the particle. Instead, hydrophobic domains will agglomerate in the center of particles forming the core of the particles [17].
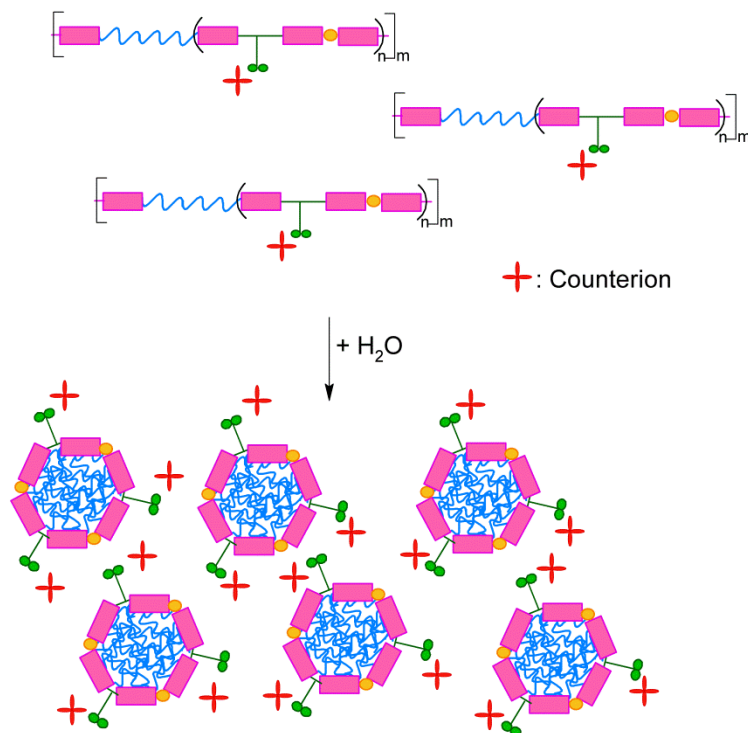
Figure 1.5 *Scheme of ionic WBPU or WBPUU particles formation*

In the case of WBPU and WBPUU the most used ionic emulsifier is DMPA, which contains carboxyl groups. For neutralizing DMPA, tryehylamine is commonly employed. Thereby, the interference of electrical double layer of different particles results in particle repulsion, leading to the stabilization mechanism of the dispersion [1,35].

WBPU and WBPUU result versatile polymers, which considering the nature of reactants, the composition or synthesis process can tailor the properties of the material. In this way, it is worth noting that the type and content of emulsifier, hard/soft segments percentages, isocyanate/hydroxyl (NCO/OH) groups ratio, among others [8–10,12,28,36], affect the particle size and stability of WBPU and

WBPUU dispersions, and thus will influence the final properties of the films. In this work, some of these variables will be considered for the preparation of WBPU and WBPUU dispersions.

1.4 Cellulose nanocrystals

With the purpose of synthesizing new environmentally friendly materials, WBPU and WBPUU can be employed in the preparation of nanocomposites. The opportunity of dispersing hydrophilic reinforcement in WBPU and WBPUU has focused attention in water dispersible entities, such as cellulose derivatives. Cellulose is the most abundant renewable biopolymer which has attracted great attention due to their availability, low cost, non-toxicity, biocompatibility and biodegradability. Cellulose is a high molecular weight homopolymer composed of D-glucose units linked by $\beta(1,4)$ glycosidic bonds, as can be observed in **Figure 1.6**.
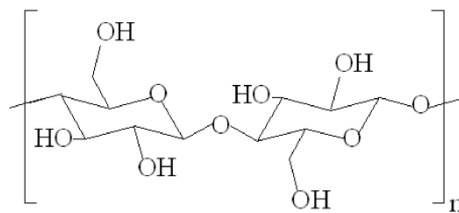
Figure 1.6 *Chemical structure of cellulose*

Cellulose is produced principally in nature by plants like cotton, jute or flax, different marine animals as tunicates, and in invertebrates, fungi, algae, bacteria, and amoeba (protozoa) in lower quantities [37,38].

Cellulose can be used in different dimensions, from macroscopic to nanoscale, and diverse assemblies such as fibers or crystals [39]. Among these, it is worth

noting the relevance of cellulose nanocrystals, which are gaining importance in diverse application fields [37,40]. The isolation of the crystalline ordered regions of cellulose lead to obtaining those highly crystalline nanoentities, possessing unique properties in the nanoscale dimension, modulated by isolation hydrolysis process [41] and origin of cellulose [38]. **Figure 1.7** shows a scheme of CNC isolation process from microcrystalline cellulose (MCC), which will be employed in this work as raw material.
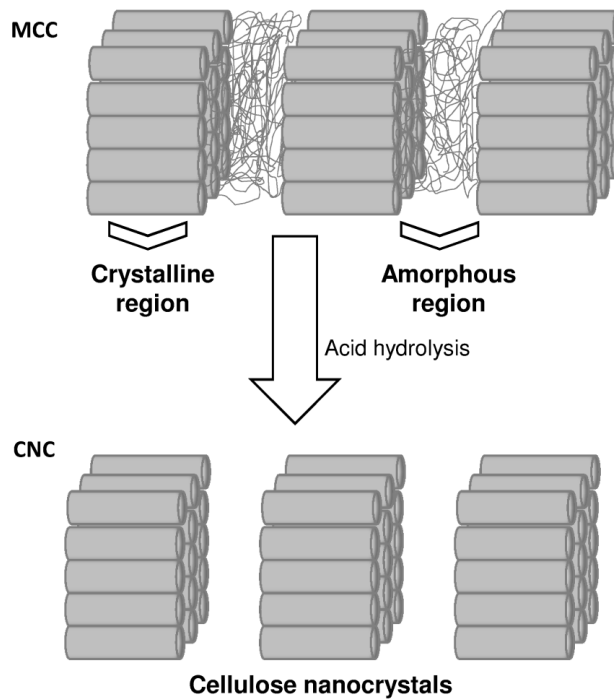
Figure 1.7 *Scheme of MCC general acid hydrolysis for obtaining CNC*

The high length/diameter (L/D) aspect ratio and high specific mechanical properties have focused the attention of CNC in nanocomposites field [42]. Several strategies have been used in order to prepare cellulose well dispersed nanocomposites, such as melt blending or solvent casting. In the former case,

depending on matrix nature, often it is difficult to obtain the adequate cellulose dispersion in the matrix and high temperatures could degrade cellulose nanocrystals [43]. By solvent casting, the slow evaporation of the solvent promotes the formation of hydrogen bonds and rigid networks, resulting in high thermomechanical stability and mechanical reinforcement in the nanocomposite film. Diverse types of polymers have been used for nanocellulose nanocomposites preparation [44]. The use of nonpolar polymers requires an appropriate organic dispersion medium or the use of surfactant or surface chemical modification of nanocellulose in order to obtain a suitable polymer matrix dispersion. Instead, the use of aqueous polymer dispersions ensures the compatibility between the polymer and nanocellulose in water, facilitating the good dispersion for homogeneous nanocomposites preparation without requiring chemical modifications or surfactants [43]. The chance to disperse hydrophilic CNC in WBPU and WBPUU has focused their attention in WBPU-CNC and WBPUU-CNC nanocomposites films preparation. In this way, the final properties of nanocomposites films can be tailored varying CNC content, as well as their incorporation route, thus broadening the range of possible applications.

1.5 Electrospinning

Electrospinning is a suitable technique for obtaining mat of fibers in the nano and micrometer diameter range from a polymer solution induced by electric fields [45]. The fundamental of the process is based on the application of an electric field between the capillary syringe tip, where the polymer solution droplet is formed, and the grounded collector, where the fibers mat is deposited. Thereby, the application of the electric field induces the change of the droplet shape into a Taylor cone form, and when the droplet surface tension is exceeded,

the solution is ejected to the collector. During the discharge, the solvent is evaporated and the dried polymer fibers are deposited in the collector [46,47]. A scheme of the process is shown in **Figure 1.8**.
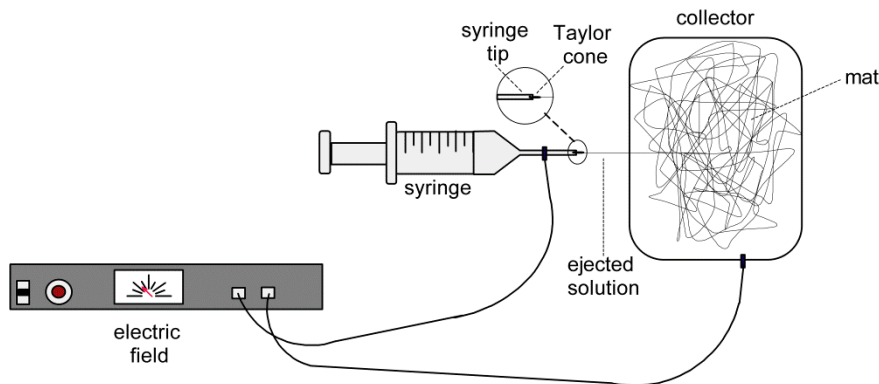
Figure 1.8 *Scheme of electrospinning process*

In this way, mats with high porosity and large surface area to volume ratio with tailored fiber diameters can be obtained, which become an attractive alternative to conventional casted coatings in different applications such as nanocatalysis, tissue engineering scaffolds, protective clothing, filtration, cosmetics and membranes among others [48–51]. The proper formation of fibers depends on several parameters which cover all aspects related with solution variables (viscosity, concentration, molecular weight, surface tension, electrical conductivity,…), processing variables (flow rate, electrical field strength, tip-to-collector distance,…) and ambient conditions (temperature, humidity,…) [52,53]. Even though, the solvent results a key parameter in the formation and final characteristics of the fibers [45]. Organic solvents can cause problems in fibers spinnability and morphology as well as corrosive effects in the collector of the equipment [54]. The election of water as solvent offers a suitable alternative,

focusing on environmentally friendly systems, and provides the opportunity of using polar polymers and aqueous dispersions such as WBPU and WBPUU. Thereby, the opportunity of electrospinning CNC reinforced WBPU and WBPUU fibers offers the possibility of tailoring the morphology and porosity of nanocomposites mats as an alternative to nanocomposites films, broadening the range of possible applications [55]. But the dispersibility of WBPU and WBPUU is not enough for the packaging of chains by entanglements in order to form a continuous fiber. Thereby, the incorporation of low contents of high molecular weight water soluble polymer acting as template polymer, such as poly(ethylene oxide) (PEO) or poly(vinyl alcohol) (PVA), favors the entanglement of the chains facilitating the spinning process [56]. In addition, the template polymer can be successfully removed at the end of the process by water extraction obtaining an electrospun of WBPU-CNC and WBPUU-CNC fiber mats.

1.6 Bioactive plant extracts

The possibility of incorporating water dispersible nanoreinforcements is not the unique advantage of WBPU and WBPUU systems. In this way, they offer also the opportunity of adding soluble additives, which provides to the polymer particular enhanced properties. For instance, in terms of antibacterial properties the incorporation of plant extracts can be a suitable chance of using enviromentally-friendly compounds derived from natural raw sources.

In this context, the use of medicinal plants for obtaining extracts with antibacterial potential has gained attention. For example, *Salvia officinalis L.* commonly known as sage, which belongs to Lamiaceae family and is usually used in culinary and medicinal preparations [57]. Their natural compounds have showed an alternative to other synthesized compounds as effective remedies to

antibacterial, antioxidant and anti-inflammatory [57,58]. On the other hand, *Melissa officinalis L.* belongs also to Lamiaceae family known as Lemon balm due to its flavor and fragrance [59]. Traditionally, Melissa tea has been used to treat headache, migraine, nervous tension,... This fact is related with the antibacterial, anti-inflammatory and antioxidant effect of extracts compounds [59–61].

In this way, the medical properties of plants can be attributed to the biologically active substances. It usually consists on secondary metabolites which are produced as intermediate or end products in secondary metabolism processes of the plant in order to complete the functioning of plant organism [60]. The main bioactive compounds of plants are alkaloids, flavonoids, tannins and phenolic compounds, among others, whose composition vary depending on the plant and their growing conditions [60,62,63] conferring the antibacterial activity to the extracts.

The extraction of the compounds can be carried out by different methods, such as infusion, decoction [64], and different solvents can be used [65]. Thereby, depending on the conditions of the extraction process, the composition of the extract will be varied and thus, the effective character against microbial agents.

In this way, the antibacterial properties of *Salvia officinalis L.* and *Melissa officinalis L.* plants extracts incorporated to WBPUU dispersions will be analyzed against Gram positive *Staphylococcus aureus* (S. aureus) and Gram negative *Escherichia coli* (E. coli) and *Pseudomonas aeruginosa* (P. aeruginosa) which are responsible for many infections and are common pathogens with difficult treatment [66].

1.7 General objectives

The main objectives of this work were the synthesis of environmentally-friendly polyurethane and polyurethane-urea dispersions for the preparation of films, and based on these preliminary results to use them thereafter for the preparation of nanocomposites incorporating cellulose nanocrystals as nanoreinforcement. In addition, other water soluble additives were incorporated, thus WBPUU dispersions containing plant extracts were synthesized.

Thus, after a brief introduction in chapter 1 and the specifications of the employed reactants and characterization methods during the work, in chapter 2:

- In chapter 3, different WBPU dispersions were synthesized varying molar composition in order to analyze the obtained dispersions as well as films final properties. Furthermore, in the second section of this chapter, the effect of annealing at room temperature after 5 months over previously prepared films was analyzed. In the third section of the chapter, based on preliminary results, the effect of varying hydroxyl/isocyanate groups ratio was analyzed.

- In chapter 4, WBPUU dispersions were synthesized considering different diamine chain extender contents. Moreover, two diamine incorporation routes were designed (homogeneous and heterogeneous media), and this effect was also studied in dispersions and films final properties.

- In chapter 5, the isolation process of cellulose nanocrystals by acid hydrolysis and their posterior characterization in order to use as renewable nanoreinforcement in WBPU and WBPUU nanocomposites was explained.

- In chapter 6, WBPU-CNC nanocomposites series were prepared considering different parameters that can alter the final properties of the films. In this way, different nanocomposites systems were prepared varying CNC content, WBPU matrix composition and CNC incorporation route.

- In chapter 7, following the objective of chapter 6, in this case previously synthesized WBPUU dispersion was employed for the preparation of WBPUU-CNC nanocomposites loaded with different CNC contents.

- In chapter 8, based on previously discussed WBPU-CNC series in chapter 6, nanocomposites containing different CNC content and prepared by two incorporation routes were employed for the preparation and characterization of nanocomposite mats by electrospinning technique.

- In chapter 9, bioactive plants extracts were obtained by infusion from *Salvia officinalis L.* and *Melissa officinalis L.* The extracts were incorporated to a WBPUU dispersion in order to enhance the antibacterial properties of the films. With this purpose, different extract contents were added to the WBPUU by three incorporation routes. Furthermore, the influence of each extract in the final properties of dispersions and films was also analyzed.

- In chapter 10, the general conclusions of the work as well as the proposed future works are presented.

1.8 References

[1]   D.K. Chattopadhyay, K.V.S.N. Raju, Structural engineering of polyurethane coatings for high performance applications, Prog. Polym. Sci. 32 (2007) 352–418.

[2]   H. Hao, J. Shao, Y. Deng, S. He, F. Luo, Y. Wu, J. Li, H. Tan, J. Li, Q. Fu, Synthesis and characterization of biodegradable lysine-based waterborne polyurethane for soft tissue engineering applications, Biomater. Sci. 4 (2016) 1682–1690.

[3]   Z. Wang, Z. Hou, Y. Wang, Fluorinated waterborne shape memory polyurethane urea for potential medical implant application, J. Appl. Polym. Sci. 127 (2013) 710–716.

[4]   I. Yilgör, E. Yilgör, G.L. Wilkes, Critical parameters in designing segmented polyurethanes and their effect on morphology and properties: A comprehensive review, Polymer 58 (2015) A1–A36.

[5]   L.S.T.J. Korley, B.D. Pate, E.L. Thomas, P.T. Hammond, Effect of the degree of soft and hard segment ordering on the morphology and mechanical behavior of semicrystalline segmented polyurethanes, Polymer 47 (2006) 3073–3082.

[6]   A. Saralegi, L. Rueda, B. Fernández-D'Arlas, I. Mondragon, A. Eceiza, M.A. Corcuera, Thermoplastic polyurethanes from renewable resources: Effect of soft segment chemical structure and molecular weight on

morphology and final properties, Polym. Int. 62 (2013) 106–115.

[7]   H.T. Lee, S.Y. Wu, R.J. Jeng, Effects of sulfonated polyol on the properties of the resultant aqueous polyurethane dispersions, Colloid Surface A 276 (2006) 176–185.

[8]   X. Jiang, J. Li, M. Ding, H. Tan, Q. Ling, Y. Zhong, Q. Fu, Synthesis anddegradation of nontoxic biodegradable waterborne polyurethanes elastomerwith poly (ε-caprolactone) and poly(ethylene glycol) as soft segment, Eur. Polym. J. 43 (2007) 1838–1846.

[9]   A.K. Nanda, D.A. Wicks, The influence of the ionic concentration, concentration of the polymer, degree of neutralization and chain extension on aqueous polyurethane dispersions prepared by the acetone process, Polymer 47 (2006) 1805–1811.

[10]   M.M. Rahman, H. Do Kim, Synthesis and characterization of waterborne polyurethane adhesives containing different amount of ionic groups (I), J. Appl. Polym. Sci. 102 (2006) 5684–5691.

[11]   Y. Li, B.A.J. Noordover, R.A.T. Van Benthem, C.E. Koning, Property profile of poly (urethane urea) dispersions containing dimer fatty acid- , sugar- and amino acid-based building blocks, Eur. Polym. J. 59 (2014) 8–18.

[12]   L.H. Bao, Y.J. Lan, S.F. Zhang, Synthesis and properties of waterborne

polyurethane dispersions with ions in the soft segments, J. Polym. Res. 13 (2006) 507–514.

[13]   M. Barikani, M.V. Ebrahimi, S.M.S. Mohaghegh, Preparation and characterization of aqueous polyurethane dispersions containing ionic centers, J. Appl. Polym. Sci. 104 (2007) 3931–3937.

[14]   M. Pohl, E. Danieli, M. Leven, W. Leitner, B. Blümich, T.E. Müller, Dynamics of polyether polyols and polyether carbonate polyols, Macromolecules 49 (2016) 8995–9003.

[15]   K. Gorna, S. Polowinski, S. Gogolewski, Synthesis and characterization of biodegradable poly(ε-caprolactone urethane)s. I. Effect of the polyol molecular weight, catalyst, and chain extender on the molecular and physical characteristics, J. Polym. Sci. Part A Polym. Chem. 40 (2002) 156–170.

[16]   V. García-Pacios, Y. Iwata, M. Colera, J.M. Martín-Martínez, Influence of the solids content on the properties of waterborne polyurethane dispersions obtained with polycarbonate of hexanediol, Int. J. Adhes. Adhes. 31 (2011) 787–794.

[17]   J. Bullermann, S. Friebel, T. Salthammer, R. Spohnholz, Novel polyurethane dispersions based on renewable raw materials-Stability studies by variations of DMPA content and degree of neutralisation, Prog. Org. Coat. 76 (2013) 609–615.

[18] J. Hong, X.Q. Yang, X. Wan, Z. Zheng, Z.S. Petrović, High value polyurethane resins from rubber seed oil, Polym. Int. 66 (2017) 126–132.

[19] S.M. Cakic, M. Spirkova, I.S. Ristic, J.K. B-Simendic, M. M-Cincovic, R. Poreba, The waterborne polyurethane dispersions based on polycarbonate diol: Effect of ionic content, Mater. Chem. Phys. 138 (2013) 277–285.

[20] Y.H. Guo, J.J. Guo, H. Miao, L.J. Teng, Z. Huang, Properties and paper sizing application of waterborne polyurethane emulsions synthesized with isophorone diisocyanate, Prog. Org. Coat. 77 (2014) 988–996.

[21] S.M. Cakic, J. V Stamenkovic, D.M. Djordjevic, I.S. Ristic, Synthesis and degradation profile of cast films of PPG-DMPA-IPDI aqueous polyurethane dispersions based on selective catalysts, Polym. Degrad. Stab. 94 (2009) 2015–2022.

[22] K. Wang, Y. Peng, R. Tong, Y. Wang, Z. Wu, The effects of isocyanate index onthe properties of aliphatic waterborne polyurethaneureas, J. Appl. Polym. Sci. 118 (2010) 920–927.

[23] S.K. Lee, B.K. Kim, High solid and high stability waterborne polyurethanes via ionic groups in soft segments and chain termini, J. Colloid Interf. Sci. 336 (2009) 208–214.

[24] L. Lei, L. Zhong, X. Lin, Y. Li, Z. Xia, Synthesis and characterization of

waterborne polyurethane dispersions with different chain extenders for potential application in waterborne ink, Chem. Eng. J. 253 (2014) 518–525.

[25]   S. Sakurai, Y. Okamoto, H. Sakaue, T. Nakamura, L. Banda, S. Nomura, Structure and properties of segmented poly(urethaneurea)s with relatively short hard-segment chains, J. Polym. Sci. Part B 38 (2000) 1716–1728.

[26]   B. Li, D. Peng, N. Zhao, Q. Mu, J. Li, The physical properties of nonionic waterborne polyurethane with a polyether as side chain, J. Appl. Polym. Sci. 127 (2013) 1848–1852.

[27]   A.M. Nelson, T.E. Long, Synthesis, Properties, and Applications of Ion-Containing Polyurethane Segmented Copolymers, Macromol. Chem. Phys. 215 (2014) 2161–2174.

[28]   X. Dang, G. Wang, D. Wang, T. Pan, L. Zhou, X. Shi, Distribution of hydrophilic monomer units and its effect on the property of the water dispersion of polyurethaneurea anionomer, J. Appl. Polym. Sci. 103 (2007) 634–640.

[29]   T.F. Garrison, Z. Zhang, H.J. Kim, D. Mitra, Y. Xia, D.P. Pfister, B.F. Brehm-Stecher, R.C. Larock, M.R. Kessler, Thermo-mechanical and antibacterial properties of soybean Oil-Based cationic polyurethane coatings: Effects of amine ratio and degree of crosslinking, Macromol.

Mater. Eng. 299 (2014) 1042–1051.

[30]   B. Fernández-D'Arlas, M. Corcuera, J. Labidi, I. Mondragon, A. Eceiza, Poly(urea)urethanes based on amorphous quaternizable hard segments and a crystalline polyol derived from castor oil, Colloid Polym. Sci. 291 (2013) 1247–1254.

[31]   M.R. Chashmejahanbin, H. Daemi, M. Barikani, A. Salimi, Noteworthy impacts of polyurethane-urea ionomers as the efficient polar coatings on adhesion strength of plasma treated polypropylene, Appl. Surf. Sci. 317 (2014) 688–695.

[32]   H. Sardon, L. Irusta, M.J. Fernández-Berridi, Synthesis of isophorone diisocyanate (IPDI) based waterborne polyurethanes: Comparison between zirconium and tin catalysts in the polymerization process, Prog. Org. Coat. 66 (2009) 291–295.

[33]   D.J. Hourston, G.D. Williams, R. Satguru, J.C. Padget, D. Pears, The influence of the degree of neutralization, the ionic moiety, and the counterion on water-dispersible polyurethanes, J. Appl. Polym. Sci. 74 (1999) 556–566.

[34]   S.H. Son, H.J. Lee, J.H. Kim, Effects of carboxyl groups dissociation and dielectric constant on particle size of polyurethane dispersions.pdf, Colloids Surfaces A 133 (1998) 295–301.

[35]   B.K. Kim, Aqueous polyurethane dispersions, Colloid Polym. Sci. 274 (1996) 599–611.

[36]   H. Lijie, D. Yongtao, Z. Zhiliang, S. Zhongsheng, S. Zhihua, Synergistic effect of anionic and nonionic monomers on the synthesis of high solid content waterborne polyurethane, Colloids Surfaces A 467 (2015) 46–56.

[37]   R.M.A. Domingues, M.E. Gomes, R.L. Reis, The potential of cellulose nanocrystals in tissue engineering strategies, Biomacromolecules 15 (2014) 2327–2346.

[38]   Y. Habibi, L.A. Lucia, O.J. Rojas, Cellulose nanocrystals: Chemistry, self-assembly, and applications, Chem. Rev. 110 (2010) 3479–3500.

[39]   G. Mondragon, S. Fernandes, A. Retegi, C. Peña, I. Algar, A. Eceiza, A. Arbelaiz, A common strategy to extracting cellulose nanoentities from different plants, Ind. Crops Prod. 55 (2014) 140–148.

[40]   S.J. Eichhorn, Cellulose nanowhiskers: Promising materials for advanced applications, Soft Matter. 7 (2011) 303–315.

[41]   X.M. Dong, J.F. Revol, D.G. Gray, Effect of microcrystallite preparation conditions on the formation of colloid crystals of cellulose, Cellulose 5 (1998) 19–32.

[42]   M.A.S.A. Samir, F. Alloin, A. Dufresne, Review of recent research into

cellulosic whiskers, their properties and their application in nanocomposite field, Biomacromolecules 6 (2005) 612–626.

[43]   M. Mariano, N. El Kissi, A. Dufresne, Cellulose nanocrystals and related nanocomposites: Review of some properties and challenges, J. Polym. Sci. Part B Polym. Phys. 52 (2014) 791–806.

[44]   A. Dufresne, Interface engineering of natural fibre composites, Interface Eng. Nat. Fibre Compos., Woodhead Publishing Limited, 2011: pp. 82–116.

[45]   S. Torres-Giner, R. Pérez-Masiá, J.M. Lagaron, A review on electrospun polymer nanostructure as advanced bioactive platforms, Polym. Eng. Sci. 56 (2016) 500–527.

[46]   A. Moheman, M. Sarwar Alam, A. Mohammad, Recent trends in electrospinning of polymer nanofibers and their applications in ultra thin layer chromatography, Adv. Colloid Interf. Sci. 229 (2016) 1–24.

[47]   T.C. Mokhena, V. Jacobs, A.S. Luyt, A review on electrospun bio-based polymers for water treatment, Express Polym. Lett. 9 (2015) 839–880.

[48]   N. Bhardwaj, S.C. Kundu, Electrospinning: A fascinating fiber fabrication technique, Biotechnol. Adv. 28 (2010) 325–347.

[49]   N. Moazeni, D. Semnani, M. Latifi, M. Sadrjahani, A novel method to

produce an artificial common bile duct using electrospinning technique, Procedia Mater. Sci. 11 (2015) 166–170.

[50]   C. Tonda-Turo, M. Boffito, C. Cassino, P. Gentile, G. Ciardelli, Biomimetic polyurethane – based fibrous scaffolds, Mater. Lett. 167 (2016) 9–12.

[51]   Z. Zhou, W. Lin, X.F. Wu, Electrospinning ultrathin continuous cellulose acetate fibers for high-flux water filtration, Colloid Surface A 494 (2016) 21–29.

[52]   S. Mohammadzadehmoghadam, Y. Dong, I.J. Davies, Recent progress in electrospun nanofibers: Reinforcement effect and mechanical performance, J. Polym. Sci. Part B 53 (2015) 1171–1212.

[53]   D.H. Reneker, A.L. Yarin, Electrospinning jets and polymer nanofibers, Polymer 49 (2008) 2387–2425.

[54]   B.N. Singh, N.N. Panda, K. Pramanik, A novel electrospinning approach to fabricate high strength aqueous silk fibroin nanofibers, Int. J. Biol. Macromol. 87 (2016) 201–207.

[55]   Y.C. Kuo, S.C. Hung, S.H. Hsu, The effect of elastic biodegradable polyurethane electrospun nanofibers on the differentiation of mesenchymal stem cells, Colloid Surface. B 122 (2014) 414–22.

[56]   L. Buruaga, H. Sardon, L. Irusta, A. González, M.J. Fernández-Berridi, J.J. Iruin, Electrospinning of waterborne polyurethanes, J. Appl. Polym. Sci. 115 (2010) 1176–1179.

[57]   N. Martins, L. Barros, C. Santos-Buelga, M. Henriques, S. Silva, I.C.F.R. Ferreira, Evaluation of bioactive properties and phenolic compounds in different extracts prepared from Salvia officinalis L., Food Chem. 170 (2015) 378–385.

[58]   M. Ghorbanpour, M. Hatami, K. Kariman, P. Abbaszadeh Dahaji, Phytochemical variations and enhanced efficiency of antioxidant and antimicrobial ingredients in Salvia officinalis as inoculated with different rhizobacteria, Chem. Biodivers. 13 (2016) 319–330.

[59]   M. Carocho, L. Barros, R.C. Calhelha, A. Ćirić, M. Soković, C. Santos-Buelga, P. Morales, I.C.F.R. Ferreira, *Melissa officinalis L.* decoctions as functional beverages: A bioactive approach and chemical characterization, Food Funct. 6 (2015) 2240–2248.

[60]   O. Stefanović, L. Comic, Synergistic antibacterial interaction between *Melissa officinalis* extracts and antibiotics, J. Appl. Pharm. Sci. 2 (2012) 1–5.

[61]   K. Dastmalchi, H.J. Damien Dorman, P.P. Oinonen, Y. Darwis, I. Laakso, R. Hiltunen, Chemical composition and in vitro antioxidative activity of a lemon balm (*Melissa officinalis L.*) extract, LWT. 41 (2008) 391–400.

[62] B. Pawlikowska-Pawlęga, L.E. Misiak, B. Zarzyka, R. Paduch, A. Gawron, W.I. Gruszecki, FTIR, ^{1}H NMR and EPR spectroscopy studies on the interaction of flavone apigenin with dipalmitoylphosphatidylcholine liposomes, Biochim. Biophys. Acta. 1828 (2013) 518–527.

[63] R. Venkataswamy, A. Doss, H.M. Mubarack, M. Sukumar, Phytochemical, HPTLC finger printing and antibacterial activity of *Acacia nilotica (L.)* Delile, Hygeia J. Drugs Med. 2 (2010) 38–42.

[64] M. Carocho, R.C. Calhelha, M.J.R.P. Queiroz, A. Bento, P. Morales, M. Soković, I.C.F.R. Ferreira, Infusions and decoctions of *Castanea sativa* flowers as effective antitumor and antimicrobial matrices, Ind. Crops Prod. 62 (2014) 42–46.

[65] K. Rashed, A. Ćirić, J. Glamočlija, R.C. Calhelha, I.C.F.R. Ferreira, M. Soković, Antimicrobial and cytotoxic activities of *Alnus rugosa L.* aerial parts and identification of the bioactive components, Ind. Crops Prod. 59 (2014) 189–196.

[66] Y. Gerasymchuk, A. Lukowiak, A. Wedzynska, A. Kedziora, G. Bugla-Ploskonska, D. Piatek, T. Bachanek, V. Chernii, L. Tomachynski, W. Strek, New photosensitive nanometric graphite oxide composites as antimicrobial material with prolonged action, J. Inorg. Biochem. 159 (2016) 142–148.

CHAPTER 2

Materials and characterization techniques

2 MATERIALS AND CHARACTERIZATION TECHNIQUES

In this chapter, the materials employed in the synthesis of WBPU and WBPUU dispersions, isolation of CNC and extraction of plant extracts are described. Furthermore, the characterization techniques and conditions used for dispersions and films analysis are also specified.

2.1 Reactants

Regarding WBPU synthesis, a difunctional poly(ε-caprolactone) diol (PCL) ($\overline{M}_w$= 2000 g mol⁻¹), purchased from BASF was selected as soft segment. Hard segment was composed by 1,4-butanediol (BD), provided from Aldrich as chain extender, 5-isocyanate-1-(isocyanate methyl)-1,3,3-trimethyl cyclohexane, as diisocyanate, kindly provided by Bayer and 2,2-bis(hydroxymethyl) propionic acid, DMPA, as internal emulsifier supplied by Aldrich. PCL, BD and DMPA were dried under vacuum at 50 °C for 4 h previous their use and dibutyl tin dilaurate, provided from Aldrich, was chosen as catalyst and used as received. Furthermore, triethylamine, purchased from Aldrich, was employed to neutralize the ionic groups in the dispersion and tetrahydrofuran (THF) was used to control the viscosity during the synthesis. Both were dehydrated with hydranal-molecular Sieve 0.3 nm (water adsorption capacity of 15%), supplied by Fluka, which was previously dried at 55 °C under vacuum for 1 day.

In the case of WBPUU systems, the synthesis was carried out using poly(ε-caprolactone) diol ($\overline{M}_w$= 2000 g mol⁻¹) provided by Solvay, IPDI, also provided by Bayer, as in the case of the IPDI used in WBPU, 1,4-butanediol and ethylenediamine (EDA) supplied by Fluka and Panreac respectively, used as

chain extenders and 2,2-bis(hydroxymethyl)propionic acid and triethylamine, purchased both from Fluka. PCL, BD and DMPA were also dried under vacuum at 50 °C for 4 h. Dry acetone, purchased from Panreac, employed during the synthesis as viscosity adjuster and dibutyl tin dilaurate, supplied by Fluka, were used without further purification.

Cellulose nanocrystals were isolated from microcrystalline cellulose powder supplied from Aldrich with sulfuric acid (96%) provided from Panreac.

Finally, for obtaining plants extracts, *Salvia officinalis L.* from Raizes da Natureza and *Melissa officinalis L.* from Tetley were employed as dry material obtained in an herbalist.

2.2 Characterization techniques

2.2.1 Dispersions characterization

2.2.1.1 pH

The pH of dispersions was measured using a pH meter GLP22 of Crison, which was calibrated with pH 4.00 and 7.00 buffer solutions standards.

2.2.1.2 Rheological properties

The rheological properties of dispersions were determined by viscosimetry in order to analyze the properties of WBPU and WBPUU containing CNC or plant extracts in water. Samples were analyzed by rotational viscosimetry in order to measure shear viscosity results. In the case of WBPU dispersions for electrospinning, rheological measurements were performed in a Haake Rheostress stress–controlled rotational viscoelastometer at 25 ± 2 °C using a cone-plate geometry (φ = 40 mm, angle of 2°). Instead, for WBPUU dispersions

containing plants extracts, the measurements were carried out using a Visco Star Fungilab of concentric cylinders rotational viscosimeter. The viscosity (η) values were determined by averaging 3 measurements using 8 mL of dispersion at 25 °C.

2.2.1.3 Dynamic light scattering

Particle size of WBPU dispersions was analyzed by dynamic light scattering (DLS). By this technique, it is possible to measure the diffusion speed of particles by means of the dispersed light in the system. In this way, the particle size and distribution profile of the particles can be determined by the hydrodynamic radio. The measurements were carried out using a BI-200SM goniometer, from Brookhaven. The intensity of dispersed light was measured using a luminous source of He-Ne laser (Mini L-30, wavelength λ = 637 nm, 400 mW) and a detector (BI–APD) placed on a rotary arm which allows measuring the intensity at 90°. Samples prepared mixing a small amount of aqueous dispersion with ultrapure water were measured at 25 °C by triplicate.

2.2.1.4 Particle analyzer

Particle size of WBPUU dispersions containing plant extracts were analyzed using a Mastersizer 3000 Hydro particle size analyzer of Marlvern. The technique is based on a laser beam diffraction measurement. When the laser passes through a dispersed particulate sample, the angular variation in intensity of the scattered light is measured. Large particles scatter light at small angles relative to the laser beam and small particles scatter light at large angles. The angular scattering intensity data is then analyzed to calculate the size of the particles and is reported as a volume equivalent sphere diameter. Samples were

analyzed at 25 °C by averaging 5 measurements of the diluting WBPUU dispersions.

2.2.2 Physicochemical characterization

2.2.2.1 Proton and Carbon nuclear magnetic resonance

The chemical structure of WBPU was analyzed by proton (^{1}H NMR) and carbon (^{13}C NMR) nuclear magnetic resonance. The technique is based on the application of an electromagnetic field and the analysis of the variation in the frequencies of proton and carbon resonances depending on the surrounding atoms of each proton or carbon nucleus. In this way, the measurement was carried out in a Bruker Avance 500 spectrometer, equipped with a BBO probe with gradient in Z axis and using a resonant frequency of 125.77 mHz. Acquisition times were established at 3 and 1.5 s averaging 64 and 32 K scans, in the case of ^{1}H NMR and ^{13}C NMR, respectively, using an interpulse delay of 2 s. A time domain of 64 K was used in a spectral width of 10000 Hz for ^{1}H NMR and 31000 Hz in ^{13}C NMR.

2.2.2.2 Gel permeation chromatography

Weight average molecular weight ($\overline{M}_w$) and polydispersity index (IP) of the synthesized WBPU were determined by gel permeation chromatography (GPC). It is a type of size exclusion chromatography, where a mobile phase carries the sample through a stationary phase circuit, which consists on a microporous packaged gel. In this way, depending on the size of the molecules, the molecules retention time for completing the whole circuit varies, considering that smaller molecules will result in longer elution times by being entrapped in the pores. Thus, the molecules of the sample will be separated according to their sizes due

to the different retention time in the circuit. The measurements were carried out using a Thermo Scientific chromatograph equipped with an isocratic Dionex UltiMate 3000 pump and a RefractoMax 521 refractive index detector. The separation was carried out at 30 °C within four Phenogel GPC columns, from Phenomenex, with 5 μm particle size and 10^5, 10^3, 100 and 50 Å porosities, respectively, located in an UltiMate 3000 Thermostated Colum Compartment. Tetrahydrofuran at a flow rate of 1 mL min^{-1} was chosen as mobile phase. The molecular weight and polydispersity index were referred to monodisperse polystyrene standards. Samples were prepared dissolving the obtained films in THF at 1 wt%.

2.2.2.3 Fourier transform infrared spectroscopy

Fourier transform infrared spectroscopy (FTIR) was used to identify characteristic functional groups and hydrogen bonding interactions. This technique is based on irradiating the sample with an infrared light source. In this way, the light absorbed by the sample is reflected in the spectrum at different wavenumbers. Spectra were recorded using a Nicolet Nexus spectrometer provided with a MKII Golden Gate accessory (Specac) with diamond crystal at a nominal incidence angle of 45° and ZnSe lens. Measurements were run after averaging 64 scans in the range between 4000 and 650 cm^{-1} in transmittance mode with a resolution of 8 cm^{-1}.

2.2.2.4 Elemental analysis

Elemental analysis (EA) was performed in order to determine the sulfate groups anchored to CNC during the hydrolysis process using a Euro EA3000 Elemental Analyzer of Eurovector. In this way, the sample is combusted in presence of

oxygen and the resultant products are analyzed in a chromatographic column. Thereby, a thermal conductivity detector provides a signal of each element and the percentage is measured.

2.2.2.5 Conductometric titration

The concentration of sulfate groups anchored to the sulfuric acid hydrolyzed CNC was determined by conductometric titration at 25 °C with a Crison EC-Meter GLP 31 conductometer calibrated with 147 μS cm^{-1}, 1413 μS cm^{-1} and 12.88 mS cm^{-1} standards. For the titration, sodium hydroxide (NaOH) and hydrochloric acid (HCl) 10 mM were used.

2.2.3 Thermal characterization

2.2.3.1 Differential scanning calorimetry

Differential scanning calorimetry (DSC) measurements were carried out in order to analyze the thermal behavior of films. The technique is based in heat provided to the analyzing sample and a reference for maintaining the same temperature. Thereby, when the sample undergoes to a thermal transition, the required heat for the sample will vary respect to the reference, and will be reflected in the thermograms. The measurements were performed using a Mettler Toledo 822^e equipment, provided with a robotic arm and with an electric intracooler as refrigerator unit. WBPU, WBPUU and nanocomposites samples with a weight between 5 and 10 mg were encapsulated in aluminum pans and were heated from −80 to 180 °C at a scanning rate of 20 °C min^{-1} under a constant nitrogen flow. A dynamic scan was also performed to the pure PCL from −80 to 180 °C and to neat IPDI–BD block from 25 to 250 °C at a scanning rate of 20 °C min^{-1}. The inflection point of heat capacity change (ΔC_p) observed

was chosen as glass transition temperature (T_g). Melting temperature (T_m) was settled as the maximum of endothermic peak taking the area under the peak as melting enthalpy (ΔH_m).

2.2.3.2 Thermogravimetric analysis

The thermal stability of CNC and WBPU and nanocomposites films was determined by thermogravimetric analysis (TGA). In this technique, the degradation process of the sample is controlled by measuring the weight of the sample in a microbalance during a heating scan. Thereby, the evolution of the weight loss respect to the sample initial weight can be determined. The analysis was performed using a TGA/SDTA 851 Mettler Toledo equipment. Between 5 and 10 mg of samples were subjected to a dynamic run from 25 to 700 °C at a heating rate of 10 °C min^{-1} in nitrogen atmosphere. The initial degradation temperature (T_i) was referred to the loss of 5 wt% of weight of the total sample whereas the maximum degradation temperature (T_m) was settled as the minimum of the degradation peak in the derivative thermogravimetric (DTG) curves.

2.2.4 Mechanical characterization

2.2.4.1 Tensile tests

Mechanical behavior of films was determined at room temperature. By this technique, the sample is subjected to a constant elongation rate where the sample is extended until failure. In this way, the equipment records the force and elongation values for the sample reflecting in stress-strain curves, where different characteristic properties of the materials are determined. In this case, a MTS Insight 10 testing machine provided with a 250 N load cell and pneumatic

grips to hold samples was employed. Films tensile modulus (E), yield stress (σ_y), stress at break (σ_b) and strain at break (ε_b) were determined from stress–strain curves obtained at a crosshead speed of 50 mm min^{-1}. Five specimens of 8 mm in length, 2.5 mm in width and 0.4 mm in thickness were analyzed for each system.

2.2.5 Thermomechanical characterization

2.2.5.1 Thermomechanical properties

Dynamic mechanical analysis (DMA) was performed in order to analyze the viscoelastic properties of films. In this way, a sinusoidal stress is applied and the strain response is measured by varying the temperature of the sample. Thereby, the phase difference between the stimulus and response are used to determine the storage modulus (E') as well as loss modulus (E''), whose relation result in the tangent of phase angle (Tanδ). In this way, the peaks in Tanδ curves can be associated with the T_g of the sample, which will be also reflected in a drop in E' curves. The thermomechanical stability of the films was determined using an Eplexor 100 N analyser Gabo equipment. The measurements carried out in tensile mode were performed from -100 to 150 °C at a scanning rate of 2 °C min^{-1}. The static strain was established as 0.05% and the operating frequency was fixed at 1 Hz.

2.2.6 Hydrophilicity

2.2.6.1 Static and dynamic water contact angle

The surface hydrophilicity of films was analyzed by either static or dynamic water contact angle measurements. This technique is based on the deposition of a deionized water drop in the surface of the film in order to analyze the

equilibrium air-water-film contact angle value, which will depend on the chemical interactions. Measurements were carried out in a Dataphysics OCA20 equipment at room temperature. In the case of static water contact angle (SWCA) six contact angle (θ) values were averaged by dropping 2 µL of deionized water over the films surface. Instead, for dynamic contact angle (DWCA) a deionized water drop of 3 µL was deposited in the surface of the film by a syringe tip. The needle was remained inside the drop, maintaining the smallest portion as possible during all experiment, in order to prevent alterations in the tests. The advancing contact angles (θ_a) values were measured by increasing the drop volume up to 10 mL adding deionized water at a constant flow of 0.5 µL, while receding contact angles (θ_r) were determined reducing the drop volume at a constant flow of 0.5 µL.

2.2.6.2 Water absorption

The evolution of water absorption (WA) of films was carried out by weight difference measurements. Thus, the capacity of films for absorbing water is analyzed. For the study, films of around 15-20 mg were immersed in deionized water at 25 °C. Samples were weighted at different times until no considerable weight changes were observed. Water absorption percentage was determined from weight increase by means of the following **Equation 2.1**:

$$WA(\%) = \frac{W_t - W_0}{W_0} \cdot 100 \qquad (2.1)$$

Where W_t and W_0 are referred to the weight at time t and the initial weight respectively. Three measurements were averaged for each sample.

2.2.7 Morphological characterization

2.2.7.1 Atomic force microscopy

The morphology of WBPU, WBPUU, CNC and their nanocomposites was determined by atomic force microscopy (AFM). The technique is based on the interactions between the tip and the sample. In this way, the tip and sample attractive-repulsion forces created a deflection in the tip, and the images are created by mapping the deflections in each point of the sample. The images were obtained at room temperature in tapping mode, using a Nanoscope IIIa scanning probe microscope (Multimode TM Digital instruments) with an integrated force generated by cantilever/silicon probes, applying a resonance frequency of about 180 kHz. The cantilever had a tip radius of 5–10 nm and was 125 μm long. The morphology of polyurethanes presented in chapter 3, was analyzed from the cross-section of samples cut in liquid nitrogen. Otherwise, the analysis of the morphology of WBPU, WBPUU, CNC, nanocomposites and bioactive films containing plant extracts samples prepared from dispersions, was carried out via *spin-coating* (Spincoater P6700) at 1200 rpm for 130 s. WBPU, WBPUU, nanocomposites and bioactive films containing plant extracts samples were prepared by spin-coating a droplet of dispersions on glass supports whereas in the case of CNC, a droplet of CNC diluted dispersion was spin-coated on a mica flake in order to analyze their morphology.

2.2.7.2 Scanning electron microscopy

The electrospun fibers morphology was analyzed by scanning electron microscopy (SEM). It is based on irradiating the surface of the sample with a high-energy electrons beam, in order to analyze the different signals obtained from the electron sample interactions. Electrospun samples were analyzed using

a Hitachi S-2700 Scanning Electron Microscope at 15 kV accelerating voltage, after putting the samples on a SEM disk and sputter-coated with an 8 nm Pt/Au layer to reduce electron charging effects.

2.2.8 Antibacterial characterization

2.2.8.1 Antimicrobial tests

The assays were performed using Gram positive bacteria *Staphylococcus aureus* ATCC 19213 and Gram negative bacteria *Escherichia coli* ATCC 10536 and *Pseudomonas aeruginosa* ATCC 9027 as test microorganisms. The method was based on the Kirby-Bauer modified test. Briefly, the bacteria inoculums were prepared by aseptically transferring 4 isolated colonies of each one, to separate test tubes containing nutrient broth, which were then incubated for 24 h at 37 °C. The inoculums were diluted to 0.5 McFarland turbidity standard (corresponding to a concentration of $1.5–3.0 \times 10^8$ CFU/mL) using sterilized Ringer solution. The concentration of the bacteria dilutions were also controlled by UV-visible spectrophotometry by measuring the absorbance at 625 nm. Then, the bacteria solutions were inoculated in Mueller Hinton Agar plates, using a sterilized swab. The inoculated plates were left to dry for a short period of time. After that, a piece of sample with 1.5 cm of diameter of the waterborne polyurethane-urea films containing plant extracts with 1.5 cm of diameter was placed in the center of the plate. The plates were incubated at 37 °C for 24 h. After this period, the plates were analyzed to measure the diameter of the inhibition zone and the growth of the bacteria on the surface or behind the film. After, the incubation maintained for a further 4 days in order to evaluate the possible growth of the inhibition zone caused by the extract diffusion and the bacteria biofilm formation on the films surface.

CHAPTER 3

Synthesis of waterborne polyurethanes

"Hay que aprender a ver las cosas por lo que son,

no por lo que tú quieres que sean"

3. SYNTHESIS OF WATERBORNE POLYURETHANES

3.1 Objective

This chapter was focused on the synthesis of waterborne polyurethane varying the reactants molar ratio for studying these parameters on the final properties. Polyurethanes with different diisocyanate/macrodiol/emulsifier/chain extender molar ratio were synthesized in order to analyze the effect on dispersions stability and films physicochemical, thermal and mechanical properties, hydrophilicity and morphology by means of dynamic light scattering, proton and carbon nuclear magnetic resonance, gel permeation chromatography, Fourier transform infrared spectroscopy, differential scanning calorimetry, mechanical tests, static water contact angle, water absorption measurements and atomic force microscopy. Then, the obtained films properties were studied focusing on the annealing effect at room conditions, after 5 months of storing. Finally, based on previous results, maintaining constant the molar composition of macrodiol, emulsifier and chain extender, different diisocyanate molar contents were used. Thus, the effect of isocyanate/hydroxyl groups ratio was analyzed for a more comprehensive study of dispersions and films properties.

3.2 Experimental

3.2.1 Synthesis of waterborne polyurethanes and films preparation

WBPU were synthesized using PCL as soft segment, BD as chain extender, DMPA as internal emulsifier and IPDI as diisocyanate. The synthesis was carried out by a two step polymerization procedure, in a 250 mL four-necked flask equipped with a mechanical stirrer, thermometer, nitrogen inlet and condenser

within a thermostatized bath. In the first step, PCL, 0.1 wt% of DBTDL (respect to WBPU total weight) and IPDI were mixed at 90 °C and left to react for 5 h. Thereafter, DMPA was added and the mixture was allowed to react until the theoretical NCO content was reached. The reaction progress was determined analyzing the NCO content by dibutylamine (DBA) back titration method according to ASTM D 2572-97. In the second step, the required amount of BD was added and the reaction evolution was also verified by DBA back titration method. Afterwards, the polymer was cooled to 55 °C while viscosity was adjusted adding low volumes of THF. After that, the necessary TEA amount was added with the purpose to neutralize all the carboxylic groups. Thereafter the system was cooled until room temperature and 75 mL of deionized water were added dropwise using a peristaltic pump under vigorous stirring for 15 min. Finally, THF was removed using a rotary evaporator at 60 °C obtaining a dispersion with about 25 wt% solids content. Scheme of polyurethane synthesis process is depicted in **Figure 3.1**.
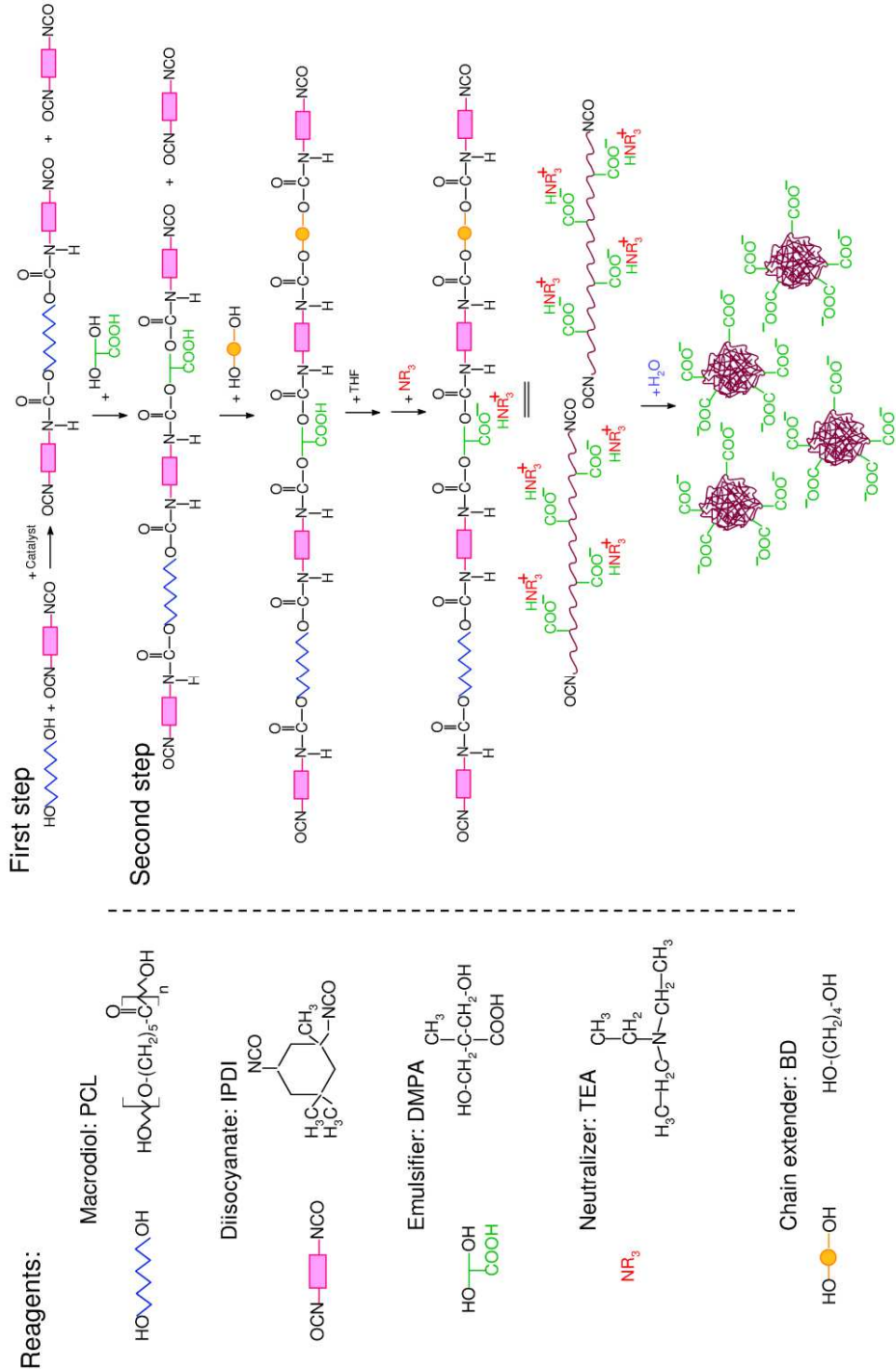
Figure 3.1 *Scheme of the WBPU synthesis process*

Films were prepared by casting 12 mL of WBPU dispersion on leveled (8 cm × 8 cm) Teflon molds and allowing them to dry in a climatic chamber at 25 °C and 50% of relative humidity during 7 days. The residual water entrapped in films was removed drying in a vacuum oven at 25 °C for 3 days at 800, 600 and 400 mbar, respectively. For comparison, neat IPDI–BD block was also synthesized following previous protocol [1]. Dispersions were characterized after their synthesis and films one week after their preparation. Films were stored in a desiccator previous their characterization.

WBPU samples with different macrodiol/emulsifier (PCL/DMPA) and diisocyanate/(macrodiol+emulsifier) (IPDI/(PCL+DMPA)) molar ratios were synthesized. Samples were named as WBPUX or WBPUX(1.5), where X denotes the molar composition of diisocyanate, and (1.5) is referred to PCL/DMPA molar ratio in cases when is different from 1. As the NCO/OH groups ratio was also varied, working in stoichiometric conditions or with a slightly excess of isocyanate groups, "s" was used in order to denote stoichiometric conditions, resulting in WBPUXs and WBPUX(1.5)s.

Reagents molar ratio and hard segment, total acid groups *(COOH$_{tot}$)* and total emulsifier *(DMPA$_{tot}$)* contents of the synthesized WBPUs are summarized in **Table 3.1**. Although the internal emulsifier was added in the first step of the synthesis, due to its low molecular weight and taking into account it was added after polyol and IPDI reaction, it might be considered part of hard segment. Furthermore, **Table 3.1** also contains pH and particle size diameter and polydispersity values of the dispersions as well as $\overline{M}_w$ and PI determined from WBPU films.

Table 3.1 *Molar composition and hard segment (HS), total acid groups, and total emulsifier contents, pH, particle size diameters and polydispersity and $\bar{M}_w$ and PI of WBPU samples*

		WBPU2(1.5)s	WBPU2(1.5)	WBPU2s	WBPU2	WBPU3(1.5)	WBPU3
Molar composition	IPDI	2	2.1	2	2.1	3.15	3.15
	PCL	0.6	0.6	0.5	0.5	0.6	0.5
	DMPA	0.4	0.4	0.5	0.5	0.4	0.5
	BD	1	1	1	1	2	2
HS (wt%)		32.6	33.4	37.3	38.1	43.4	48.3
$COOH_{tot}$ (wt%)		1.00	0.99	1.39	1.38	0.84	1.15
$DMPA_{tot}$ (wt%)		2.97	2.94	4.15	4.10	2.50	3.42
pH		8.09	7.87	7.79	8.20	8.18	8.57
Diameter (nm)		38.7 ± 0.7	39.7 ± 0.8	28.2 ± 0.8	32.3 ± 1.6	59.2 ± 0.9	52.3 ± 0.5
Polydispersity		0.13 ± 0.02	0.12 ± 0.03	0.26 ± 0.03	0.18 ± 0.11	0.15 ± 0.02	0.08 ± 0.05
$\bar{M}_w$ (g mol^{-1})		58231	71639	47608	86748	56001	67353
PI		3.04	2.80	2.71	3.04	2.96	3.22

3.3 WBPU varying molar composition

3.3.1 WBPU dispersions characterization

The interactions between acid groups and water provided dispersion stability due to the stabilization mechanism of the particles. The presence of ionic groups at particle interface reduces the particle size due to the increase of surface hydrophilicity. This fact, causes acid groups-water interactions and increases dispersion stability owing to the formation of electrical double layer between ionic constituents and their counterions, which migrate into water phase around particles [2–4]. The interference of electrical double layer of different particles results in particles repulsion, leading to the stabilization mechanism of the dispersion [2]. If the added carboxylic groups are not enough to maintain an electrostatic repulsive force between particles, those would form aggregates which would precipitate [3]. **Figure 3.2** shows an image of the synthesized WBPU dispersions. In this case, the carboxylic groups content (2.5 wt% the lowest value) of the synthesized WBPU was enough to support the electrostatic repulsive forces between particles remaining visually stable for over 6 months.
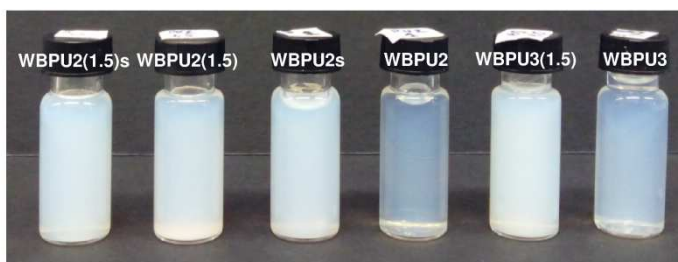

Figure 3.2 *Image of synthesized WBPU dispersions*

As observed in **Figure 3.2**, dispersions appearance varied with particle size. At lower particle sizes, that is, low IPDI/(PCL + DMPA) molar ratio, translucent dispersions were observed, whereas bigger particle sizes observed at higher IPDI/(PCL + DMPA) molar ratio, led to milky dispersions. In addition, for the same IPDI/(PCL + DMPA) ratio as DMPA content increased, slightly lighter dispersions were obtained, as consequence of the smaller particle sizes.

Regarding pH of dispersions showed in **Table 3.1**, indicated that carboxylic groups were successfully neutralized. This values were in the range of that found in the literature [5,6].

Otherwise, particle size distribution is a key parameter to evaluate WBPU dispersions stability. In general, large particle sizes (> 1 µm) result in unstable dispersions due to precipitation of the biggest particles. Instead, smaller particles results in more stable dispersions, which allow storage for months. Furthermore, the high surface energy owing to the small particle size of dispersion leads to a strong driving force for film formation [2]. When water is added to the system, polyurethane chains are arranged leading to nano-sized particles which adopt a core-shell structure. Generally, the segment containing ionic groups is located in the surface forming the shell while hydrophobic segment remains protected constituting the core within the nanoparticle [3,7] as it can be seen in **Figure 3.3**. Particle size distribution of synthesized WBPU dispersions and their average diameter measured by DLS varying the PCL/DMPA and IPDI/(PCL+DMPA) molar ratios and NCO/OH groups ratio, which differ in hard segment, acid groups and emulsifier content, are shown in **Table 3.1**.
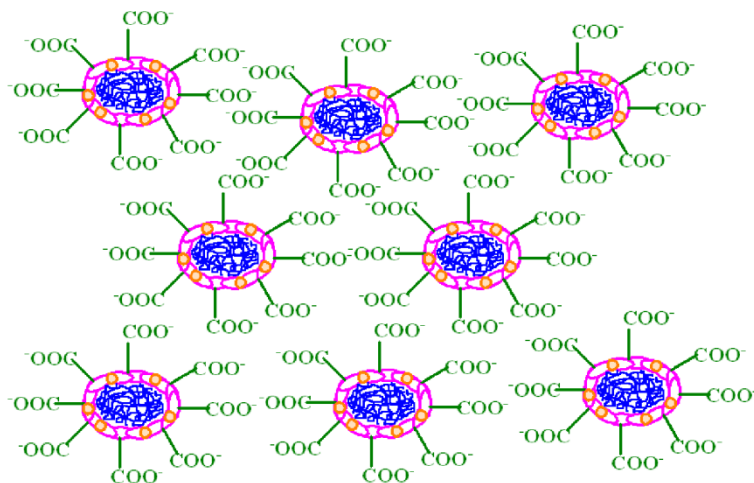
Figure 3.3 *Core–shell structure adopted by polyurethane chains in the dispersion*

As can be observed, narrow particle size distribution has been obtained in all synthesized WBPUs with a polydispersity between 0.08 and 0.26. The effect of IPDI content has been analyzed. As can be observed in **Table 3.1**, particle size increases as IPDI/(PCL + DMPA) molar ratio between 30 and 60 nm. The flexibility of chains adjacent to ionic groups influences in the mobility of ionic groups and therefore, in nanoparticles formation. Thus, at lower IPDI/(PCL + DMPA) molar ratio, that is, at higher polyol content, greater is the flexibility of polyurethane chains resulting in a better dispersion in the aqueous phase under agitation, obtaining smaller particles [4,5,7]. Moreover, the content of carboxylic groups decreases as IPDI/(PCL + DMPA) molar ratio increases. Attending to PCL/DMPA molar ratio, as DMPA content increases particle size decreases due to the higher amount of carboxylic groups. Thus, the hydrophilicity of polymer increases [3,8] and repulsion forces between particles are enhanced resulting in

lower particle size. For the same PCL/DMPA molar ratio, slightly bigger particles were obtained as the NCO/OH groups ratio was increased. For NCO/OH > 1, the residual NCO groups that remain after chain extension can react with water where unstable carbamic acid is obtained and decomposed to carbon dioxide and amino groups. These amino groups can react with other residual isocyanate groups resulting in urea linkages [2], as can be observed in **Figure 3.4**.
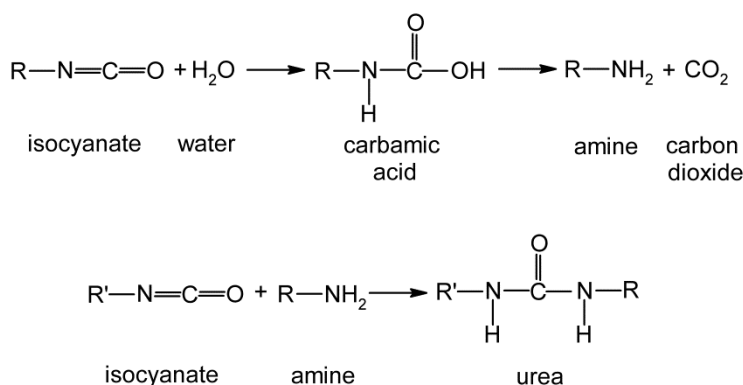

Figure 3.4 *Scheme of isocyanate water reaction*

The presence of urea linkages favors hydrogen bonding formation and restricts chains movements so, less hydrophilic groups are located in particles surface [9] which tend to aggregate longer polymer fragments.

3.3.2 Properties of WBPU films

3.3.2.1 Physicochemical properties

Weight average molecular weight and polydispersity index of WBPU films measured by GPC are shown in **Table 3.1**. The synthesis protocol followed in this work led to high molecular weights, even higher than reported in bibliography for similar systems [10]. As IPDI/(PCL + DMPA) molar ratio increased the M_w value decreased. It was attributed to the lower proportion of polyol which was the reagent with the highest molar mass [11]. In the same way, when stoichiometric molar ratio is used, molecular weight decreased as polyol content was decreased (comparing WBPU2s respect to WBPU2(1.5)s), leading to shorter chains [12]. However, when NCO/OH groups ratio 1.05 was employed, $\overline{M}_w$ increased with increasing DMPA content (comparison of WBPU2 and WBPU3 respect to, WBPU2(1.5) and WBPU3(1.5) respectively). This fact could be related with the conformation of polymer chain, which favors the reaction of residual NCO groups with water, resulting in longer chains.

Regarding to WBPU synthesis, in order to verify that reaction proceeded correctly, the structure of WBPU3 sample was determined by ^{1}H and ^{13}C NMR analysis.

Regarding to WBPU synthesis, the reaction was verified by ^{1}H and ^{13}C NMR spectroscopy. Thereby, in **Figure 3.5** the structure and ^{13}C NMR spectrum of WBPU3 sample are shown.
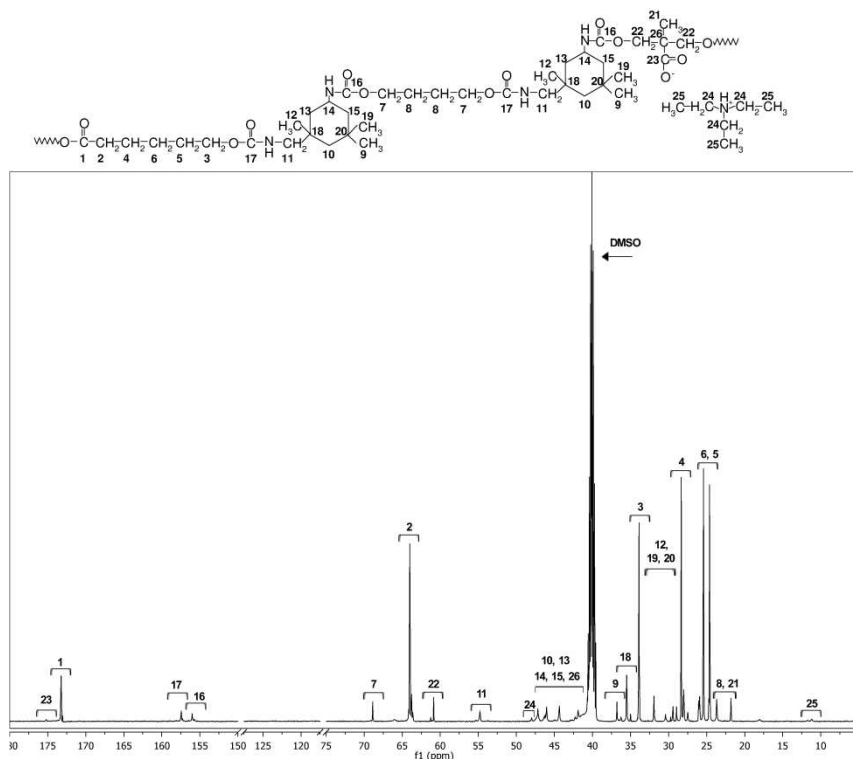
Figure 3.5 *¹³C NMR spectrum and structure of WBPU3*

According to ¹³C NMR results, the absence of NCO groups peaks around 123-121 ppm indicated that the synthesis reaction proceed completely [13,14] and the peaks around 156 and 157 ppm implied the formation of urethane groups [14,15]. The carbonyl (C=O) characteristic group of PCL soft segment was related with the peak at 173 ppm, whereas –OCH₂ and –CH₂OCO of PCL groups carbons were attributed to the peaks at 63-64 and 34 ppm respectively [16][16]. The rest of the PCL carbon groups were involved in the peaks between 30-40 ppm [16]. The peaks from 24 to 45 ppm were related with the methyl and skeleton of IPDI and DMPA carbons [14,15] and that about 55 ppm was assigned to the IPDI carbon linked to urethane groups [15]. Moreover, the peak at 47 ppm indicated the presence of ethylene carbons of the triethylammonium form

of TEA [15].

The polyurethane structure was also analyzed by ^{1}H NMR. **Figure 3.6** shows the spectrum and structure of WBPU3 polyurethane.
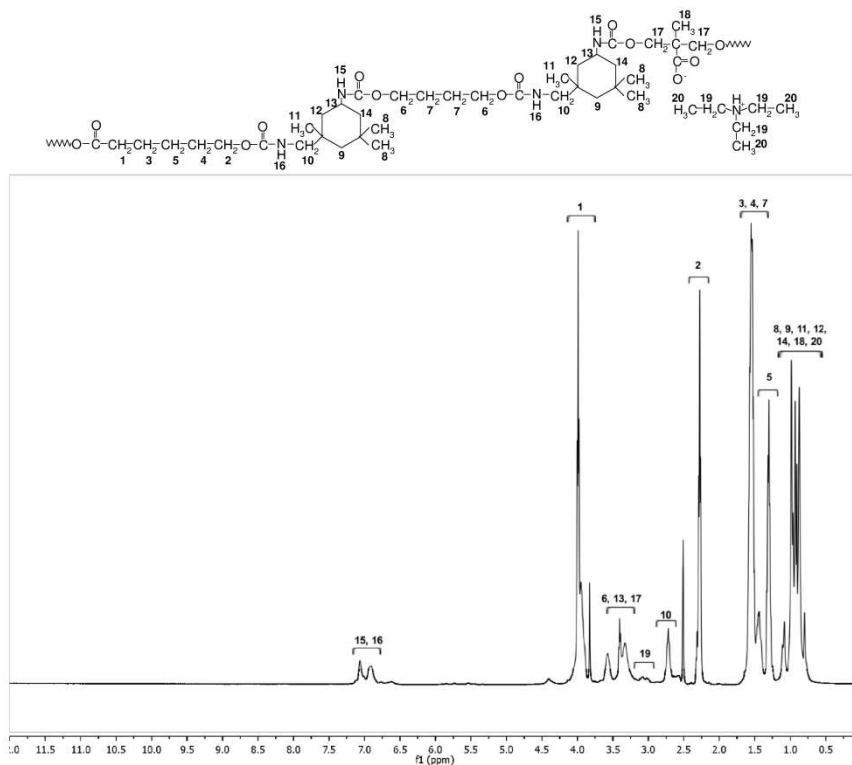
Figure 3.6 *^{1}H NMR spectrum and structure of WBPU3*

The different peaks were assigned to the corresponding characteristic protons of the polyurethane backbone. The peaks at 6.95 and 7 ppm confirmed the presence of urethane groups without the formation of allophanate NH groups, due to the absence of a peak at 7.52 ppm [14], which are generated by isocyanate side reactions during the synthesis. Considering SS, the peaks around 4, 2.3 and 1.55 and 1.3 ppm were related to PCL, –OCH$_2$, –CH$_2$OCO and methylene

groups' protons, respectively [17]. The peaks in the range between 0.8 and 1.6 ppm were assigned to methyl and ethylene protons in IPDI, DMPA and BD [14,15] backbone whereas around 2.4-3.8 ppm IPDI protons near to urethane groups were appreciated. Furthermore, TEA $-CH_2$ group protons attached to tertiary amine nitrogen were observed about 3 ppm.

Furthermore, WBPU functional groups structure and hydrogen bonding interactions were studied by FTIR. WBPU films, pure polyol and IPDI spectra are shown in **Figure 3.7**. Primarily, it was observed the absence of the stretching vibration bands at 2270 cm^{-1} and 3500 cm^{-1} referred to NCO and OH groups respectively, indicative that WBPU synthesis reaction proceeded completely [1]. In WBPU structures, different regions were differentiated. The band associated to N-H stretching vibration of urethane group at 3330 cm^{-1} [18,19] increased as IPDI/(PCL + DMPA) molar ratio was increased, due to the higher quantity of urethane linkages. Moreover, a new band related to C-N stretching and N-H bending of urethane functional group, in amide II region, was observed at 1527 cm^{-1} [20], which also increased in intensity as IPDI/(PCL + DMPA)molar ratio increased. In order to study the influence of reagents molar ratio in the formation of urethane carbonyl band and also hydrogen bonding, an amplification of the carbonyl stretching vibration in amine I region is included in **Figure 3.7b**. C=O group stretching vibration band appears at different wavenumber if the C=O group belongs to polyol or urethane functional groups [21]. Moreover, carbonyl group shifts to different wavenumbers if it is free or hydrogen bonded [18,19,22]. The stretching vibration bands of free and hydrogen bonded urethane C=O groups appear around 1733 and 1700–1690 cm^{-1}, respectively [18,19]. In the polyol spectrum a peak at 1720 cm^{-1} related to ester C=O group was observed, which was also observed in WBPU films.
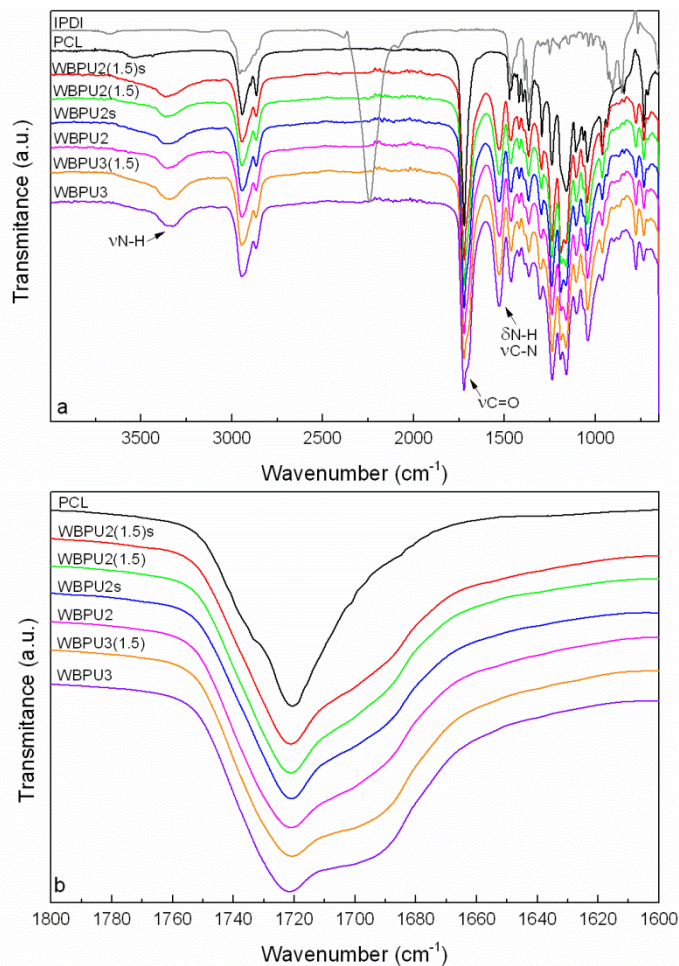
Figure 3.7 *a) FTIR spectra of PCL and WBPU films and b) amplification of carbonyl spectral region*

In addition, at 1700–1690 cm^{-1}, a shoulder corresponding to hydrogen bonded urethane carbonyl groups was observed in WBPU. As IPDI/(PCL + DMPA) molar ratio increased, the intensity of hydrogen bonded urethane carbonyl peak increased due to higher urethane groups density. Furthermore, in cases when excess of isocyanate was employed and considering the absence of the stretching band at 2270 cm^{-1}, it could be ensured that residual isocyanate groups reacted with water molecules leading to urea linkages. Nevertheless, the low isocyanate

excess implied that it was not observed significant variation in WBPU spectra in relation to the formation of urea groups.

3.3.2.2 Thermal properties

The thermal behavior of WBPU films was analyzed by differential scanning calorimetry and their thermograms are shown in **Figure 3.8**. To a better interpretation of WBPU thermal behavior, pure polyol and neat IPDI–BD block thermograms were also included in the inset of **Figure 3.8**.
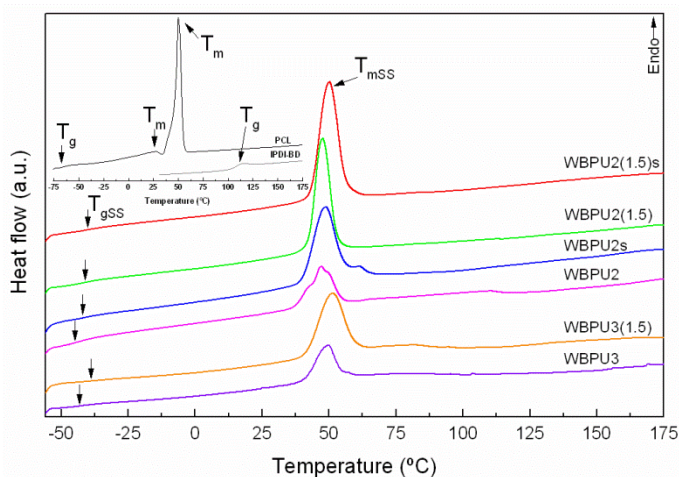
Figure 3.8 *DSC thermograms of WBPU films and PCL and IPDI-BD block in the inset*

Soft segment glass transition temperature (T_{gSS}) and soft segment melting temperature (T_{mSS}) and enthalpy (ΔH_{mSS}) values, determined from the thermograms are summarized in **Table 3.2**.

PCL shows a glass transition temperature at –65.4 °C and two melting peaks at 27.5 and 49.8 °C with an enthalpy of 2.7 and 83.5 J g^{-1} respectively. IPDI–BD neat block showed a T_g at 108.5 °C. Highly ordered hard segments arrangement

was hindered by the asymmetrical IPDI structure, no presenting melting peaks [23] like in blocks based on HDI or MDI [1,24].

Table 3.2 *Thermal properties of WBPU films*

Sample	T_{gss} (°C)	T_{mss} (°C)	ΔH_{mss} (J g^{-1})
WBPU2(1.5)$_s$	-40.7	50.2	30.6
WBPU2(1.5)	-41.0	47.7	24.3
WBPU2$_s$	-41.7	48.7	24.9
WBPU2	-44.4	47.0	12.1
WBPU3(1.5)	-38.0	51.4	21.4
WBPU3	-42.7	49.5	10.8

Regarding WBPU, as IPDI/(PCL + DMPA) molar ratio increases soft domain melting enthalpy decreases. It may be due to an inhibition in the growth of large, well-ordered soft segment crystallites in addition to the lower soft segment content. Besides, it can be observed an increment of 2–3 °C in soft domain glass transition temperature which could be related with restrictions in chain mobility and phase mixing increase. Thermal properties are also affected by ionic groups content. For the same IPDI/(PCL + DMPA) molar ratio, as DMPA content increases, a decrease of T_{gss} was observed which could be due to a better phase separation between hard and soft segments. The increase of ionic groups content provides major hydrogen bonds or columbic forces interactions between hard segment where DMPA molecules are located. Hence, hard segment chains tend to group instead of dissolving in soft domains. In addition, the steric hindrance of DMPA methyl groups restricts PCL crystallization

ability, enabling the formation of amorphous soft domains [25], being reduced the melting enthalpy to the half. The effect of NCO/OH groups ratio was also analyzed. As NCO/OH groups ratio increased, the formation of urea groups by the reaction of excess of NCO groups with water enhanced interactions between hard segment resulting in lower T_{gss} values [26] and ΔH_{mss}, indicating that PCL chains tended to settle in amorphous domains rather than arranged in crystalline domains.

3.3.2.3 Mechanical properties

The mechanical properties of WBPU are directly related to hard segment amount [1] although other parameters such as DMPA content [27] or NCO/OH groups ratio [8,9] should also be taken into account. Moreover, the structure adopted by chains is important in order to determine the morphology, thermal and mechanical behavior of WBPU films [28]. Generally, while hard segments improve mechanical resistance, soft segments confer elastomeric properties [1]. The mechanical properties of WBPU films were determined by tensile tests at room temperature and stress-strain curves are shown in **Figure 3.9**. Furthermore, yield stress, stress at break, tensile modulus and strain at break values of WBPU films obtained from the stress-strain curves are summarized in **Table 3.3**.

As IPDI/(PCL + DMPA) molar ratio increased, yield stress, stress at break and modulus increased, even double and triple comparing WBPU2 and WBPU3 samples, whereas strain at break of films decreased, which can be attributed to the increase of hydrogen bonds interactions between chains [29] owed to higher urethane groups density [1]. Nonetheless, in cases where high HS values were reached (even about 50 wt%), high deformability was maintained.
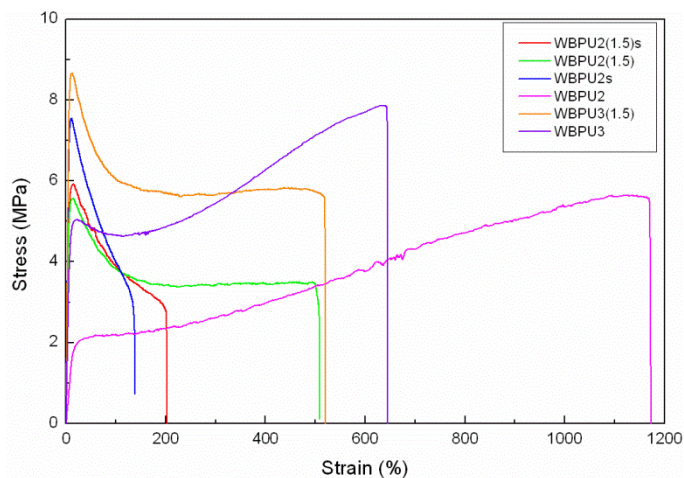
Figure 3.9 *Stress–strain curves of WBPU films*

Table 3.3 *Mechanical properties of WBPU films*

Sample	σ_y (MPa)	σ_b (MPa)	E (MPa)	ε_b (%)
WBPU2(1.5)s	5.8 ± 0.3	3.0 ± 0.2	106.0 ± 6.6	208 ± 40
WBPU2(1.5)	5.7 ± 0.3	3.6 ± 0.2	87.8 ± 2.0	497 ± 68
WBPU2s	7.3 ± 0.3	3.7 ± 0.5	126.9 ± 6.5	131 ± 42
WBPU2	2.3 ± 0.1	5.5 ± 0.2	13.1 ± 2.0	1197 ± 41
WBPU3(1.5)	8.8 ± 0.6	5.6 ± 0.2	147.5 ± 18.0	492 ± 34
WBPU3	4.6 ± 0.3	7.9 ± 0.4	54.8 ± 5.7	735 ± 102

Analyzing NCO/OH groups ratio, it was observed a reduction in yield stress and modulus values, as well as an increase in strain at break as the NCO/OH groups ratio was increased. Instead, according to bibliography [8,23], as NCO/OH groups ratio is enhanced an increase in yield stress and modulus and a decrease in strain at break should be expected due to the formation of additional urea groups which contribute to hydrogen bonding. This fact indicated the greater

influence of soft and hard domains arrangement rather than NCO/OH groups ratio influence in mechanical properties of WBPU films. The effect of DMPA content was also analyzed for a fixed NCO/OH groups ratio. For NCO/OH stoichiometric ratio, as DMPA content increased yield stress, stress at break and modulus increased while strain at break decreased, related with the enhancement of interchain coulombic forces or hydrogen bonding interactions between acid groups and urethane linkages due to the increase of ionic centers [30]. Instead when excess of NCO was employed, the increase of DMPA content led to lower yield stress and modulus values, whereas strain at break improved considerably from about 490 to 1197 and 735 % in WBPU2 and WBPU3 respectively, probably due to the lower soft segment crystallinity as observed by DSC results. Furthermore, amorphous soft domains were able to align in the stress applied direction leading to strain induced crystallization [31]. Thus, WBPU2 and WBPU3 samples showed higher stress at break than WBPU2(1.5) and WBPU3(1.5), respectively.

Soft segment chains rearrangement in mechanically tested WBPU2 sample was analyzed by means of DSC and the thermograms are shown in **Figure 3.10**.
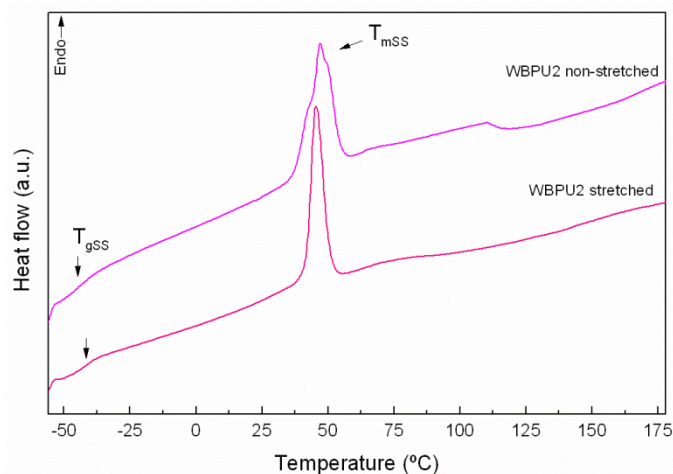
Figure 3.10 *DSC thermograms of WBPU2 sample before and after being stretched by tensile tests*

Comparing to non-stretched sample, an increase of T_{gSS} (from -44.4 to -41.7 °C) and a decrease in soft domains heat capacity (ΔC_{pSS}) (from 0.15 to 0.10 J g^{-1}K^{-1}) were observed due to soft segment rearrangement which hindered amorphous chains mobility. In addition, a narrower soft domain melting peak was observed indicating that more uniform crystals were formed. During the stretching test, the existing crystals can be disrupted and arranged giving new crystals so, ΔH_{mSS} varied (from 12.1 to 11.4 J g^{-1}).

3.3.2.4 Morphology

The structure and morphology adopted by soft crystalline domains at nanoscale were analyzed by AFM. **Figure 3.11** shows phase images of the cross section of WBPU cut films.
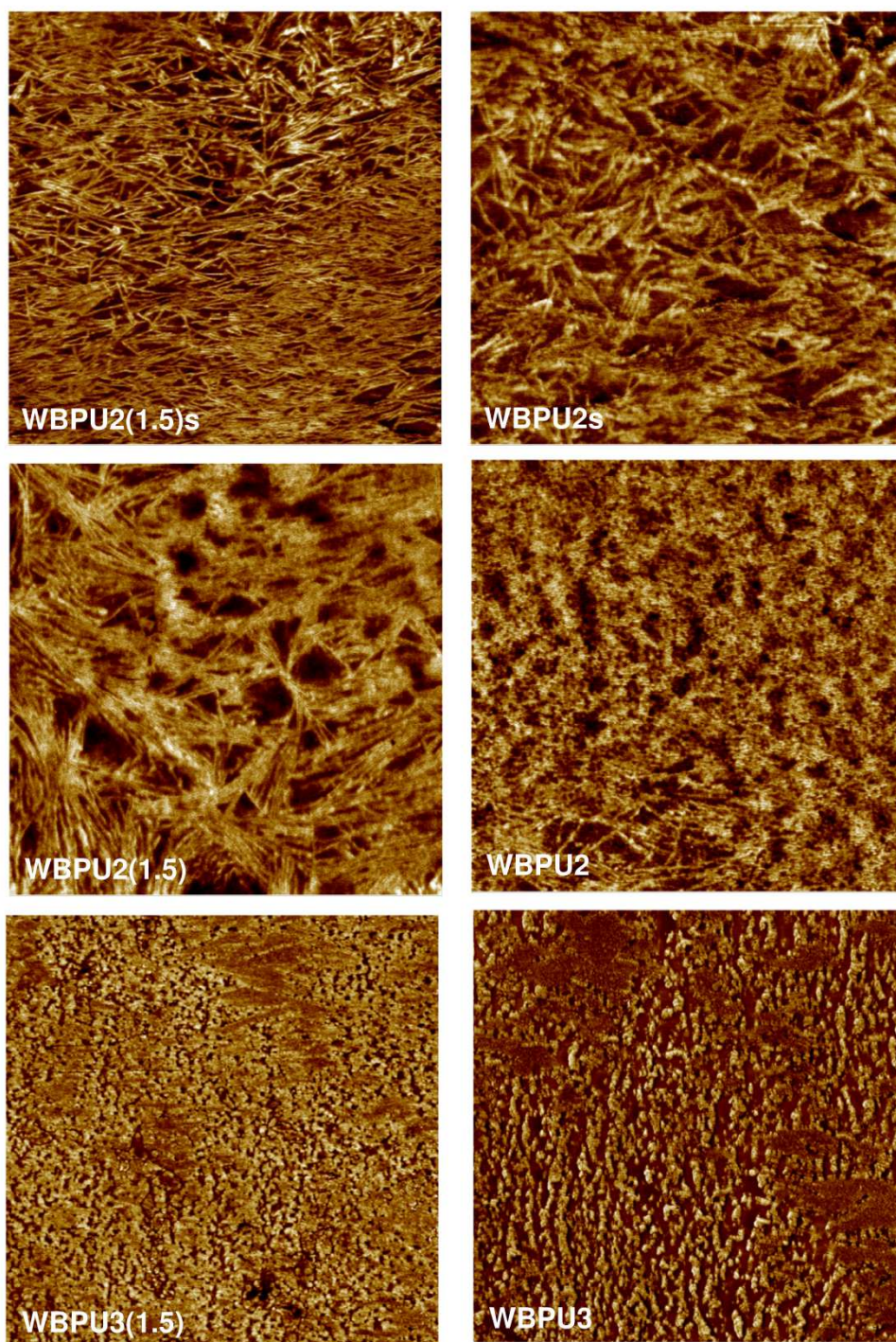
Figure 3.11 *AFM phase images of WBPU cut films (size: 3x3 µm²)*

Bright and dark regions were observed which were mainly related with the crystalline and amorphous domains, respectively. At low IPDI/(PCL + DMPA) molar ratios, soft segment was able to crystallize adopting a rod-like structure (WBPU2(1.5)s, WBPU2s, WBPU2(1.5) and WBPU2). Furthermore, as PCL/DMPA molar ratio increased, as observed by DSC results, soft segment chains showed a greater capacity of crystallize leading to longer and well defined rod-like structures. However, at higher IPDI/(PCL + DMPA) molar ratios, smaller crystallites were randomly dispersed in a continuous amorphous domain (WBPU3(1.5) and WBPU3). Regarding NCO/OH groups ratio, the increase of NCO/OH ratio led to larger dark domains and less defined crystals were observed, in agreement with the lower T_{gss} and melting temperature and enthalpy values determined by DSC results.

3.3.2.5 Hydrophilicity

Static water contact angle and water absorption measurements were carried out in order to analyze the wettability or hydrophilic–hydrophobic properties of polyurethane films. Regarding water contact angles, it is accepted that a surface is hydrophilic if the contact angle value is less than 90° [32]. Water contact angle values of WBPU films are shown in **Table 3.4**.

It was observed a decrease in contact angle values as the IPDI/(PCL + DMPA) molar ratio increased, due to increase of HS content and so, urethane polar groups, which induces to a more hydrophilic surface. Generally, the increase in DMPA content tends to decrease contact angle values [27] due to carboxylic groups polarity. At higher IPDI/(PCL + DMPA) molar ratio, the behavior is accomplished from 76.7 to 65.0°, but at lower ratios similar contact angle values around 79° were obtained. Analyzing NCO/OH groups ratio, it was observed

that NCO/OH ratio increase led to a decrease in water contact angles, attributable to the more polar surface of WBPU films owing to the formation of urea groups by the reaction between excess of NCO groups and water.

Table 3.4 *Water contact angle values of WBPU films*

Sample	Angle (°)
WBPU2(1.5)s	82.6 ± 3.2
WBPU2(1.5)	78.3 ± 3.6
WBPU2s	81.8 ± 5.5
WBPU2	79.6 ± 3.1
WBPU3(1.5)	76.7 ± 3.7
WBPU3	65.0 ± 2.5

Regarding water absorption measurements, it is an important parameter of polymeric films since it could limit the use, storing or type of application [23]. The water absorption may be attributed to the localized polarity, number of ionic groups at the surface and sample crystallinity. **Figure 3.12** shows the water absorption percentage of WBPU films as function of time at 25 °C.

The water absorption rate increased as PCL/DMPA molar ratio decreased due to higher amount of carboxylic hydrophilic groups [30,33] and also to their lower crystallinity, which could favor water uptake as a result of a better water molecules diffusion process.
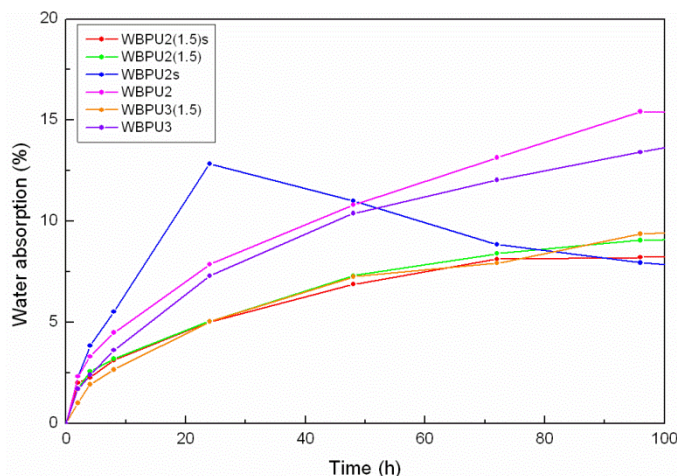
Figure 3.12 *Water absorption percentages of WBPU films over time*

Instead, IPDI/(PCL+DMPA) molar ratio as well as NCO/OH groups ratio did not present a strong influence in the water absorption behavior of WBPU films, except for WBPU2s where a considerable increase in water absorption values was observed which would be related with highest DMPA percentage and the lowest molecular weight of the sample comparing with other WBPU films [34].

3.3.3 Conclusions

Different visually stable WBPU dispersions with small particle sizes and narrow distribution were synthesized varying the molar ratio of IPDI, PCL, DMPA and BD. The synthesized dispersions were used for the preparation of casted films that were characterized by several experimental techniques. For the study, IPDI/(PCL+DMPA) and PCL/DMPA molar ratios and NCO/OH groups ratio were varied. Results revealed that the increase of IPDI/(PCL+DMPA) molar ratio led to stiffer films. Furthermore, it is worth noting that DMPA content increase resulted in lower ΔH_{mss} values, promoting strain induced crystallization behavior in cases when NCO/OH groups ratio of 1.05 was employed. In general,

it was observed that relatively small variations in WBPU molar composition led to remarkable variations in the final properties, broadening the range of applicability.

3.4 Effect of annealing at room temperature of WBPU films

Considering other reported works [10,35–37], PCL is able to evolve in more crystalline systems with time by the annealing at room temperature. In this way, in order to analyze the effect of PCL evolution in the polyurethane microphases, annealed WBPU films were studied from the viewpoint of physicochemical, thermal and mechanical properties after 5 months. Samples were coded preceded by "A" before the name of the corresponding non annealed samples.

3.4.1 Properties of WBPU films

3.4.1.1 Physicochemical properties

The characteristic groups of WBPU after the annealing were analyzed by FTIR, and the spectra of films are shown in **Figure 3.13**.

Analyzing the spectra of A-WBPU films it was observed that the characteristic N-H stretching peak about 3290 cm^{-1} and the peak at 1527 cm^{-1} related to C-N stretching and N-H bending of urethane functional groups were similar to the films before the annealing, discerning the same tendencies as molar compositions were varied. In order to analyze the carbonyl spectral region, an amplification of the region is shown in **Figure 3.13b** and compared with the spectra of the films before the annealing.
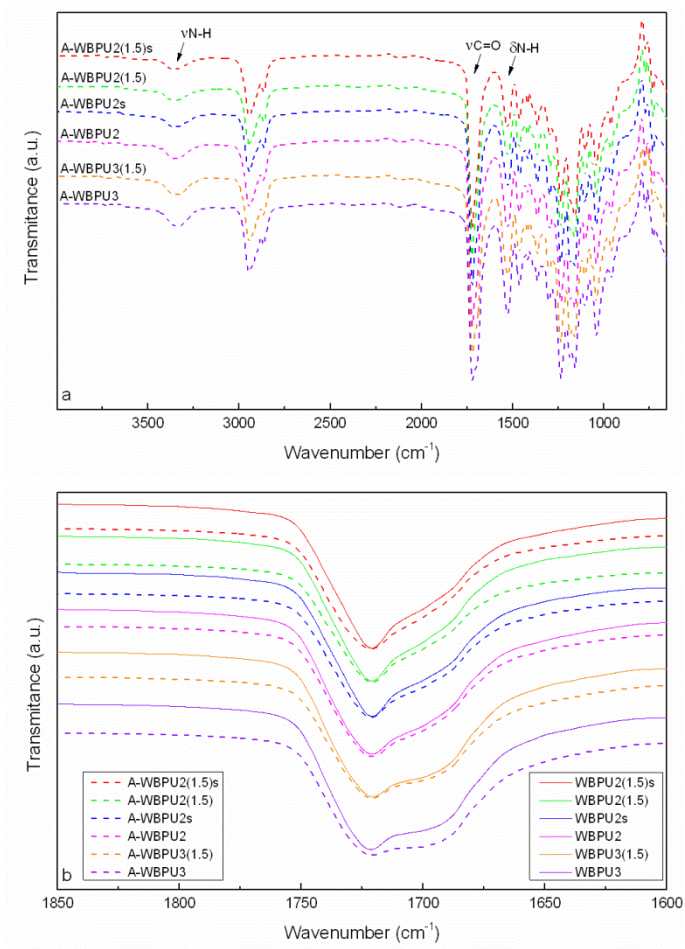
Figure 3.13 *a) FTIR spectra of A-WBPU films and b) amplification of carbonyl spectral region of WBPU films before (continuous line) and after the annealing (dashed line)*

It was observed that the annealing promoted the broadening of carbonyl peak, indicating the generation of hydrogen bonding interactions. This effect was more notable in A-WBPU3, the less crystalline sample before the annealing, which would favor a more pronounced crystallinity evolution.

3.4.1.2 Thermal properties

The thermal properties of WBPU films after the annealing at room temperature were analyzed and thermograms are shown in **Figure 3.14**. T_{gSS}, T_{mSS} and ΔH_{mSS} values of A-WBPU films obtained from the thermograms are shown in **Table 3.5**.
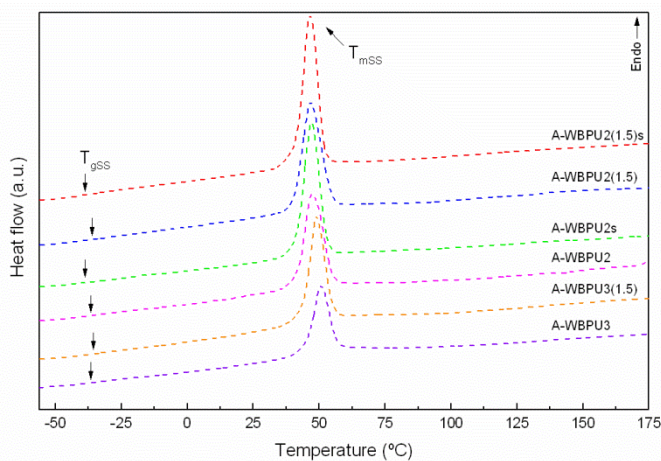

Figure 3.14 *DSC thermograms of A-WBPU films*

Table 3.5 *Thermal properties of A-WBPU films*

Sample	T_{gSS} (°C)	T_{mSS} (°C)	ΔH_{mSS} (J g^{-1})	$\Delta_{\Delta H_{mSS}}$ (%)
A-WBPU2(1.5)s	-38.4	46.5	40.1	31.0
A-WBPU2(1.5)	-36.0	47.2	36.8	51.4
A-WBPU2s	-38.7	46.6	34.7	39.6
A-WBPU2	-36.7	47.2	31.2	157.9
A-WBPU3(1.5)	-35.7	48.9	29.7	38.8
A-WBPU3	-36.7	50.7	20.1	86.1

Furthermore, the increase of melting enthalpy value after the annealing ($\Delta_{\Delta H_{mSS}}$) respect to the initial melting enthalpy value of each WBPU sample, due to the crystallinity increase was calculated by **Equation 3.1**:

$$\Delta_{\Delta H_{mSS}} = \frac{\Delta H_{mSS}(annealed) - \Delta H_{mSS}(non-annealed)}{\Delta H_{mSS}(non-annealed)} \cdot 100 \quad (\mathbf{3.1})$$

Comparing the results of A-WBPU films with their respective non-annealed WBPU, in general an increase in T_{gSS} values was observed due to the restriction of soft segment amorphous chains mobility induced by the increase in crystallinity. Increasing IPDI/(PCL+DMPA) molar ratio, lower crystallinity increase was observed attributable to the lower amount of PCL and higher hard segment content, which would hinder soft domains arrangement in ordered domains. Both, DMPA content as well as NCO/OH groups ratio increase led to lower ΔH_{mSS} values in the same way as in the non-annealed WBPU films. However, the increase of crystallinity was enhanced, leading to higher $\Delta_{\Delta H_{mSS}}$ values. This fact is related with the initial ΔH_{mSS} values, where in more crystalline WBPU samples the crystallization induced by annealing was more limited. In general, a decrease in T_{mSS} values was observed comparing with the respective non-annealed WBPU films, except for A-WBPU2 and A-WBPU3, where a slight increase was appreciated. Their lower ΔH_{mSS} values just after film formation implied higher mobility of soft segment amorphous domains, presenting a greater ability of soft segment rearrangement over time, showing the highest increase of ΔH_{mSS} after annealing.

3.4.1.3 Mechanical properties

The evolution of the crystalllinity had influence in the mechanical properties of WBPU samples over time. In **Figure 3.15** stress-strain curves of A-WBPU samples are shown and yield stress, stress at break, tensile modulus and strain at break values obtained from stress-strain curves are summarized in **Table 3.6**.
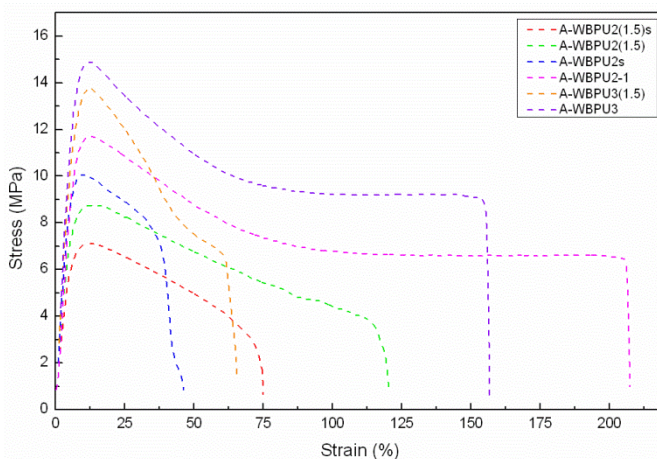

Figure 3.15 *Stress-strain curves of A-WBPU films*

Comparing the mechanical properties with the results of WBPU samples after film formation, all A-WBPU samples showed an increase in σ_y, σ_b and E values as well as a decrease in ε_b values due to the increase of crystallinity after the annealing. However, different properties evolution was observed depending on the reagents molar ratio. While the effect of composition in samples with stoichiometric NCO/OH ratio was the same as observed for non-annealed samples, in A-WBPU films with NCO/OH of 1.05 some variations were observed.

Table 3.6 *Mechanical properties of A-WBPU films*

Sample	σ_y (MPa)	σ_b (MPa)	E (MPa)	ε_b (%)
A-WBPU2(1.5)s	7.1 ± 0.2	5.5 ± 0.3	140.0 ± 7.5	46 ± 5
A-WBPU2(1.5)	8.9 ± 0.1	4.6 ± 0.6	167.1 ± 6.2	98 ± 26
A-WBPU2s	10.1 ± 0.2	10.1 ± 0.2	200.6 ± 2.0	10 ± 1
A-WBPU2	11.5 ± 0.5	6.3 ± 0.4	174.1 ± 17.1	210 ± 34
A-WBPU3(1.5)	13.5 ± 0.7	9.7 ± 1.2	229.3 ± 3.7	36 ± 5
A-WBPU3	14.2 ± 1.6	9.1 ± 1.1	212.2 ± 14.0	131 ± 41

The most significant change was observed in A-WBPU2 and A-WBPU3, considering that those samples led to a higher increase of ΔH_{mSS}, resulting in a greater increase in E and σ_y and lower ε_b values. Furthermore, the greater increase of crystallinity, hindered the capacity of amorphous soft segments to align in the stress applied direction, losing strain induced crystallization ability.

3.4.1.4 Thermomechanical properties

The thermomechanical properties of WBPU samples were studied by DMA, and curves are shown in **Figure 3.16**.

At low temperatures, a drop in E' curves was observed and reflected as a peak in Tanδ curves, which were associated to the T_{gSS} values of the A-WBPU films. Similar T_{gSS} values about -25 °C were obtained in all A-WBPU samples.
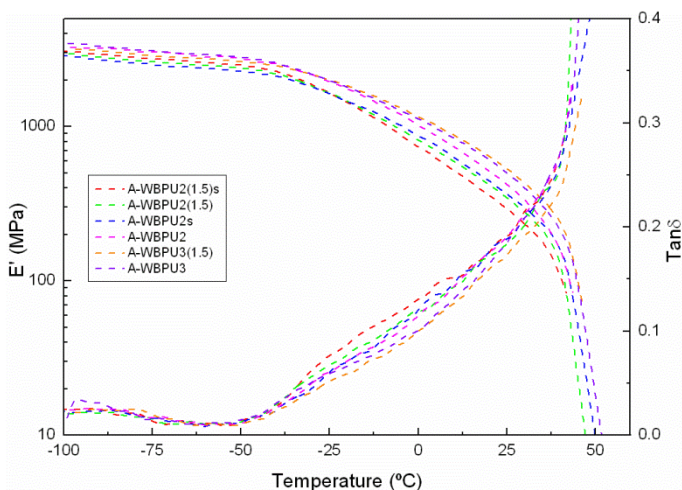
Figure 3.16 *Storage modulus and Tanδ curves of A-WBPU films*

At higher temperature, a sharp E' decrease was observed, related with the disruption of soft segment crystalline domains. Then, as IPDI hard segment did not show melting transition [30], the films started to flow. Besides the elevated E' values of A-WBPU3(1.5) and A-WBPU3 due to their higher IPDI/(PCL + DMPA) molar ratio, A-WBPU2 showed high E' values influenced by the evolution of the crystallization during the annealing process.

3.4.2 Conclusions

The effect of annealingWBPU films at room temperature for 5 months was analyzed in order to study the evolution of crystallinity with time. It was observed that soft segment evolved to more crystalline domains being more notable in the samples with initially lower ΔH_{mSS} values, favoring higher σ_y and E values and lower ε_b percentages. Therefore, with the global perception of films properties, both annealed and not, WBPU3 system was chosen for further analysis. For simplicity, hereafter, the sample will be denoted as WBPU.

3.5 Modulating the microstructure of WBPU varying the NCO/OH groups ratio

Based on WBPU3 molar composition new WBPU were synthesized increasing NCO/OH groups ratio to 1.2 and 1.4, following the same synthesis and film formation protocol. In this way, the already studied WBPU with a NCO/OH groups ratio of 1.05 was compared with the WBPU shown in **Table 3.7**. For simplification, samples will be coded as WBPU$_x$, where x denotes the NCO/OH groups ratio (1.2 or 1.4).

Table 3.7 *Molar composition and NCO/OH groups ratio, hard segment, total acid groups, and total emulsifier contents and particle size diameters and polydispersity of WBPU samples*

Sample			WBPU	WBPU$_{1.2}$	WBPU$_{1.4}$
Molar composition		IPDI	3.15	3.6	4.2
		PCL	0.5	0.5	0.5
		DMPA	0.5	0.5	0.5
		BD	2	2	2
NCO/OH groups ratio			1.05	1.2	1.4
HS (wt%)			48.3	50.8	53.8
DMPA$_{tot}$ (wt%)			3.42	3.26	3.06
Diameter (nm)			52.3 ± 0.5	46.8 ± 0.2	73.3 ± 0.1
Polydispersity			0.08 ± 0.05	0.09 ± 0.01	0.02 ± 0.01

3.5.1 Characterization of dispersions

The appearance of WBPU dispersions synthesized based on WBPU and varying NCO/OH groups ratio are shown in **Figure 3.17**.
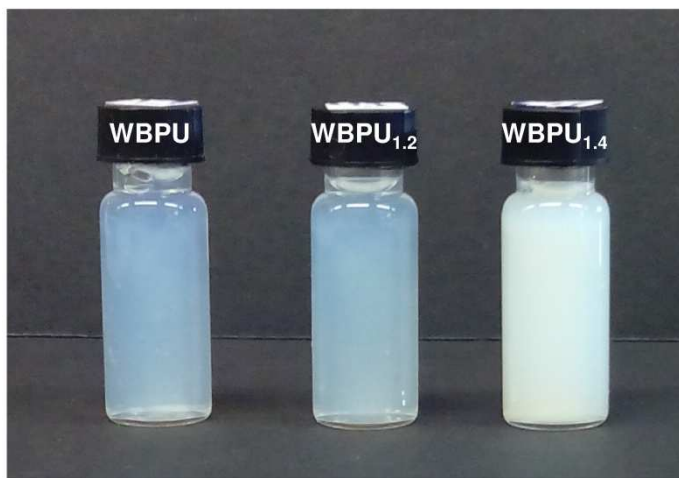
Figure 3.17 *Image of synthesized WBPU dispersions*

The small particle sizes and narrow distribution of WBPU$_{1.2}$ and WBPU$_{1.4}$ (**Table 3.7**) favored the stability of dispersions, resulting visually stable over 6 months, in accordance with the previously analyzed WBPU. Analyzing the effect of NCO/OH groups ratios it was observed that WBPU and WBPU$_{1.2}$ resulted in translucent dispersions according to their lower particle size, being slightly lighter in the case of WBPU$_{1.2}$ due to the lower particle size. Instead, WBPU$_{1.4}$ dispersion presented milky appearance in relation with the higher particle sizes obtained in the synthesis process.

Particle size and polydispersity of WBPU dispersions, where the NCO/OH groups ratio was varied, analyzed by DLS are summarized in **Table 3.7**. WBPU and WBPU$_{1.2}$ showed similar particle size, however higher values were measured for WBPU$_{1.4}$. In this case, the particles formation was greatly affected by the higher NCO residual free groups which reacted with water during the water addition step, resulting in urea groups and leading to bigger particles [38].

The morphology of the dispersions was also analyzed. AFM images were obtained from films of WBPU dispersions obtained by *spin-coating*. AFM phase images are shown in **Figure 3.18**.

It was observed that nanoparticles conformation was more discernible in the images where NCO/OH molar ratio was higher. In WBPU and WBPU$_{1.2}$, cohesion between nanoparticles was observed, whereas in case of WBPU$_{1.4}$, nanoparticles remained isolated without forming a continuous phase.
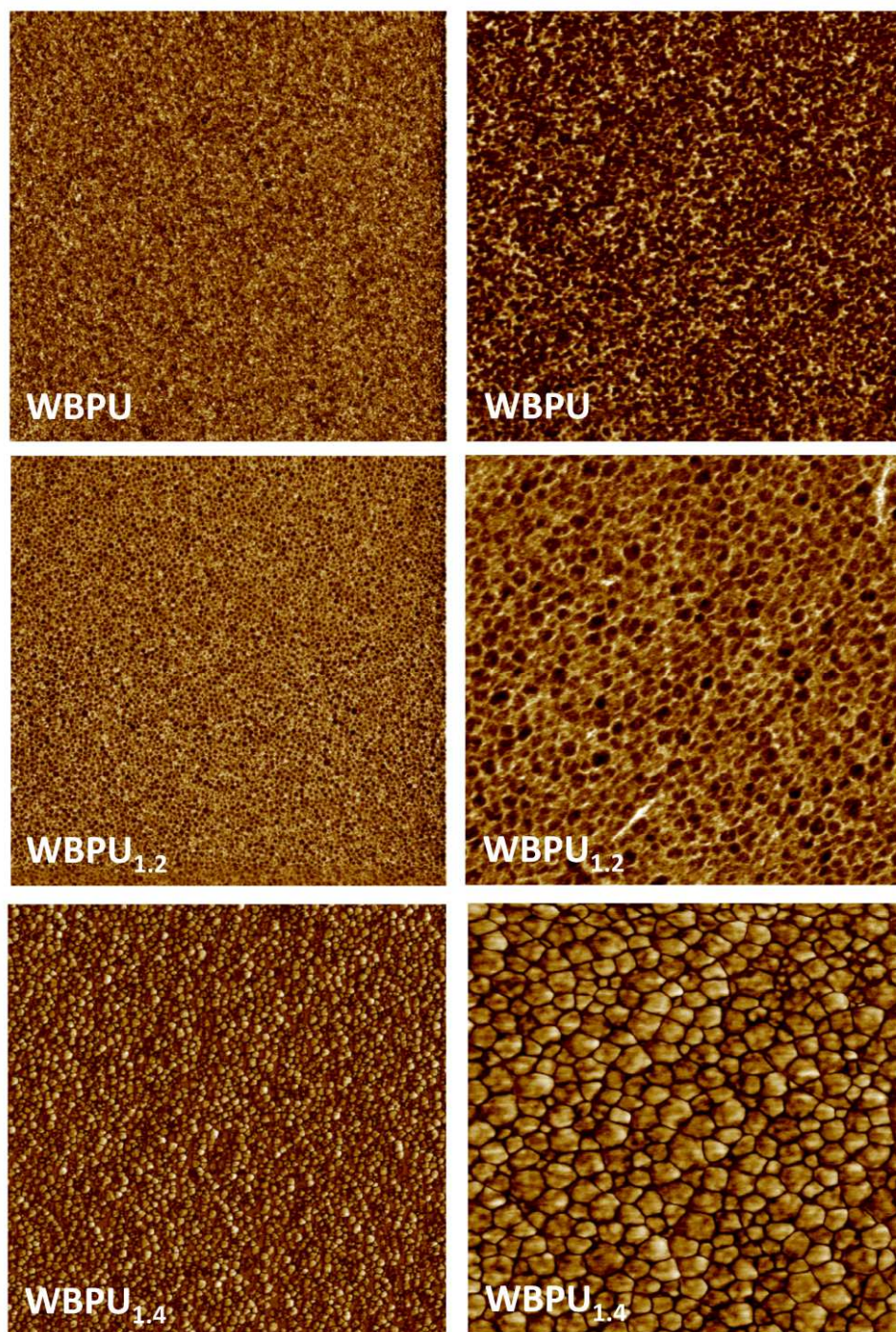
Figure 3.18 *AFM phase images of WBPU samples (size: 3x3 µm² (left) and 1x1 µm² (right))*

3.5.2 Properties of WBPU films

3.5.2.1 Appearance and solubility of WBPU films

Films prepared by casting are shown in **Figure 3.19**.

Figure 3.19 *WBPU films varying NCO/OH groups ratio prepared by casting*

In the case of WBPU and WBPU$_{1.2}$, homogeneous transparent films were observed, while in WBPU$_{1.4}$ it was not possible to obtain a continuous film. In this case, the morphology observed by AFM where isolated nanoparticles were viewed, corroborated the hindering for the formation of a continuous film. Hence, the study of WBPU with different NCO/OH groups ratio was more centered in the comparison of WBPU and WBPU$_{1.2}$ films properties, which were stored in a desiccator for 1 week previous their characterization.

Analyzing the solubility of films in THF it was observed that WBPU film resulted soluble in THF, whereas WBPU$_{1.2}$ was insoluble. This fact supported the greater generation of urea groups by the reaction of NCO free groups with water, which restricted the solubility of the material [39].

3.5.2.2 Physicochemical, thermal and mechanical properties

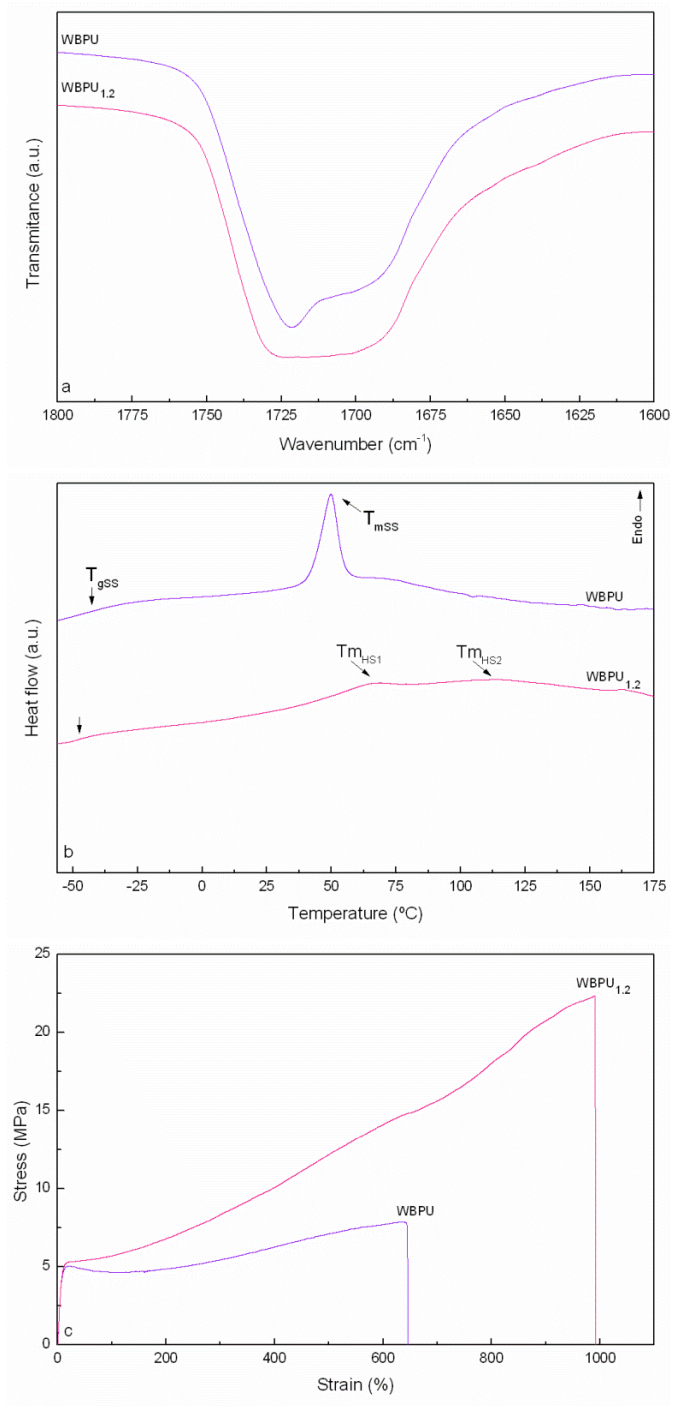FTIR spectra, DSC thermograms and stress-strain curves of WBPU and WBPU$_{1.2}$ are shown in **Figure 3.20**.

Figure 3.20 *a) FTIR spectra, b) DSC thermograms and c) stress-strain curves of WBPU films with different NCO/OH groups ratio*

FTIR spectra of WBPU and WBPU$_{1.2}$ were similar and only differences in amide I region were observed. With the purpose of analyzing the C=O groups interactions formed in the WBPU films varying NCO/OH groups ratio, an amplification of the carbonyl region between 1800 and 1600 cm^{-1} is shown in **Figure 3.20a**. In WBPU a peak about at 1722 and a shoulder about 1700-1690 cm^{-1} were observed related to the ester C=O of PCL and free C=O of urethane and hydrogen bonded C=O of urethane groups respectively, whereas in WBPU$_{1.2}$ the peak corresponding to the ester C=O of PCL and free C=O groups was appreciated around 1725 cm^{-1}, and the shoulder broaded comparing with WBPU, suggesting the greater amount of interactions and urea groups formation due to the reaction of residual NCO groups with water, being the effect higher as NCO/OH groups ratio was increased.

Regarding thermal properties, it was observed that soft and hard domains structure strongly depended on NCO/OH groups ratio. Thermal transitions are summarized in **Table 3.8**.

Table 3.8 *Thermal properties of WBPU films with different NCO/OH groups ratio*

Sample	T_{gSS} (°C)	T_{mSS} (°C)	ΔH_{mSS} (J g^{-1})	T_{mHS1} (°C)	ΔH_{mHS1} (J g^{-1})	T_{mHS2} (°C)	ΔH_{mHS2} (J g^{-1})
WBPU	-42.7	49.5	10.8	-	-	-	-
WBPU$_{1.2}$	-47.3	-	-	65.9	1.4	119.0	5.3

In the case of WBPU, a glass transition and an endothermic peak were observed, associated to the soft segment amorphous and ordered domains respectively. However, in WBPU$_{1.2}$, lower T_{gSS} value was observed and the melting enthalpy related with the ordered soft domains was not appreciable. Instead, the

transitions about 65 and 119 °C, related with the short and long range order of hard segment domains (T_{mHS1}) and (T_{mHS2}), respectively, were distinguished [40]. The increase of hard segment content by the presence of greater amount of isocyanate content, increased the possibility of free NCO groups reaction with water, leading to urea groups [41]. Thereby, hard to hard segment interactions were favored, which can act as physical crosslinks, and contribute to HS different ordering domains. By this way, SS ordering was hindered and SS chain mobility was facilitated, justified by the decreased in T_{gSS} value comparing with WBPU [23].

Concerning mechanical properties, yield stress, stress at break, tensile modulus and strain at break values obtained from stress-strain curves are summarized in **Table 3.9**.

Table 3.9 *Mechanical properties of WBPU films with different NCO/OH groups ratio*

Sample	σ_y (MPa)	σ_b (MPa)	E (MPa)	ε_b (%)
WBPU	4.6 ± 0.3	7.9 ± 0.4	54.8 ± 5.7	735 ± 102
WBPU$_{1.2}$	5.3 ± 0.2	23.1 ± 1.3	48.9 ± 9.5	995 ± 50

It was observed that WBPU showed higher E value comparing with WBPU$_{1.2}$ due to the ordered soft segment domains, which provides stiffness to the film. Instead, higher σ_y value was obtained in WBPU$_{1.2}$ attributable to the presence of higher hydrogen bonding interactions [29,42–44]. In addition, the effect of alignment under stress applied direction [31] of sample WBPU$_{1.2}$ was more discernible owing to the mobility of soft segment amorphous chains [45], thus observing considerably higher ε_b and σ_b values comparing with WBPU.

Furthermore, the physical crosslinks would also contribute to the increase of ε_b and σ_b.

3.5.2.3 Hydrophilicity

The hydrophilicity of WBPU films surface was measured by water contact angle and the water diffusion trough WBPU films was analyzed by water absorption measurements. Comparing water contact angle values, $65.0 \pm 2.5°$ was obtained in the case of WBPU and $88.2 \pm 1.4°$ was determined for WBPU$_{1.2}$. This fact could be attributed to the lower DMPA content and thus, lower COOH groups in WBPU$_{1.2}$ sample [27].

Water absorption measurements of WBPU and WBPU$_{1.2}$ over time are shown in **Figure 3.21**.
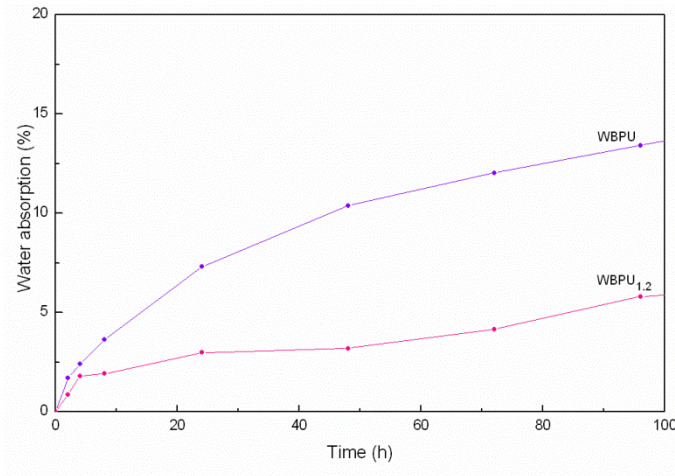
Figure 3.21 *Water absorption percentages of WBPU films with different NCO/OH groups ratio*

The water diffusion process through the film is governed by domains order [46]. Comparing WBPU and WBPU$_{1.2}$, the increase in NCO/OH groups ratio

decreased the water absorption ability of the films. The additional urea groups generated by the residual NCO and water molecules would increased the rigidity of the chains, avoiding to water molecules to diffuse through the film [23]. Furthermore, the stronger hydrogen bonding interactions of hard segments [47] leading to the more ordered hard segment domains in WBPU$_{1.2}$, hindered the water diffusion in a greater extent than the retarded provided by soft segment ordered domains in WBPU.

3.5.3 Conclusions

In this section, a more exhaustive study was carried out based on previously analyzed WBPU varying NCO/OH groups ratio in 1.05, 1.2 and 1.4. The morphology of the films formed from the dispersions were analyzed by AFM. Results revealed that only increasing NCO/OH groups ratio, WBPU dispersions resulted in very different morphologies. AFM phase images showed a lack of cohesiveness between nanoparticles synthesized at high NCO/OH groups ratio (1.4), which hindered the formation of a continuous film. Moreover, it was observed that just by varying NCO/OH ratio, the polyurethane microstructure can be tailored resulting in SS crystalline domains in the case of WBPU or SS amorphous domains with certain HS ordered structures in WBPU$_{1.2}$. It was observed that the mechanical properties as well as hydrophilicity of films was directly related with the microstructure of films. Thus WBPU$_{1.2}$ films showed a greater strain induced crystallization effect due to the mobility provided by soft segment amorphous chains. In contrast, water absorption ability of the film was difficulted by the ordered hard segment domains which hindered the diffusion of water molecules through WBPU$_{1.2}$ film.

Thereby, just by varying NCO/OH groups ratio, WBPU microstructure can be altered resulting in different order structures and presenting the opportunity of modulating the properties of the final material towards the desired application.

3.6 References

[1]   A. Saralegi, L. Rueda, B. Fernández-d'Arlas, I. Mondragon, A. Eceiza, M.A. Corcuera, Thermoplastic polyurethanes from renewable resources: Effect of soft segment chemical structure and molecular weight on morphology and final properties, Polym. Int. 62 (2013) 106–115.

[2]   B.K. Kim, Aqueous polyurethane dispersions, Colloid Polym. Sci. 274 (1996) 599–611.

[3]   J. Bullermann, S. Friebel, T. Salthammer, R. Spohnholz, Novel polyurethane dispersions based on renewable raw materials-Stability studies by variations of DMPA content and degree of neutralisation, Prog. Org. Coat. 76 (2013) 609–615.

[4]   S.K. Lee, B.K. Kim, High solid and high stability waterborne polyurethanes via ionic groups in soft segments and chain termini, J. Colloid Interface Sci. 336 (2009) 208–214.

[5]   V.D. Athawale, M.A. Kulkarni, Effect of dicarboxylic acids on the performance properties of polyurethane dispersions, J. Appl. Polym. Sci. 117 (2010) 572–580.

[6]   V. García-Pacios, Y. Iwata, M. Colera, J. Miguel Martín-Martínez, Influence of the solids content on the properties of waterborne polyurethane dispersions obtained with polycarbonate of hexanediol, Int. J. Adhes. Adhes. 31 (2011) 787–794.

[7]   K. Mequanint, R. Sanderson, Hydrolytic stability of nano-particle polyurethane dispersions: Implications to their long-term use, Eur. Polym. J. 42 (2006) 1145–1153.

[8]   M. Ramli, E.S.M. Negim, B. Saad, L. Bekbayeva, M.I. Saleh, Preparation and characterization of water dispersion polyurethane, World Appl. Sci. J. 12 (2011) 1145–11150.

[9]   C. Song, Q. Yuan, D. Wang, Effect of the content of urea groups on the particle size in water-borne polyurethane or polyurethane/polyacrylate dispersions, Colloid Polym. Sci. 282 (2004) 642–645.

[10]   J. Čulin, M. Andreis, I. Šmit, Z. Veksli, A. Anžlovar, M. Žigon, Motional heterogeneity and phase separation of functionalized polyester polyurethanes, Eur. Polym. J. 40 (2004) 1857–1866.

[11]   L. Tatai, T.G. Moore, R. Adhikari, F. Malherbe, R. Jayasekara, I. Griffiths, P.A. Gunatillake, Thermoplastic biodegradable polyurethanes: The effect of chain extender structure on properties and in-vitro degradation, Biomaterials 28 (2007) 5407–5417.

[12]   J.Y. Jang, Y.K. Jhon, I.W. Cheong, J.H. Kim, Effect of process variables on molecular weight and mechanical properties of water-based polyurethane dispersion, Colloid Surface A 196 (2002) 135–143.

[13]   C. Fu, Z. Zheng, Z. Yang, Y. Chen, L. Shen, A fully bio-based waterborne

polyurethane dispersion from vegetal oils: From synthesis of precursors by thiol-ene to study of final material, Prog. Org. Coat. 77 (2014) 53–60.

[14]   Q. Yong, F. Nian, B. Liao, L. Huang, L. Wang, H. Pang, Synthesis and characterization of solvent-free waterborne polyurethane dispersion with both sulfonic and carboxylic hydrophilic chain-extending agents for matt coating applications, RSC Adv. 5 (2015) 107413–107420.

[15]   H. Daemi, M. Barikani, M. Barmar, Compatible compositions base on aqueous polyurethane dispersions and sodium alginate, Carbohydr. Polym. 92 (2013) 490–496.

[16]   B. Rajkumar, T. Dhanalakshmi, B. Meenarathi, R. Anbarasan, Synthesis and characterization of novel fluorescent amphiphilic diblock copolymer, Polym. Bull. 73 (2016) 2147-2163.

[17]   X. Peng, Y. Zhang, Y. Chen, S. Li, B. He, Synthesis and crystallization of well-defined biodegradable miktoarm star PEG-PCL-PLLA copolymer, Mater. Lett. 171 (2016) 83–86.

[18]   L.H. Bao, Y.J. Lan, S.F. Zhang, Synthesis and properties of waterborne polyurethane dispersions with ions in the soft segments, J. Polym. Res. 13 (2006) 507–514.

[19]   X. Jiang, J. Li, M. Ding, H. Tan, Q. Ling, Y. Zhong, et al., Synthesis anddegradation of nontoxic biodegradable waterborne polyurethanes

elastomerwith poly (ε-caprolactone) and poly(ethylene glycol) as soft segment, Eur. Polym. J. 43 (2007) 1838–1846.

[20]   P. Król, B. Król, Surface free energy of polyurethane coatings with improved hydrophobicity, Colloid Polym. Sci. 290 (2012) 879–893.

[21]   Y.K. Jhon, I.W. Cheong, J.H. Kim, Chain extension study of aqueous polyurethane dispersions, Colloid Surface A 179 (2001) 71–78.

[22]   E. Princi, S. Vicini, K. Castro, D. Capitani, N. Proietti, L. Mannina, On themicro-phase separation in waterborne polyurethanes, Macromol. Chem. Phys. 210 (2009) 879–889.

[23]   K. Wang, Y. Peng, R. Tong, Y. Wang, Z. Wu, The effects of isocyanate index on the properties of aliphatic waterborne polyurethaneureas, J. Appl. Polym. Sci. 118 (2010) 920–927.

[24]   L. Ugarte, B. Fernández-d'Arlas, A. Valea, M.L. González, M.A. Corcuera, A. Eceiza, Morphology-properties relationship in high-renewable content polyurethanes, Polym. Eng. Sci. 54 (2014) 2282–2291.

[25]   S.M. Cakic, M. Spirkova, I.S. Ristic, J.K. B-Simendic, M. M-Cincovic, R. Poreba, The waterborne polyurethane dispersions based on polycarbonate diol: Effect of ionic content, Mater. Chem. Phys. 138 (2013) 277–285.

[26] M.S. Sánchez-Adsuar, E. Papon, J.J. Villenave, Influence of the prepolymerization on the properties of thermoplastic polyurethane elastomers. Part II. Relationship between the prepolymer and polyurethane properties, J. Appl. Polym. Sci. 76 (2000) 1602–1607.

[27] M. Barikani, M.V. Ebrahimi, S.M.S. Mohaghegh, Preparation and characterization of aqueous polyurethane dispersions containing ionic centers, J. Appl. Polym. Sci. 104 (2007) 3931–3937.

[28] D.K. Chattopadhyay, K.V.S.N. Raju, Structural engineering of polyurethane coatings for high performance applications, Prog. Polym. Sci. 32 (2007) 352–418.

[29] C.C. Santos, M.C. Delpech, F.M.B. Coutinho, Thermal and mechanical profile of cast films from waterborne polyurethanes based on polyether block copolymers, J. Mater. Sci. 44 (2009) 1317–1323.

[30] Y.S. Kwak, E.Y. Kim, B.H. Yoo, H. Do Kim, Preparation and properties of waterborne poly(urethane urea)s for adhesives: The effects of the 2,2-bis(hydroxylmethyl) propionic acid content on the properties, J. Appl. Polym. Sci. 94 (2004) 1743–1751.

[31] B. Fernández-d'Arlas, J.A. Ramos, A. Saralegi, M.A. Corcuera, I. Mondragon, A. Eceiza, Molecular engineering of elastic and strong supertough polyurethanes, Macromolecules 45 (2012) 3436–3443.

[32]   Y.C. Jung, B. Bhushan, Contact angle, adhesion and friction properties of micro-and nanopatterned polymers for superhydrophobicity, Nanotechnology 17 (2006) 4970–4980.

[33]   M.M. Rahman, H. Do Kim, Synthesis and characterization of waterborne polyurethane adhesives containing different amount of ionic groups (I), J. Appl. Polym. Sci. 102 (2006) 5684–5691.

[34]   Z. Wang, X. Zhang, L. Zhang, T. Tan, H. Fong, Nonisocyanate biobased poly(ester urethanes) with tunable properties synthesized via an environment-friendly route, ACS Sustain. Chem. Eng. 4 (2016) 2762–2770.

[35]   J. Čulin, I. Šmit, M. Andreis, Z. Veksli, A. Anžlovar, M. Žigon, Motional heterogeneity and phase separation of semi-interpenetrating networks and mixtures based on functionalised polyurethane and polymethacrylate prepolymers, Polymer 46 (2005) 89–99.

[36]   J. Čulin, I. Šmit, Z. Veksli, A. Anžlovar, M. Žigon, Phase morphology of functionalized polyester polyurethanes. Effect of functional group concentration, Polym. Int. 55 (2006) 285–291.

[37]   M.E.V. Hormaiztegui, V.L. Mucci, A. Santamaria-Echart, M.A. Corcuera, A. Eceiza, M.I. Aranguren, Waterborne polyurethane nanocomposites based on vegetable oil and microfibrillated cellulose, J. Appl. Polym. Sci. 133 (2016) 44207/1-44207-12.

[38]   E. Delebecq, J.P. Pascault, B. Boutevin, F. Ganachaud, On the versatility of urethane/urea bonds: Reversibility, blocked isocyanate, and non-isocyanate polyurethane, Chem. Rev. 113 (2013) 80–118.

[39]   I. Yilgör, E. Yilgör, G.L. Wilkes, Critical parameters in designing segmented polyurethanes and their effect on morphology and properties: A comprehensive review, Polymer 58 (2015) A1–A36.

[40]   C. Fang, X. Zhou, Q. Yu, S. Liu, D. Guo, R. Yu, S. Liu, D. Guo, R. Yu, J. Hu, Synthesis and characterization of low crystalline waterborne polyurethane for potential application in water-based ink binder, Prog. Org. Coat. 77 (2014) 61–71.

[41]   I. Poljansek, E. Fabjan, D. Moderc, D. Kukanja, The effect of free isocyanate content on properties of one component urethane adhesive, Int. J. Adhes. Adhes. 51 (2014) 87–94.

[42]   C.Y. Li, Y.H. Li, K.H. Hsieh, W.Y. Chiu, High-molecular-weight polyurethanes prepared by one-step miniemulsion polymerization, J. Appl. Polym. Sci. 107 (2008) 840–845.

[43]   Y.H. Guo, J.J. Guo, S.C. Li, X. Li, G.S. Wang, Z. Huang, Properties and paper sizing application of waterborne polyurethane emulsions synthesized with TDI and IPDI, Colloid Surface A 427 (2013) 53–61.

[44]   L. Lei, L. Zhong, X. Lin, Y. Li, Z. Xia, Synthesis and characterization of

waterborne polyurethane dispersions with different chain extenders for potential application in waterborne ink, Chem. Eng. J. 253 (2014) 518–525.

[45]   M.L. Auad, M.A. Mosiewicki, T. Richardson, M.I. Aranguren, N.E. Marcovich, Nanocomposites made from cellulose nanocrystals and tailored segmented polyurethanes, J. Appl. Polym. Sci. 115 (2010) 1215–1225.

[46]   L. Rueda, B. Fernandez d'Arlas, M.A. Corcuera, A. Eceiza, Biostability of polyurethanes. Study from the viewpoint of microphase separated structure, Polym. Degrad. Stab. 108 (2014) 195-200.

[47]   Y.H. Guo, J.J. Guo, H. Miao, L.J. Teng, Z. Huang, Properties and paper sizing application of waterborne polyurethane emulsions synthesized with isophorone diisocyanate, Prog. Org. Coat. 77 (2014) 988–996.

<div align="right">

CHAPTER 4

</div>

Synthesis of waterborne polyurethane-ureas

"Quando falas, só estás a repetir o que já sabes.

Mas se escutas, pode que aprendas algo novo"

4. SYNTHESIS OF WATERBORNE POLYURETHANE-UREAS

4.1 Objective

In this chapter, a systematic and comprehensive analysis of the synthesis process and its effect on the final properties of a waterborne polyurethane-urea system was carried out. In this way, besides the macrodiol, diisocyanate, internal emulsifier and diol chain extender reagents employed in the previous chapter for the preparation of polyurethane, in this chapter a diamine chain extender will be also used. Considering the few works studying the diamine chain extension step, this study was focused on the synthesis of different polyurethane-ureas, where diamine extension was carried out either by the classical heterogeneous reaction medium, or also by the alternative homogeneous medium, besides varying diamine chain extender content. The corresponding polyurethane, i.e. a dispersion without diamine chain extender was also synthesized in order to compare the influence of urethane or urethane and urea moieties in the polymer chain. Dispersions as well as films prepared from dispersions have been later extensively characterized by dynamic light scattering, atomic force microscopy, optical microscopy, Fourier transform infrared spectroscopy, differential scanning calorimetry, mechanical tests, dynamic mechanical analysis, static water contact angle, and water absorption measurements.

4.2 Experimental

4.2.1 Synthesis of waterborne polyurethane and polyurethane-urea dispersions and films preparation

For the synthesis of waterborne polyurethane-ureas the same PCL, IPDI, DMPA, and BD used for the synthesis of waterborne polyurethanes were selected. EDA was used as diamine chain extender. The molar composition of PCL, DMPA and BD was maintained equal to WBPU, 0.5:0.5:2 respectively, and EDA and IPDI were varied in order to synthesize WBPUU with different diamine contents. WBPUU dispersions were synthesized by a two-step polymerization process, varying EDA content from 0 to about 4.5 wt%. The reaction was carried out in a 500 mL four neck jacketed reactor with an intracooler as a temperature controller. The reactor was equipped with a mechanical stirrer and a thermocouple connected to a computer for monitoring and controlling the reaction conditions. The synthesis was performed under nitrogen atmosphere and the reaction progress was followed by the dibutylamine back titration method according to ASTM D 2572-97. PCL, 0.037 wt% of DBTDL catalyst and IPDI were charged in the reactor at 80 °C and allowed to react until the amount of residual NCO groups reached the theoretical value. Once the mixture was cooled to 50 °C, and in order to effectively incorporate the internal emulsifier, previously mixed DMPA and TEA (dissolved in a small amount of acetone), were added. This procedure ensured the addition of DMPA as its triethylammonium salt. The reaction proceeded until the theoretical NCO was reached and then, the NCO terminated prepolymer was heated to 80 °C and BD was added for the first chain extension with a diol. The system was cooled to 45 °C while the viscosity was adjusted

with dry acetone. Afterwards, two alternative methods were chosen to carry out the second extension reaction with the diamine:

1. In the first method, EDA addition in homogeneous medium, EDA was dissolved in 30 mL of dry acetone and added at a flow rate of 0.5 mL min^{-1}. Thereafter, by the phase inversion process, a polyurethane-urea dispersion was obtained adding distilled water dropwise under vigorous stirring at 25 °C.

2. In the second method, EDA addition in heterogeneous medium, EDA was added after phase inversion.

In both cases, the added amount of EDA was calculated assuming a chain extension of 80%. In either situation, acetone was removed using a rotary evaporator at 40 °C and 350 mbar, obtaining final dispersions with solids content around 35 wt%. In addition, a dispersion without EDA was also synthesized. Scheme of the synthesis route as well as reagents molecular structure used in the polymerization process are depicted in **Figure 4.1**.

Polyurethane and polyurethane-urea films were prepared by casting following the same drying protocol used for WBPU. Samples were stored in a desiccator for 1 week previous their characterization. Samples were coded as WBPUUXy where X describes EDA molar ratio (0.6, 1.2 or 1.8) and subindex y specifies a homogeneous (hom) or heterogeneous (het) medium for the EDA chain extension step. The dispersion without EDA addition was named WBPU.
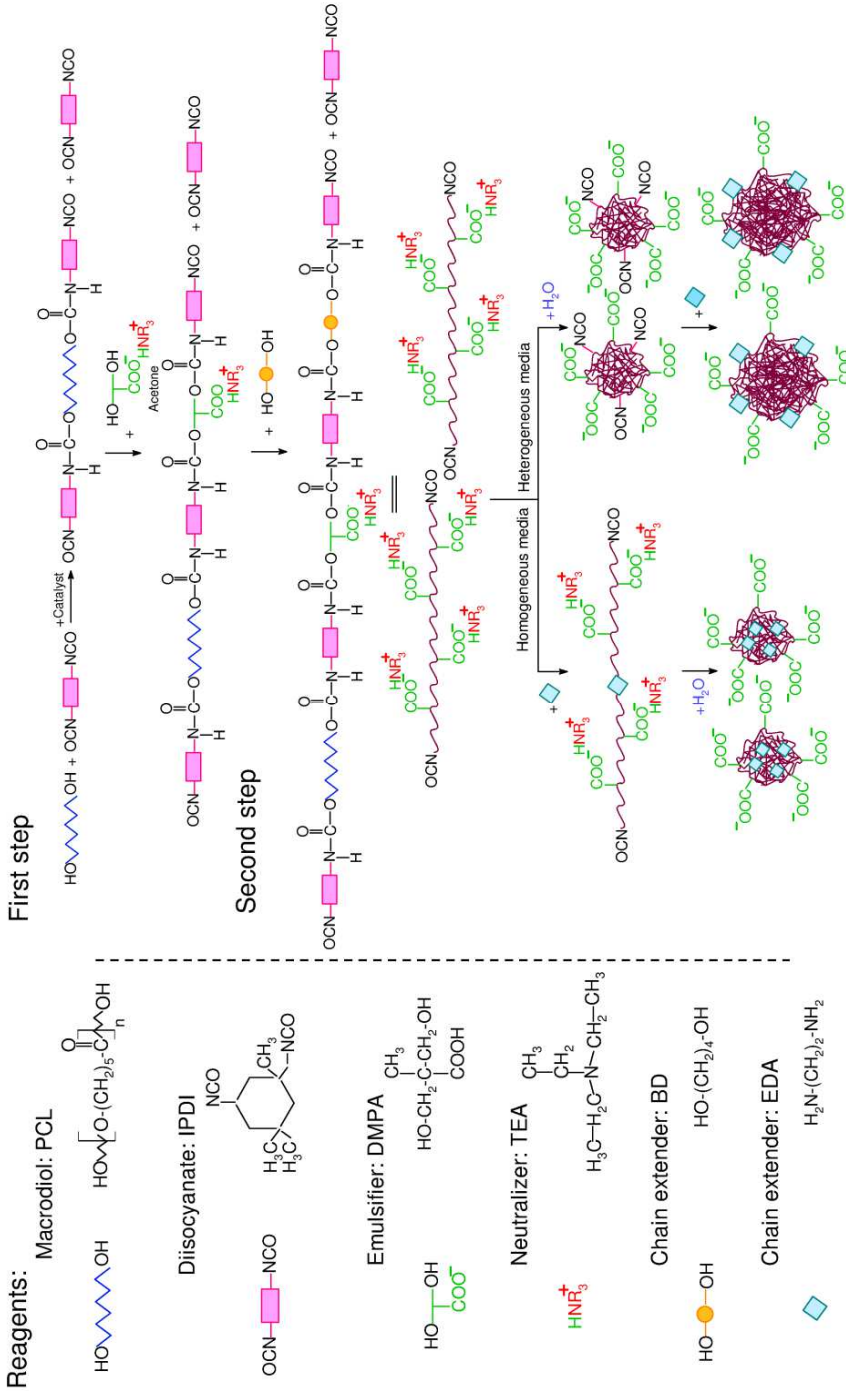
Figure 4.1 *Scheme of the WBPUU synthesis routes and reactants used in the polymerization process*

Molar composition of reagents and hard segment, EDA and DMPA content expressed as weight percentage of the synthesized WBPU and WBPUU both in homogeneous and heterogeneous media are summarized in **Table 4.1**.

Table 4.1 *Molar composition and hard segment, EDA and DMPA contents of WBPU and WBPUU samples*

			WBPU	WBPUU0.6$_y$	WBPUU1.2$_y$	WBPUU1.8$_y$
Molar composition		**IPDI**	3.15	3.6	4.2	4.8
		PCL	0.5	0.5	0.5	0.5
		DMPA	0.5	0.5	0.5	0.5
		BD	2	2	2	2
		EDA	0	0.6	1.2	1.8
HS (wt%)			48.3	52.0	55.6	58.7
DMPA$_{tot}$ (wt%)			3.42	3.22	2.98	2.77
EDA$_{tot}$ (wt%)			0	1.73	3.20	4.47

The y subindex denotes the EDA reaction medium, which refers to homogeneous or heterogeneous media

4.3 Results and discussion

4.3.1 WBPUU dispersions characterization

4.3.1.1 Particle size and distribution

The dispersions particle size has no direct influence on the physical properties of polyurethane and polyurethane-urea cast films. However, particle size is a significant variable to consider depending on the final application of the polyurethane and polyurethane-urea dispersion [1,2]. Usually, small particle size dispersions are preferable for the preparation of deep penetrating coatings, whereas larger particle sizes promote the formation of fast drying coatings [1,3].

The particle size distribution of the polyurethane and polyurethane-ureas determined by light scattering is shown in **Figure 4.2**.
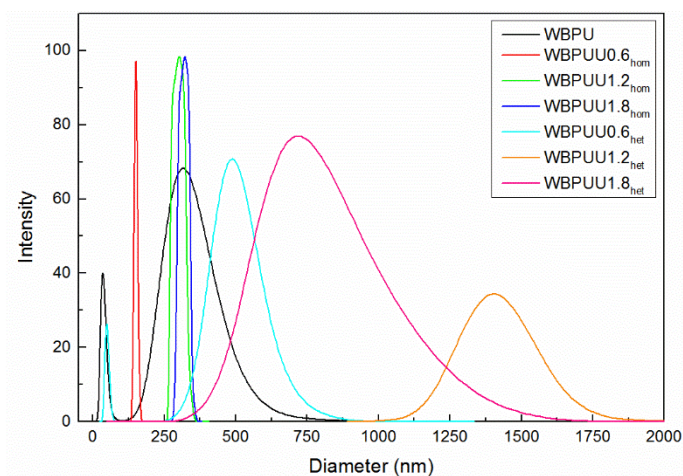
Figure 4.2 *Particle size distribution of WBPU and WBPUU dispersions*

Furthermore, the average particle size of the WBPU and WBPUU dispersions is summarized in **Table 4.2**. It was observed that larger particles and broader particle size distribution profiles were obtained as EDA content increased. The addition of EDA resulted in higher HS content, which caused a decrease in the flexibility of polymer chains hindering their ability to be dispersed into small particles [4]. In addition, the decrease in DMPA content as EDA content was increased, contributed to the formation of larger particles due to the lower repulsion forces generated among them [5]. In the case of WBPU, a bimodal distribution was observed, resulting in particles around 35 and 342 nm. The smaller particles presented a narrow distribution whereas the distribution of larger sized particles resulted broader.

Table 4.2 *Particle size of WBPU and WBPUU dispersions*

Sample	Particle size (nm)
WBPU	34.3 ± 1.1; 342.3 ± 41.0
WBPUU0.6hom	153.4 ± 1.3
WBPUU1.2hom	298.1 ± 1.4
WBPUU1.8hom	308.6 ± 1.6
WBPUU0.6het	56.8 ± 7.6; 483.5 ± 26.4
WBPUU1.2het	1411.6 ± 412.2
WBPUU1.8het	838.7 ± 179.7

The influence of the EDA chain extension step in the average particle size and distribution was also examined. The results revealed that EDA reaction in homogeneous medium, led to a narrow unimodal distribution with rather small particles. However, when EDA chain extension was carried out in a heterogeneous medium, bimodal or very broad particle size distributions were observed. The broad peak consisting of larger particles could result from the growth of smaller particles during EDA chain extension step and possible agglomerations. It has to be noted that once phase inversion has occurred, NCO free groups can react with EDA or water, being the reactivity with EDA higher, and resulting in urea linkages in both cases. As observed in **Figure 4.3**, the reaction of NH_2 groups of EDA is supposed to take place mainly close to the particles surface. The NCO free groups positioned at or near the particle surface show greater accessibility than those located inside particles [6,7]. However, EDA and water molecules have also the ability to penetrate into the particles and react with remaining NCO groups. Therefore, despite the possibility of reactions inside the particles, it is expected that chain extension would mainly

occur at the particles surface [7], thus contributing to achieve larger particle sizes, as compared with their homologues synthesized in a homogeneous medium.
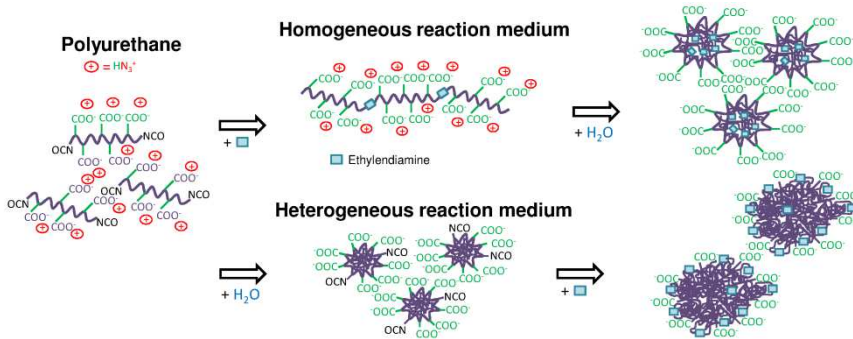
Figure 4.3 *WBPUU particles formation process during water dispersion step*

4.3.1.2 Morphology

In order to analyze the morphology of WBPUU dispersions, AFM images were obtained from films WBPUU dispersions prepared by *spin-coating*. Height and phase images of WBPUU synthesized by EDA chain extension step in homogeneous medium at 5 and 1 μm are shown in **Figure 4.4** and **Figure 4.5**.

Analyzing those AFM images was observed that WBPUU0.6$_{hom}$ sample seemed to present considerable cohesiveness between particles leading to a homogeneous film surface where spherical particles could barely be differentiated. Alternatively, as EDA content was increased, the cohesiveness between larger particles became weaker resulting in observable slightly isolated particles in the case of WBPUU1.8$_{hom}$.
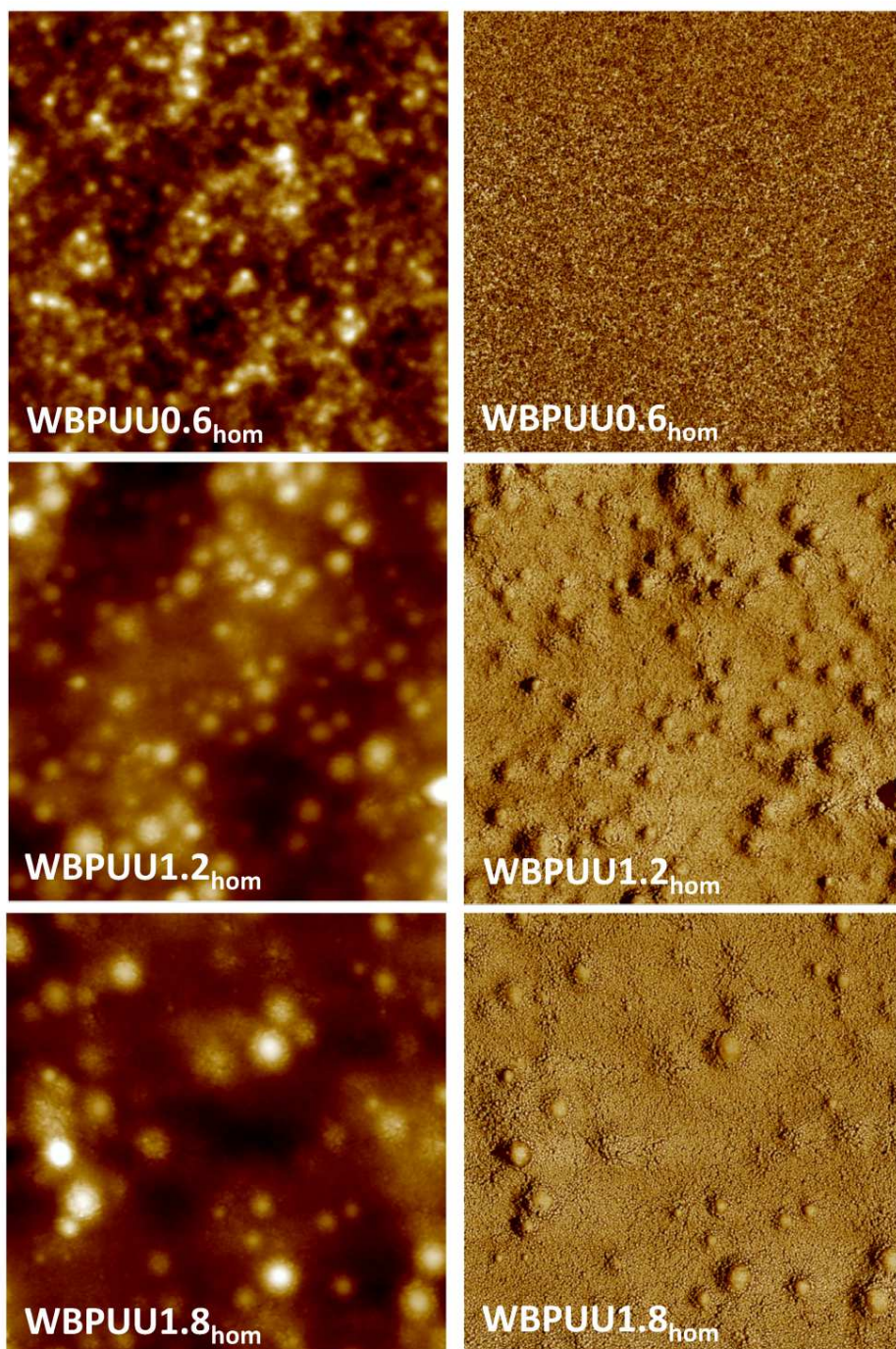
Figure 4.4 *AFM height (left) and phase (right) images of WBPUU dispersions synthesized in homogeneous medium (size: 5x5 μm²)*
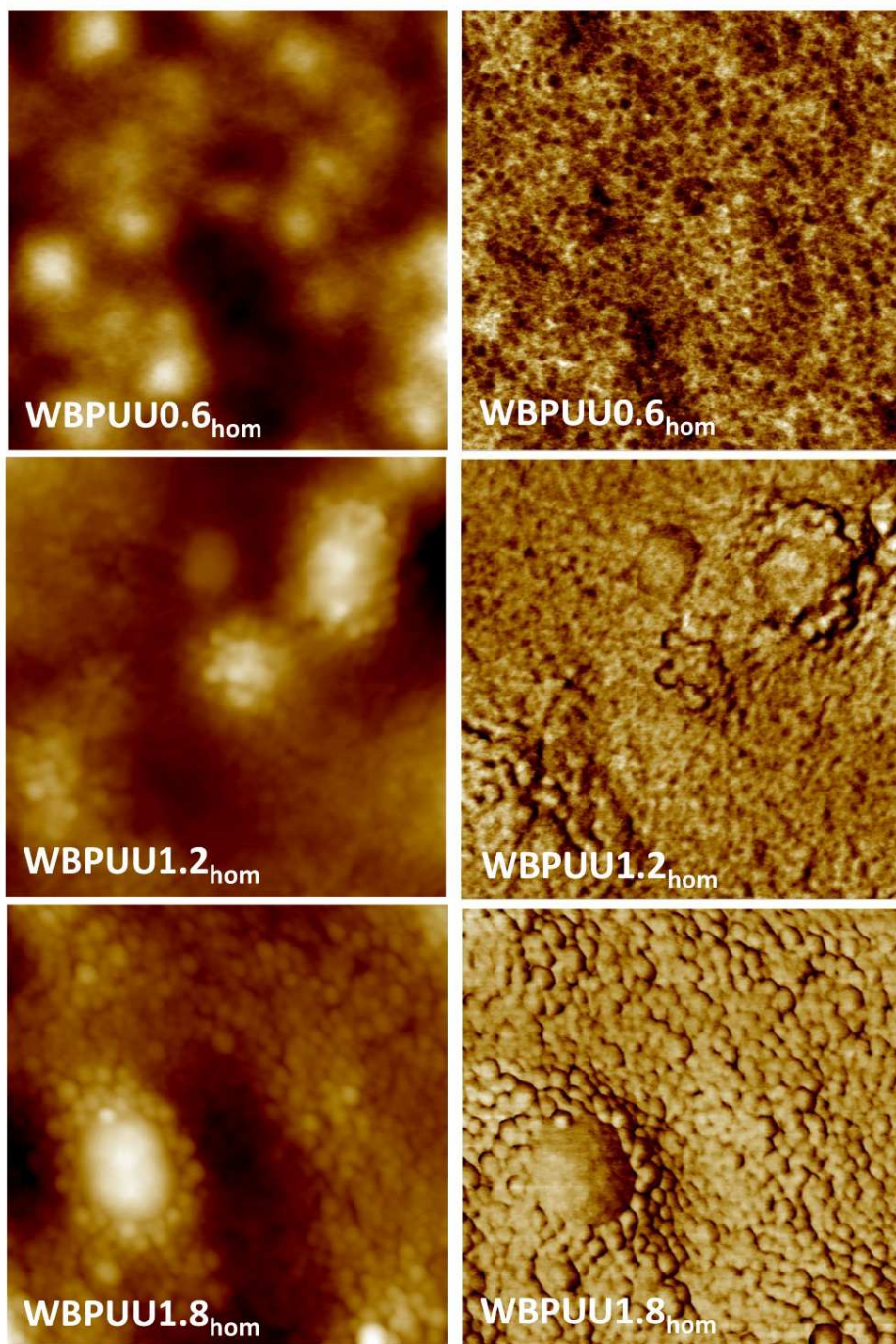
Figure 4.5 *AFM height and phase images of WBPUU dispersions synthesized in homogeneous medium (size: 1x1 μm²)*

Since it was not possible to obtain AFM images from dispersions prepared in heterogeneous medium, an optical microscopy image of WBPUU0.6$_{het}$ sample is displayed in **Figure 4.6**.
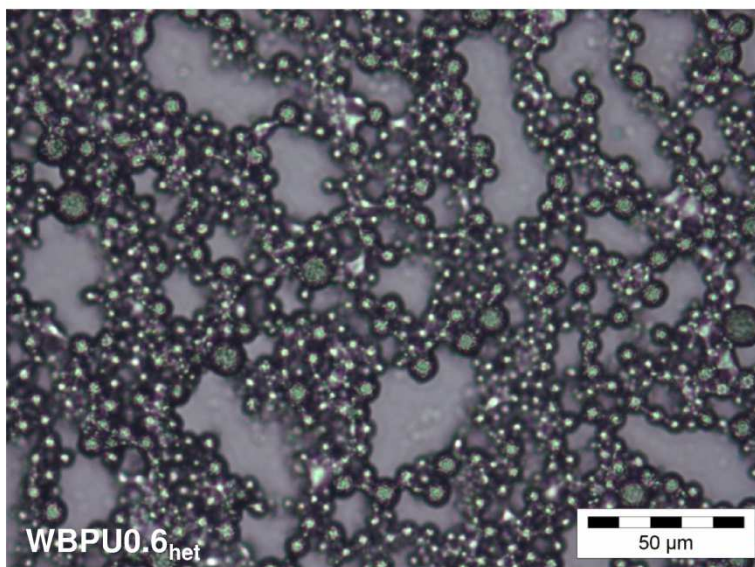
Figure 4.6 *Optical microscopic image of WBPUU0.6$_{het}$ sample*

In this case, no homogeneously dispersed particles, heterogeneous in size, were observed resulting in lower driving force for film formation. These results corroborated the particle size and distribution previously discussed in 4.3.1.1 section.

4.3.2 Properties of WBPUU films

4.3.2.1 Physicochemical properties

The characteristic functional groups of polyurethane and polyurethane-ureas were analyzed by FTIR. Spectra of WBPU and WBPUU films are shown in **Figure 4.7**.
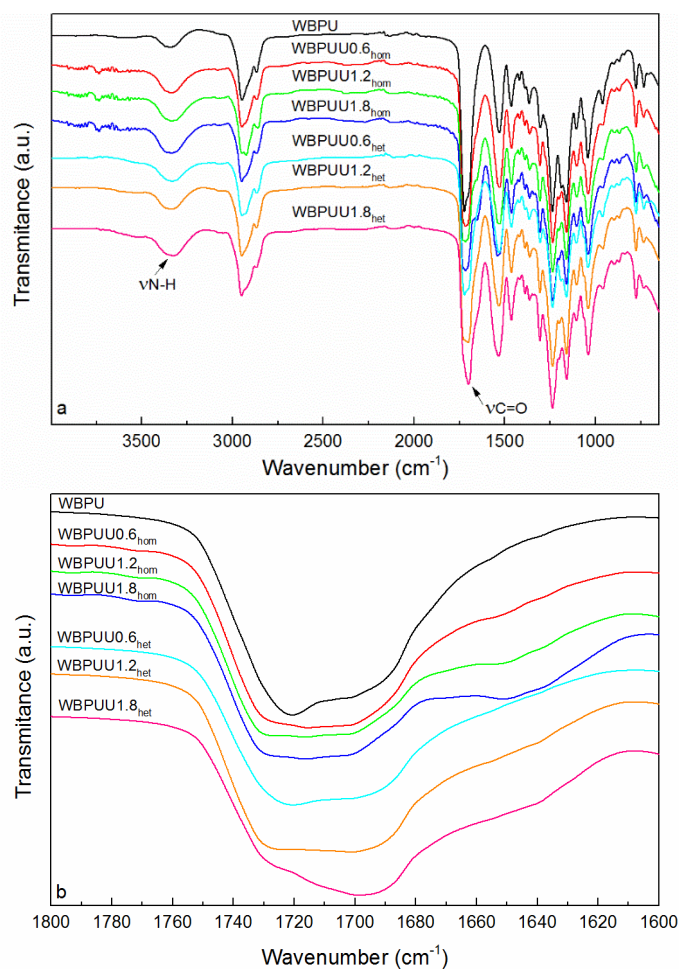
Figure 4.7 *a) FTIR spectra of WBPU and WBPUU films and b) amplification of carbonyl stretching region*

The band at 2270 cm^{-1} associated with NCO groups is not detected in any spectra, indicating that isocyanate conversion proceeded completely in all synthesis. Regarding the region between 3500 and 3100 cm^{-1} attributed to urea and urethane N-H groups, two peaks, located about 3450 and 3320 cm^{-1} are often observed, that can be assigned to hydrogen-bonded and non hydrogen-bonded N-H of urethane and urea groups [8]. In this case, only a single peak around 3336 cm^{-1} was observed, indicating that most N-H groups are involved in hydrogen bonds.

Regarding amide I region [9], an amplification of the spectra in that region between 1800 and 1600 cm^{-1} is included in **Figure 4.7b**, which concerns the peak corresponding to stretching vibration of carbonyl groups. In this region, depending on the C=O groups nature and hydrogen bonding ability, stretching vibration peaks appear at different wavenumbers [8,10–12]. In WBPU a sharp peak was distinguished around 1720 cm^{-1} and a shoulder about 1700 cm^{-1} attributable to the C=O of the free urethane and PCL ester groups, and C=O hydrogen bonded of urethane groups, respectively. In the case of EDA reaction in homogeneous medium, C=O carbonyl stretching region presented different bands at about 1730 and 1701 cm^{-1}. In addition, a band close to 1650 cm^{-1} related with the hydrogen bonded urea C=O groups was observed, becoming more noticeable as EDA content increased, and therefore, indicating that EDA addition favored urea C=O hydrogen bonding interactions. In samples where the chain extension with EDA was performed in heterogeneous medium, similar bands to WBPU were observed. The peak about 1720 cm^{-1} shifted to higher wavenumber values (1720 cm^{-1} in WBPUU0.6$_{het}$, 1726 cm^{-1} in WBPUU1.2$_{het}$ and 1728 cm^{-1} in WBPUU1.8$_{het}$) as EDA content increased, probably due to the presence of a great amount of free C=O urethane groups. In addition, the

relative intensity of the band about 1700 cm^{-1} increased due to the presence of more C=O of urea groups with EDA addition. The bands related with the hydrogen bonded C=O urea groups, around 1640 cm^{-1} were perceptible at high EDA contents (WBPUU1.2$_{het}$ and WBPUU1.8$_{het}$) suggesting that urea C=O groups tend to associate in hydrogen bonding interactions when EDA content increased.

4.3.2.2 Thermal properties

Thermal behavior of WBPU and WBPUU films was analyzed by differential scanning calorimetry and the thermograms are shown in **Figure 4.8**.
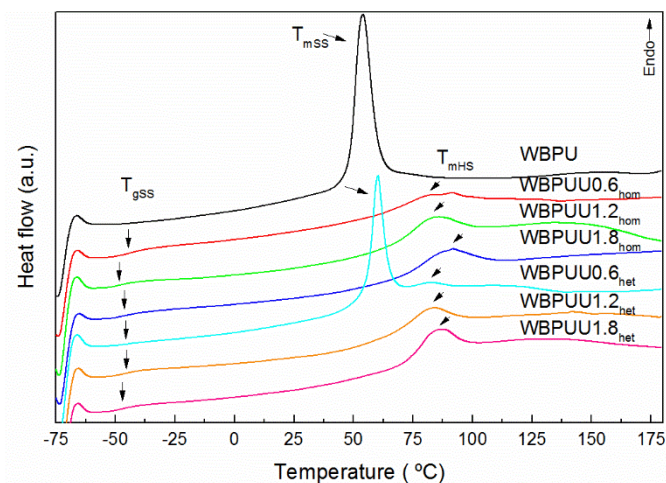
Figure 4.8 *DSC thermograms of WBPU and WBPUU films*

Furhtermore, **Table 4.3** summarizes the corresponding soft segment glass transition temperature, melting temperature and enthalpy as well as hard segment melting temperature (T$_{mHS}$) and enthalpy (ΔH$_{mHS}$) determined from the thermograms.

Table 4.3 *Thermal properties of WBPU and WBPUU films*

Sample	T_{gSS} (°C)	T_{mSS} (°C)	ΔH_{mSS} (J g^{-1})	T_{mHS} (°C)	ΔH_{mHS} (J g^{-1})
WBPU	-	53.6	27.6	-	-
WBPUU0.6$_{hom}$	-44.4	-	-	81.5	13.5
WBPUU1.2$_{hom}$	-48.4	-	-	83.4	11.7
WBPUU1.8$_{hom}$	-46.4	-	-	91.9	10.8
WBPUU0.6$_{het}$	-45.7	60.5	13.5	82.1	3.3
WBPUU1.2$_{het}$	-45.7	-	-	82.7	15.1
WBPUU1.8$_{het}$	-47.1	-	-	85.3	14.6

For WBPU, an endothermic peak about 50 °C related with the ordered soft domains was observed. In WBPUUX$_{hom}$ systems, it was observed that EDA addition hindered the possibility of soft segments to arrange in soft crystalline domains, since no soft endothermic peak was detected, providing mobility and decreasing T_{gSS} as EDA content increased. However, in heterogeneous medium, WBPUU0.6$_{het}$ showed soft segment melting enthalpy. In this case, EDA is added after the polyurethane chains have adopted the conformation expected with core-shell particles, where PCL moves inside the particle, forming part of the core [5]. The amine tends to stay and later react close to the particle surface, as previously explained in 4.3.1.1 section, and consequently, EDA interferes in a lesser extent with PCL facilitating the ability to form soft crystalline domains. Nevertheless, ΔH_{mSS} decreased comparing with WBPU. At higher EDA contents SS crystallization was hindered.

Around 80 °C, in both homogeneous and heterogeneous systems, an endothermic transition was observed attributable to the short range ordering of

hard segments [13]. It was observed that the increase of EDA content decreased ΔH_{mHS} values and shifted the transition to higher temperature, due to stronger hydrogen bonding interactions. However, in case of heterogeneous reaction medium, higher and broader ΔH_{mHS} were obtained. When EDA reaction occurs after chains have adopted a conformation typical of particles, EDA tends to react in the outer shell of the particles remaining more accessible to interactions and thus favoring ordered structures.

4.3.2.3 Mechanical properties

The mechanical behavior was analyzed in tensile mode and stress-strain curves of WBPU and WBPUU films are shown in **Figure 4.9**.
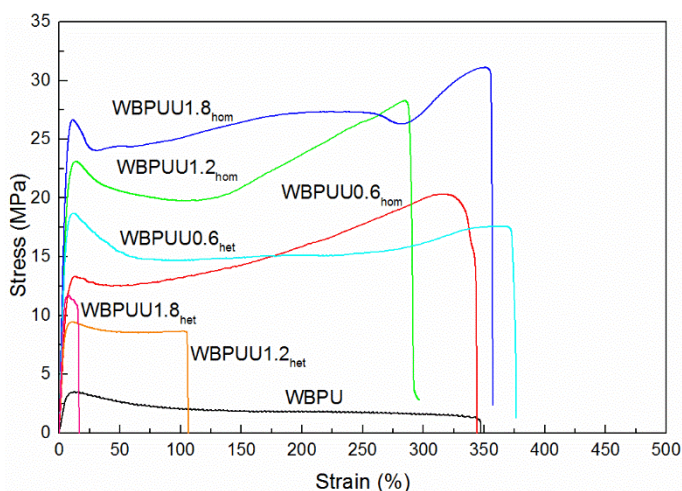
Figure 4.9 *Stress–strain curves of WBPU and WBPUU films*

Furthermore, yield stress, stress at break, tensile modulus and strain at break values of WBPU and WBPUU films obtained from the stress-strain curves are summarized in **Table 4.4**.

Table 4.4 *Mechanical properties of WBPU and WBPUU films*

Sample	σ_y (MPa)	σ_b (MPa)	E (MPa)	ε_b (%)
WBPU	4.1 ± 0.7	1.8 ± 0.6	76.9 ± 14.4	337 ± 63
WBPUU0.6$_{hom}$	12.7 ± 0.5	20.6 ± 2.6	209.7 ± 14.9	329 ± 42
WBPUU1.2$_{hom}$	21.5 ± 1.3	26.6 ± 1.2	331.6 ± 13.9	296 ± 37
WBPUU1.8$_{hom}$	26.2 ± 2.2	29.7 ± 1.4	387.1 ± 51.5	343 ± 59
WBPUU0.6$_{het}$	14.5 ± 0.2	18.0 ± 0.8	337.7 ± 9.6	373 ± 22
WBPUU1.2$_{het}$	9.3 ± 0.5	8.5 ± 0.9	222.9 ± 28.6	113 ± 44
WBPUU1.8$_{het}$	11.5 ± 1.0	11.0 ± 1.0	279.0 ± 11.5	13 ± 3

It was observed a considerable improvement of polyurethane-ureas mechanical performance comparing with WBPU, behavior attributable to the stronger hydrogen bonding provided by urea groups as compared with urethane groups of hard segments [8]. The yield stress, stress at break and modulus values improved considerably in WBPUU comparing with WBPU, even up 540, 1570 and 400%, respectively in WBPUU1.8$_{hom}$. The increase of EDA content resulted in a greater amount of urea groups thus leading to an increase of the hydrogen bonds, as observed by FTIR results in 4.3.2.1 section, resulting in tougher films [14]. In addition, in most of the samples high strain at break values were observed. In the case of heterogeneous medium, and comparing samples with the same EDA content of the homogeneous series, except for WBPUU0.6$_{het}$, lower values of stress modulus and strain at break were obtained. This could be related to a distinct pattern of the particles formation during the synthesis process. In homogeneous systems, a narrower size distribution together with lower average particle sizes were obtained leading to an improved homogeneous

cohesion between particles during the drying process of film formation. Therefore, interactions would be favored as observed in FTIR results, and the presumably lower amount of failure points, owing to the film homogeneity, would facilitate the stress transfer in the films. The larger values of yield stress, stress at break and modulus in sample WBPUU0.6$_{het}$ would be due to the additional stiffness conferred by the soft segment crystallization.

4.3.2.4 Thermomechanical properties

The thermomechanical behavior of WBPU and WBPUU films was studied by DMA by analyzing the evolution of storage modulus and Tanδ with increasing temperature, as observed in **Figure 4.10**.
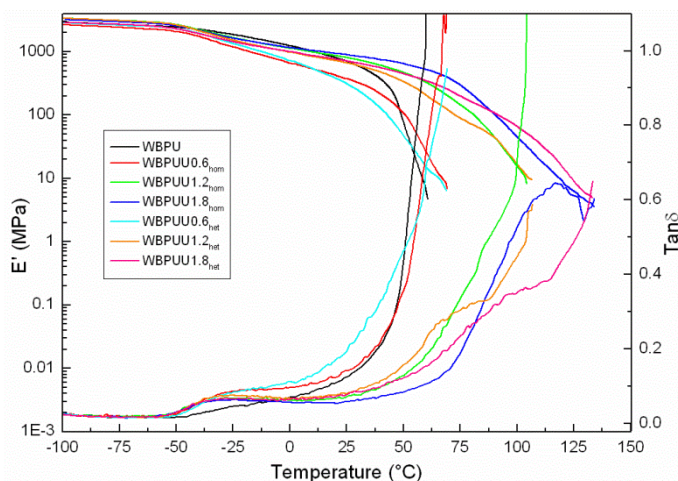
Figure 4.10 *Storage modulus and Tanδ curves of WBPU and WBPUU films*

It was observed that at low temperatures all samples showed similar E' values in the glassy state, followed by a drop between -50 and 25 °C related with the T$_{gSS}$, which was also reflected in a small peak in Tanδ curve. Analyzing this peak, it was observed that the transition was less pronounced in the case of the plain

polyurethane, corroborating the results obtained by DSC in 4.3.2.2 section, as T_{gss} was hard to observe. Moreover, E' values for that polyurethane was slightly higher in this rubbery plateau, due to the higher crystallinity of soft segments as compared to polyurethane-ureas [8]. With larger urea content, the T_{gss} transition in the Tanδ curve became more pronounced with almost unchanged temperature values. At higher temperatures, it was appreciated that WBPU presented lower thermomechanical stability comparing with polyurethane-ureas. Despite presenting around 90% higher E' values than in the case of WBPUU0.6$_{hom}$ and WBPUU0.6$_{het}$ at room temperature, when soft domains crystals melted about 50 °C, as observed in DSC results, the sample started to flow. In polyurethane-ureas, the increase of EDA content provided greater thermomechanical stability due to the contribution of urea groups' interactions as observed by FTIR and DSC results. In the case of homogeneous chain extension reaction, an improvement of about 55 and 100% was observed in the thermomechanical stability temperature (referred to the beginning of the sharp drop) for WBPUU1.2$_{hom}$ and WBPUU1.8$_{hom}$ respect to WBPUU0.6$_{hom}$, whereas with heterogeneous system the improvement resulted into about 75 and 120% for WBPUU1.2$_{het}$ and WBPUU1.8$_{het}$ respectively as compared to WBPUU0.6$_{het}$.

4.3.2.5 Hydrophilicity

The surface hydrophilicity of WBPU and WBPUU films was put into evidence through static water contact angle determinations, whereas in order to study the behavior of films immersed in water, WBPUU films were subjected to weight change measurements by water absorption analysis at 25 °C. Static water contact angles of WBPU and WBPUU films are summarized in **Table 4.5**.

Table 4.5 *Water contact angle values of WBPU and WBPUU films*

Sample	Angle (°)
WBPU	87.4 ± 0.6
WBPUU0.6hom	80.9 ± 1.0
WBPUU1.2hom	75.5 ± 0.7
WBPUU1.8hom	73.1 ± 1.3
WBPUU0.6het	81.6 ± 1.1
WBPUU1.2het	79.7 ± 0.8
WBPUU1.8het	90.0 ± 0.7

From the water contact angle values it was observed that WBPU showed in general higher values as compared with polyurethane-ureas containing urea groups, which presented higher polarity. In general, in both, EDA reaction in homogeneous and heterogeneous media, it was observed a decrease in contact angle values as EDA content increased, due to the greater density of urea groups. This drop was slightly lower in the case of EDA reaction in heterogeneous medium. Indeed, it could be influenced by the EDA addition after dispersion formation in the synthesis. As explained in DLS results in 4.3.1.1 section, EDA would react preferably in the particle external boundary and probably would interfere with the location of the ionic groups at the surface. In the case of WBPUU1.8het, the higher surface roughness could also contribute to the increase of the water contact angle value [15].

Regarding the behavior of WBPU and WBPUU films immersed in water at 25 °C, water absorption measurements are displayed in **Figure 4.11**.
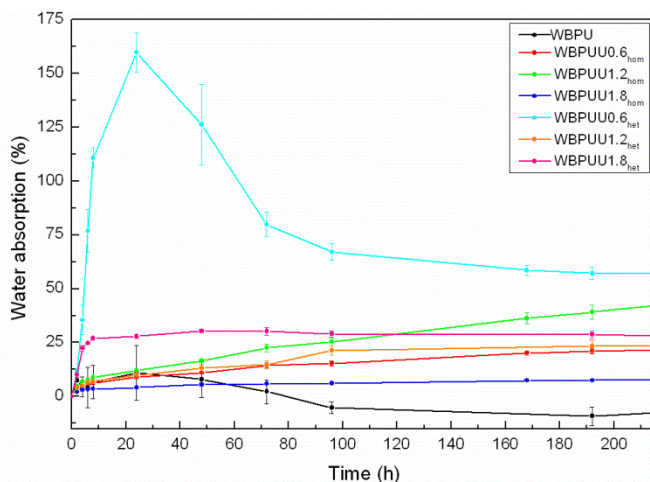
Figure 4.11 *Water absorption percentages of WBPU and WBPUU films over time*

It was observed that water absorption of WBPU reached a maximum and then decreased due to a weight loss [16]. With respect to EDA reaction in homogeneous medium, as the EDA content increased, a higher water absorption capacity was observed, attributed to the greater amount of urea polar groups, except for WBPUU1.8hom, which could be related to the inhomogeneity of the film. In the case of EDA reaction in heterogeneous medium, the same tendency was observed, being the obtained values generally higher as compared to the corresponding homologues of the homogeneous series. This would be related with the film formation ability. The broader bimodal particle size distribution of the heterogeneous systems would lead to films with lower uniformity and cohesiveness among particles which may result in possible gaps among them and thereby, facilitate the transport of water molecules through the film. In the case of WBPUU0.6het, a similar behavior to WBPU was observed, corroborated by the similar soft and hard segment structures as observed in DSC results in 4.3.2.2 section. Furthermore, the higher water absorption percentage achieved in

WBPUU0.6het would present more influence in the weight loss effect in that sample due to the greater accessibility of water molecules extending through the film until weaker points [16].

4.4 Conclusions

In this chapter a series of polyurethane and polyurethane-urea dispersions, with varied EDA content and following two different chain extender addition procedures (in homogeneous or heterogeneous media), were produced. From these dispersions films were prepared and also characterized. As the EDA content was increased, and thereby HS content, dispersions with larger particles were obtained as a result of the polymer chain flexibility reduction. Moreover, the used addition step also influenced the particle size distribution. In homogeneous medium unimodal distributions with lower particle sizes were observed, whereas in heterogeneous medium broader distributions with larger particle sizes resulted, behavior attributed to the preferential EDA reaction at the particles' surface, once in this last case diamine addition followed particle formation. Dispersions produced in homogenous medium with low EDA contents gave rise to films imparting significant cohesiveness among particles, whereas slightly isolated particles start to be perceived as the EDA content was increased. Moreover, DSC results revealed that soft segment crystallization ability was hindered by EDA addition, although endothermic transition related to short range ordering of hard segment domains was promoted.

Comparatively with polyurethane counterparts, polyurethane-urea presented better mechanical performance showing values of stress at yield, stress at break and modulus values up to 540, 1570, and 400%, respectively in WBPU1.8hom, while keeping proximate values of strain at break. In addition, a higher EDA

content led to improved stress and modulus, particularly if EDA was added in homogeneous medium. A narrow particle size distribution facilitated cohesiveness and interactions during film formation, thus favoring stress transfer. DMA results corroborated the thermomechanical stability conferred by EDA addition. An improvement of about 100 and 120% was observed in thermomechanical stability temperature values for samples WBPUU1.8$_{hom}$ and WBPUU1.8$_{het}$ respect to WBPUU0.6$_{hom}$ and WBPUU0.6$_{het}$ respectively. Water absorption exhibited a growing tendency as the EDA content increased. In the case of using heterogeneous medium for chain extension, higher levels of water absorption were achieved in comparison with the corresponding homogeneous counterparts, attributable to the influence of particle size in the film formation process.

4.5 References

[1]   Y.S. Kwak, E.Y. Kim, B.H. Yoo, H. Do Kim, Preparation and properties of waterborne poly(urethane urea)s for adhesives: The effects of the 2,2-bis(hydroxylmethyl) propionic acid content on the properties, J. Appl. Polym. Sci. 94 (2004) 1743–1751.

[2]   Q.B. Meng, S.I. Lee, C. Nah, Y.S. Lee, Preparation of waterborne polyurethanes using an amphiphilic diol for breathable waterproof textile coatings, Prog. Org. Coat. 66 (2009) 382–386.

[3]   M.M. Rahman, H. Do Kim, Effect of polyisocyanate hardener on adhesive force of waterborne polyurethane adhesives, J. Appl. Polym. Sci. 104 (2007) 3663–3669.

[4]   L.H. Bao, Y.J. Lan, S.F. Zhang, Effect of NCO/OH molar ratio on the structure and properties of aqueous polyurethane from modified castor oil, Iran. Polym. J. 15 (2006) 737–746.

[5]   A. Santamaria-Echart, A. Arbelaiz, A. Saralegi, B. Fernández-d'Arlas, A. Eceiza, M.A. Corcuera, Relationship between reagents molar ratio and dispersion stability and film properties of waterborne polyurethanes, Colloid Surface A 482 (2015) 554–561.

[6]   Y.H. Guo, J.J. Guo, H. Miao, L.J. Teng, Z. Huang, Properties and paper sizing application of waterborne polyurethane emulsions synthesized with isophorone diisocyanate, Prog. Org. Coat. 77 (2014) 988–996.

[7]   Y.K. Jhon, I.W. Cheong, J.H. Kim, Chain extension study of aqueous polyurethane dispersions, Colloid Surface A 179 (2001) 71–78.

[8]   I. Yilgör, E. Yilgör, G.L. Wilkes, Critical parameters in designing segmented polyurethanes and their effect on morphology and properties: A comprehensive review, Polymer 58 (2015) A1–A36.

[9]   L. Ugarte, B. Fernandez-d'Arlas, A. Valea, M.L. González, M.A. Corcuera, A. Eceiza, Morphology-properties relationship in high-renewable content polyurethanes, Polym. Eng. Sci. 54 (2014) 2282–2291.

[10]   M.A. Pérez-Limiñana, F. Arán-Aís, A.M. Torró-Palau, C. Orgilés-Barcel, J.M. Martín-Martínez, Influence of the hard-to-soft segment ratio on the adhesion of water-borne polyurethane adhesive, J. Adhes. Sci. Technol. 21 (2007) 755–773.

[11]   M.S. Yen, P.Y. Chen, H.C. Tsai, Synthesis , properties, and dyeing application of nonionic waterborne polyurethanes with different chain length of ethyldiamines as the chain extender, J. Appl. Polym. Sci. 90 (2003) 2824–2833.

[12]   J.T. Garrett, R. Xu, J. Cho, J. Runt, Phase separation of diamine chain-extended poly(urethane) copolymers: FTIR spectroscopy and phase Transitions, Polymer 44 (2003) 2711–2719.

[13]   C. Fang, X. Zhou, Q. Yu, S. Liu, D. Guo, R. Yu, J. Hu, Synthesis and

characterization of low crystalline waterborne polyurethane for potential application in water-based ink binder, Prog. Org. Coat. 77 (2014) 61–71.

[14]   S. Sakurai, Y. Okamoto, H. Sakaue, T. Nakamura, L. Banda, S. Nomura, Structure and properties of segmented poly(urethaneurea)s with relatively short hard-segment chains, J. Polym. Sci. Part B 38 (2000) 1716–1728.

[15]   K. Malkappa, T. Jana, Hydrophobic, water-dispersible polyurethane: Role of polybutadiene diol structure, Ind. Eng. Chem. Res. 54 (2015) 7423–7435.

[16]   A. Marcos-Fernández, G.A. Abraham, J.L. Valentín, J. San Román, Synthesis and characterization of biodegradable non-toxic poly(ester-urethane-urea)s based on poly(ε-caprolactone) and amino acid derivatives, Polymer 47 (2006) 785–798.

CHAPTER 5

Isolation of cellulose nanocrystals

"Lo que hoy está comprobado, una vez solo pudo ser imaginado"

5. ISOLATION OF CELLULOSE NANOCRYSTALS

5.1 Objective

The synthesis of waterborne polyurethane as well as polyurethane-ureas provided the opportunity of incorporating water dispersible nanoentities and focusing on eco-friendly materials. In this sense, CNC have gained attention as nanoreinforcement in the field of nanocomposites [1] due to their exceptional properties conferred by the elevated L/D aspect ratio and high specific mechanical properties. Moreover, the negatively charged sulfate groups anchored to CNC during the H_2SO_4 hydrolysis favor the formation of stable dispersions of CNC in water [2] becoming a suitable nanoreinforcement for the direct incorporation to aqueous polymeric matrixes such as WBPU and WBPUU ensuring their compatibility, without requiring chemical modifications or the addition of surfactants [3]. Furthermore, additional drying steps would not be required, which would difficult their redispersion, even in water [2]. Thus, in this chapter, microcrystalline cellulose was used for the isolation of cellulose nanocrystals.

5.2 Experimental

5.2.1. Isolation of cellulose nanocrystals

Cellulose nanocrystals were isolated from microcrystalline cellulose via sulfuric acid hydrolysis removing the amorphous regions of cellulose. For the process, MCC was mixed with H_2SO_4 (64 wt%) at 45 °C for 30 min. The suspension was diluted for stopping the process with deionized water and washed by successive centrifugation cycles at 4000 rpm. The resulting suspension was dialyzed against

deionized water until pH 5-6 was reached. A scheme of the hydrolysis process is shown in Figure 5.1.
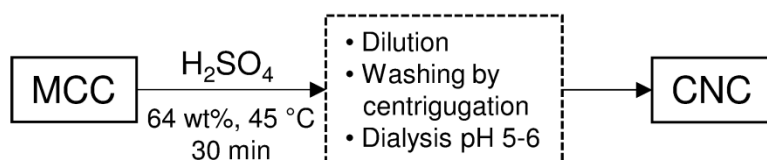
Figure 5.1 *Scheme of MCC acid hydrolysis process for obtaining CNC*

In this way, as can be seen in **Figure 5.2**, CNC dispersion with about 0.5 wt% solids content was obtained determined by UNE-EN ISO 638.

Figure 5.2 *CNC suspension in water*

5.3 Characterization of cellulose nanocrystals

5.3.1 Morphology

AFM height and phase images of CNC are shown in **Figure 5.3**.
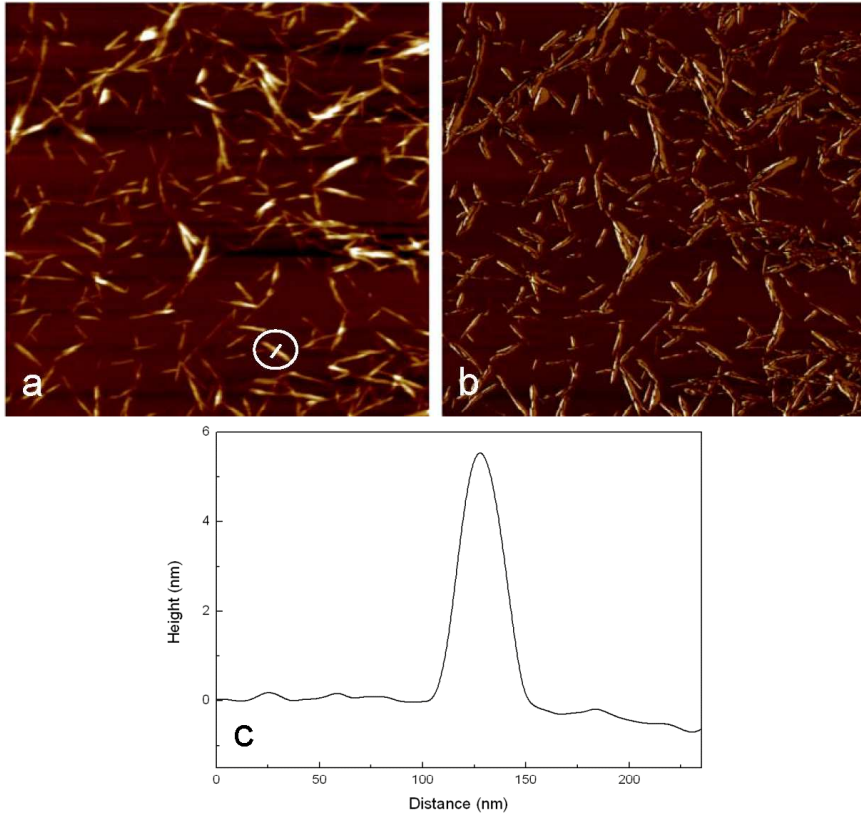
Figure 5.3 *AFM a) height and b) phase images of cellulose nanocrystals (size: 3x3 μm²). c) Height profile of cellulose nanocrystal indicated in height image*

AFM images corroborated the isolation of CNC nanoentities via acid hydrolysis, showing a rod-like morphology. Furthermore, with the purpose of determining the length/diameter aspect ratio, around 100 CNC were measured and averaged. The length of CNC was determined in the height image, whereas the diameters were measured in the AFM height profiles, assuming their cylindrical shape [4]. **Figure 5.3c** shows the height profile taken from the white line marked just above a nanocrystal in **Figure 5.3a**. Thereby, CNC with an average length about 167 ± 31 nm and diameter of 5.4 ± 1.5 nm were obtained, corresponding to an L/D aspect ratio of about 31.

5.3.2 Physicochemical characterization

The sulfate groups anchored in the CNC surface during the hydrolysis led to an electrostatic repulsion between CNC, which improves their dispersibility in polar solvents [5,6]. The CNC sulfate content was measured by conductometric titration [5,7]. In this way, 5 mg of CNC in 25 mL of deionized water were sonicated and after the addition of 10 mL of HCl (10 mM) the mixture was titrated with NaOH (10 mM). Thereby considering the NaOH employed for the CNC sample and the blank the charge density (expressed as sulfur content) can be calculated using **Equation 5.1**.
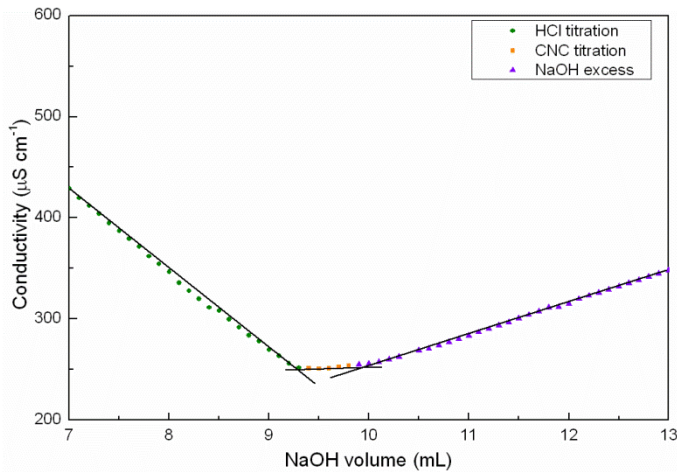
Figure 5.4 *Conductometric titration curve of cellulose nanocrystals*

$$S(\%) = \frac{32 \cdot M \cdot V}{\omega} \cdot 100 \qquad (\mathbf{5.1})$$

where M is the NaOH concentration and ω the weight of used CNC. V is referred to the NaOH volume necessary for the titration of CNC after subtracting the volume necessary to titrate the blank. These values are obtained

from titration curves. The titration curve obtained from CNC dispersion is shown in **Figure 5.4**. The curve can be fitted into 3 lines which would correspond to the NaOH employed for the titration of the HCl, the sample and the excess of NaOH respectively. Thus, considering the intersection points between the lines, the required volume of NaOH employed for the sample titration is calculated. Therefore, based on NaOH curves, and according to **Equation 5.1** a sulfur content of 1.22% was determined.

Elemental analysis was also performed in order to determine the sulfur content of CNC. In this case, a sulfur content of 1.28% was obtained. This value supported the conductometric titration measurements as well as confirmed the modification of negatively charged CNC surface, as a result of the hydrolysis.

5.4 Conclusions

In this chapter, cellulose nanocrystals were successfully isolated from microcrystalline cellulose. By AFM analysis, rod-like shape nanoentities were observed, corroborating the nanometric scale of the isolated cellulose nanocrystals. Furthermore, AFM height image and profile were employed for the determination of the length and diameter values of CNC, resulting in an L/D aspect ratio of 31. In addition, the sulfate groups anchored to the surface of CNC during the hydrolysis process, which favor the formation of stable CNC dispersions in water, was calculated by conductometric titration and elemental analysis, obtaining 1.22 and 1.28% values respectively.

5.5 References

[1]   M.A.S.A. Samir, F. Alloin, A. Dufresne, Review of recent research into cellulosic whiskers, their properties and their application in nanocomposite field, Biomacromolecules 6 (2005) 612–626.

[2]   S. Beck, J. Bouchard, R. Berry, Dispersibility in Water of dried nanocrystalline cellulose, Biomacromolecules 13 (2012) 1486–1494.

[3]   M. Mariano, N. El Kissi, A. Dufresne, Cellulose nanocrystals and related nanocomposites: Review of some properties and challenges., J. Polym. Sci. Part B 52 (2014) 791–806.

[4]   I. Kvien, B.S. Tanem, K. Oksman, Characterization of cellulose whiskers and their nanocomposites by atomic force and electron microscopy, Biomacromolecules 6 (2005) 3160–3165.

[5]   X.M. Dong, J.F. Revol, D.G. Gray, Effect of microcrystallite preparation conditions on the formation of colloid crystals of cellulose, Cellulose 5 (1998) 19–32.

[6]   T. Abitbol, E. Kloser, D.G. Gray, Estimation of the surface sulfur content of cellulose nanocrystals prepared by sulfuric acid hydrolysis, Cellulose (2013) 785–794.

[7]   S. Camarero Espinosa, T. Kuhnt, E.J. Foster, C. Weder, Isolation of thermally stable cellulose nanocrystals by phosphoric acid hydrolysis,

Biomacromolecules 14 (2013) 1223–1230.

CHAPTER 6

Waterborne polyurethane cellulose nanocrystals

nanocomposites

"Si buscas resultados distintos, no hagas siempre lo mismo"

6. WATERBORNE POLYURETHANE CELLULOSE NANOCRYSTALS NANOCOMPOSITES

6.1 Objective

This chapter is focused on the preparation of nanocomposites based on previously non-dried CNC aqueous dispersions and water dispersible polymers such as waterborne polyurethane as an environmentally sustainable attractive via for obtaining advanced materials. Thus, in this chapter, different WBPU-CNC nanocomposites systems were studied in order to perform an exhaustive analysis, considering how the characteristic of matrix, cellulose nanocrystals content and addition route can affect the final properties of the nanocomposites films. With this purpose, three different WBPU-CNC series were prepared by solvent-casting. In the first case, different CNC contents (from 0 to 5 wt%) were incorporated to a previously studied WBPU (in chapter 3) in order to analyze the influence of the reinforcement content in the nanocomposite. Then, the analysis was focused on the influence of the matrix, thus, in this case CNC were incorporated to previously synthesized WBPU$_{1.2}$ (chapter 3), and results were compared with previously prepared nanocomposites in order to analyze the effect of matrix compositions, WBPU and WBPU$_{1.2}$. Furthermore, an additional study was carried considering nanocomposites preparation variables. Two CNC incorporation routes were designed for analyzing the influence of CNC disposition in the WBPU matrix: the classical mixing by sonication after WBPU synthesis and the alternative *in-situ* during the WBPU nanoparticles formation in the synthesis process. The resultant nanocomposites were analyzed from the viewpoint of morphology and CNC disposition in the matrix as well as

considering their physicochemical, thermal, mechanical, thermomechanical and hydrophilicity properties.

6.2 Influence of cellulose nanocrystals content

6.2.1 WBPU-CNC nanocomposite films preparation

Nanocomposites were prepared from the waterborne polyurethane WBPU, previously synthesized in chapter 3, with a IPDI/PCL/DMPA/BD of 3.15/0.5/0.5/2 and different contents of CNC isolated in chapter 5. WBPU-CNC nanocomposites were prepared by casting. CNC suspension was sonicated for 1 h, and after the addition to WBPU waterborne polyurethane dispersion, the mixture was sonicated for another 1 h. The resulting mixture was poured in Teflon mold and dried as previously explained. Varying the total weight content of CNC, films with a thickness of about 0.4 mm were prepared by adding 0.5, 1, 3 and 5 wt% of CNC to WBPU dispersion. Nanocomposite films were stored for 1 week in a desiccators previous their characterization. For comparison, a film of WBPU matrix was also prepared. The samples designation was WBPU-X, where X was referred to CNC weight content in the nanocomposite (0.5, 1, 3 and 5 wt%).

6.2.2 Properties of WBPU-CNC nanocomposites

6.2.2.1 Physicochemical properties

Nanocomposites characteristic functional groups were analyzed by FTIR and the spectra are shown in **Figure 6.1**.

Two typical regions were differentiated related to N-H stretching vibration of urethane and hydroxyl (O-H) groups of CNC between 3600 and 3100 cm^{-1} and carbonyl stretching vibration of urethane linkages in 1800 - 1600 cm^{-1} interval.
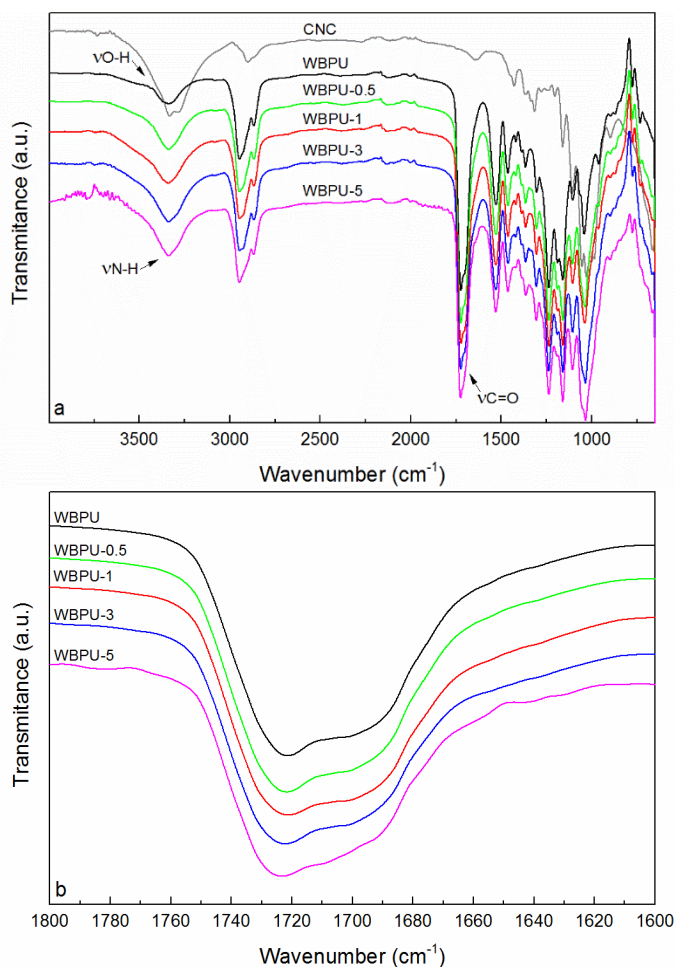
Figure 6.1 *a) FTIR spectra of CNC, WBPU matrix and nanocomposites and b) amplification of carbonyl stretching region*

In the stretching region between 3600 and 3100 cm^{-1}, a band around 3340 cm^{-1} was observed in WBPU and nanocomposites attributed to hydrogen bonded N-H groups, whereas CNC showed two peaks at 3332 and 3287 cm^{-1} referred to O-H groups stretching vibration [1]. In nanocomposites, an increase in the peak

intensity was appreciated as CNC content was increased, related with the overlapping with the O-H stretching vibration band observed in the neat CNC spectrum. With the purpose of analyzing WBPU and nanocomposites C=O characteristic bands, an amplification of the spectra is included in **Figure 6.1b**. The band about 1720 cm^{-1} was related with the C=O of PCL and free urethane C=O groups, whereas the shoulder about 1700 cm^{-1} was attributable to hydrogen bonded urethane C=O groups. It was observed that free C=O groups band shifted to higher wavenumbers whereas the shoulder referred to hydrogen bonded C=O groups was broadened as CNC content increased, suggesting the generation of new WBPU-CNC interactions.

6.2.2.2 Thermal properties

Thermal behavior of WBPU matrix and their nanocomposite films was analyzed by differential scanning calorimetry and thermograms are shown in **Figure 6.2**.
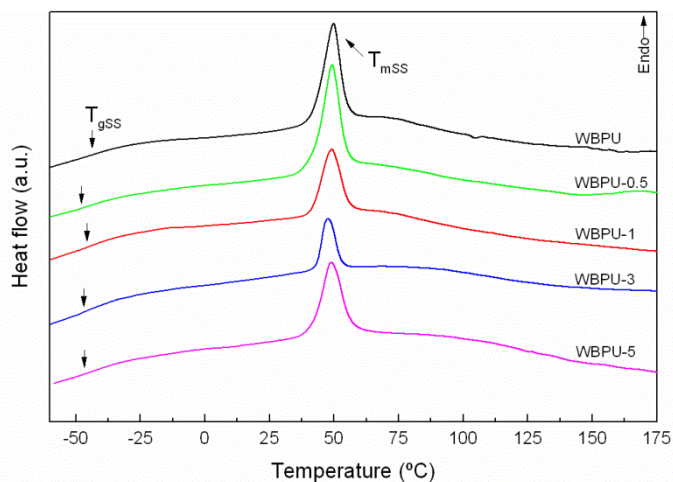
Figure 6.2 *DSC thermograms of WBPU and nanocomposites*

Soft segment glass transition temperature, melting temperature and enthalpy determined from the thermograms are summarized in **Table 6.1**.

Table 6.1 *Thermal properties of WBPU matrix and nanocomposites*

Sample	T_{gSS} (°C)	T_{mSS} (°C)	ΔH_{mSS} (J g^{-1})	X_{cSS}
WBPU	-43.2	49.8	9.9	1
WBPU-0.5	-47.8	49.1	11.1	1.13
WBPU-1	-45.8	49.1	7.1	0.72
WBPU-3	-47.5	47.5	4.1	0.43
WBPU-5	-47.5	48.8	9.0	0.96

A slight decrease in T_{gSS} of the nanocomposites comparing with the matrix was observed. The addition of CNC interfered in the matrix interactions providing greater mobility to chains [2]. Regarding the endothermic peak, it is possible to calculate the relative soft segment crystallinity (χ_{cSS}) with respect to the neat WBPU, in order to obtain more accurate information about the crystallinity of the SS in each nanocomposite. χ_{cSS} was determined by means of the following **Equation 6.1** [3]:

$$\chi_{cSS} = \frac{\Delta H_{mSS}}{\omega \cdot \Delta H_{100}} \tag{6.1}$$

where ΔH_{100} is referred to the melting enthalpy of the neat WBPU, ω the weight fraction of WBPU in the nanocomposite and ΔH_{mSS} the melting enthalpy of the corresponding nanocomposite. At low reinforcement content (0.5 wt%), an

increase of the χ_{cSS} was observed due to the formation of new interactions between CNC and the matrix, comparing with the neat polyurethane, which promoted the ordering of soft domains [4]. Otherwise as CNC content was increased, a decrease in χ_{cSS} was observed. The creation of new WBPU-CNC interactions and the greater amount of reinforcement gradually hindered soft domains crystallization [5,6]. In the case of 5 wt% of CNC, a raise in χ_{cSS} was observed instead, reaching a value similar to WBPU matrix. The possible formation of agglomerates tended to prevail CNC-CNC interactions over CNC-WBPU interactions, favoring the ordering of soft segment in crystalline domains.

6.2.2.3 Mechanical properties

Mechanical behavior of WBPU matrix and nanocomposites films was analyzed by performing tensile tests. **Figure 6.3** shows stress-strain curves of WBPU matrix and their nanocomposites.
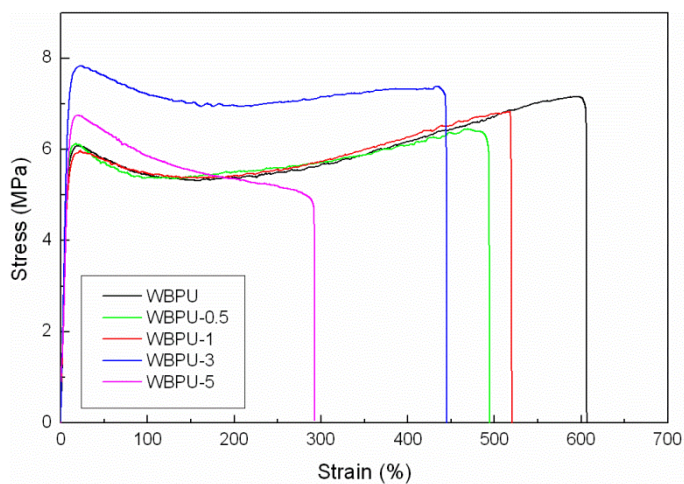
Figure 6.3 *Stress–strain curves of WBPU matrix and nanocomposites*

Yield stress, stress at break, tensile modulus and strain at break values of WBPU matrix and nanocomposites films obtained from the stress-strain curves are summarized in **Table 6.2**.

Table 6.2 *Mechanical properties of WBPU matrix and nanocomposites*

Sample	σ_y (MPa)	σ_b (MPa)	E (MPa)	ε_b (%)
WBPU	6.1 ± 0.5	7.3 ± 0.5	76.4 ± 3.5	612 ± 28
WBPU-0.5	5.7 ± 0.4	6.5 ± 0.1	83.6 ± 2.0	501 ± 38
WBPU-1	5.7 ± 0.8	6.4 ± 0.5	79.0 ± 0.9	472 ± 29
WBPU-3	8.3 ± 0.7	7.4 ± 0.6	88.1 ± 2.5	391 ± 58
WBPU-5	6.5 ± 0.1	5.1 ± 0.2	73.9 ± 5.9	220 ± 74

It was observed that, in general, nanocomposites showed higher modulus and lower strain at break values comparing with the matrix, due to the reinforcement effect of CNC. The high modulus value observed in the case of 0.5 wt% of CNC could be related to the higher crystallinity observed by DSC. Taking into account the reinforcement L/D aspect ratio, the theoretical volume fraction of CNC (V_{R_C}) needed in order to reach the percolation threshold in the nanocomposite was estimated by means of the **Equation 6.2** [7]:

$$V_{R_C} = \frac{0.7}{\left(L/D\right)} \tag{6.2}$$

Considering 1.08 and 1.5 g cm^{-1} WBPU and CNC densities respectively [8], values of 2.26 vol% and 3.2 wt% were obtained. Regarding the nanocomposite

with 3 wt% of CNC, the highest modulus and stress at yield values were observed (showing an improvement of 16 and 36% in E and σ_y respectively, comparing with the matrix). This fact supported the theoretically calculated value. At higher CNC content (5 wt%), though an improvement in stress at yield was observed, the modulus and stress and strain at break values decreased in the nanocomposite. Above the theoretical percolation threshold, the possible presence of some agglomerates could reduce WBPU-CNC interfacial area, hindering stress transfer in the nanocomposite [9].

6.2.2.4 Thermomechanical properties

The thermomechanical behavior of WBPU matrix and nanocomposites films was studied by DMA, analyzing the evolution of storage modulus and Tanδ with increasing temperature, as observed in **Figure 6.4**.
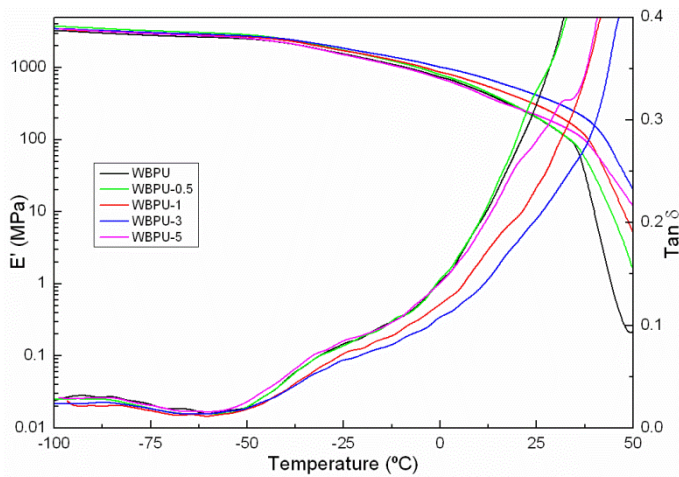
Figure 6.4 *Storage modulus and Tanδ curves of WBPU matrix and nanocomposites*

At low temperatures, in the glassy state, nanocomposites showed similar E' values comparing with the matrix. By increasing temperature, between -50 and -30 °C, a decrease in E' values was observed associated with the T_{gss} of the matrix, as observed in DSC results in 6.3.1.2 section. This transition was also reflected as a peak in Tanδ curves which became less intense with CNC addition, except for 5 wt%. This fact could be related with the WBPU-CNC interactions, which would reduce the amount of mobile chains in the matrix [10,11]. In the case of WBPU-5, the possible formation of some aggregates, as suggested by DSC and mechanical properties results, could promoted CNC-CNC interactions, providing again greater mobility to WBPU chains. In the rubbery plateau, higher E' values were observed in the nanocomposites comparing with the matrix, attributable to the effective reinforcement of CNC [12]. In this region, as temperature increased, a progressive drop in E' value was observed and, as it approached to the soft segments melting region, the WBPU-CNC network collapsed and the film started to flow [13]. Nevertheless, CNC addition retarded even up to 10 °C the thermomechanical stability of nanocomposites, except again for 5 wt%.

6.2.2.5 Hydrophilicity

The surface hydrophilicity of WBPU matrix and nanocomposite films was analyzed by static water contact angle measurements, and films behavior immersed in water was analyzed by water absorption measurements. Static water contact angle values are summarized in **Table 6.3**.

Contact angle measurement is a suitable technique in order to comprehend the affinity of the materials surface with liquids [14]. WBPU matrix presented a considerably hydrophobic character which was reduced as CNC content was increased, even around 15° for WBPU-5. These results were attributable to the

greater hydrophilicity of the nanocomposites provided by the hydrophilic character of CNC [10,15,16].

Table 6.3 *Static water contact angle values of WBPU matrix and nanocomposites*

Sample	Angle (°)
WBPU	102.1 ± 1.9
WBPU-0.5	99.0 ± 1.8
WBPU-1	90.6 ± 2.0
WBPU-3	91.7 ± 2.8
WBPU-5	87.5 ± 2.9

Similar deviation values of 2–3° were observed in the nanocomposites, suggesting the homogeneous uniformity of films. Furthermore, student's t-test was performed comparing each nanocomposite against WBPU matrix in order to assure whether the variation in WCA values was significant. Considering a statistical significance (α) of 0.05, p-values of 4.99×10^{-3}, 3.29×10^{-6}, 1.37×10^{-3} and 2.80×10^{-5} were obtained for WBPU-0.5, WBPU-1, WBPU-3 and WBPU-5, respectively. The fact that nanocomposites show p-values lower than α, indicated that nanocomposites presented a significant variation in WCA values in comparison with the matrix.

The hydrophilic behavior of WBPU matrix and nanocomposites was also analyzed by water absorption measurements at 25 °C as it is displayed in **Figure 6.5**.
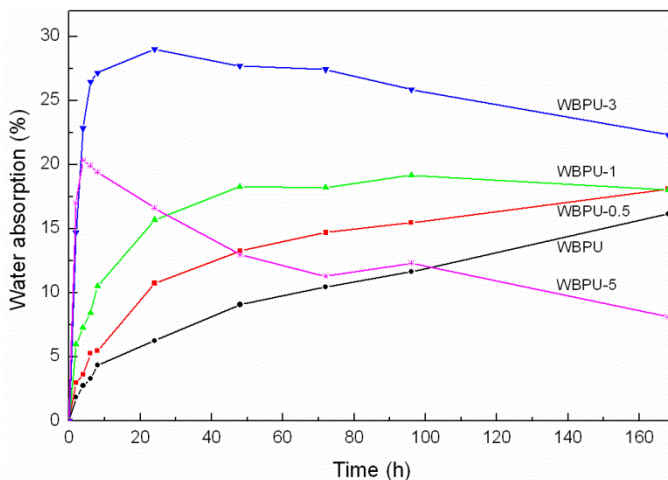
Figure 6.5 *Water absorption percentages of WBPU matrix and nanocomposite films over time*

The same tendency observed in water contact angles was observed in this case, resulting in WA values increase with the increase of CNC content. Water molecules diffuse through the material and tend to approach the WBPU-CNC interface where CNC are located, [5] and which resulted greater as CNC content was increased. In addition, once the percolation threshold was established, the diffusion of water molecules was promoted [17], and that could be the reason of the considerable increase in WA values observed for the sample with 3 wt% of CNC. At higher CNC content, for WBPU-5, the possible aggregates formed in the nanocomposite, would tend to locate CNC in certain areas, decreasing WA values respect to WBPU-3. However, it is worth noting that a decrease in WA values was observed over time in some of the samples. It is true that in the nanocomposite of 5 wt% of CNC lower water absorption values were observed comparing with nanocomposite of 3 wt%, but nevertheless, the beginning of the weight loss phenomena is sharper. In the case of 3 wt% of CNC, the formation of the network confers more stability to the film, contributing to a more

controlled weight loss of the nanocomposite. However, the agglomerates formed in the case of 5 wt%, resulted in located weak points where water could access more easily, which could provoke weight loss.

6.2.2.6 Morphology

The morphology of the matrix and CNC dispersion in the nanocomposites was analyzed by AFM from samples prepared *spin-coating*. The height and phase images at 5 and 1 μm are shown in **Figure 6.6** and **Figure 6.7**, respectively.

In the matrix, dark and bright regions were appreciated, attributed to the amorphous and crystalline domains, respectively [18]. Regarding the nanocomposites, similar morphological structure was observed comparing with the matrix, suggesting that CNC barely alter WBPU morphology. Furthermore, greater quantity of CNC were observed as CNC content was increased, showing an effective homogeneous dispersion of CNC in the matrix [19]. This fact favored the creation of WBPU-CNC interactions [4] as was also observed in FTIR and DSC results. Analyzing height images, in the case of 1 wt% nanocomposite, rod-like CNC were observed isolated from each other, whereas for 3 wt% an interrelated CNC mat was appreciated, which could be related with the network structure. Nevertheless, in the case of 5 wt% some located agglomerates were appreciated, being responsible of variations in the tendencies of the properties, as explained previously.
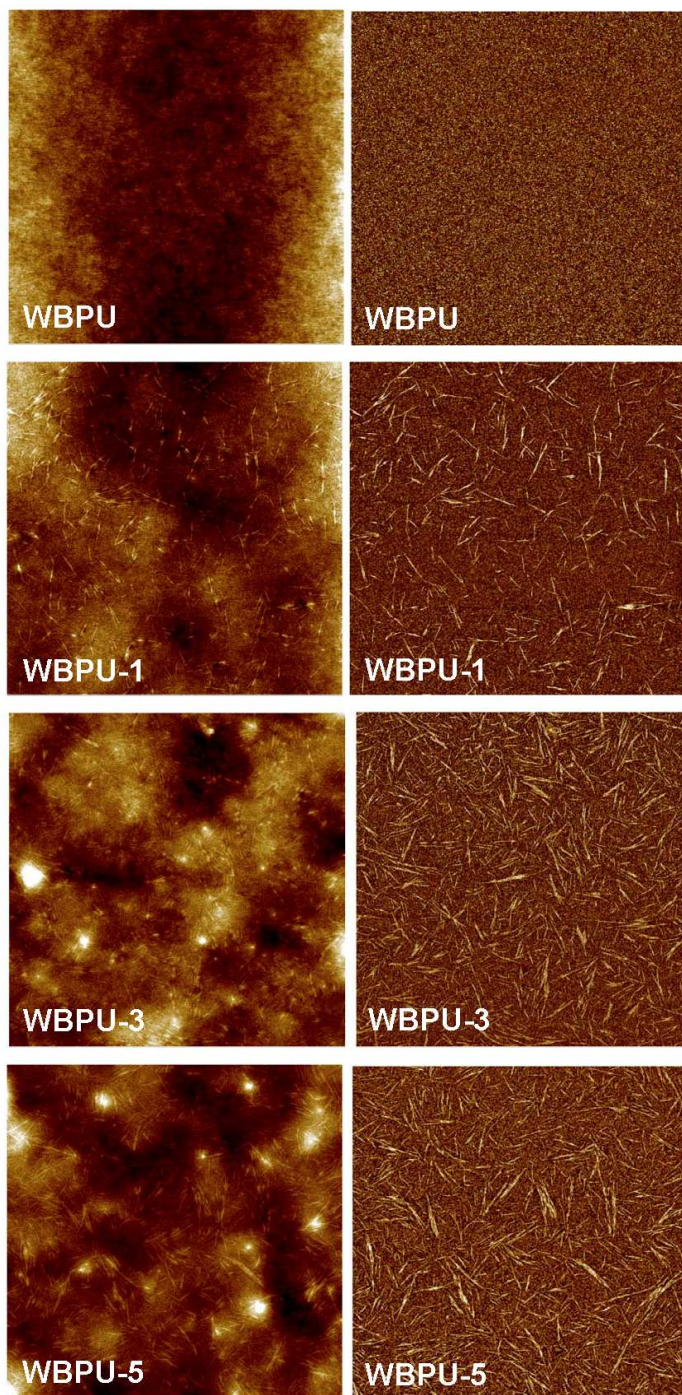
Figure 6.6 *AFM height (left) and phase (right) images of WBPU matrix and nanocomposites (size: 5x5 μm²)*
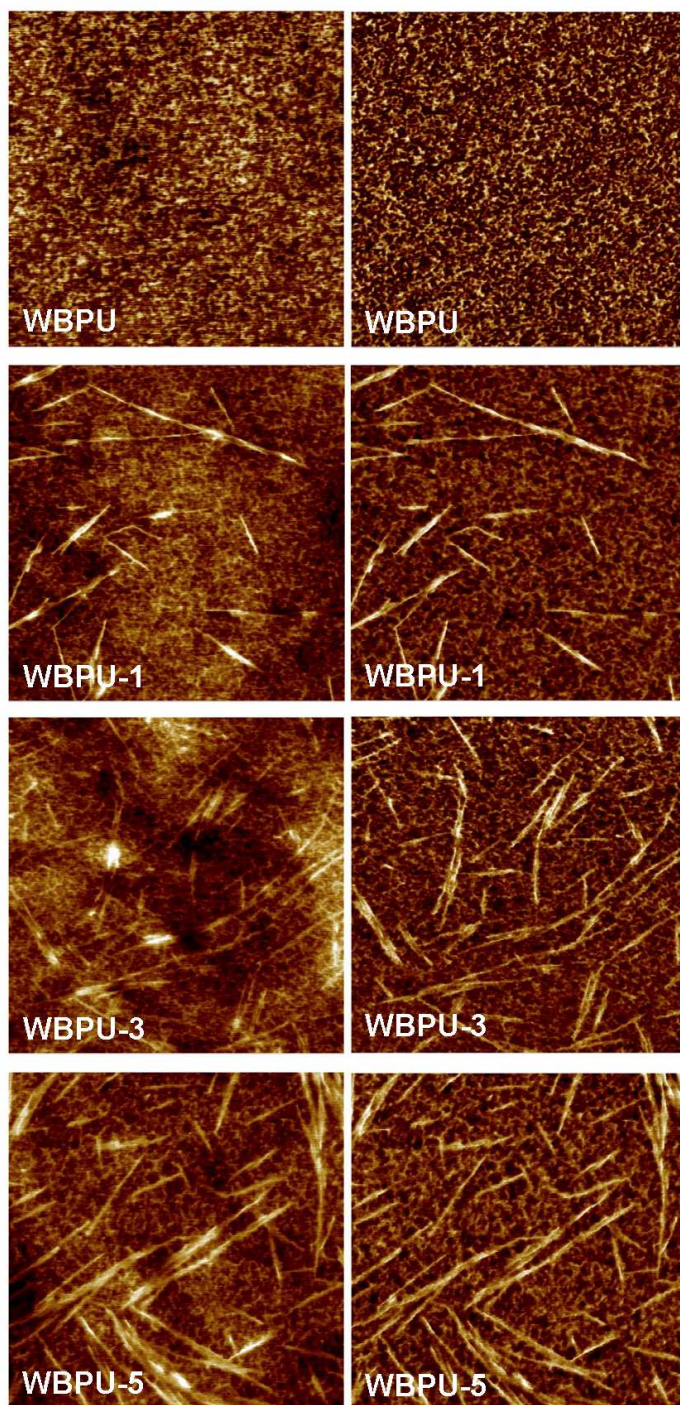
Figure 6.7 *AFM height (left) and phase (right) images of WBPU matrix and nanocomposites (size: 1x1 µm²)*

6.2.3 Conclusions

In this section, previously synthesized waterborne polyurethane of high hard segment content was employed for the preparation of nanocomposites with different CNC content, previously isolated from MCC, with an elevated L/D aspect ratio. DSC results revealed that low CNC content favored the crystallization of soft domains, while as CNC content was increased, in general, a progressive decrease in soft domains crystallization was observed due to the generation of WBPU-CNC interactions, as observed by FTIR. Furthermore, by a theoretical approach, a theoretical percolation threshold about 3 wt% was estimated and was experimentally corroborated. Mechanical tests showed a considerable improvement in stress at yield and modulus values when the percolation threshold was reached, as well as DMA results which showed that the thermomechanical stability enhancement was more remarkable at CNC 3 wt%. However, above percolation threshold, at 5 wt% of CNC, a decrease in mechanical and thermomechanical properties was observed due to the formation of some located agglomerates which acted as failure points. The presence of those agglomerates in 5 wt% of CNC film was observed by AFM. Nevertheless, the homogeneous dispersibility of CNC in the nanocomposites was also corroborated. Furthermore, WCA and WA measurements revealed an increase of the hydrophilic character of the films along with CNC addition.

6.3 Influence of waterborne polyurethane composition

6.3.1 WBPU-CNC nanocomposite films preparation

In order to analyze the effect of matrix composition, previously synthesized (chapter 3) two different WBPU dispersions were employed, WBPU and

WBPU$_{1.2}$, which differ in NCO/OH groups ratio. This section was focused on the effect of CNC incorporation attending to the microstructure of WBPU matrix. The suspension of CNC isolated in chapter 5 was employed in this section. Nanocomposite films were prepared by casting, following the same protocol employed previously in 6.2.1 section. Nanocomposites were coded as WBPU-X and WBPU$_{1.2}$-X, where X was referred to CNC weight content in the nanocomposite (1, 3 and 5 wt%).

6.3.2 Properties of WBPU-CNC and WBPU$_{1.2}$-CNC nanocomposites
6.3.2.1 Physicochemical, thermal, mechanical and thermomechanical properties

The effect of the matrix nature on the final properties of nanocomposites was analyzed by several physicochemical, thermal, mechanical and thermomechanical measurements. **Figure 6.8** shows FTIR spectra and DSC thermograms of WBPU and WBPU$_{1.2}$ and their respective nanocomposites.

The spectra of nanocomposites based on WBPU$_{1.2}$ were similar to the spectra of the homologous WBPU. In this way, considering amide I region one of the characteristic regions of waterborne polyurethanes in order to analyze the effect of NCO/OH groups ratio in the interactions between the matrix and CNC, only an amplification of the carbonyl region between 1800 and 1600 cm^{-1} is shown in **Figure 6.8a**.
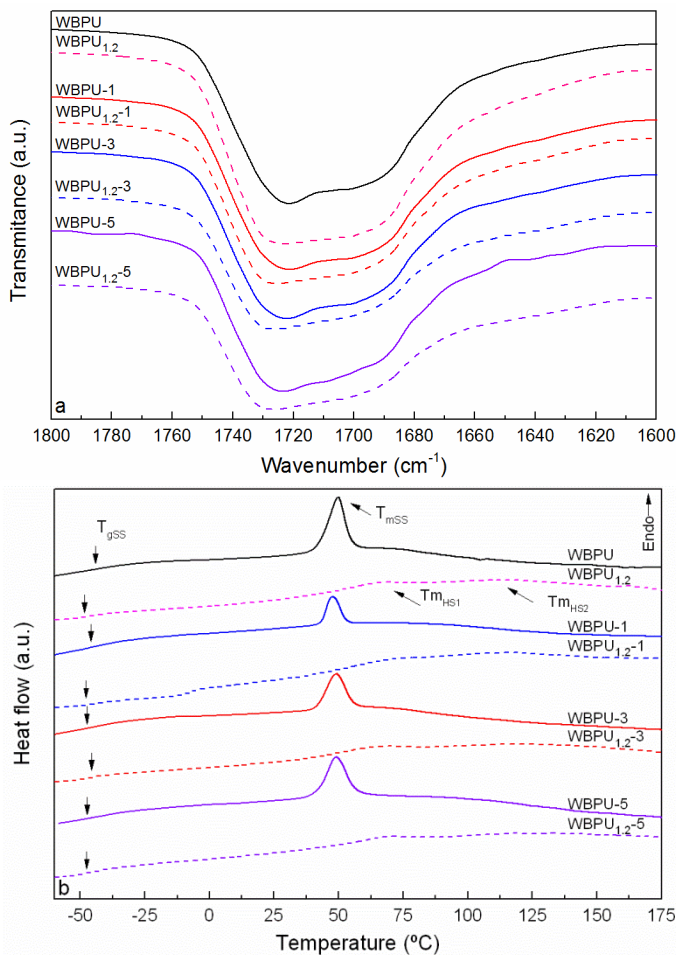
Figure 6.8 *a) Carbonyl stretching region of FTIR spectra and b) DSC thermograms of WBPU and WBPU_{1.2} matrices and their respective nanocomposites*

As in the case of previously discussed WBPU nanocomposites serie, analyzing the addition of CNC to WBPU_{1.2} matrix, it was observed that the peak corresponding to the free C=O groups shifted to higher wavenumbers and the shoulder associated to the hydrogen bonded C=O groups became broaden, suggesting that CNC incorporation favored the formation of new WBPU_{1.2}-CNC interactions.

Comparing thermograms obtained for both nanocomposites series, showed in **Figure 6.8b**, differences in soft and hard domains transitions were appreciated. **Figure 6.9** compares the glass transition temperature, melting temperature and enthalpy associated to the soft segment and melting temperatures and enthalpies associated to hard segment transitions of WBPU and WBPU$_{1.2}$ series and their evolution with CNC content is also displayed.
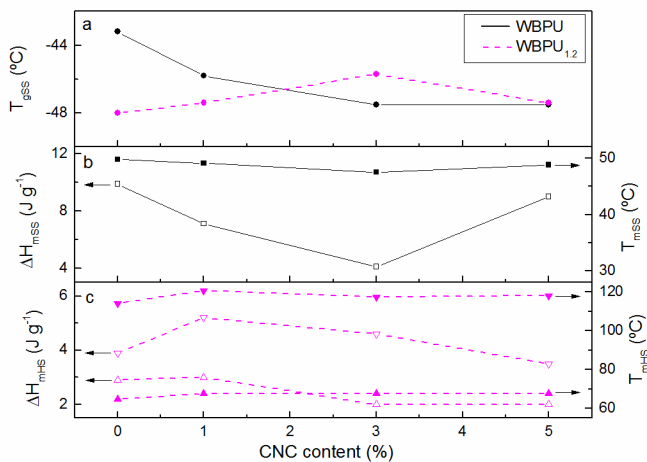
Figure 6.9 *a) (●) T_{gSS}, b) (■) T_{mSS} and (□) ΔH_{mSS}, c) (▲) T_{mHS1} and (△) ΔH_{mHS1}, (▼) T_{mHS2} and (▽) ΔH_{mHS2} thermal properties of WBPU (–) and WBPU$_{1.2}$ (- -) series*

The addition of CNC to WBPU matrix, as already discussed, hindered soft segment crystallization at 1 and 3 wt% of CNC [20] and seemed to favor at 5 wt% of CNC [21,22]. Concerning to WBPU$_{1.2}$ nanocomposites, the increase observed in short and long order range region temperatures suggested that CNC interacted with HS domains [9]. For 1 wt% of CNC, an increase in both, ΔH_{mHS1} and ΔH_{mHS2} was observed, indicating that CNC acted as nucleating agent promoting the ordered structures in the HS [6], discerning soft segment mobility

as observed by the increase of T_{gSS}. However, at high CNC content, despite nanocomposites presented higher T_{mHS} values than the matrix, lower ΔH_{mHS} were obtained, which could be attributed to the hindrance generated by the more ordered domains.

Regarding to mechanical and thermomechanical behavior, **Figure 6.10** shows stress-strain curves and DMA results.
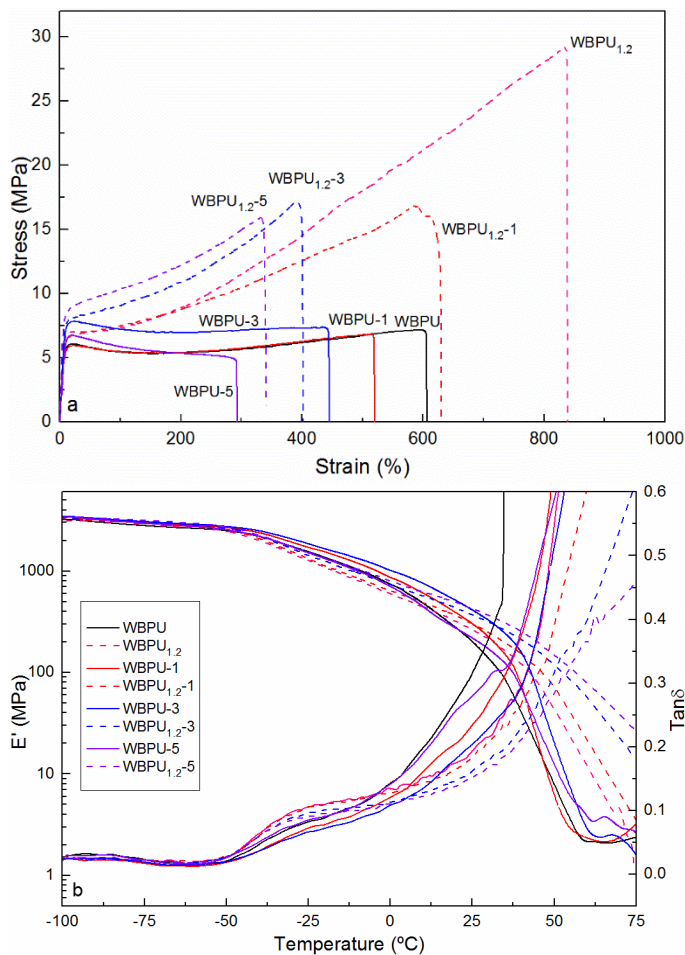
Figure 6.10 *a) Stress-strain curves and b) storage modulus and Tanδ curves of WBPU and WBPU$_{1.2}$ matrices and their respective nanocomposites*

From the stress-strain curves of **Figure 6.10a**, modulus, stress at yield, stress at break and strain at break values of both nanocomposites series with different CNC content were obtained and compared in **Figure 6.11**.
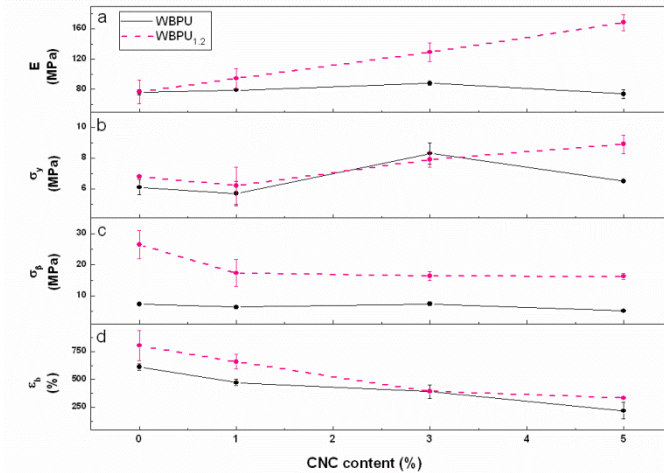
Figure 6.11 *a) Modulus, b) stress at yield, c) stress at break and d) strain at break values of WBPU (–) and WBPU$_{1.2}$ (- -) series*

The incorporation of CNC contributed to the increase of modulus and yield strength values, although considering the type of matrix, the enhancement was different. In the case of WBPU$_{1.2}$, CNC acted as nucleating agents inducing HS to order. However, in WBPU, as previously discussed, the restriction of SS crystallinity [13], caused a lower enhancement in E values. In turn, a progressive decrease in σ_b and ε_b values was observed independent of the matrix nature due to the matrix-CNC interactions, which decreased matrix mobility.

The thermomechanical properties of nanocomposites based on WBPU and WBPU$_{1.2}$ matrices were also compared in **Figure 6.10b**.

Analyzing the series, it was observed that storage modulus values of WBPU and their nanocomposites were maintained above WBPU$_{1.2}$ at low temperatures, as a

result of the soft segment ordered domains. Once soft segment fusion was reached, the cohesiveness of the material was collapsed and induced films to flow before in the case of WBPU serie. In this way, in WBPU$_{1.2}$ and their nanocomposites the thermomechanical stability was extended in about 15 °C due to the short and long range ordered regions as observed in DSC results, as well as by the WBPU-CNC interactions.

6.3.2.2 Hydrophilicity

Static water contact angle and water absorption measurements were carried out in order to analyze hydrophilicity of WBPU and WBPU$_{1.2}$ nanocomposites. Results are shown in **Figure 6.12**.

Concerning water contact angle values, it was observed a similar tendency in both nanocomposites series, which resulted in a decrease in WCA values with CNC incorporation due to the hydrophilic character of the reinforcement [15,16].

The water absorption in both nanocomposites series was compared in **Figure 6.12b**, where it was observed that the addition of CNC increased in both systems the water absorption capacity of the films, also due to the hydrophilicity of CNC [23,24]. Nevertheless, the water absorption ability of both matrices was different, which would be related with the microstructure of soft and hard segments. The formation of more ordered hard domains in the case of WBPU$_{1.2}$ serie, hindered in a greater extent the diffusion of water molecules trough the film comparing with WBPU serie.
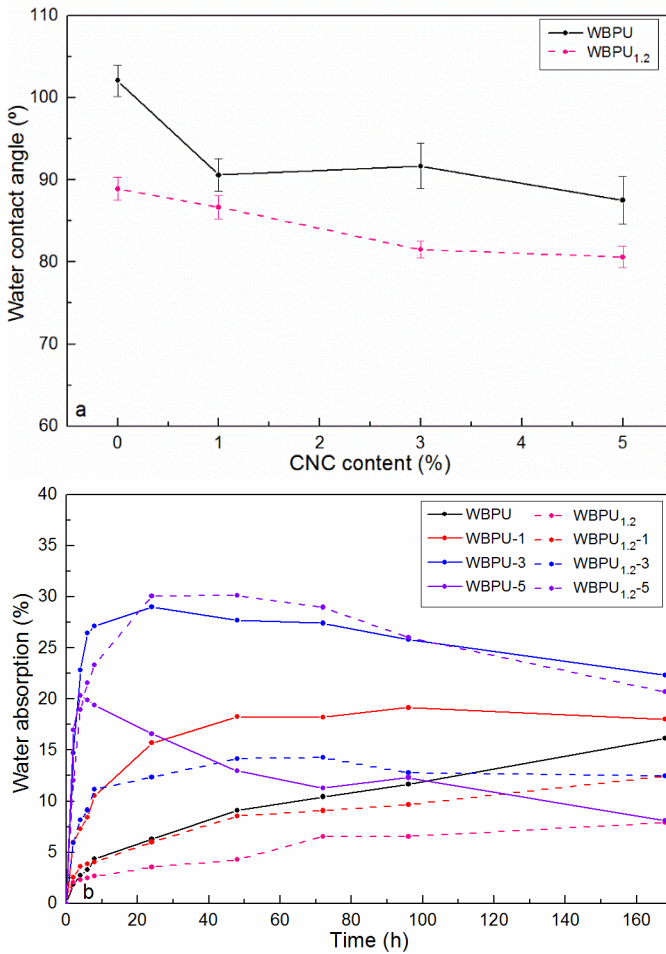
Figure 6.12 *a) Static water contact angle measurements and b) water absorption percentages over time of WBPU and WBPU$_{1.2}$ matrices and their respective nanocomposites*

6.3.2.3 Morphology

The morphology of WBPU and WBPU$_{1.2}$ matrices as well as the dispersion of CNC in their respective nanocomposites was analyzed by AFM. Phase images of 3 μm are shown in **Figures 6.13**.
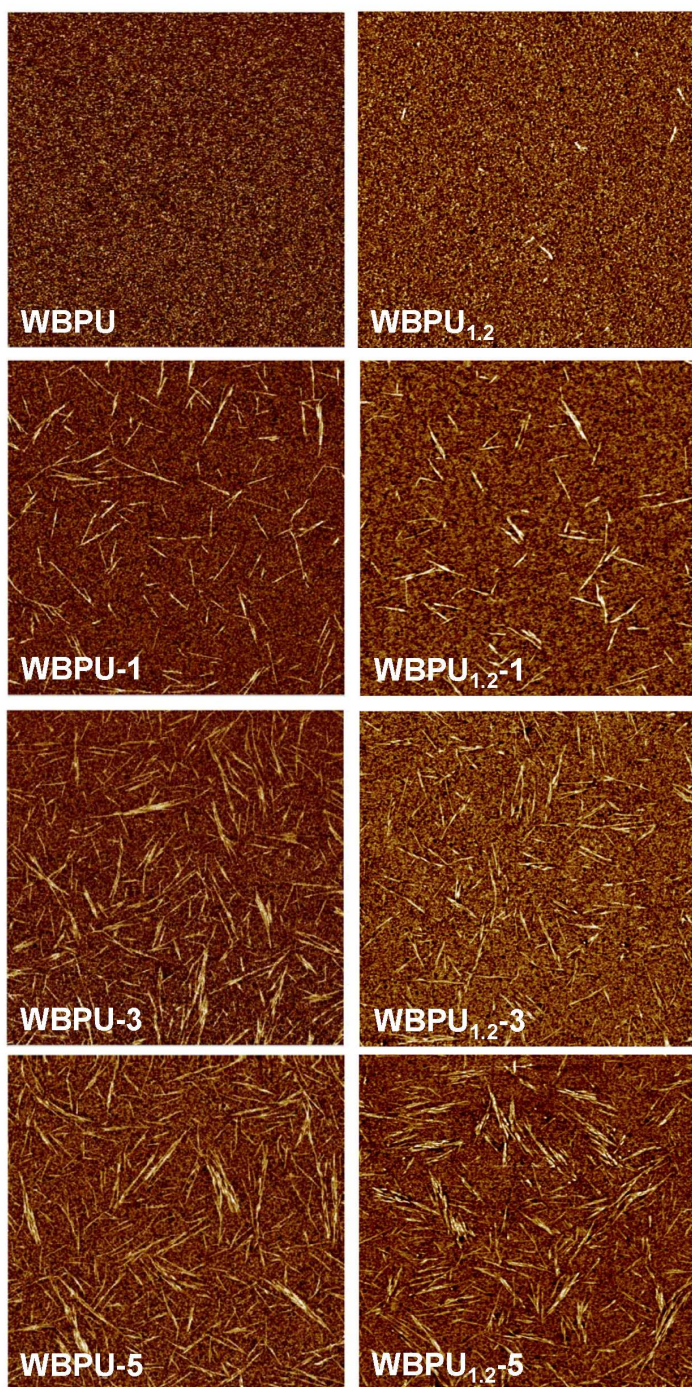
Figure 6.13 AFM phase images of WBPU (left) and WBPU1.2 (right) matrices and their respective nanocomposites (size: 3x3 μm²)

It was viewed the relative homogeneous CNC distribution in the *spin-coated* films of nanocomposites emphasizing the effective CNC incorporation in the matrices.

6.3.3 Conclusions

In this section, the effect of the matrix nature in the final properties of nanocomposites containing 1, 3 and 5 wt% of CNC were compared. While the addition of CNC to WBPU matrix contributed to the decrease in the crystallinity of the SS, the addition to $WBPU_{1.2}$, enhanced HS short and long order range regions since CNC acted as nucleating agents. In this way, an improvement of modulus and stress at yield values was observed in all CNC contents in $WBPU_{1.2}$ matrix serie. Furthermore, films based on $WBPU_{1.2}$ presented higher thermomechanical stability. Otherwise, CNC incorporation increased the hydrophilicity of both nanocomposites series. Regarding the surface hydrophilicity, WBPU nanocomposites serie showed more hydrophobic surfaces comparing with $WBPU_{1.2}$ serie. Nevertheless, WBPU serie exhibited greater water absorption capacity. This fact would be related with the microstructure adopted by the soft and hard segments that favored the diffusion of water molecules through the film in WBPU serie.

Thereby, the tailorable structure and properties of WBPU with enhanced properties by CNC incorporation, present the innovative opportunity of modulating the properties of the final material towards the desired application.

6.4 Influence of cellulose nanocrystals incoporporation route

6.4.1 WBPU-CNC nanocomposites preparation by in-situ incorporation route

In order to analyze the effect of CNC incorporation route, dispersions containing 1 and 3 wt% of CNC were prepared adding CNC during the waterborne polyurethane synthesis process. The molar ratio of IPDI/PCL/DMPA/BD was 3.15/0.5/0.5/2, the same as WBPU sample. This pathway will be coded as *in-situ* route. The effect of CNC arrangement in the WBPU matrix was analyzed in the alternative *in-situ* route and compared to the classical mixing by sonication route after WBPU synthesis, containing also 1 and 3 wt% of CNC. By *in-situ* route, previously sonicated CNC dispersion was incorporated to the polyurethane in the water addition step of the synthesis.

Nanocomposite films were also prepared by casting following previous protocol and drying conditions. Designation of obtained films is expressed as WBPU-X$_{\text{in-situ}}$, where X denotes CNC weight content in the nanocomposite. Films were also stored in a desiccator for 1 week before their characterization.

6.4.2 Characterization of WBPU-CNC nanocomposite dispersions

The particle size and distribution of *in-situ* synthesized WBPU-1$_{\text{in-situ}}$ nanocomposite dispersion are similar to the obtained previously for the WBPU matrix. In the case of WBPU-1$_{\text{in-situ}}$ a diameter and polydispersity values of 52.6 ± 0.2 nm and 0.06 ± 0.02 were obtained, respectively, whereas for WBPU sample 52.3 ± 0.5 nm and 0.08 ± 0.05 values were previously determined in chapter 3. It was observed that small particles with a narrow distribution were obtained, leading to visually stable dispersions over 6 months. Moreover, the addition of 1

wt% of CNC *in-situ* during the water addition process, did not affect the formation of the particles. Despite the higher length of CNC, the particle size and polydispersity were similar to the measured for the matrix. Instead, in the case of WBPU-3$_{in\text{-}situ}$, it was not possible to determine the particle size since the higher CNC content interfered in its determination.

6.4.3 Comparison of properties of WBPU-CNC nanocomposite films prepared by two different incorporation routes

6.4.3.1 Films appearance

WBPU-CNC nanocomposites films prepared by casting dispersions with CNC incorporated by *in-situ* route resulted in transparent films, in the same way as the films obtained from WBPU and CNC incorporated by mixing by sonication, as can be observed in **Figure 6.14**. In addition, all samples were completely soluble in THF and DMF.

Figure 6.14 *WBPU and nanocomposite films prepared by two CNC incorporation routes*

6.4.3.2 Physicochemical properties

The hydrogen bonding interactions between CNC and WBPU attending to the incorporation route, mixing by sonication or *in-situ*, were studied by FTIR. **Figure 6.15** shows the spectra of CNC, WBPU matrix and nanocomposites with 1 and 3 wt% of CNC.
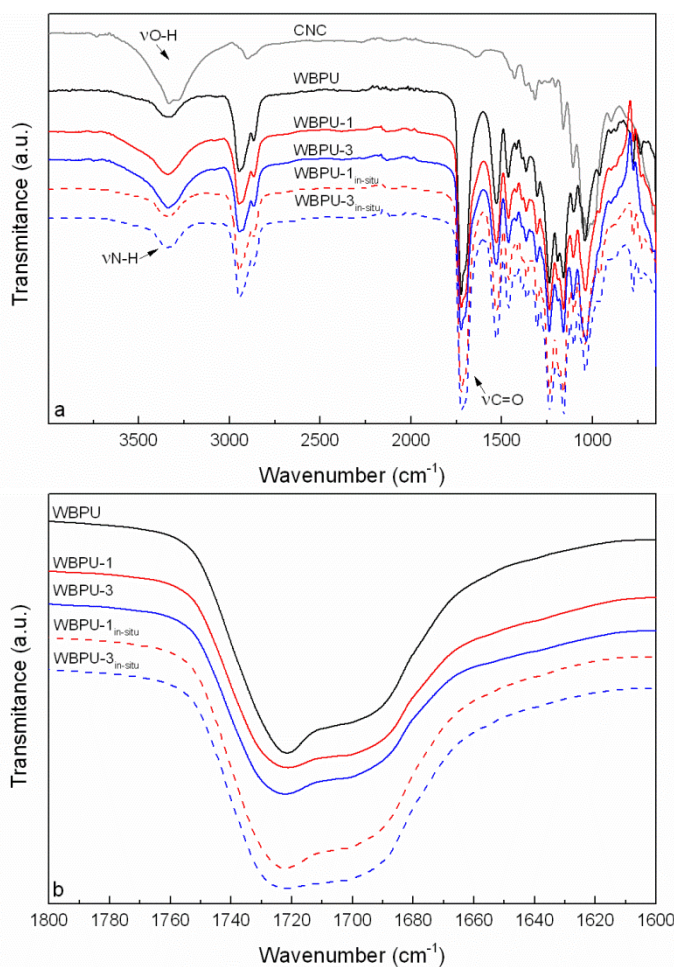
Figure 6.15 *a) FTIR spectra of CNC, WBPU matrix and nanocomposites and b) amplification of carbonyl stretching region*

Regarding FTIR spectra, two typical regions were analyzed, the interval from 3600 to 3100 cm^{-1}, where the stretching vibration related to N-H of urethane groups and OH stretching vibration of CNC were observed [9]. Slight differences were observed between nanocomposites. The peak about 3340 cm^{-1} was related with the N-H vibration of urethane groups associated by hydrogen bonding interactions. The extended shoulder around 3530 cm^{-1} observed in WBPU-1 and WBPU-3 samples related to CNC was barely noticeable in WBPU-1$_{in\text{-}situ}$ and WBPU-3$_{in\text{-}situ}$. It could be associated with the CNC disposition in the nanocomposite. In the case of mixing components by sonication, CNC were homogeneously dispersed in WBPU and OH groups of CNC were also appreciable by broadening the peak in that region to higher wavenumbers, similar to the peak observed in CNC spectrum. However, *in-situ* incorporation route favored the intercalation of CNC in WBPU particles during dispersion formation, and considering FTIR as surface physicochemical analysis, it is thought that CNC could result embedded in the matrix during film formation, hindering the visualization of CNC hydroxyl groups, but favoring interactions between them. In this way, a scheme of CNC disposition in the matrix considering the incorporation route is shown in **Figure 6.16**

Figure 6.15b shows the carbonyl stretching vibration region of spectra. Both nanocomposites presented similar features. The broadening and increase of the relative intensity of the peak related with the hydrogen bonded C=O groups around 1700 cm^{-1} respect to the free C=O groups about 1720 cm^{-1}, suggested the existence of WBPU-CNC interactions in the nanocomposites, which increased with CNC content, as was also previously discussed.
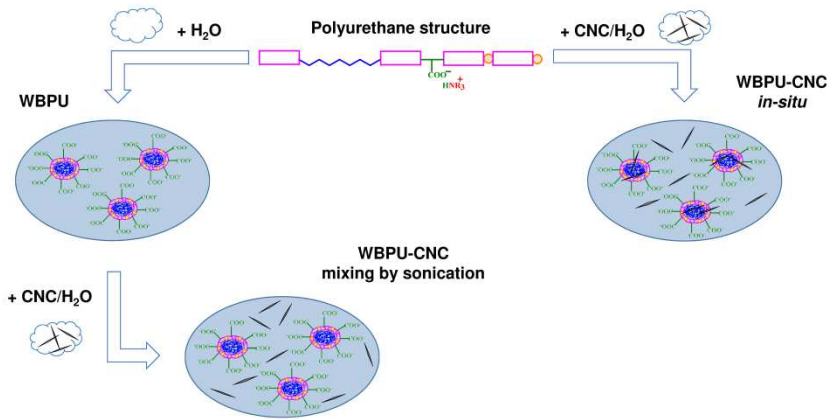
Figure 6.16 *Scheme of CNC disposition in WBPU matrix considering the two different incorporation routes for nanocomposites preparation*

6.4.3.3 Thermal properties

Thermal behavior of WBPU-X$_{in-situ}$ nanocomposite films was also studied by DSC and thermograms together with those of their homologues prepared by sonication and WBPU matrix are displayed in **Figure 6.17**.
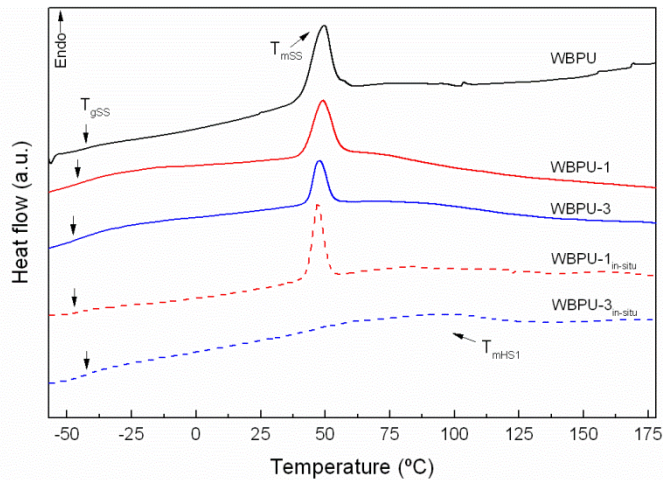
Figure 6.17 *DSC thermograms of WBPU matrix and nanocomposites prepared by two CNC incorporation routes*

Table 6.4 summarizes the thermal transition values corresponding to the soft domain glass transition temperature, melting temperature and enthalpy values of nanocomposites prepared by *in-situ* as well as the respective nanocomposites prepared by sonication route and WBPU matrix.

Table 6.4 *Thermal properties of WBPU matrix and nanocomposites prepared by two CNC incorporation routes*

Sample	T_{gSS} (°C)	T_{mSS} (°C)	ΔH_{mSS} (J g^{-1})	T_{mHS1} (°C)	ΔH_{mHS1} (J g^{-1})
WBPU	-42.7	49.5	10.8	-	-
WBPU-1	-45.8	49.1	7.1	-	-
WBPU-3	-47.5	47.5	4.1	-	-
WBPU-1$_{in\text{-}situ}$	-47.3	47.2	6.0	-	-
WBPU-3$_{in\text{-}situ}$	-42.0	-	-	83.9	15.4

Comparing both nanocomposites, it was observed that the addition of CNC by *in-situ* route resulted in lower T_{mSS} and ΔH_{mSS} values in WBPU-1$_{in\text{-}situ}$ comparing with WBPU-1, suggesting greater WBPU-CNC interactions, which would hinder in a greater extent crystals growth. Indeed, at higher CNC content, for WBPU-3$_{in\text{-}situ}$, soft domain crystallization was totally hindered. In this case, WBPU-CNC interactions led to a clearer broad transition around 84 °C related with the short range order of hard segment [25], which restricted soft segment chains mobility and increased slightly T_{gSS}.

Thermal stability of nanocomposite films was analyzed by TGA. **Figure 6.18** displays TGA and DTG curves of both nanocomposites, prepared by *in-situ* and and by sonication, as well as the WBPU matrix and CNC.
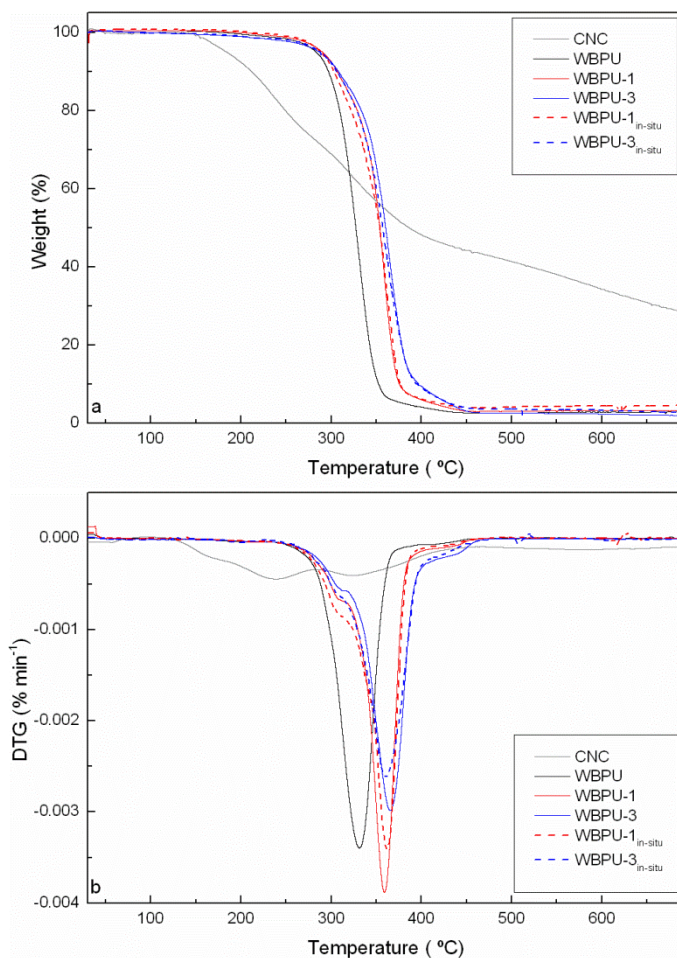
Figure 6.18 *a) TGA and b) DTG curves of CNC, WBPU matrix and nanocomposites prepared by two CNC incorporation routes*

The initial degradation temperature, the maximum degradation temperature and the temperature of the shoulder (T_s) observed in WBPU and nanocomposites obtained from the thermograms are summarized in **Table 6.5**.

In polyurethanes, a unique degradation stage as well as multiple degradation stages can be observed, influenced by the polyurethane nature, composition,

crystallinity and microphase separation degree of the system, among others [26–28].

Table 6.5 *Thermal stability properties of WBPU matrix and nanocomposites prepared by two CNC incorporation routes*

Sample	T_i (°C)	T_m (°C)	T_s (°C)
WBPU	281	331	-
WBPU-1	288	359	322
WBPU-3	287	365	316
WBPU-1in-situ	286	362	323
WBPU-3in-situ	288	361	313

In this case, the neat WBPU showed a single decomposition peak with the maximum degradation temperature centered at 331 °C, whereas in both nanocomposites a shoulder was also appreciated. Furthermore, an increase in T_i and T_m values of the nanocomposites was observed, comparing with the matrix, attributable to the stabilization of urethane groups by interactions of WBPU and CNC and the enhancement of the thermal resistance with CNC addition. Analyzing T_i and T_m values, the CNC addition by sonication and *in-situ* caused a delay of 5-7 °C in the start of the degradation process and a delay around 30 °C in the T_m values. This remarkable improvement, could be owed to a suitable dispersion of the CNC in the WBPU matrix [2,29] providing interactions. Analyzing CNC degradation curves, multiple decomposition steps were observed related with sulfate groups [30,31], where the maximum degradation temperatures were centered at 239 and 325 °C. Otherwise, the shoulder

observed around 315-320 °C in the degradation of the nanocomposites could be attributed to the less ordered domains induced by the interactions between WBPU and CNC in the polyurethane. In addition, both nanocomposites showed a similar degradation profile, suggesting that thermal stability was not so affected by CNC incorporation route.

6.4.3.4 Mechanical properties

The effect of CNC addition route in the mechanical behavior was analyzed performing tensile tests. For comparison, stress-strain curves of WBPU matrix as well as nanocomposites films obtained from both CNC incorporation routes are shown in **Figure 6.19**.
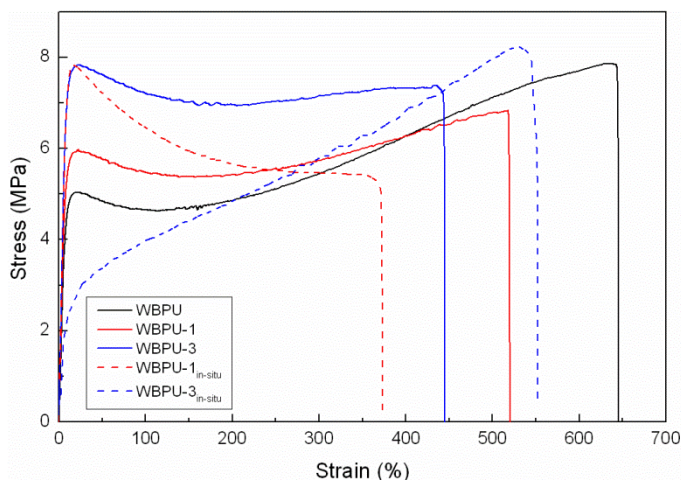
Figure 6.19 *Stress–strain curves of WBPU matrix and nanocomposites prepared by two CNC incorporation routes*

In order to analyze the effect of CNC addition, stress at yield, stress at break, modulus and strain at break values determined from the matrix and both type of nanocomposites curves are summarized in **Table 6.6**.

Table 6.6 *Mechanical properties of WBPU matrix and nanocomposites prepared by two CNC incorporation routes*

Sample	σ_y (MPa)	σ_b (MPa)	E (MPa)	ε_b (%)
WBPU	4.6 ± 0.3	7.9 ± 0.4	54.8 ± 5.7	735 ± 102
WBPU-1	5.7 ± 0.8	6.4 ± 0.5	79.0 ± 0.9	472 ± 29
WBPU-3	8.3 ± 0.7	7.4 ± 0.6	88.1 ± 2.5	391 ± 58
WBPU-1$_{in\text{-}situ}$	7.8 ± 0.3	5.5 ± 0.2	88.2 ± 5.9	374 ± 79
WBPU-3$_{in\text{-}situ}$	3.2 ± 0.1	8.4 ± 0.6	31.9 ± 3.3	533 ± 30

It was observed that mechanical properties depended on both, CNC content as well as CNC addition route. In the case of CNC addition by sonication, where WBPU soft segments ordered in crystalline domains, higher modulus and stress at yield values and lower strain at break values were obtained as CNC content was increased [19]. In the case of *in-situ* method and at 1 wt% of CNC, an increase in modulus and stress at yield values and a decrease in strain at break value were also observed comparing with the matrix. However at 3 wt% of CNC, modulus and stress at yield decreased, attributable to the absence of soft ordered domains, as observed previously by DSC results. In turn, stress at break and strain at break values increased respect to 1 wt% of CNC owing to the additional resistance provided by CNC and chain mobility. These improvements suggested the effective reinforcement effect caused by CNC due to new interactions with the WBPU, maintaining a suitable stress transfer in the nanocomposite besides their morphology with an elevated L/D aspect ratio [32]. Otherwise, due to NCO/OH groups ratio of 1.05, the possible reaction of residual isocyanate groups with hydroxyl groups of CNC could only occur by *in-situ*

method during water/CNC addition step, which could contribute to enhance the interactions between them [33]. By this way, tailored mechanical properties can be obtained attending to the CNC addition method as well as content. When CNC were added by sonication, the strain induced crystallization of the matrix was maintained. Nevertheless, when CNC were added during the synthesis process, the system resulted in sharper WBPU-CNC interactions, hindering the orientation and crystallization of the WBPU under strain [6].

6.4.3.5 Thermomechanical properties

The thermomechanical stability of the nanocomposite films obtained by *in-situ* route was analyzed by monitoring the evolution of storage modulus and Tanδ curves as a function of temperature, which are shown together with the WBPU matrix and nanocomposites prepared by sonication in **Figure 6.20**.
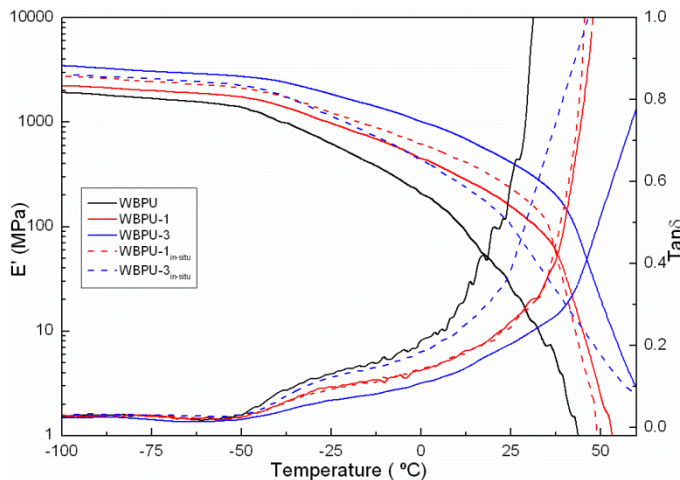
Figure 6.20 *Storage modulus and Tanδ curves of WBPU matrix and nanocomposites prepared by two CNC incorporation routes*

At low temperatures, in the glassy state, it was observed that nanocomposites showed higher E' values comparing with the matrix, which increased with CNC addition, due to the effective CNC reinforcement [11] and soft segment ordered structures. In the case of WBPU-3$_{in\text{-}situ}$, the absence of soft segment crystallization resulted in similar E' values to WBPU-1$_{in\text{-}situ}$. In the range between -50 and -30 °C, a pronounced decrease was observed owing to a glassy relaxation. This change in E' curves, generally reflected by a peak in Tanδ curves, was associated with the T$_{gss}$ of the films. Once amorphous WBPU chains acquired mobility, as temperature was increased, a progressive decrease was observed in E', resulting sharper next to soft segment crystalline domains melting transition. Afterwards, an abrupt drop was observed (between 30 and 50 °C) in agreement with DSC results. In the case of WBPU-3$_{in\text{-}situ}$, though E' values remained always above the matrix due to the reinforcement provided by the CNC, the absence of soft ordered domains led to the earlier E' drop as T$_{gss}$ was exceeded. Moreover, the effective CNC dispersion in the nanocomposites provided an improvement in the thermomechanical stability of nanocomposites. Regarding to the CNC reinforcement and incorporation route effect, it is possible to estimate the physical crosslinking density (vs/V) of the nanocomposites analyzing the E' in the rubbery plateau by the following **Equation 6.3** and **Equation 6.4** [34]:

$$^{vs}/_V = A exp\left(^{E_a}/_{RT}\right) \qquad (6.3)$$

$$E' = \left(^{vs}/_V\right)RT = ARTexp\left(^{E_a}/_{RT}\right) \qquad (6.4)$$

Equation 6.4, can be also expressed by:

$$\ln{E'}/_T = lnRA + {E_a}/_{RT} \qquad (6.5)$$

where A is a constant, E_a is the apparent activation energy of hydrogen bonding dissociation, R is the gas constant and T is the absolute temperature. Thereby, plotting ln E'/T versus 1/T, it is possible to determine E_a and A values from **Equation 6.5**. In this case, considering curves as straight lines, E_a values of 28.7, 20.2, 16.9, 18.3 and 25.1 kJ mol^{-1} and A values of 2.9×10^{-7}, 2.7×10^{-5}, 2.6×10^{-4}, 8.8×10^{-5} and 3.1×10^{-6} mol m^{-3} were determined for WBPU, WBPU-1, WBPU-3, WBPU-1$_{in\text{-}situ}$ and WBPU-3$_{in\text{-}situ}$ respectively. As a result, (vs/V) was quantified in function of temperature from **Equation 6.3** as it is displayed in **Figure 6.21**.
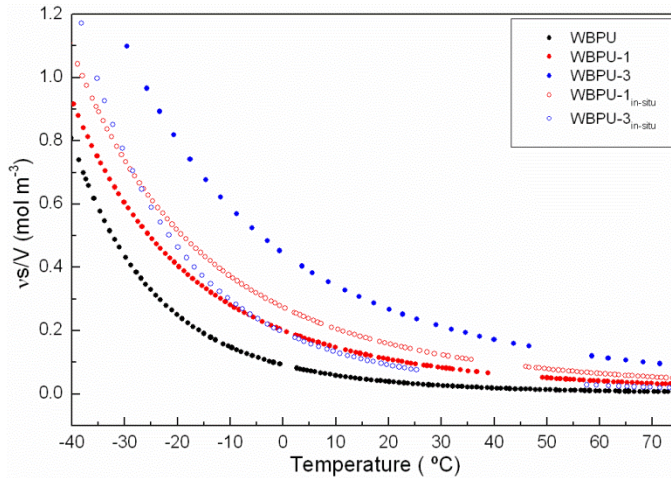
Figure 6.21 *Physical crosslinking density of WBPU matrix and nanocomposite films prepared by two CNC incorporation routes*

As it was expected, and in accordance with mechanical test results, the physical crosslinking density increased considerably with the addition of CNC, except for WBPU-3$_{in\text{-}situ}$ once T_{gss} was exceeded. In addition, it was appreciated a drop in

(vs/V) regarding to the crosslinking disruption as temperature increased, which was retarded with CNC incorporation, once again except for WBPU-3$_{in-situ}$. It could be attributed to the different structure adopted by the polyurethane in the WBPU-3$_{in-situ}$ as observed in DSC results.

6.4.3.6 Hydrophilicity

Dynamic contact angle values of WBPU matrix and nanocomposites, which reveal the hydrophilicity of the films, are shown in **Figure 6.22**.
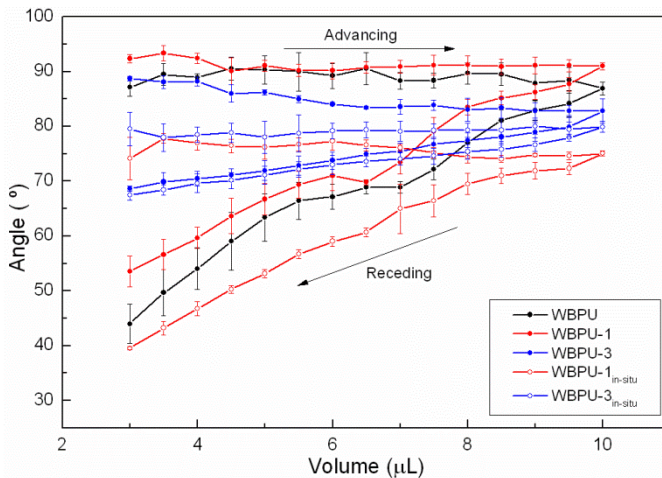
Figure 6.22 Advancing and receding water contact angles of WBPU matrix and nanocomposites prepared by two CNC incorporation routes

Generally, three main regions can be observed during dynamic water contact angle measurements. The first region corresponds to the advancing contact angle regime, where θ remains nearly constant while the drop volume and radius are increased. In this region, $θ_a$ is determined by averaging the advancing contact angle values measured in this domain [35]. In addition, usually the advancing contact angle values are quite similar to the values obtained by static contact

angle method [36]. In the region corresponding to the receding contact angle, generally lower contact angle values are obtained, and different slopes can be observed derived from the variations in water–surface interactions. The second region is related with the domain just after starting to reduce the volume of the drop, where the base diameter remains unchanged. The third region is related with the simultaneous reduction of the receding contact angle and drop base diameter [37]. Attending to the slope variation in the receding contact angles values curve, due to the second and third region, and considering this transition as θ_r [38], it is possible to calculate the equilibrium contact angle (θ_e) based on **Equation 6.6**, **Equation 6.7** and **Equation 6.8** proposed by Tadmor [38,39]:

$$\theta_e = arcos\left(\left(\Gamma_a \cos\theta_a\right) + \left(\Gamma_r \cos\theta_r\right) \middle/ \left(\Gamma_a + \Gamma_r\right) \right) \qquad (6.6)$$

$$\Gamma_a = \left(sin^3\theta_a \middle/ \left(2 - 3\cos\theta_a + cos^3\theta_a\right) \right)^{1/3} \qquad (6.7)$$

$$\Gamma_r = \left(sin^3\theta_r \middle/ \left(2 - 3\cos\theta_r + cos^3\theta_r\right) \right)^{1/3} \qquad (6.8)$$

Matrix and nanocomposite films showed the equilibrium contact angle values displayed in **Table 6.7**.

Table 6.7 *Equilibrium contact angle values of WBPU matrix and nanocomposites prepared by two CNC incorporation routes*

Sample	θ_e
WBPU	82.8
WBPU-1	84.8
WBPU-3	76.6
WBPU-1$_{in\text{-}situ}$	71.0
WBPU-3$_{in\text{-}situ}$	70.0

Equilibrium contact angle values indicated the different hydrophilic behavior of the nanocomposites even though having the same composition. Slightly higher θ_e value were obtained for WBPU-1 nanocomposite comparing with WBPU matrix, although higher CNC content induced to lower values. Instead, in the case of WBPU-1$_{in\text{-}situ}$, quite lower θ_e value were observed. It could be due to the arrangement of the CNC in the matrix. As it was viewed in WBPU-1 AFM images, CNC seemed to be deposited over the WBPU implying that probably, despite the hydrophilic character, CNC could interfere in the diffusion of water molecules through the film surface considering their high aspect ratio. The decrease in θ_e observed in WBPU-1$_{in\text{-}situ}$, up to 13°, suggested different disposition of CNC in the WBPU matrix. Instead, the lower decrease observed at higher CNC content, implied that in addition to CNC disposition, θ_e could be also influenced by the different microstructure adopted by the matrix, as observed in DSC results, where hard segment was able to arrange in short range ordered domains in WBPU-3$_{in\text{-}situ}$, hindering water molecules diffusion.

6.4.3.7 Morphology

The morphology of WBPU matrix and the effect of CNC incorporation route to the nanocomposites dispersions was analyzed by AFM. For comparison of both CNC incorporation routes, 5 and 1 μm height and phase AFM images of WBPU matrix and nanocomposites prepared by mixing by sonication are shown again together with AFM images obtained for nanocomposites prepared by *in-situ* in **Figures 6.23** and **Figure 6.24**.

Analyzing nanocomposites, independent of CNC addition route, light and dark regions were appreciated associated to the crystalline and amorphous domains observed for the WBPU matrix. Moreover, a homogeneous distribution of CNC in the WBPU was observed, without the presence of agglomerates implying the proper dispersion of the reinforcement in the matrix and the formation of WBPU–CNC interactions during film forming by casting. However, some differences were distinguished comparing both nanocomposites images. In the case of nanocomposites prepared by mixing by sonication, CNC in all of its length and dispersed homogeneously in the matrix were observed. In samples prepared by *in-situ* method instead, CNC seemed to be shorter despite possessing the same aspect ratio and that presented lower CNC quantity comparing with their respective nanocomposites prepared by mixing by sonication. So, this fact would imply that CNC were partially embedded in the matrix due to the greater intercalation among WBPU particles when were added during such particles formation.
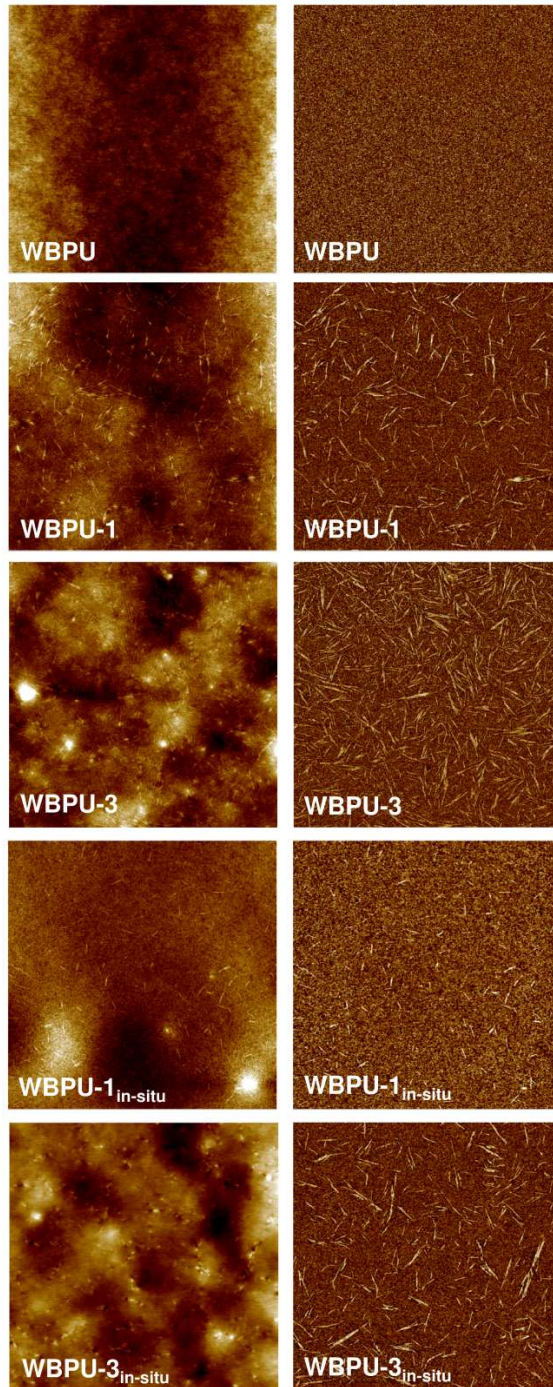
Figure 6.23 *AFM height (left) and phase (right) images of WBPU matrix and nanocomposites prepared by two CNC incorporation routes (size: 5x5 μm²)*
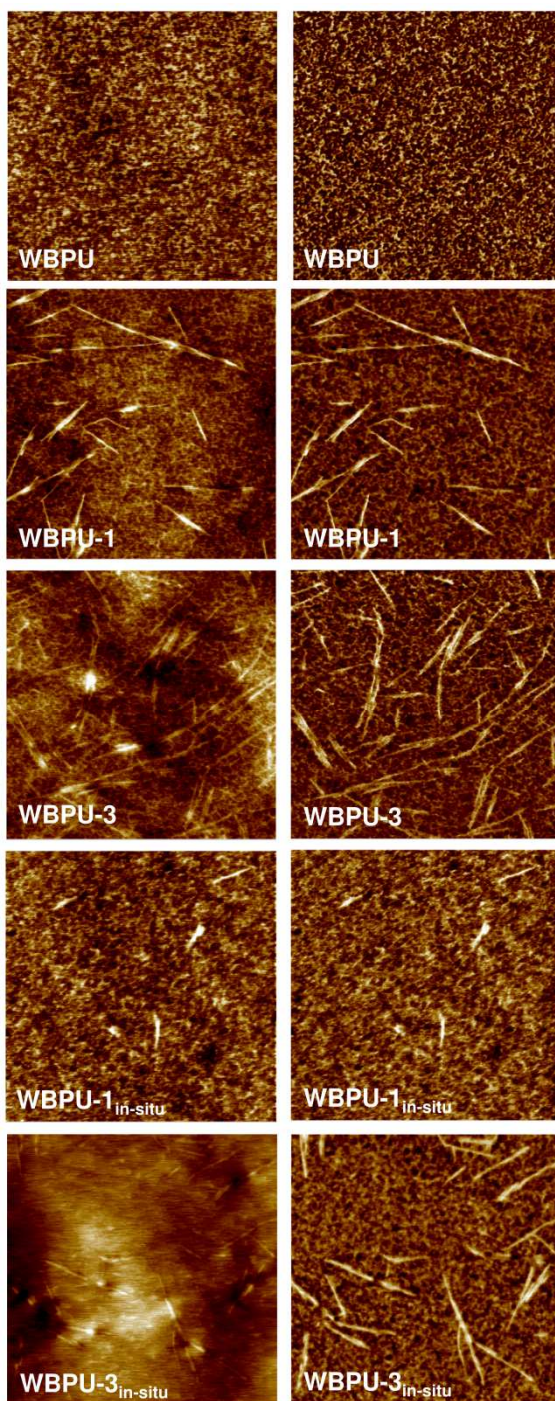
Figure 6.24 *AFM height (left) and phase (right) images of WBPU matrix and nanocomposites prepared by two CNC incorporation routes (size: 1x1 μm²)*

It is worth noting that in the case of WBPU-3$_{in\text{-}situ}$ the synthesized dispersion had to be diluted for the preparation of *spin-coated* sample in order to facilitate the observation of CNC by AFM. Although presenting the same solids content comparing with WBPU and WBPU-1$_{in\text{-}situ}$ samples, it was too viscous for preparing a thin film for the observation of CNC. As can be observed in **Figure 6.25**, the thickness for both WBPU-3$_{in\text{-}situ}$ samples (non-diluted and diluted) was measured. It was observed that the thickness was reduced from 1.40 ± 0.03 to 0.29 ± 0.00 μm facilitating thus CNC visualization.
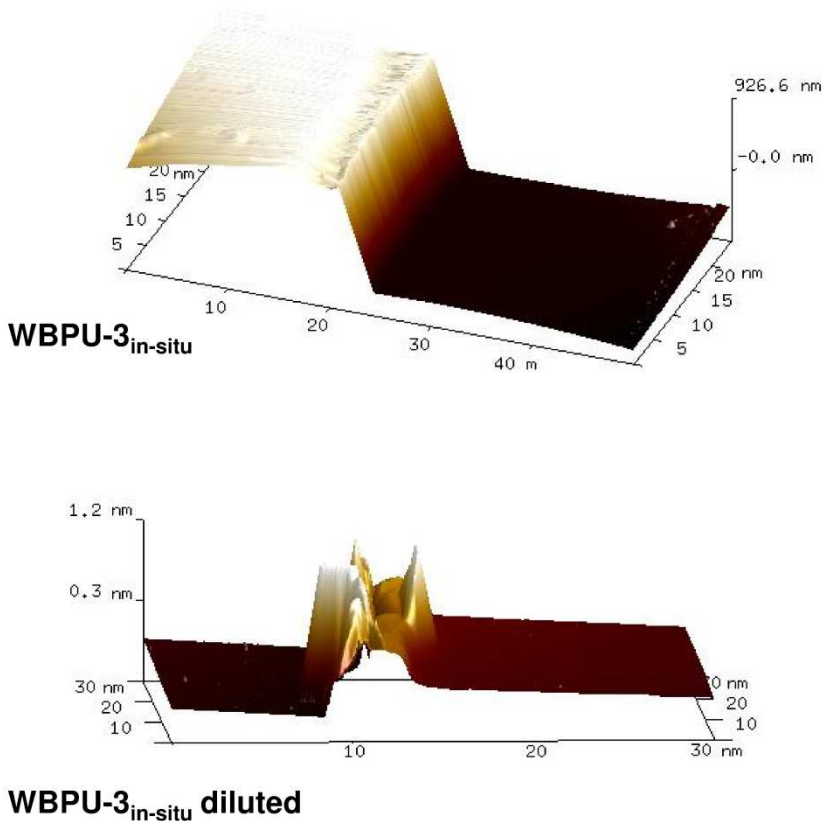
Figure 6.25 AFM height images of WBPU-3$_{in\text{-}situ}$ and diluted WBPU-3$_{in\text{-}situ}$ samples for thickness measurements

Furthermore, it should be noted that despite the dilution of WBPU-3$_{in\text{-}situ}$ sample, CNC seemed also shorter and lower in quantity comparing with WBPU-3, corroborating that CNC would be partially embedded in the matrix. Thereby, the diverse arrangement adopted by CNC in the nanocomposites, justified the variation in the physicochemical and mechanical properties of the films.

6.4.4 Conclusions

In this work, the alternative *in-situ* route was used to prepare homogeneous WBPU-CNC dispersions first, and thereafter by casting, nanocomposites films containing 1 and 3 wt% of high aspect ratio CNC. The homogeneous dispersion facilitated the suitable casting process promoting WBPU-CNC interactions during the transparent films formation. Results were compared with WBPU matrix and nanocomposites with the same CNC content prepared by mixing by sonication, in order to analyze the effect of CNC incorporation route and disposition in the matrix. AFM images showed a homogeneous distribution of CNC in both type of nanocomposites without the presence of agglomerates. The entire length of dispersed CNC were observed in nanocomposite prepared by casting whereas shorter CNC were observed in nanocomposite prepared by *in-situ*, suggesting that CNC were partially embedded in the matrix due to intercalation among WBPU particles when were added during such particles formation. FTIR results supported this observation. The alternative *in-situ* route resulted in enhanced WBPU-CNC interactions, which hinder the soft segments chains to arrange in ordered structures, avoiding even completely the crystallization of soft domain in WBPU-3$_{in\text{-}situ}$ sample. Thus, WBPU-CNC interactions provided higher E' values than the matrix and an improvement in

the thermomechanical stability. TGA results revealed also that WBPU-CNC interactions improved the stabilization of urethane groups delaying the T_m value about 30 °C comparing with the matrix. Regarding to mechanical properties of the films, it was observed that CNC addition route, as well as content, influenced in the mechanical performance of the films, showing always an effective reinforcing effect. Nanocomposites exhibited different hydrophilic behavior, which would be related with the disposition of CNC in the nanocomposite.

6.5 References

[1]   A. Santamaria-Echart, L. Ugarte, A. Arbelaiz, N. Gabilondo, M.A. Corcuera, A. Eceiza, Two different incorporation routes of cellulose nanocrystals in waterborne polyurethane nanocomposites, Eur. Polym. J. 76 (2016) 99–109.

[2]   H. Liu, S. Cui, S. Shang, D. Wang, J. Song, Properties of rosin-based waterborne polyurethanes/cellulose nanocrystals composites, Carbohydr. Polym. 96 (2013) 510–515.

[3]   B. Wunderlich, Thermal analysis of polymeric materials, Springer, 2005.

[4]   L. Rueda, A. Saralegui, B. Fernández, Q. Zhou, L.A. Berglund, M.A. Corcuera, et al., Cellulose nanocrystals/polyurethane nanocomposites. Study from the viewpoint of microphase separated structure, Carbohydr. Polym. 92 (2013) 751–757.

[5]   K. Benhamou, H. Kaddami, A. Magnin, A. Dufresne, A. Ahmad, Bio-based polyurethane reinforced with cellulose nanofibers: A comprehensive investigation on the effect of interface, Carbohydr. Polym. 122 (2015) 202–211.

[6]   A. Saralegi, L. Rueda, L. Martin, A. Arbelaiz, A. Eceiza, M.A. Corcuera, From elastomeric to rigid polyurethane/cellulose nanocrystal bionanocomposites, Compos. Sci. Technol. 88 (2013) 39–47.

[7]   Y. Habibi, L.A. Lucia, O.J. Rojas, Cellulose nanocrystals: Chemistry, self-assembly, and applications, Chem. Rev. 110 (2010) 3479–3500.

[8]   X. Cao, H. Dong, C.M. Li, New nanocomposite materials reinforced with flax cellulose nanocrystals in waterborne polyurethane, Biomacromolecules 8 (2007) 899–904.

[9]   Z. Gao, J. Peng, T. Zhong, J. Sun, X. Wang, C. Yue, Biocompatible elastomer of waterborne polyurethane based on castor oil and polyethylene glycol with cellulose nanocrystals, Carbohydr. Polym. 87 (2012) 2068–2075.

[10]   B. Ly, W. Thielemans, A. Dufresne, D. Chaussy, M.N. Belgacem, Surface functionalization of cellulose fibres and their incorporation in renewable polymeric matrices, Compos. Sci. Technol. 68 (2008) 3193–3201.

[11]   L. Rueda, B. Fernández d'Arlas, Q. Zhou, L.A. Berglund, M.A. Corcuera, I. Mondragon, A. Eceiza, Isocyanate-rich cellulose nanocrystals and their selective insertion in elastomeric polyurethane, Compos. Sci. Technol. 71 (2011) 1953–1960.

[12]   A. Pei, J.M. Malho, J. Ruokolainen, Q. Zhou, L.A. Berglund, Strong nanocomposite reinforcement efects in polyurethane elastomer with low volume fraction of cellulose nanocrystals, Macromolecules 44 (2011) 4422–4427.

[13]   M.L. Auad, M.A. Mosiewicki, T. Richardson, M.I. Aranguren, N.E. Marcovich, Nanocomposites made from cellulose nanocrystals and tailored segmented polyurethanes, J. Appl. Polym. Sci. 115 (2010) 1215–1225.

[14]   O.S. Kushwaha, C.V. Avadhani, R.. Singh, Effect of UV rays on degradation and stability of high performance polymer membranes, Adv. Mater. Lett. 5 (2014) 272–279.

[15]   A. Ashori, M. Babaee, M. Jonoobi, Y. Hamzeh, Solvent-free acetylation of cellulose nanofibers for improving compatibility and dispersion, Carbohydr. Polym. 102 (2014) 369–375.

[16]   M.A. Hubbe, D.J. Gardner, W. Shen, contact angles and wettability of cellulosic surfaces: A review of proposed mechanisms and test strategies, Bioresources 10 (2015) 8657–8749.

[17]   M. Mariano, N. El Kissi, A. Dufresne, Cellulose nanocrystals and related nanocomposites: Review of some properties and challenges., J. Polym. Sci. Part B 52 (2014) 791–806.

[18]   P. Schön, K. Bagdi, K. Molnár, P. Markus, B. Pukánszky, G.J. Vancso, Quantitative mapping of elastic moduli at the nanoscale in phase separated polyurethanes by AFM, Eur. Polym. J. 47 (2011) 692–698.

[19]   H. Liu, J. Song, S. Shang, Z. Song, D. Wang, Cellulose nanocrystal/silver

nanoparticle composites as bifunctional nanofillers within waterborne polyurethane, ACS Appl. Mater. Interf. 4 (2012) 2413–2419.

[20]   A.O. Sanches, L.H. Siliano Ricco, L.F. Malmonge, M.J. Da Silva, W.K. Sakamoto, J.A. Malmonge, Influence of cellulose nanofibrils on soft and hard segments of polyurethane/cellulose nanocomposites and effect of humidity on their mechanical properties, Polym. Test. 40 (2014) 99–105.

[21]   L. Rueda, A. Saralegi, B. Fernández-d'Arlas, Q. Zhou, A. Alonso-Varona, L. a. Berglund, I. Mondragon, M.A. Corcuera, A. Eceiza, In situ polymerization and characterization of elastomeric polyurethane-cellulose nanocrystal nanocomposites. Cell response evaluation, Cellulose 20 (2013) 1819–1828.

[22]   A. Santamaria-Echart, L. Ugarte, C. García-Astrain, A. Arbelaiz, M.A. Corcuera, A. Eceiza, Cellulose nanocrystals reinforced environmentally-friendly waterborne polyurethane nanocomposites, Carbohydr. Polym. 151 (2016) 1203–1209.

[23]   J. Mendez, P.K. Annamalai, S.J. Eichhorn, R. Rusli, S.J. Rowan, E.J. Foster, C. Weder, Bioinspired mechanically adaptive polymer nanocomposites with water-activated shape-memory effect, Macromolecules 44 (2011) 6827–6835.

[24]   K.L. Dagnon, A.E. Way, S.O. Carson, J. Silva, J. Maia, S.J. Rowan, Controlling the rate of water-induced switching in mechanically

dynamic cellulose nanocrystal composites, Macromolecules 46 (2013) 8203–8212.

[25] C. Fang, X. Zhou, Q. Yu, S. Liu, D. Guo, R. Yu, J. Hu, Synthesis and characterization of low crystalline waterborne polyurethane for potential application in water-based ink binder, Prog. Org. Coat. 77 (2014) 61–71.

[26] D.K. Chattopadhyay, D.C. Webster, Thermal stability and flame retardancy of polyurethanes, Prog. Polym. Sci. 34 (2009) 1068–1133.

[27] F.M.B. Coutinho, M.C. Delpech, T.L. Alves, A.A. Ferreira, Degradation profiles of cast films of polyurethane and poly(urethane-urea) aqueous dispersions based on hydroxy-terminated polybutadiene and different diisocyanates, Polym. Degrad. Stab. 81 (2003) 19–27.

[28] S.M. Cakic, J. V Stamenkovic, D.M. Djordjevic, I.S. Ristic, Synthesis and degradation profile of cast films of PPG-DMPA-IPDI aqueous polyurethane dispersions based on selective catalysts, Polym. Degrad. Stab. 94 (2009) 2015–2022.

[29] X. Cao, Y. Habibi, L.A. Lucia, One-pot polymerization, surface grafting, and processing of waterborne polyurethane-cellulose nanocrystal nanocomposites, J. Mater. Chem. 19 (2009) 7137–7145.

[30] M. Roman, W.T. Winter, Effect of sulfate groups from sulfuric acid hydrolysis on the thermal degradation behavior of bacterial cellulose,

Biomacromolecules 5 (2004) 1671–1677.

[31]   N. Wang, E. Ding, R. Cheng, Thermal degradation behaviors of spherical cellulose nanocrystals with sulfate groups, Polymer 48 (2007) 3486–3493.

[32]   Q. Zhao, G. Sun, K. Yan, A. Zhou, Y. Chen, Novel bio-antifelting agent based on waterborne polyurethane and cellulose nanocrystals, Carbohydr. Polym. 91 (2013) 169–174.

[33]   P.S. De Oliveira Patricio, I.M. Pereira, N.C. Ferreira Da Silva, E. Ayres, F. Vargas Pereira, R. Lambert Oréfice, Tailoring the morphology and properties of waterborne polyurethanes by the procedure of cellulose nanocrystal incorporation, Eur. Polym. J. 49 (2013) 3761–3769.

[34]   Y. Wang, H. Tian, L. Zhang, Role of starch nanocrystals and cellulose whiskers in synergistic reinforcement of waterborne polyurethane, Carbohydr. Polym. 80 (2010) 665–671.

[35]   C.N.C. Lam, R. Wu, D. Li, M.L. Hair, A.W. Neumann, Study of the advancing and receding contact angles: Liquid sorption as a cause of contact angle hysteresis, Adv. Colloid Interface Sci. 96 (2002) 169–91.

[36]   D. Polster, H. Graaf, Advancing and receding angles-dynamic contact angle measurements on mixed alkyl monolayers, Appl. Surf. Sci. 265 (2013) 88–93.

[37]   P.R. Waghmare, S.K. Mitra, Contact angle hysteresis of microbead suspensions, Langmuir 26 (2010) 17082–17089.

[38]   W. Zhang, P.R. Waghmare, L. Chen, Z. Xu, S.K. Mitra, Interfacial rheological and wetting properties of deamidated barley proteins, Food Hydrocoll. 43 (2015) 400–409.

[39]   R. Tadmor, Line energy and the relation between advancing, receding, and young contact angles, Langmuir 20 (2004) 7659–7664.

CHAPTER 7

Waterborne polyurethane-urea cellulose

nanocrystals nanocomposites

"Nada en este mundo sucede por casualidad"

7. WATERBORNE POLYURETHANE-UREA CELLULOSE NANOCRYSTALS NANOCOMPOSITES

7.1 Objective

Taking into account that the addition of CNC modulates the final properties of WBPU, in this chapter the effect of CNC incorporation to WBPUU will be analyzed. Therefore, in this chapter, a serie of nanocomposites was prepared using a previously analyzed WBPUU matrix (chapter 4) loaded with different cellulose nanocrystals contents (from 0 to 5 wt%). WBPUU0.6$_{hom}$ was selected since it presented the highest similarity (52 wt% HS and IPDI/PCL:/DMPA/BD/EDA molar ratio of 3.6/0.5/0.5/2/0.6) to the WBPU matrix (48.3 wt% HS and IPDI/PCL/DMPA/BD molar ratio of 3.15/0.5/0.5/2) employed in previously analyzed nanocomposites. In this way, nanocomposites films were prepared by casting and a comprehensive study was carried out focusing on the effect of CNC content in the final properties of the films from the viewpoint of physicochemical, thermal, mechanical, thermomechanical and hydrophylicity properties as well as morphology.

7.2 Experimental

7.2.1 WBPUU-CNC nanocomposite films preparation

WBPUU-CNC nanocomposites were prepared by casting following the same protocol used for WBPU films preparation. Nanocomposites containing 0.5, 1, 3 and 5 wt% of CNC were prepared adding CNC to WBÛU0.6$_{hom}$ the dispersion by mixing by sonication. The matrix was also prepared as reference in the same conditions. In order to simplify the designation of samples, the matrix was

denoted as WBPUU, instead of WBPUU0.6$_{hom}$, and nanocomposites as WBPUU-X, where X was referred to CNC weight content in the nanocomposite.

7.3 Results and discussion

7.3.1 Properties of WBPUU-CNC nanocomposites

7.3.1.1 Physicochemical properties

CNC, WBPUU and nanocomposites characteristic functional groups were characterized by FTIR and the spectra are shown in **Figure 7.1**.

Nanocomposites FTIR spectra showed a progressive increase in the N-H stretching vibration region of the WBPUU, which became sharper with CNC addition due to the overlapping with the O-H groups peak of CNC in that region. Nanocomposites showed another characteristic band in amide I region showed in **Figure 7.1b**, between 1800 and 1600 cm^{-1} related with the carbonyl groups of PCL, urethane and urea groups which shifted to different wavenumbers depending the nature and hydrogen bonding ability of C=O groups [1]. Regarding nanocomposites, it was observed that the addition of CNC promoted that the peak about 1720 cm^{-1} observed in WBPUU shifted to higher wavenumbers, whereas the shoulder at 1700 cm^{-1} was broaden to lower wavenumbers as in the case of WBPU nanocomposite serie. This fact indicated that CNC influenced in the disruption of hydrogen bonds, resulting in greater free C=O groups. Anyway, CNC favored the generation of new hydrogen bonding interactions supported by the broadening of the shoulder to lower wavenumbers.
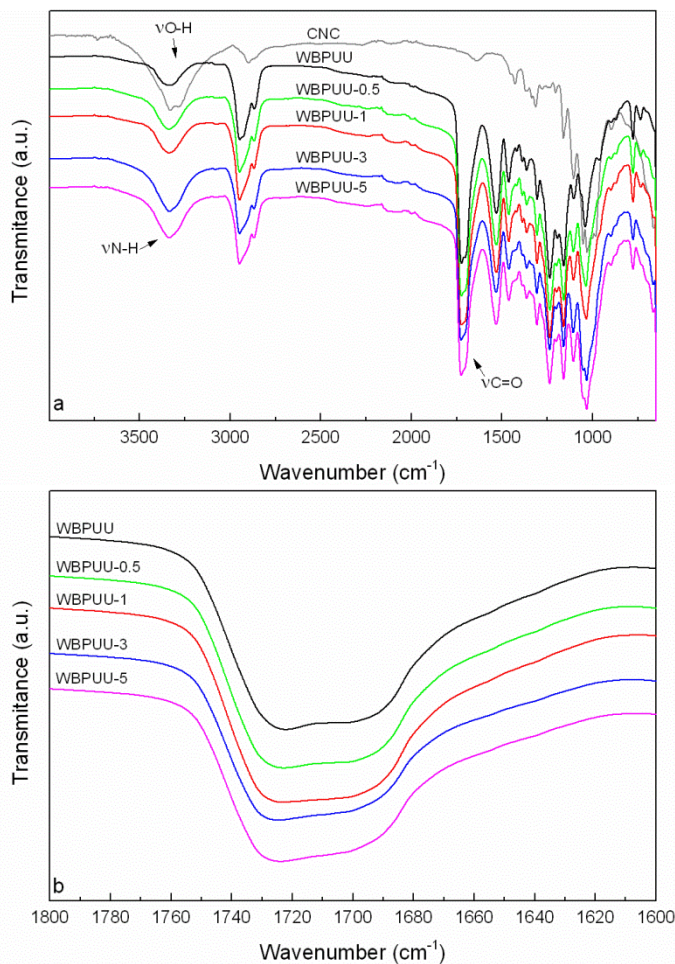
Figure 7.1 *a) FTIR spectra of CNC, WBPUU matrix and nanocomposites and b) amplification of carbonyl stretching region*

7.3.1.2 Thermal properties

Thermal behavior of WBPUU matrix and nanocomposites films was analyzed by DSC and thermograms are shown in **Figure 7.2**.
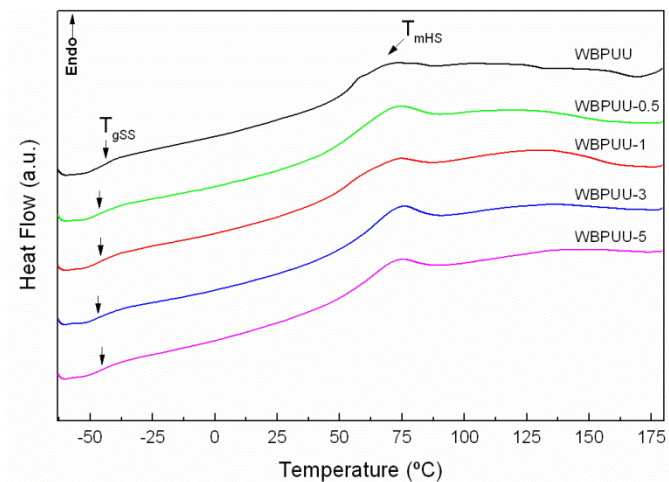
Figure 7.2 *DSC thermograms of WBPUU matrix and nanocomposites*

Soft segment glass transition temperature, and hard segment melting temperature and enthalpy obtained from thermograms are shown in **Table 7.1**.

Table 7.1 *Thermal properties of WBPUU matrix and nanocomposites*

Sample	T_{gSS} (°C)	T_{mHS} (°C)	ΔH_{mHS} (J g^{-1})	X_{cHS}
WBPUU	-43.7	68.7	6.5	1
WBPUU-0.5	-46.4	71.4	7.0	1.08
WBPUU-1	-45.7	72.1	5.73	0.89
WBPUU-3	-47.1	73.4	6.5	1.03
WBPUU-5	-45.7	72.7	5.8	0.94

Regarding soft segment, it was observed that in general, CNC addition conferred greater mobility to amorphous soft segment domains, resulting in lower T_{gSS} values [2]. Otherwise, with the purpose of interpreting the transition associated

to the short range order transition of hard segment [3], the relative hard segment crystallinity of nanocomposites (χ_{cHS}) with respect to the neat WBPUU was determined. In this way, it was possible to analyze in more detail HS behavior in each nanocomposite. Thus, χ_{cHS} was calculated by means of the following **Equation 7.1** [4]:

$$\chi_{cHS} = \frac{\Delta H_{mHS}}{\omega \cdot \Delta H_{100}}$$

(**7.1**)

where ΔH_{100} is referred to the melting enthalpy of the neat WBPUU, ω the weight fraction of WBPUU in the nanocomposite and ΔH_{mHS} the melting enthalpy of the corresponding nanocomposite. It has to be worth noting that CNC addition provided higher T_{mHS} values comparing with the matrix, indicating that CNC acted as nucleating agent [5,6]. At low CNC content (0.5 wt%) it was observed that CNC could act as nucleating points, resulting in higher T_{mHS} and enthalpy, obtaining thus slightly higher relative hard segment crystallinity. Despite nanocomposites presented higher T_{mHS} values than the matrix, ΔH_{mHS} tended to decrease, which could be attributed to the hindrance generated by the higher ordered domains.

7.3.1.3 Mechanical properties

Mechanical behavior of WBPUU matrix and nanocomposites is shown by stress-strain curves in **Figure 7.3**.
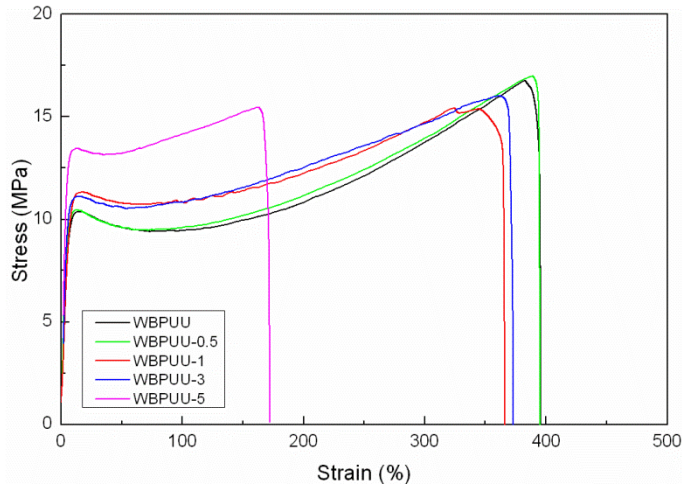
Figure 7.3 *Stress-strain curves of WBPUU matrix and nanocomposites*

Yield stress, stress at break, tensile modulus and strain at break values of WBPUU matrix and nanocomposites films obtained from the stress-strain curves are summarized in **Table 7.2**.

Table 7.2 *Mechanical properties of WBPUU matrix and nanocomposites*

Sample	σ_y (MPa)	σ_b (MPa)	E (MPa)	ε_b (%)
WBPUU	10.6 ± 0.6	16.9 ± 1.5	169.3 ± 5.0	389 ± 20
WBPUU-0.5	10.2 ± 1.1	16.0 ± 1.9	186.9 ± 24.8	377 ± 23
WBPUU-1	11.5 ± 0.6	16.0 ± 1.2	194.5 ± 19.9	334 ± 9
WBPUU-3	11.3 ± 0.8	15.5 ± 1.0	218.8 ± 14.7	333 ± 53
WBPUU-5	13.4 ± 0.3	15.5 ± 0.7	317.4 ± 26.0	189 ± 37

It was observed that CNC contributed to the increase of E maintaining σ_y, σ_b and ε_b values similar to those of the matrix in the case of nanocomposites with up to 3 wt% of CNC. This fact was related with the effective CNC reinforcement

effect [7], resulting in stiffer films. At 5 wt% of CNC content, ε_b was considerably reduced due to the restriction of WBPUU chains mobility by CNC addition [2].

7.3.1.4 Thermomechanical properties

The thermomechanical behavior of WBPUU matrix and nanocomposite films was studied by DMA, analyzing the evolution of storage modulus and Tanδ with increasing temperature, as is shown in **Figure 7.4**.
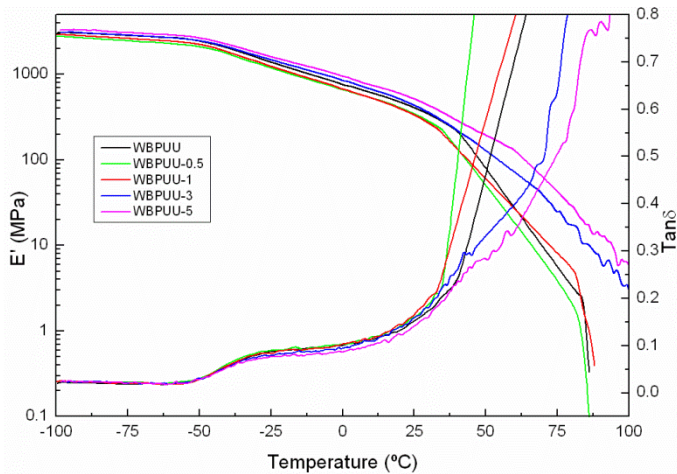
Figure 7.4 *Storage modulus and Tanδ curves of WBPUU matrix and nanocomposites*

It was observed that in the glassy state all samples showed similar E' values, although slightly higher values were reached in the case of high CNC contents (3 and 5 wt%). At higher temperatures, in the range between –50 and -30 °C, a drop in E' curves was observed associated to the T_{gSS} of films. This transition was also reflected as a peak in Tanδ curves. It was observed that the peak resulted broader and less intense at high CNC contents, where the influence of CNC in

the restriction of WBPUU chains mobility would be more notable [8–11]. As temperature was increased, at low CNC contents (0.5 and 1 wt%), lower E' values were observed in both cases comparing with the matrix. This fact could be ascribed to the low CNC content and the way of interfering in the WBPUU neat interactions. Nevertheless, it is worth noting that the thermomechanical stability of WBPUU-1 nanocomposite was slightly enhanced. Nanocomposites loaded with 3 and 5 wt% of CNC, E' curves showed higher values comparing with the matrix, attributed to the effective reinforcement effect of CNC, providing more interactions with the matrix, as observed by FTIR, and conferring higher rigidity to the nanocomposites [12]. Furthermore, the second drop in E' curves referred to melting of the short range order of hard segment domains was significantly retarded denoting the higher thermomechanical stability of nanocomposites to start flowing, conferred by CNC incorporation [13].

7.3.1.5 Hydrophilicity

The hydrophilicity of WBPUU matrix and nanocomposites films was analyzed by static water contact angle measurements and water absorption measurements. Water contact angle values are summarized in **Table 7.3**.

Concerning contact angle measurements, 90° is the reference value, which differs the hydrophobic (>90°) or hydrophilic (< 90°) character of films surface [1]. WBPUU matrix showed a moderate hydrophilic character showing a value around 79°. In the case of nanocomposites, the incorporation of CNC contributed to a slightly more hydrophilic character of the films.

Table 7.3 *Static water contact angle values of WBPUU matrix and nanocomposites*

Sample	Angle (°)
WBPUU	79.1 ± 0.7
WBPUU-0.5	78.9 ± 1.4
WBPUU-1	79.9 ± 0.2
WBPUU-3	77.8 ± 0.6
WBPUU-5	76.8 ± 0.8

Nevertheless, WCA values did not varied significantly. This fact could be related with the structure adopted by the WBPUU matrix. As observed in DSC results, CNC acting as nucleating agents may remain more covered, which could restrict the ability of water molecules to interact in the surface of films despite the hydrophilic character of CNC [14]. Furthermore, the similar deviation values (1-2°) observed in the nanocomposites, suggested the homogeneous surface of films. In order to analyze the hydrophilic behavior of WBPUU matrix and nanocomposites immersed in water, water absorption measurements at 25 °C were carried out, and curves are shown in **Figure 7.5**.

Analyzing the results it was observed that in general, CNC incorporation contributed to the greater capacity of water absorption in the nanocomposites, considering that water molecules tend to diffuse where CNC nanoentities are located [15]. At low CNC contents (0.5 wt%), it was observed an analogous to matrix water absorption behavior, showing a similar water diffusion process but greater absorption capacity due to the hydrophilic character of CNC [16]. At higher CNC content, the water absorption behavior changed, where it was appreciated a sharp increase in water absorption percentages at low times, which was reduced and stabilized at longer time.
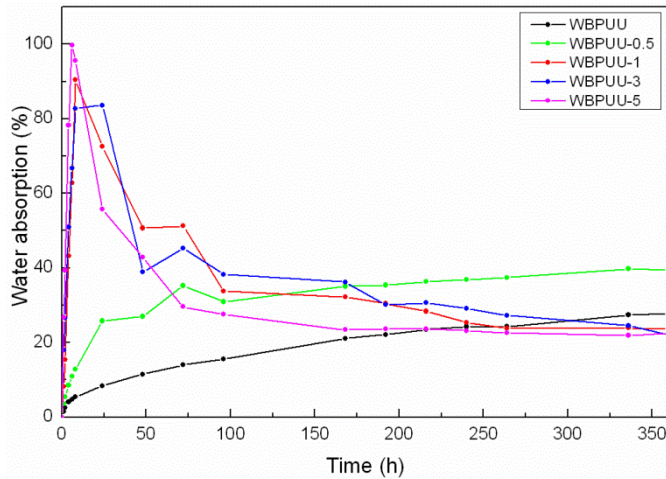
Figure 7.5 *Water absorption percentages of WBPUU matrix and nanocomposites films over time*

Furthermore, it was observed that water absorption capacity increased with CNC content, but influenced by WBPUU microstructure [17]. In the case of WBPUU-1, the lower crystallinity degree would favor slightly the diffusion of water molecules through the film as consequence of presenting greater quantity of amorphous regions. At higher CNC contents, both the microstructure and CNC content, contribute to the increase of water absorption at low times.

7.3.1.7 Morphology

The morphology of WBPUU and the dispersion of CNC in the nanocomposites were analyzed by AFM, and the height and phase images of 5 and 1 μm are shown in **Figures 7.6** and **Figure 7.7**.
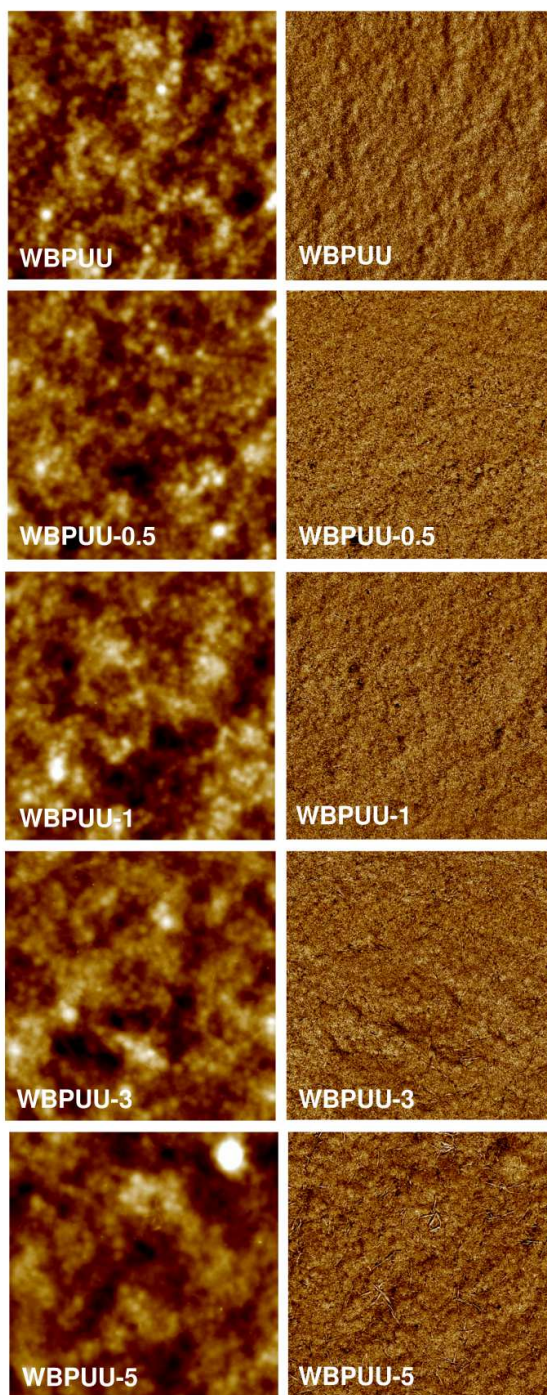
Figure 7.6 *AFM height (left) and phase (right) images of WBPUU matrix and nanocomposites (size: 5x5 µm²)*
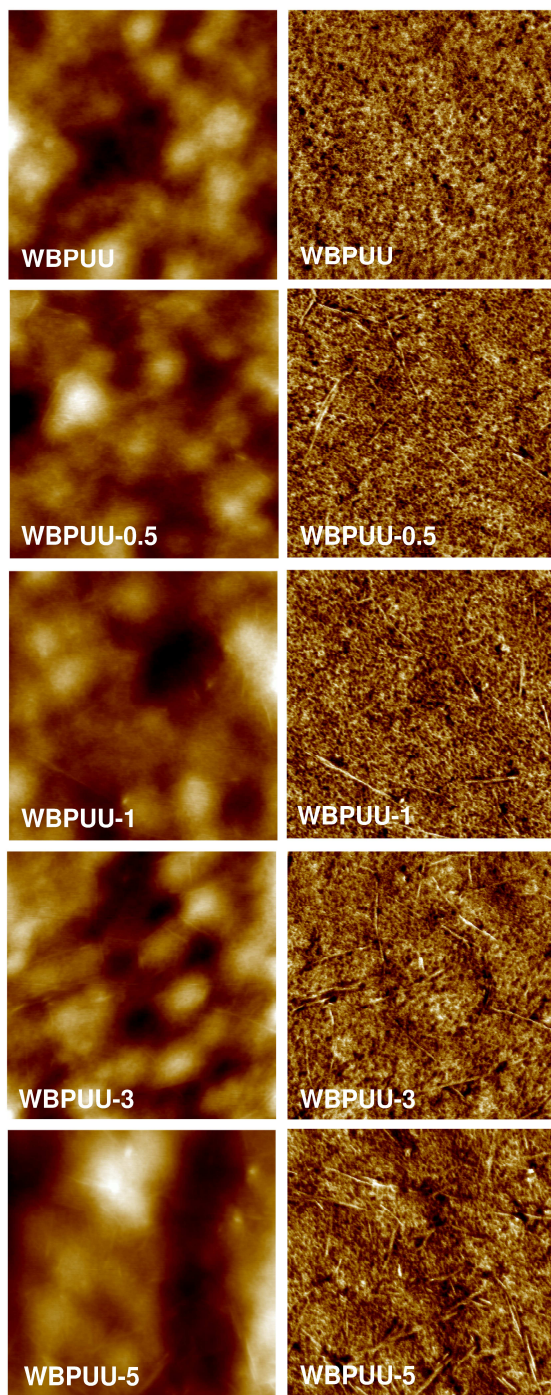
Figure 7.7 *AFM height (left) and phase (right) images of WBPUU matrix and nanocomposites (size: 1x1 μm²)*

AFM images showed WBPUU matrix morphology, where bright and dark regions were appreciated, related to the hard and soft domains, being indicative of the existence of a microphase morphology [18]. Furthermore, it was observed that CNC incorporation hardly varied the morphology of the matrix. Analyzing AFM height and phase images, the presence of greater quantity of CNC was appreciated. Moreover, it is worth noting that CNC showed a suitable dispersion, being homogeneously distributed in the matrix [19]. In this way, AFM images supported the idea that the creation of WBPUU-CNC interactions was facilitated as it was observed in FTIR and DSC results.

In addition, as it can be seen in **Figure 7.6** and **Figure 7.7** AFM images, CNC seemed to be surrounded by WBPUU, which could be the responsible of the little variation in the hydrophilicity of nanocomposites films surface, reflected in the similar SWCA values.

7.4 Conclusions

In this chapter, a serie of nanocomposites loaded with different CNC contents (from 0 to 5 wt%) were prepared by casting from a previously synthesized WBPUU. The morphological analysis by AFM corroborated the effective dispersion of CNC in the matrix, which favored the creation of WBPUU-CNC interactions as observed by FTIR and DSC. Furthermore, thermal analysis revealed that CNC presented the capacity of acting as nucleating agents, providing greater mobility to chains, reflected in lower T_{gSS} comparing with the matrix and increasing T_{mHS}. In addition, an enhancement in the thermomechanical stability was observed, especially in nanocomposites with high CNC content (3 and 5 wt%). In general, the effective CNC incorporation resulted in stiffer films, showing an increase in E and σ_y and reduction in ε_b

values at high CNC contents. Regarding hydrophilicity of films, slight differences were appreciated in WCA values, indicating the similar surface hydrophilicity of the nanocomposites. Nevertheless, more meaningful variations were appreciated in water absorption measurements, where the increase in CNC content favored water molecules diffusion process through the film, being also influenced by the matrix microstructure.

7.5 References

[1]   I. Yilgör, E. Yilgör, G.L. Wilkes, Critical parameters in designing segmented polyurethanes and their effect on morphology and properties: A comprehensive review, Polymer 58 (2015) A1–A36.

[2]   H. Liu, S. Cui, S. Shang, D. Wang, J. Song, Properties of rosin-based waterborne polyurethanes/cellulose nanocrystals composites, Carbohydr. Polym. 96 (2013) 510–515.

[3]   C. Fang, X. Zhou, Q. Yu, S. Liu, D. Guo, R. Yu, J. Hu, Synthesis and characterization of low crystalline waterborne polyurethane for potential application in water-based ink binder, Prog. Org. Coat. 77 (2014) 61–71.

[4]   B. Wunderlich, Thermal analysis of polymeric materials, Springer, 2005.

[5]   J.C. Liu, D.J. Martin, R.J. Moon, J.P. Youngblood, Enhanced thermal stability of biomedical thermoplastic polyurethane with the addition of cellulose nanocrystals, J. Appl. Polym. Sci. 132 (2015) 41970/1–41970/8.

[6]   Z. Gao, J. Peng, T. Zhong, J. Sun, X. Wang, C. Yue, Biocompatible elastomer of waterborne polyurethane based on castor oil and polyethylene glycol with cellulose nanocrystals, Carbohydr. Polym. 87 (2012) 2068–2075.

[7]   X. Cao, H. Dong, C.M. Li, New nanocomposite materials reinforced with flax cellulose nanocrystals in waterborne polyurethane,

Biomacromolecules 8 (2007) 899–904.

[8]   S.H. Park, K.W. Oh, S.H. Kim, Reinforcement effect of cellulose nanowhisker on bio-based polyurethane, Compos. Sci. Technol. 86 (2013) 82–88.

[9]   M.L. Auad, V.S. Contos, S. Nutt, M.I. Aranguren, N.E. Marcovich, Characterization of nanocellulose-reinforced shape memory polyurethanes, Polym. Int. 57 (2008) 651–659.

[10]   B. Ly, W. Thielemans, A. Dufresne, D. Chaussy, M.N. Belgacem, Surface functionalization of cellulose fibres and their incorporation in renewable polymeric matrices, Compos. Sci. Technol. 68 (2008) 3193–3201.

[11]   L. Rueda, B. Fernández d'Arlas, Q. Zhou, L.A. Berglund, M.A. Corcuera, I. Mondragon, A. Eceiza, Isocyanate-rich cellulose nanocrystals and their selective insertion in elastomeric polyurethane, Compos. Sci. Technol. 71 (2011) 1953–1960.

[12]   L. Rueda, A. Saralegui, B. Fernández, Q. Zhou, L.A. Berglund, M.A. Corcuera, I. Mondragon, A. Eceiza, Cellulose nanocrystals/polyurethane nanocomposites . Study from the viewpoint of microphase separated structure, Carbohydr. Polym. 92 (2013) 751–757.

[13]   M.L. Auad, M.A. Mosiewicki, T. Richardson, M.I. Aranguren, N.E. Marcovich, Nanocomposites made from cellulose nanocrystals and

tailored segmented polyurethanes, J. Appl. Polym. Sci. 115 (2010) 1215–1225.

[14]   A. Ashori, M. Babaee, M. Jonoobi, Y. Hamzeh, Solvent-free acetylation of cellulose nanofibers for improving compatibility and dispersion, Carbohydr. Polym. 102 (2014) 369–375.

[15]   K. Benhamou, H. Kaddami, A. Magnin, A. Dufresne, A. Ahmad, Bio-based polyurethane reinforced with cellulose nanofibers: A comprehensive investigation on the effect of interface, Carbohydr. Polym. 122 (2015) 202–211.

[16]   M.A. Hubbe, D.J. Gardner, W. Shen, contact angles and wettability of cellulosic surfaces: A review of proposed mechanisms and test strategies, Bioresources 10 (2015) 8657–8749.

[17]   L. Rueda, B. Fernandez d'Arlas, M.A. Corcuera, A. Eceiza, Biostability of polyurethanes. Study from the viewpoint of microphase separated structure, Polym. Degrad. Stab. 108 (2014) 195–200.

[18]   S. Das, P. Pandey, S. Mohanty, S.K. Nayak, Influence of NCO/OH and transesterified castor oil on the structure and properties of polyurethane: Synthesis and characterization, Mater. Express 5 (2015) 377–389.

[19]   H. Liu, J. Song, S. Shang, Z. Song, D. Wang, Cellulose nanocrystal/silver nanoparticle composites as bifunctional nanofillers within waterborne

polyurethane, ACS Appl. Mater. Interf. 4 (2012) 2413–2419.

CHAPTER 8

Electrospinning waterborne polyurethane nanocomposites loaded with cellulose nanocrystals by two incorporation routes

"Lo importante es no dejar de hacerse preguntas"

8. ELECTROSPINNING WATERBORNE POLYURETHANE NANOCOMPOSITES LOADED WITH CELLULOSE NANOCRYSTALS BY TWO INCORPORATION ROUTES

8.1 Objective

In this chapter, previously prepared dispersions of WBPU-CNC nanocomposites were employed in order to obtain electrospun nanocomposites mats assisted by poly(ethylene oxide) as polymer template. A WBPU mat was also electrospun as a reference. Previously studied two CNC incorporation routes were selected for the preparation of WBPU nanocomposite dispersions containing PEO for mats preparation loaded with 1 and 3 wt% of CNC: the classical method, mixing by sonication after WBPU synthesis, and the innovative *in-situ* route, where CNC were incorporated during the water addition step in the synthesis process. The effects of CNC content and the incorporation route were analyzed in the final properties of the dispersions prepared for electrospinning and in electrospun mats morphology, as well as in their surface behavior. Moreover, the extraction of PEO, the template polymer, washing with water resulted in continuous mats composed just by WBPU-CNC showing different properties comparing with their homologous with PEO, which opens the opportunity of focusing towards new and diverse applications. In this way, dispersions have been characterized by rheological measurements, whereas nanocomposites mats were studied from the viewpoint of physicochemical and hydrophilicity properties as well as morphology.

8.2 Experimental

8.2.1 Dispersions for electrospinning

The spinnability of dispersions depends on several factors, such as molecular weight, concentration and viscosity, among others. In case of the synthesized WBPU, due to the low molecular weight (67350 g mol^{-1}, determined in chapter 3 by GPC) for the electrospinning of the dispersion, more concentrated dispersions would be needed for a suitable spinnability [1,2]. In this way, the elevated molecular weight of PEO (900000 g mol^{-1}), in addition to its high solubility in water, contributed to the formation of entanglements or physical crosslinks between chains, facilitating the spinnability of the polymer at low solution concentrations. Thereby, considering previous works [3] 4 wt% of PEO respect to water was employed in the WBPU dispersion with 25 wt% of solids content. In this way, PEO facilitated the effective WBPU spinnability acting as a template polymer [4].

Therefore, dispersions for the electrospinning process were prepared by adding 4 wt% of PEO respect to total water content in the previously prepared WBPU and WBPU-X and WBPU-X$_{in\text{-}situ}$ nanocomposites dispersions, prepared by mixing by sonication and *in-situ*, respectively. The dispersions were subjected to a magnetic stirring until PEO was dissolved and dispersion was homogenized.

8.2.2 Electrospinning

The dispersion was charged in a 18-gage blunt-end needle which was mounted on a syringe pump (Cole-Parmer). Randomly oriented fibers were electrospun by applying a voltage between 12-14 kV to the needle using a Spellman CZE1000R high voltage supply (0–30 kV, -CZE1000R;

Spellman High Voltage Electronics Corp.), with a low current output (limited to a few microampere). The ground plate (aluminum steel sheet on a screen) was placed at 30 cm from the needle tip. The syringe pump delivered the polymer dispersion at a controlled flow rate of 0.5 mL h^{-1}. The resulting fibers were collected (for 1 h) on the screen in order to produce a sheet of nonwoven fabric. The electrospinning process was controlled by observing the output of the dispersion from the needle tip by an optical microscope.

The template polymer, PEO, was removed from electrospun fibers by water extraction treatment. The standard procedure was as follows: fibers mats were immersed in distilled water for at least 24 h at room temperature. After this treatment, mats were dried in air for 24 h before characterization. The designation selected for electrospun mats is the same employed in the homologues casted films. Thus, mats were coded as WBPU and WBPU-X and WBPU-X$_{in\text{-}situ}$, where X is referred to CNC weight content in the nanocomposite (1 or 3), followed by the words "before" or "after" depending if the mat has been already subjected or not to the washing treatment.

8.3 Results and discussion

8.3.1 Dispersions characterization

8.3.1.2 Rheological properties of dispersions

Viscosity is a relevant parameter influencing the electrospinning of dispersions. Too low viscosity is not enough for electrospinning a continuous fiber, while very high viscosity values, hinder the jet to stretch [1]. The viscosity of WBPU-PEO and WBPU-CNC-PEO dispersions in function of shear rate is shown in

Figure 8.1.
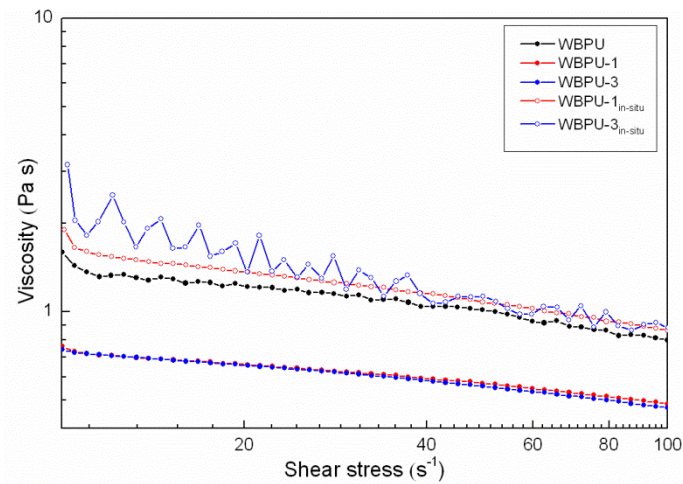
Figure 8.1 *Viscosity of WBPU-PEO and WBPU-CNC-PEO dispersions in function of shear rate*

It was observed a slight decrease in viscosity as shear rate was increased, which was related with a shear thinning behavior [5,6]. This fact could be attributable to the interactions originated in the dispersion which provided certain order to the system and thereby, induced to higher viscosities at low shear rates. In this way, the increase in shear rate interfered in the interactions which could not be recovered and, in consequence a gradual reduction in the viscosity was observed [6]. Analyzing the incorporation of CNC to the systems, two tendencies were observed respect to the matrix, where the viscosity varied principally attending to the CNC incorporation route. On the one hand, when CNC were mixed by sonication, it has to be noted that previously isolated CNC are maintained in form of dispersion for avoiding the formation of agglomerates during the redispersion in water [7]. Thereby, due to an additional dilution of the dispersion the viscosity was reduced comparing with the matrix, which barely

varied with CNC content. On the other hand, the incorporation of CNC by *in-situ* method did not imply a dilution effect. In this case, the solids content was maintained constant and an increase in viscosity values were observed respect to the matrix. The effect was related with the interactions generated with the increase of CNC content, being more discernible at low shear rates where the system presented the capacity of recovering from shear stress forces. The fluctuation of viscosity values observed in the sample WBPU-3$_{in-situ}$ could be attributed to the more favorable interactions between cellulose nanocrystals and the polymer matrix at their highest concentration.

8.3.2 Properties of electrospun nanocomposite mats

8.3.2.1 Appearance of electrospun mats

WBPU matrix and WBPU-1 nanocomposite mats digital image before and after the water treatment for the removal of PEO are shown in **Figure 8.2**.
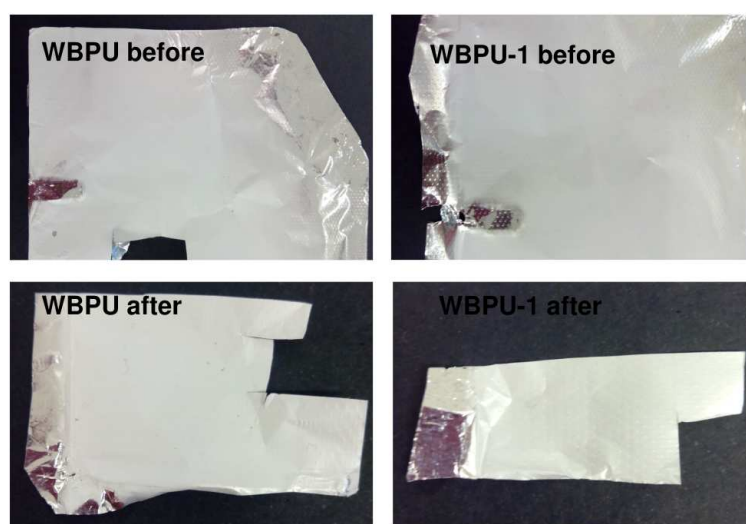
Figure 8.2 *WBPU matrix and WBPU-1 nanocomposite electrospun mats digital image before and after the water washing treatment*

As can be seen in **Figure 8.2**, white mats were obtained coating the aluminum foil used for collecting the electrospun nanofibers. Although only WBPU matrix and WBPU-1 nanocomposite are shown, it was observed that all samples showed similar appearance. Furthermore, it was observed that after subjecting the samples to the washing treatment, the appearance was maintained without disrupting mats structure.

8.3.2.2 Physicochemical properties

The resultant electrospun mats were subjected to a washing process in order to remove the PEO which acted as auxiliary polymer facilitating the electrospinning of WBPU and WBPU-CNC nanocomposites. Hence, with the purpose of verifying the elimination of PEO, FTIR measurements were carried out. **Figure 8.3**, shows FTIR spectra of PEO and 1 wt% of CNC containing mats, by both incorporation routes, previous and after the extraction of PEO with water.

It has to be worth noting that WBPU presented two typical regions from 3600 to 3100 cm^{-1} and between 1800 and 1500 cm^{-1}, related with the characteristic N-H and carbonyl of urethane groups, respectively [8]. Furthermore, CNC showed a representative broad peak about 3340 cm^{-1} attributable to the hydroxyl groups [9,10], as previosly discussed in chapter 6. Those distinctive peaks were discernible in FTIR spectra before and after washing treatment. Instead, the reduction or disappearance of some peaks was observed in spectra after the treatment, comparing with their homologues before washing process.
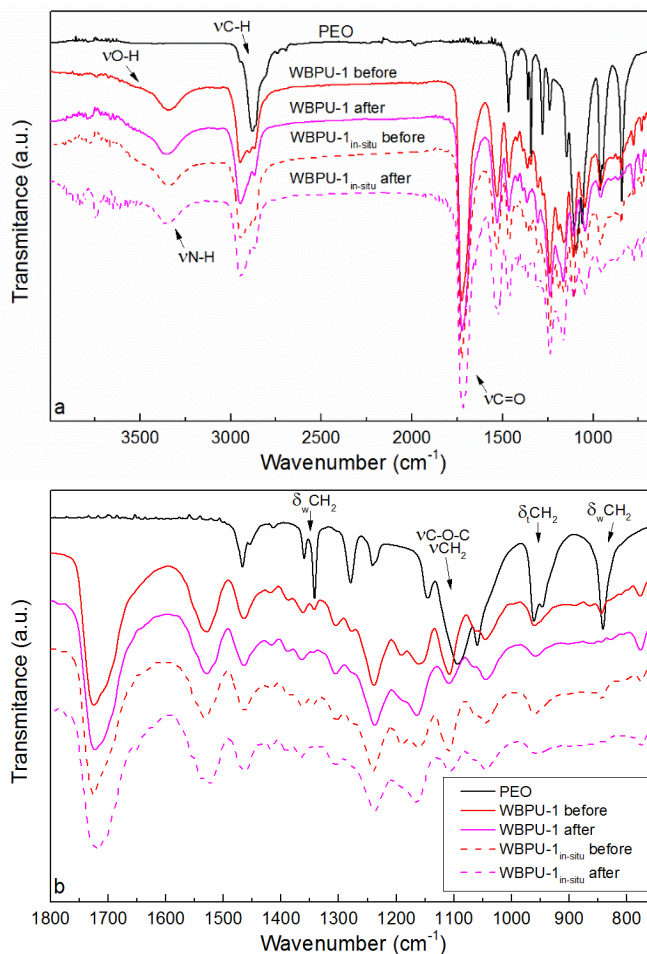
Figure 8.3 *a) FTIR spectra of PEO and 1 wt% CNC containing nanocomposite mats before and after washing treatment and b) amplification of the spectra region between 1800 and 750 cm^{-1}*

In both CNC incorporation routes, it was appreciated the disappearance or intensity decrease of the peaks around 2896, 1360 and 1340, 1189 and 1106, 960 and 843 cm^{-1} which corresponds to PEO C-H stretching, methylene (CH$_2$) wagging, the combination of ether (C-O-C) and CH$_2$ groups stretching, CH$_2$ twisting and CH$_2$ wagging, respectively [11–13]. This fact indicated that the washing process was carried out satisfactorily, extracting PEO by dissolving in

water and, thus obtaining a mat composed only by WBPU and CNC.

8.3.2.3 Morphology

The morphology of WBPU and nanocomposites mats was analyzed by SEM before and after washing treatment, and the images are shown in **Figure 8.4** and **Figure 8.5**.

It was observed that all samples exhibited a suitable spinnability resulting in continuous mats whose morphology varied influenced by the addition of CNC as well as their incorporation route. It is noteworthy that even though CNC were not appreciated in nanocomposites, the continuous and smooth surface presented by fibers implied de homogeneous distribution of CNC without discerning agglomerates. Furthermore, the mats configuration after the washing treatment was maintained, although weaker points were observed due to the removal of PEO. Fibers prepared by *in-situ* supported similar diameters in comparison with those prior to the treatment. In general, CNC addition promoted the spinnability of thinner fibers comparing with the matrix. It is worth noting that the incorporation of polyelectrolytes to the solutions promote the formation of smaller diameter fibers. As a result of their ionic strengths by nature, the charge density of the solutions is enhanced, which contribute to more intense elongation forces facilitating the ejection of the fiber [14]. In this way, CNC possessed sulfate groups anchored to the surface during the isolation process by acid hydrolysis. These negative charges acted just as polyelectrolyte salts favoring the formation of finer fibers [15,16], besides providing reinforcing effect. Thereby, as CNC content was increased slightly smaller diameters were observed, except for WBPU-3$_{in-situ}$, which could be associated with the higher viscosity of the sample.
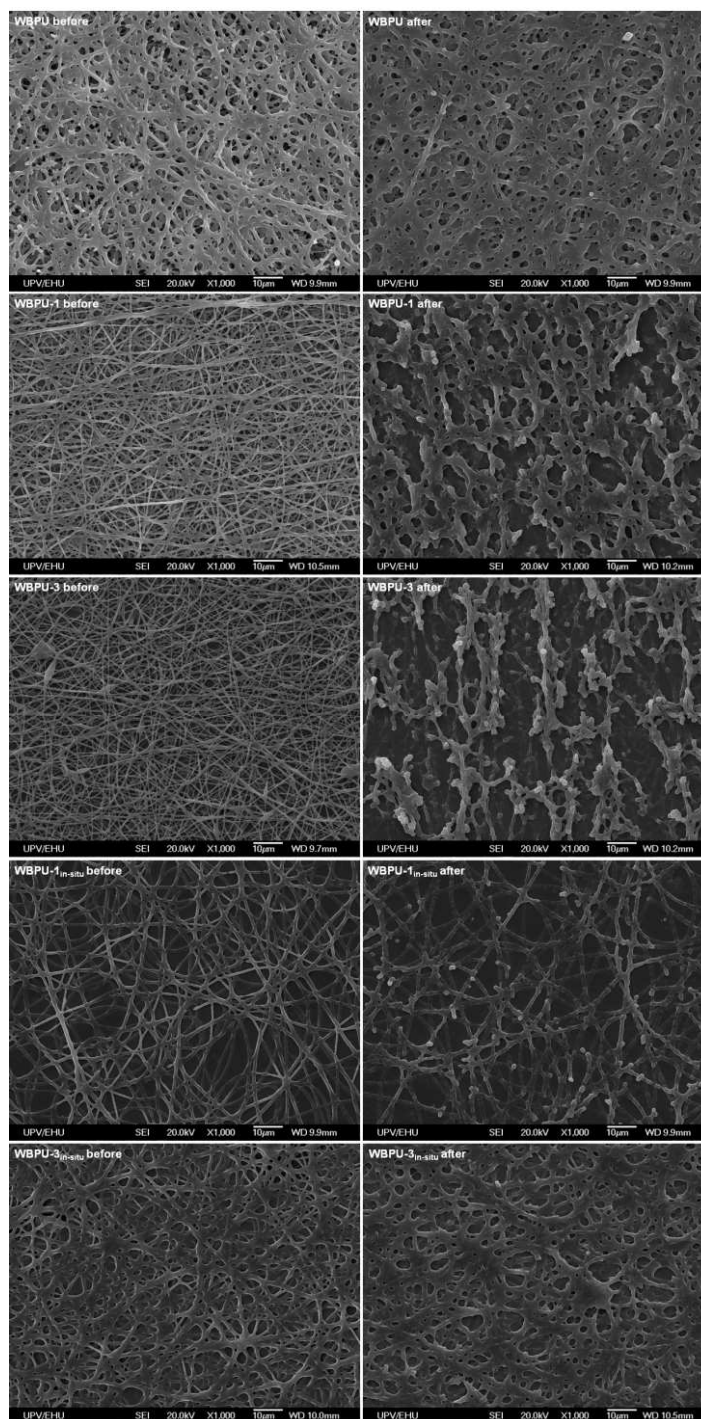
Figure 8.4 *SEM images of WBPU matrix and nanocomposite mats before and after washing treatment (size: x1000 magnifications)*
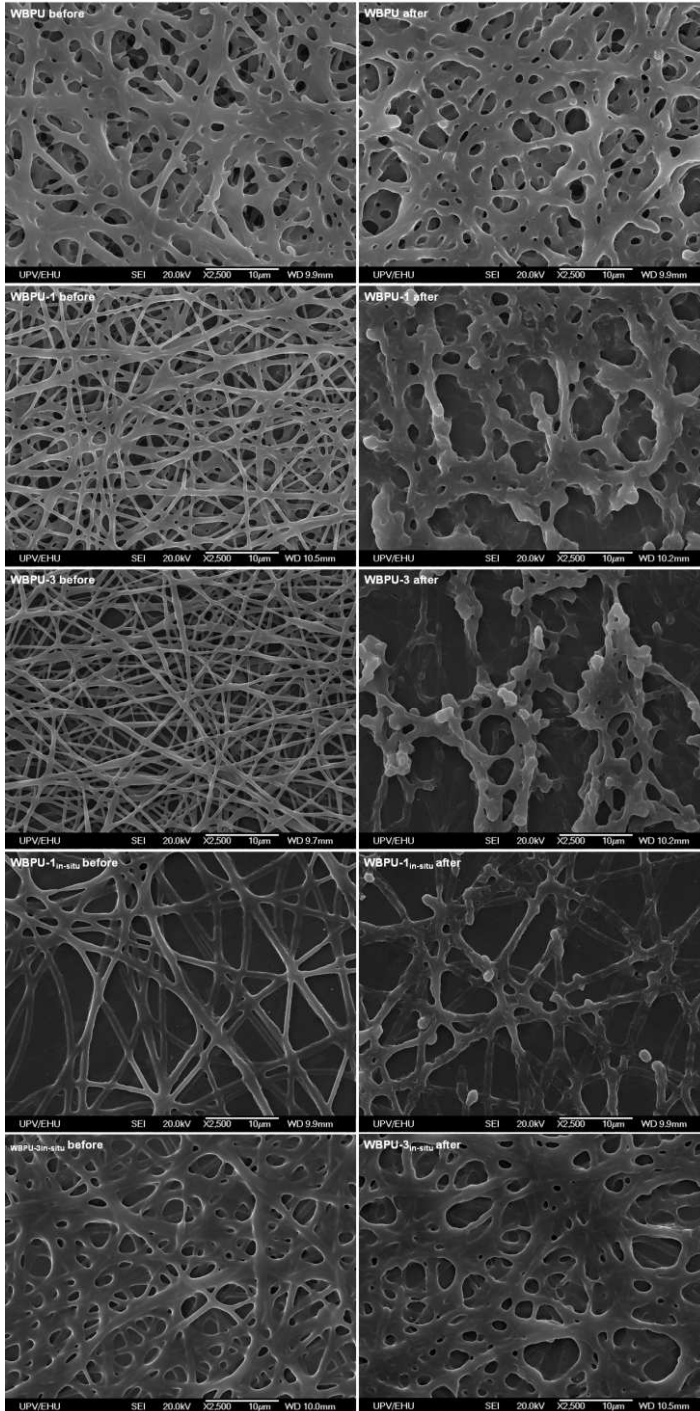
Figure 8.5 *SEM images of WBPU matrix and nanocomposite mats before and after washing treatment (size: x2500 magnifications)*

Analyzing the incorporation route before the washing treatment, it was observed that CNC addition by sonication resulted in thinner diameters than by adding *in-situ*, due to their greater surface exposure favoring the spinnability process. In the case of nanocomposites prepared by sonication, some bead defects were appreciated, which were related with the viscosity of the dispersions [17]. If the viscosity is too low, the system does not promote sufficient surface tension in order to contribute to the fiber spinnability inducing to beads formation [18]. Thereby, higher viscosities are preferred to avoid beads defects [19]. Comparing the morphology of mats after the washing treatment, it was appreciated that mats containing CNC incorporated by *in-situ* showed more uniformity than the respective added by sonication. Considering previous works [20], it is worth noting that CNC addition route altered their disposition in the matrix. By both routes, CNC were homogeneously dispersed in the matrix, but by *in-situ* method, the incorporation of CNC during dispersion formation step promoted the intercalation of CNC between WBPU nanoparticles, remaining embedded in the matrix. In this way, *in-situ* method favored the interactions contributing to support the fibrillar structure of the mats when the template polymer was removed, while the influence of adding CNC by sonication, was less effective.

8.3.2.4 Hydrophilicity

Dynamic contact angle measurements performed in electrospun mats before and after the washing treatment are shown in **Figure 8.6** and **Figure 8.7**, respectively.
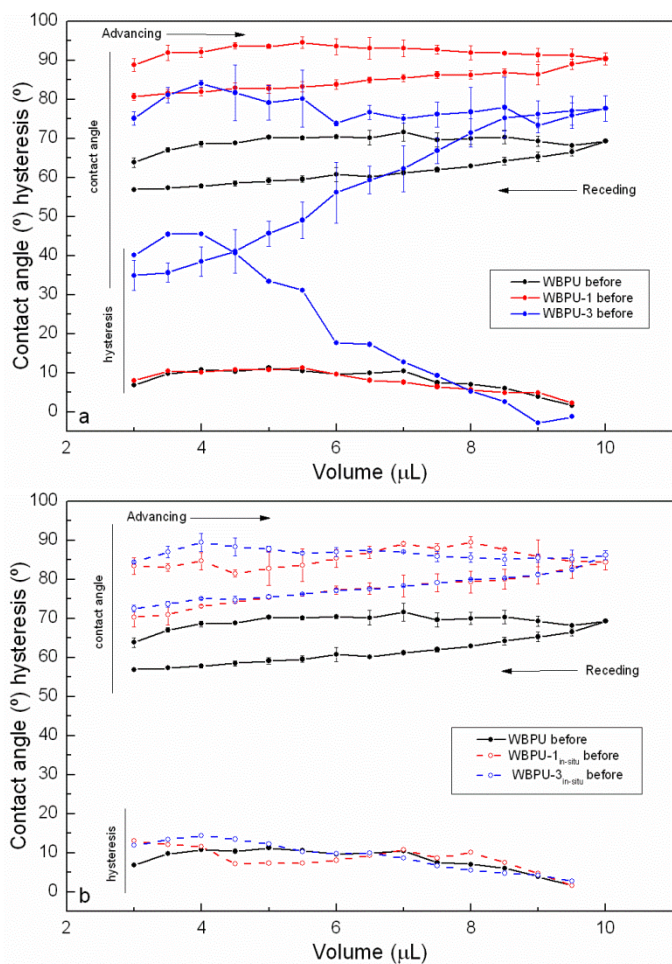
Figure 8.6 *Advancing and receding dynamic contact angle and hysteresis of WBPU matrix and nanocomposites prepared by a) mixing by sonication and by b) in-situ before the washing treatment*
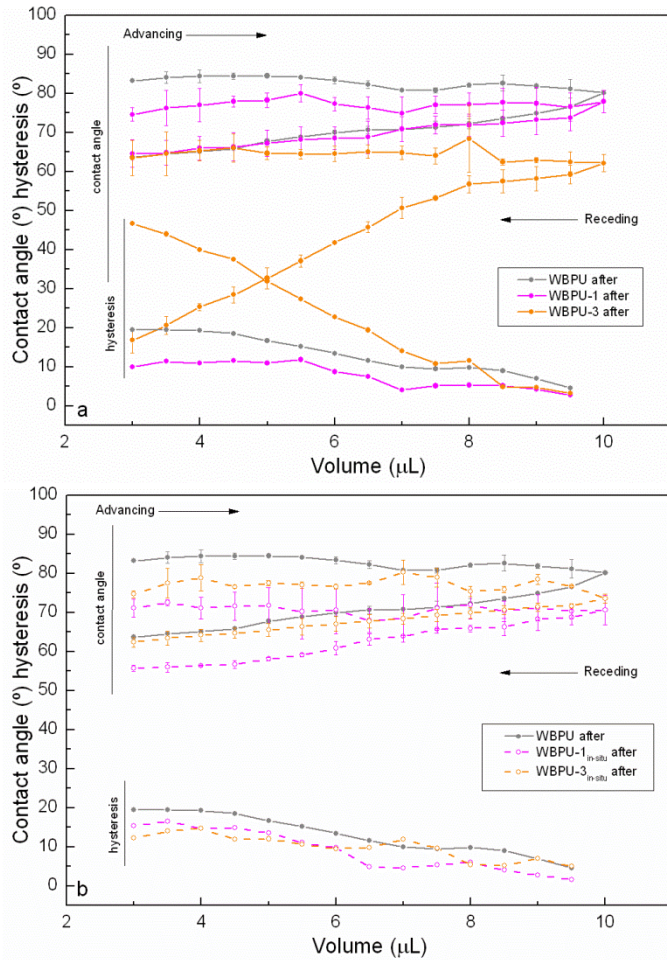
Figure 8.7 *Advancing and receding dynamic contact angle and hysteresis of WBPU matrix and nanocomposites prepared by a) mixing by sonication and by b) in-situ after the washing treatment*

Contact angle hysteresis, shown in **Figure 8.6** and **Figure 8.7**, resulted from the difference between the advancing and receding contact angle values and is an indicative of the surface wettability [21,22]. It was observed that prior to washing treatment the matrix showed advancing contact angles around 70°, while nanocomposites, independent of the incorporation route, presented higher values between 80 and 90° denoting their more hydrophobic superficial

character despite containing hydrophilic CNC. This fact was related with the electrospun fibers formation that, favored by the CNC incorporation, were thinner and more defined as observed in SEM results. It is worth noting that the formation of lower fiber diameters implies a lower liquid-solid contact area, promoting liquid-air contact area and thus resulting in higher contact angle values [23]. Analyzing CNC content, it was observed that at 1 wt% of CNC, the incorporation by sonication method showed slightly higher contact angle values considering thinner fibers diameters. Instead, at 3 wt% of CNC content by sonication method, a significant decrease in contact angle values was appreciated. As explained previously in SEM results, the incorporation route induces to different CNC dispositions and, although both methods led to a suitable CNC dispersion, by *in-situ* method, CNC resulted embedded in the matrix. Thereby, in this case the contact angle values are hardly altered with CNC content. However by sonication incorporation method, CNC kept a greater exposure on the surface. In this way, the more susceptible hydrophilic CNC located in the surface were able to reorient towards water in order to interact with water [24,25], thus observing a significant difference in contact angle and contact angle hysteresis values, resulting in more wettable mats. After the washing treatment, the matrix presented more pronounced hydrophobic character showing advancing contact angles between 80 and 90° which was attributed to the extraction of the hydrophilic PEO component. However, in nanocomposites, both prepared by sonication and *in-situ*, a decrease to 60-70° was observed. In this case, the extraction of PEO would promote CNC exposition leading to more hydrophilic surfaces. Regarding the CNC incorporation route, the same tendency was observed comparing with their homologues prior to washing treatment.

8.4 Conclusions

In this chapter, suitable dispersion for electrospinning were prepared assisted by PEO as polymer template in order to prepare electrospun nanocomposites mats. The spinnability of WBPU-CNC dispersions containing different CNC contents (1 and 3 wt%), incorporated by two different routes, the classical mixing by sonication and the alternative *in-situ* route, was analyzed. The electrospun mats were subjected to a successful washing treatment, for the extraction of PEO, corroborated by FTIR. The final properties of mats were compared prior and after the water treatment, as well as attending to the influence of CNC content and their incorporation route. It was observed that WBPU-CNC-PEO dispersions prepared by sonication method led to lower viscosity values, both at 1 and 3 wt% of CNC, considering the diluting effect of incorporating CNC dispersed in water, whereas the increase of CNC content resulted in slightly higher viscosity values by *in-situ* method. SEM results revealed that samples showed a continuous fiber structure whose morphology varied depending on CNC content as well as their incorporation route. Before washing treatment, CNC addition favored the formation of lower fiber diameters, being the effect more discernible when CNC were added mixing by sonication due to their greater surface exposure favoring the spinnability process. Instead, by *in-situ* method, as CNC resulted embedded in the matrix, the mat showed lower weaker points after the washing treatment. Furthermore, the morphology of fibers influenced the wettability of mats prior to PEO extraction, where it was observed that mats tended to be more hydrophobic as fibers diameters decreased. However, once PEO was removed, the disposition of CNC played a decisive role in the hydrophilicity. The more exposed CNC incorporated by sonication method, promoted the increase of hydrophilicity of mats, while the

embedded CNC incorporated by *in-situ* method, hardly altered contact angle values.

8.5 References

[1]   N. Bhardwaj, S.C. Kundu, Electrospinning: A fascinating fiber fabrication technique, Biotechnol. Adv. 28 (2010) 325–347.

[2]   F. Yalcinkaya, B. Yalcinkaya, O. Jirsak, Influence of salts on electrospinning of aqueous and nonaqueous polymer solutions, J. Nanomater. 2015 (2015) 134251/1-144251/12.

[3]   L. Buruaga, H. Sardon, L. Irusta, A. González, M.J. Fernández-Berridi, J.J. Iruin, Electrospinning of waterborne polyurethanes, J. Appl. Polym. Sci. 115 (2010) 1176–1179.

[4]   J. Pal, S. Singh, S. Sharma, R. Kulshreshtha, B. Nandan, R.K. Srivastava, Emulsion electrospun composite matrices of poly(ε-caprolactone)-hydroxyapatite: Strategy for hydroxyapatite confinement and retention on fiber surface, Mater. Lett. 167 (2016) 288–296.

[5]   E. Orgilés-Calpena, F. Arán-Aís, A.M. Torró-Palau, C. Orgilés-Barceló, J.M. Martín-Martínez, Influence of the chemical structure of urethane-based thickeners on the properties of waterborne polyurethane adhesives, J. Adhes. 85 (2009) 665–689.

[6]   A. Rahmatpour, B. Kaffashi, S. Maghami, Preparation and rheological properties of functionalized multiwalled carbon nanotube/waterborne polyurethane nanocomposites, J. Macromol. Sci. Part B Phys. 50 (2011) 1834–1846.

[7]   S. Beck, J. Bouchard, R. Berry, Dispersibility in water of dried nanocrystalline cellulose, Biomacromolecules 13 (2012) 1486–1494.

[8]   I. Yilgör, E. Yilgör, G.L. Wilkes, Critical parameters in designing segmented polyurethanes and their effect on morphology and properties: A comprehensive review, Polymer 58 (2015) A1–A36.

[9]   D.R. Da Silva Souza, J.P. De Mesquita, R. Montero Lago, L. Durães Caminhas, F. Vargas Pereira, Cellulose nanocrystals: A versatile precursor for the preparation of different carbon structures and luminiscent carbon dots, Ind. Crop. Prod. 93 (2016) 121–128.

[10]   A. Santamaria-Echart, L. Ugarte, C. García-Astrain, A. Arbelaiz, M.A. Corcuera, A. Eceiza, Cellulose nanocrystals reinforced environmentally-friendly waterborne polyurethane nanocomposites, Carbohydr. Polym. 151 (2016) 1203–1209.

[11]   I. Pucić, T. Jurkin, FTIR assessment of poly(ethylene oxide) irradiated in solid state, melt and aqeuous solution, Radiat. Phys. Chem. 81 (2012) 1426–1429.

[12]   S. Ramesh, T.F. Yuen, C.J. Shen, Conductivity and FTIR studies on PEO-LiX [X: $CF_3SO_3^-$, SO_4^{2-}] polymer electrolytes, Spectrochim. Acta, Part A. 69 (2008) 670–675.

[13]   J.C. Wang, M.W. Chang, Z. Ahmad, J.S. Li, Fabrication of patterned

polymer-antibiotic composite fibers via electrohydrodynamic (EHD) printing, J. Drug Deliv. Sci. Technol. 35 (2016) 114–123.

[14] W.K. Son, J.H. Youk, T.S. Lee, W.H. Park, The effects of solution properties and polyelectrolyte on electrospinning of ultrafine poly(ethylene oxide) fibers, Polymer 45 (2004) 2959–2966.

[15] C.F. Bellani, E. Pollet, A. Hebraud, F. V Pereira, G. Schlatter, L. Avérous, R.E.S. Bretas, M.C. Branciforti, Morphological, thermal, and mechanical properties of poly(ε-caprolactone) / poly(ε-caprolactone)-grafted-cellulose nanocrystals mats produced by electrospinning, J. Appl. Polym. Sci. 133 (2016) 43445/1-43445/8.

[16] M.S. Peresin, Y. Habibi, J.O. Zoppe, J.J. Pawlak, O.J. Rojas, Nanofiber composites of polyvinyl alcohol and cellulose nanocrystals: manufacture and characterization, Biomacromolecules 11 (2010) 674–681.

[17] T.C. Mokhena, V. Jacobs, A.S. Luyt, A review on electrospun bio-based polymers for water treatment, Express Polym. Lett. 9 (2015) 839–880.

[18] E. Borg, A. Frenot, P. Walkenström, K. Gisselfält, C. Gretzer, P. Gatenholm, Electrospinning of degradable elastomeric nanofibers with various morphology and their interaction with human fibroblasts, J. Appl. Polym. Sci. 108 (2008) 491–497.

[19] E. Elias, S.C. Chandran, N. Chandran, F.G. Souza, S. Thomas, Segmental

dynamics, morphology and thermomechanical properties of electrospun poly(ε-caprolactone) nanofibers in the presence of an interacting filler, RSC Adv. Adv. 6 (2016) 21376–21386.

[20]   A. Santamaria-Echart, L. Ugarte, A. Arbelaiz, N. Gabilondo, M.A. Corcuera, A. Eceiza, Two different incorporation routes of cellulose nanocrystals in waterborne polyurethane nanocomposites, Eur. Polym. J. 76 (2016) 99–109.

[21]   S.J. Pogorzelski, P. Rochowski, J. Szurkowski, Pinus sylvestris L. needle surface wettability parameters as indicators of atmospheric environment pollution impacts: Novel contact angle hysteresis methodology, Appl. Surf. Sci. 292 (2014) 857–866.

[22]   A.E. Wiącek, Effect of surface modification on strach biopolymer wettability, Food Hydrocoll. 48 (2015) 228–237.

[23]   Y. Ji, K. Liang, X. Shen, G.L. Bowlin, Electrospinning and characterization of chitin nanofibril/polycaprolactone nanocomposite fiber mats, Carbohydr. Polym. 101 (2014) 68–74.

[24]   Y. Cho, H.S. Sundaram, J.A. Finlay, M.D. Dimitriou, M.E. Callow, J.A. Callow, E.J. Kramer, C.K. Ober, Reconstruction of surfaces from mixed hydrocarbon and PEG components in water: Responsive surfaces aid fouling release, Biomacromolecules 13 (2012) 1864–1874.

[25]   H.Y. Erbil, The debate on the dependence of apparent contact angles on drop contact area or three-phase contact line: A review, Surf. Sci. Rep. 69 (2014) 325–365.

CHAPTER 9

Different incorporation routes

of bioactive plant extracts in waterborne

polyurethane-urea dispersions

"Só sei que nada sei"

9. DIFFERENT INCORPORATION ROUTES OF BIOACTIVE PLANT EXTRACTS IN WATERBORNE POLYURETHANE-UREA DISPERSIONS

9.1 Objective

The employment of renewable raw materials in the form of reinforcement, filler or additive, becomes an interesting approach to explore the specific and intrinsic properties of these materials, which can provide improved or even additional properties to the matrix. Among others, the use of plant extracts, incorporated as biologically active agents, can enhance the antimicrobial properties of polymeric systems, in general, and WBPU or WBPUU synthesized in this work, in particular. They can be added through different incorporation routes, being able to modify or maintain the final properties of the polymer.

Thus, in this chapter, different WBPUU-plant extract systems were analyzed with the purpose of studying the influence of the used plant extract origin, as well as its content and incorporation route, in the final properties of the obtained dispersions and films, including their effect on the antibacterial properties. Hence, different plant extracts were extracted by the infusion method and incorporated into the WBPUU for the preparation of different films by solvent-casting.

In this sense, for the work two plants were selected, *Salvia officinalis L.* (sage) and *Melissa officinalis L.* (Lemon balm). Moreover, three incorporation pathways were designed, where the extracts were added at different contents (1, 3 and 5 wt%), and considering both extracts.

The design of the incorporation routes was defined based on the stage at which the extract was added: in the first route, post-method, the extract was added dissolved in water once WBPUU dispersion was synthesized. In the second via, *in-situ* method, the extract was previously dissolved in the distilled water used for the phase inversion, whereby the extract was incorporated during the WBPUU nanoparticles formation step. In the third alternative, pre-method, the extract was incorporated dissolved in a small amount of distilled water, during the phase inversion step, just before nanoparticles formation. The resultant series dispersions were studied in terms of pH, viscosity and particle size, whereas the prepared films were analyzed from the viewpoint of morphology and physicochemical, thermal, mechanical and thermomechanical properties, as well as antibacterial properties.

9.2 Experimental

9.2.1 Salvia and Melissa extracts obtainment

Extracts were obtained from *Salvia officinalis L.* and *Melissa officinalis L.* plants by the infusion method. These extracts were chosen due there recognized antimicrobial activity as described in literature [1–3]. Briefly, around 20 g of triturated plant was added to 800 mL of boiling distilled water and maintained for 5 min. Then, the resultant suspension was filtered and lyophilized, and the extract rich in bioactive compounds obtained in powder form. **Figure 9.1** shows Salvia and Melissa products during the extraction process.
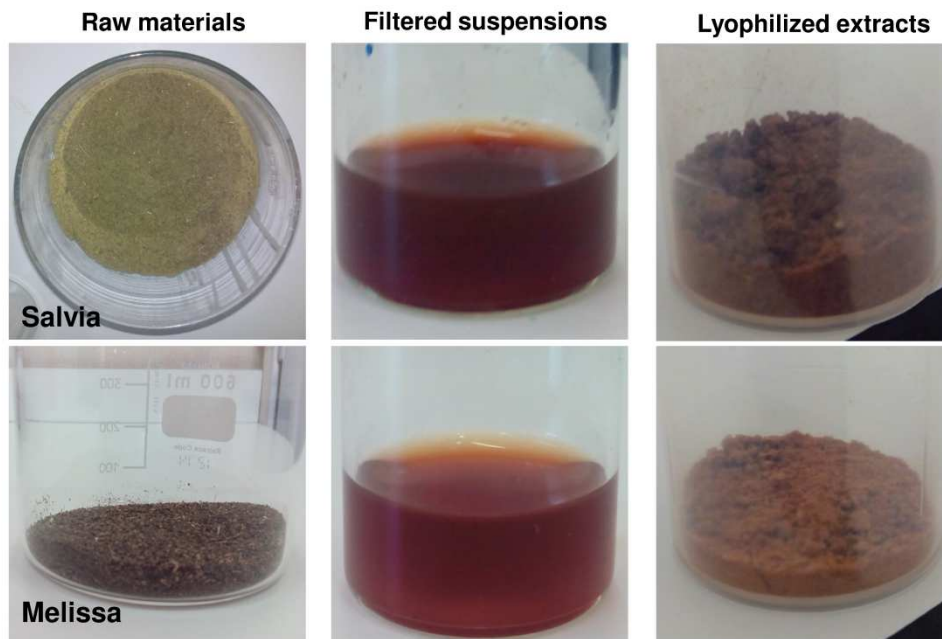
Figure 9.1 *Images of raw material, filtered suspension and lyophilized extracts of Salvia and Melissa*

For each plant, the extraction efficiency of the process was calculated by the following **Equation 9.1**:

$$Efficiency \ (\%) = \frac{W_i - W_f}{W_i} \cdot 100 \qquad (9.1)$$

Where W_i and W_f are referred to the initial plant weight and the weight of the resultant extract, respectively. In this way, an efficiency of 13 ± 1% and 17 ± 2% were obtained for Salvia and Melissa extracts, respectively, values dependent on the composition of the raw material.

9.2.2 Preparation of the Salvia- and Melissa-based WBPUU dispersions

Waterborne polyurethane-urea dispersion was synthesized following a two-step polymerization process in heterogeneous medium, as previously described in chapter 4, but differing from this protocol where only EDA diamine chain extender was employed. In this way, the composition varied slightly. WBPUU was prepared using a NCO/OH groups ratio of 1.67 in the prepolymer, and 5 wt% of DMPA, resulting in a hard segment content around 31.7 wt%. Finally, a chain extension of 40% was calculated for the addition of EDA in heterogeneous medium resulting in final dispersions with solids content around 35-40 wt%.

Three alternative incorporation routes were designed for the preparation of the Salvia- and Melissa-based WBPUU at contents of 1, 3 and 5% (wt, prepolymer-basis):

1. In the first method, post-method, the required amount of extract was dissolved in distilled water and incorporated dropwise to the synthesized WBPUU under mechanical stirring. This procedure was done previously to the corresponding film preparation. For that 10 mL of dispersion were mixed with 10 mL of the extract solution using the required amount of extract.

2. In the second method, *in-situ* method, the extract was dissolved in the amount of distilled water employed for the phase inversion step. In this way, the extract was incorporated progressively during the WBPUU nanoparticles formation during the phase inversion step of the synthesis process.

3. In the third method, pre-method, the extract was dissolved in a small amount of distilled water (15 mL) and incorporated to the reactor just before

water addition to initialize the phase inversion step, i.e. previously to the WBPUU nanoparticles formation.

9.2.3 Preparation of films from Salvia- and Melissa-based WBPUU

Films of Salvia- and Melissa-based WBPUU were prepared by the solvent casting method. Briefly, the needed volume of dispersion (around 20 mL) was poured into a Teflon mold and allowed to dry at room conditions during 1 week. Finally, films were dried at 60 °C at 800 mbar for 1 day. The resultant films were stored in a desiccator before characterization. Waterborne polyurethane-urea samples were coded as $SalviaX_y$ or $MelissaX_y$, where "X" was referred to Salvia or Melissa weight content in the polyurethane-urea and "y" specifies extract incorporation route "post", "in-situ" or "pre" Furthermore, neat polyurethane-urea was coded as WPUU.

The produced films were coded based on the former used dispersions as described in the previous section.

9.3 Results and discussion

9.3.1 Properties of the Salvia- and Melissa-based WBPUU dispersions

9.3.1.1 Appearance of WBPUU dispersions

The base WBPUU (WBPUU without added extract), as well as the Salvia- and Melissa-based WBPUU prepared using the *in-situ* and pre-method (i.e. the dispersions prepared with the addition of the extract during the synthesis process) are shown in **Figure 9.2** and **Figure 9.3**, respectively.
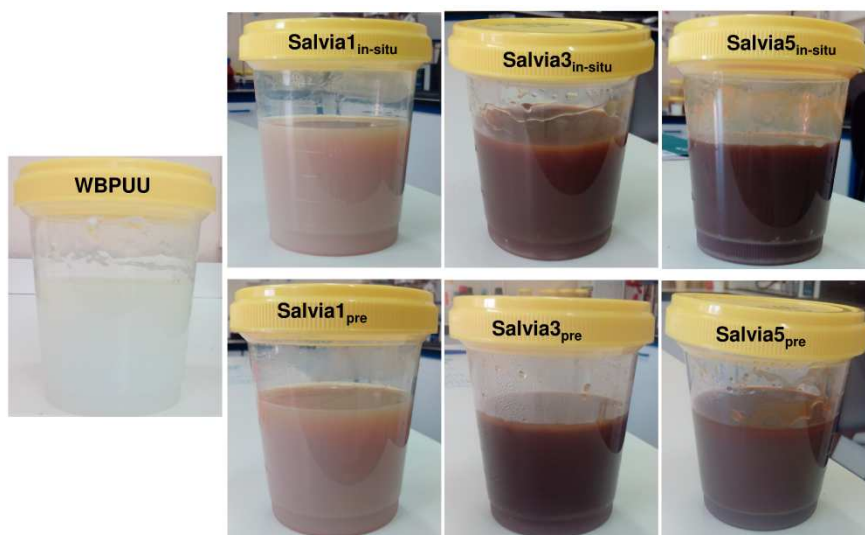
Figure 9.2 *Image of synthesized base WBPUU and WBPUU containing bioactive Salvia extracts dispersions*
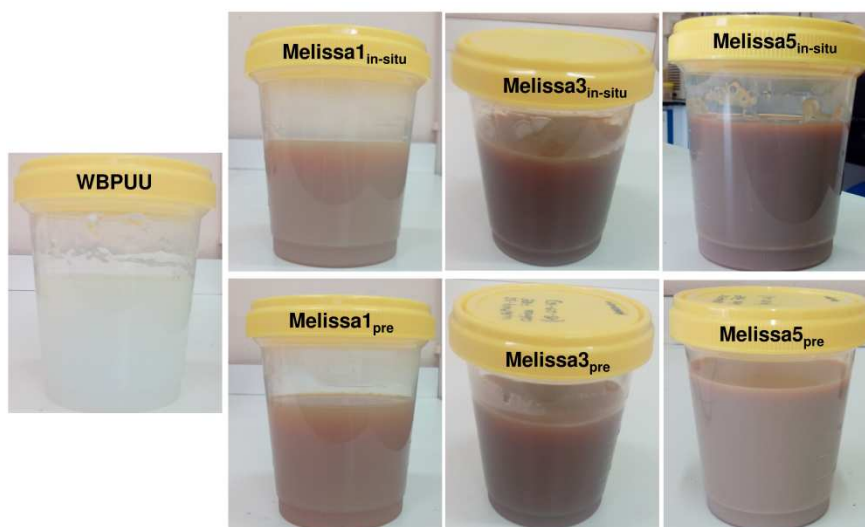
Figure 9.3 *Image of synthesized base WBPUU and WBPUU containing bioactive Melissa extracts dispersions*

The base WBPUU dispersion presented white and translucent appearance. Instead, the Salvia- and Melissa-based WBPUU dispersions, presented a

browner-like aspect. This fact was attributed to the own color of the extract, whereby dispersions color became darker and more intense as the extract content was increased. Furthermore, it was observed that in the case of using Melissa extract, lighter dispersions were obtained when compared with their homologous prepared with Salvia.

9.3.1.2 pH of the WBPUU dispersions

The pH of the Salvia- and Melissa-based WBPUU dispersions is shown in **Table 9.1** and **Table 9.2**, respectively. In the case of Salvia- and Melissa-based solutions, a pH value of 5.52 and 5.67 was obtained, fact attributed to the presence of extracted compounds, such as phenolic and flavonoids, that presented acidic groups among others [2]. For the base WBPUU dispersion, a value of 7.29 was measured, which resulted in the range founded in literature, corroborating that carboxylic groups were successfully neutralized [4,5].

Table 9.1 *pH values of WBPUU containing Salvia extracts bioactive dispersions*

Sample	pH		
	post	*in-situ*	pre
Salvia1	8.22	7.63	7.53
Salvia3	8.14	7.66	7.57
Salvia5	7.76	7.67	7.63

Analyzing the pH values of the Salvia- and Melissa-based dispersions, fluctuations in pH values were observed concerning the used extract content, as well as, the incorporation route.

Table 9.2 *pH values of WBPUU containing Melissa extracts bioactive dispersions*

Sample	pH		
	post	*in-situ*	pre
Melissa1	7.85	7.67	7.50
Melissa3	7.51	8.50	7.51
Melissa5	7.42	7.44	7.25

In the case of post-method, higher pH values were obtained comparing with the base WBPUU, but the value decrease with the addition of extract content. However, when using *in-situ* and the pre-method incorporation routes, Salvia and Melissa extracts were added during the synthesis process, bioactive compounds would be further restricted and less significant variations were observed. This fact could be related with the greater mobility or freedom of the bioactive compounds incorporated by post-method, resulting in greater ability of interacting and in this way, their ionic character would displace the equilibrium.

9.3.1.3 Viscosity and solids content of WBPUU dispersions

The viscosity and solids content of the base WBPUU and the Salvia- and Melissa-based WBPUU dispersions prepared by *in-situ* and pre-methods are shown in **Table 9.3** and **Table 9.4**, respectively.

Analyzing the viscosity values obtained in **Table 9.3** and **Table 9.4**, it was observed that, in general, the increase of the extract content, led to an increase in the dispersion viscosity, fact that could be related with the variation in the surface shear stress and interactions in the system [6].

Table 9.3 *Viscosity and solids content values of base WBPUU and WBPUU containing Salvia extracts bioactive dispersions prepared by in-situ and pre-methods*

Sample	Viscosity (mPa s)	Solids content (%)
WBPUU	23.4 ± 0.1	37.4 ± 0.0
Salvia1 in-situ	21.4 ± 0.2	37.1 ± 0.1
Salvia3 in-situ	49.7 ± 0.6	35.2 ± 0.1
Salvia5 in-situ	216.2 ± 0.6	35.5 ± 0.0
Salvia1 pre	22.6 ± 0.3	37.5 ± 0.2
Salvia3 pre	79.7 ± 0.6	34.5 ± 0.0
Salvia5 pre	69.3 ± 0.6	36.6 ± 0.2

Table 9.4 *Viscosity and solids content values of base WBPUU and WBPUU containing Melissa extracts bioactive dispersions prepared by in-situ and pre-methods*

Sample	Viscosity (mPa s)	Solids content (%)
WBPUU	23.4 ± 0.1	37.4 ± 0.0
Melissa1 in-situ	21.5 ± 0.3	37.5 ± 0.2
Melissa 3 in-situ	1797.0 ± 1.2	31.8 ± 0.5
Melissa 5 in-situ	88.9 ± 0.2	33.1 ± 0.2
Melissa 1 pre	19.2 ± 0.3	37.1 ± 0.1
Melissa 3 pre	22.1 ± 0.4	34.0 ± 0.0
Melissa 5 pre	9.4 ± 0.2	30.2 ± 0.4

Nevertheless, at low Salvia and Melissa extract content (1 wt%), lower viscosity values were obtained, when compared with the base WBPUU dispersion. This fact could be related with the hydrophilic groups attributed to the phenolic

compounds presented in the extract, favoring the dispersion formation and stability of the polyurethane-urea particles, where they can act as a surfactant [7]. In turn, when the extract content was increased, this effect was relieved by the hindrance and intensification of interactions, resulting in a viscosity growth. In addition, considering the effectiveness of extract favoring the dispersion formation which would lead to slightly smaller nanoparticles, as will be seen later, but more numerous, which would lead to a viscosity increase [8]. Furthermore, although bioactive dispersions prepared by post-method are not shown in **Table 9.3** and **Table 9.4**, it is worth noting that the addition of the extract dissolved in additional distilled water caused a dilution effect in the system, leading to lower viscosity values.

9.3.1.4 Particle size of WBPUU dispersions

The particle size distribution of the base WBPUU and the Salvia- and Melissa-based WBPUU dispersions prepared by *in-situ* and by the pre-methods and containing 1, 3 and 5 wt% of Salvia and Melissa extracts were measured by particle size analyzer and results are shown in **Figure 9.4**.

Furthermore, the particle sizes obtained from the curves analyzed for 10 (D_{10}), 50 (D_{50}) and 90% (D_{90}) of the number of nanoparticles in each sample, are included in **Table 9.5** and **Table 9.6**.
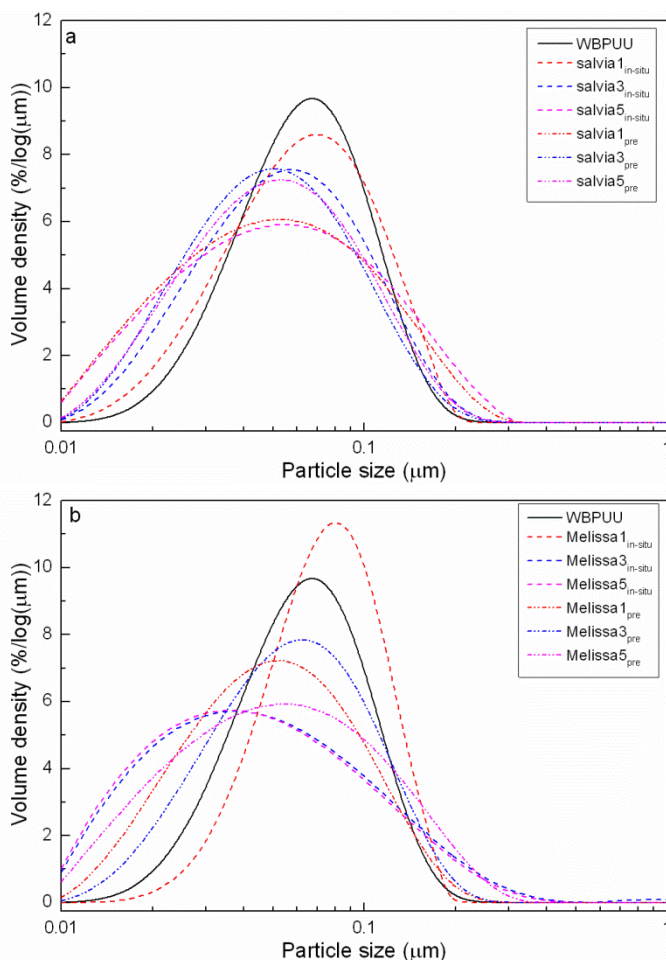
Figure 9.4 *Particle size distributions of base WBPUU and WBPUU containing a) Salvia and b) Melissa extracts bioactive dispersions prepared by in-situ and pre-methods*

It was observed that, in general, and in comparison with the base WBPUU, the particle size distribution broaden to smaller particle sizes as a consequence of extract incorporation, both for Salvia and Melissa extracts.

Table 9.5 *Particle sizes of base WBPUU and WBPUU containing Salvia extracts bioactive dispersions to 10, 50 and 90 % of the number of nanoparticles measured in the samples. The deviation in all samples was lower than 10^{-3}*

Sample	Particle size (nm)		
	D_{10}	D_{50}	D_{90}
WBPUU	34.7	69.0	135
Salvia1$_{in-situ}$	30.1	67.0	130
Salvia3$_{in-situ}$	24.9	58.4	131
Salvia5$_{in-situ}$	19.6	55.0	148
Salvia1$_{pre}$	19.3	52.7	138
Salvia3$_{pre}$	23.0	52.4	119
Salvia5$_{pre}$	22.9	54.5	127

Table 9.6 *Particle sizes of base WBPUU and WBPUU containing Melissa extracts bioactive dispersions to 10, 50 and 90 % of the number of nanoparticles measured in the samples. The deviation in all samples was lower than 10^{-3}*

Sample	Particle size (nm)		
	D_{10}	D_{50}	D_{90}
WBPUU	34.7	69.0	135
Melissa1$_{in-situ}$	42.7	79.6	133
Melissa3$_{in-situ}$	17.4	46.6	148
Melissa5$_{in-situ}$	17.1	45.1	143
Melissa1$_{pre}$	22.7	54.0	127
Melissa3$_{pre}$	27.0	62.3	135
Melissa5$_{pre}$	19.6	54.6	147

This fact was related with the nature of some of the bioactive compounds, whose character and chemical structure can promote their activity as natural

surfactants [9–11], favoring the dispersion formation and thus contributing to the achievement of smaller particles. Furthermore, some differences were observed depending on the employed incorporation method. In the case of *in-situ* method a reduction in D_{10} and D_{50} values was noticed, which became more noticeable with the increase of extract content. In contrast, in pre-method, a reduction in the particle size was also observed, but remained unchangeable with the increase of extract content. Thereby, the incorporation route of the extract influenced the dispersion formation. In the case of *in-situ* method, since the extract was incorporated progressively with water addition, its effect was more perceptible with the extract content increase, considering that it is progressively incorporated across water dropwise. In turn, in pre-method, taking into account that the total amount of extract was incorporated prior to the dispersion formation, it will be intercalated between polyurethane chains, causing a more discernible effect at low extract contents, and therefore, despite increasing the extract content increase, only a slightly variation was observed.

9.3.2 Properties of WBPUU bioactive films

9.3.2.1 Appearance of WBPUU bioactive films

Films prepared from the base WBPUU and the Salvia- and Melissa-based WBPUU dispersions, using the solvent-casting method, are shown in **Figure 9.5** and **Figure 9.6**, respectively.
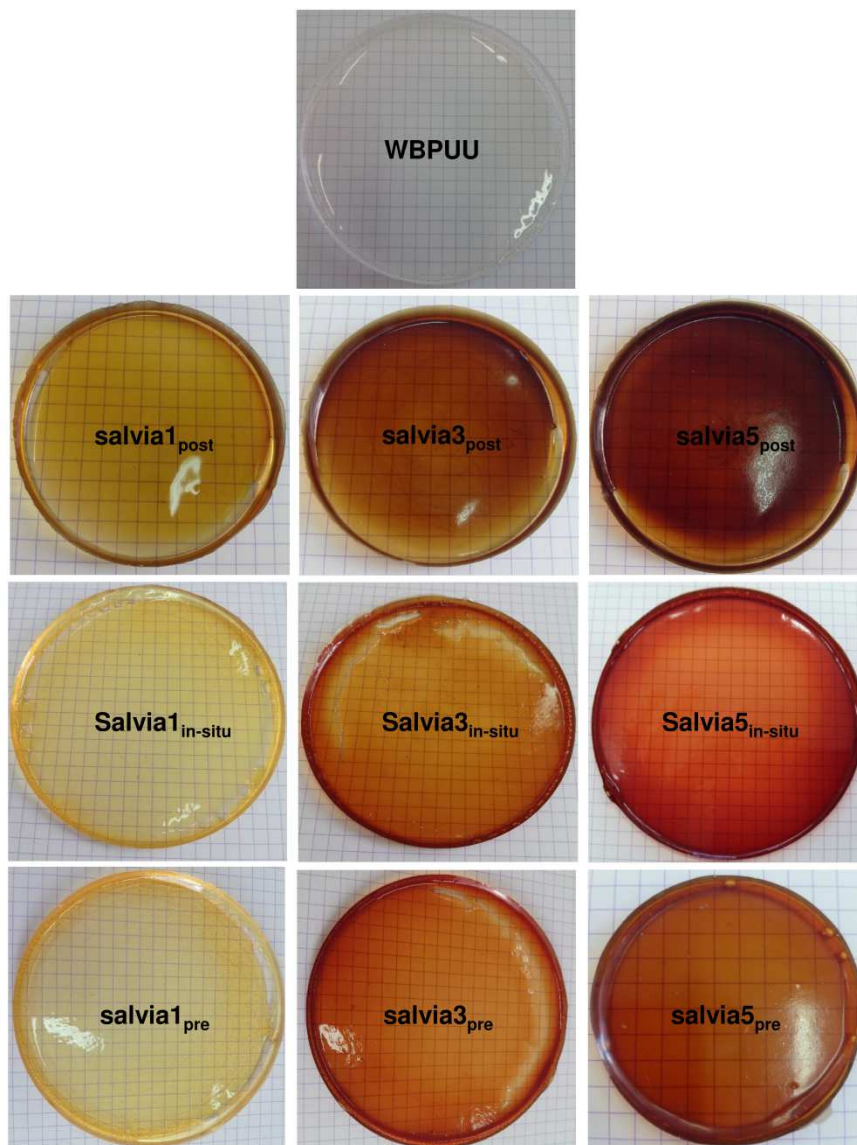
Figure 9.5 *Image of base WBPUU and WBPUU bioactive films containing Salvia extracts prepared by solvent-casting*
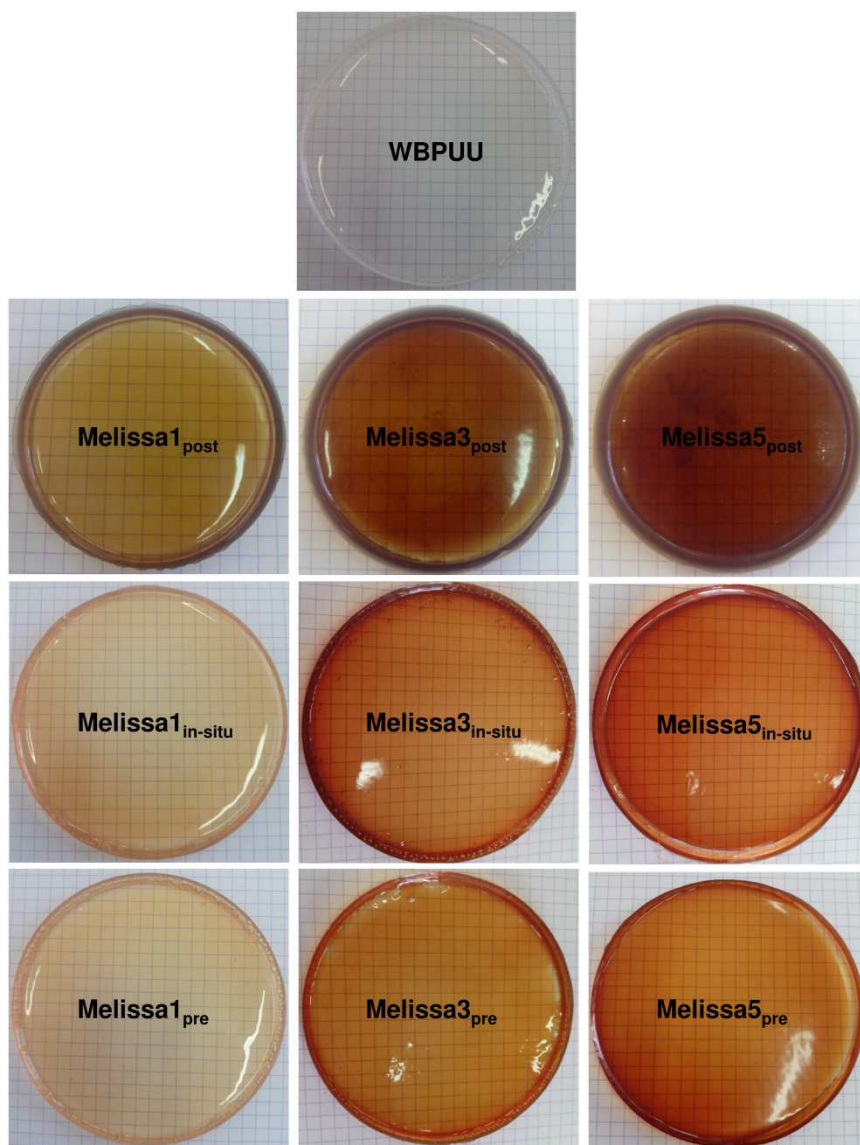
Figure 9.6 *Image of base WBPUU and WBPUU bioactive films containing Melissa extracts prepared by solvent-casting*

Analyzing the images, it was observed that the base WBPUU dispersion resulted in bright and transparent films. The addition of extract rendered the films

browner, being the effect more significant as the extract content increased, but maintaining the translucent quality in all the series.

Furthermore, it is worth noting that film's color intensity varied according to the extract incorporation route. In the case of post-method, it is believed that the extract became intercalated between WBPUU nanoparticles, and thus the variation of films color intensity was more remarkable. In addition, films containing 3 and 5 wt% prepared by post-method, resulted in a matte aspect. Otherwise, by *in-situ* method, and considering that the extract was progressively incorporated with water during dispersion formation, it is supposed that besides the intercalation of bioactive compounds among WBPUU nanoparticles, it would also tend to remain embedded inside nanoparticles. Thereby, lighter films were obtained comparing with their homologues prepared by post-method, but maintaining the brightness obtained in films prepared from the base WBPUU dispersion. In pre-method, taking into account that the extract was already incorporated between polyurethane chains during the dispersion formation, in this method, the bioactive compounds could remain both, inside and outside the nanoparticles, showing a greater surfactant effect comparing with *in-situ* method at low contents. Furthermore, lighter films were obtained by this method, in comparison with the respective films prepared by post-method, but being also matte in the case of 5 wt%. These facts, suggested that a low portion of the extract would remained embedded in the nanoparticles comparing with those prepared by *in-situ* method. The proposed mechanism of polyurethane-urea nanoparticles intercalation with bioactive compounds are shown in **Figure 9.7**.
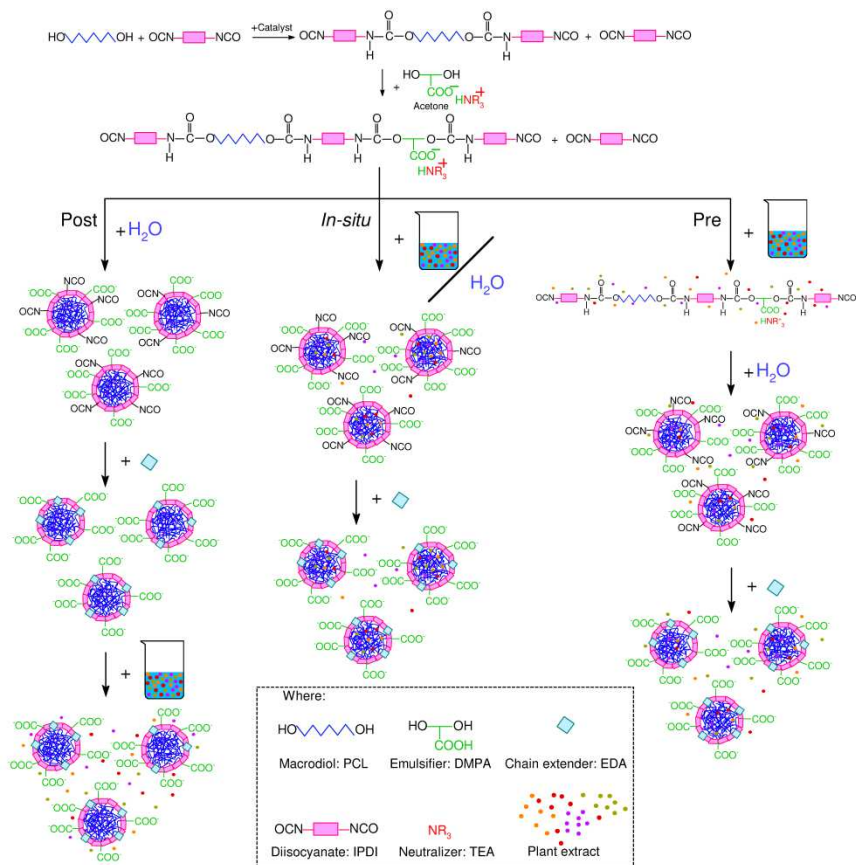
Figure 9.7 *Scheme of WBPUU nanoparticles intercalation mechanisms proposed considering the extracts incorporation route*

9.3.2.2 Fourier transform infrared spectroscopy

The functional groups, and the hydrogen bonding interactions of the base WBPUU and the Salvia- and Melissa-based WBPUU bioactive films were analyzed by FTIR and the spectra are shown in **Figure 9.8** and **Figure 9.9**, respectively.
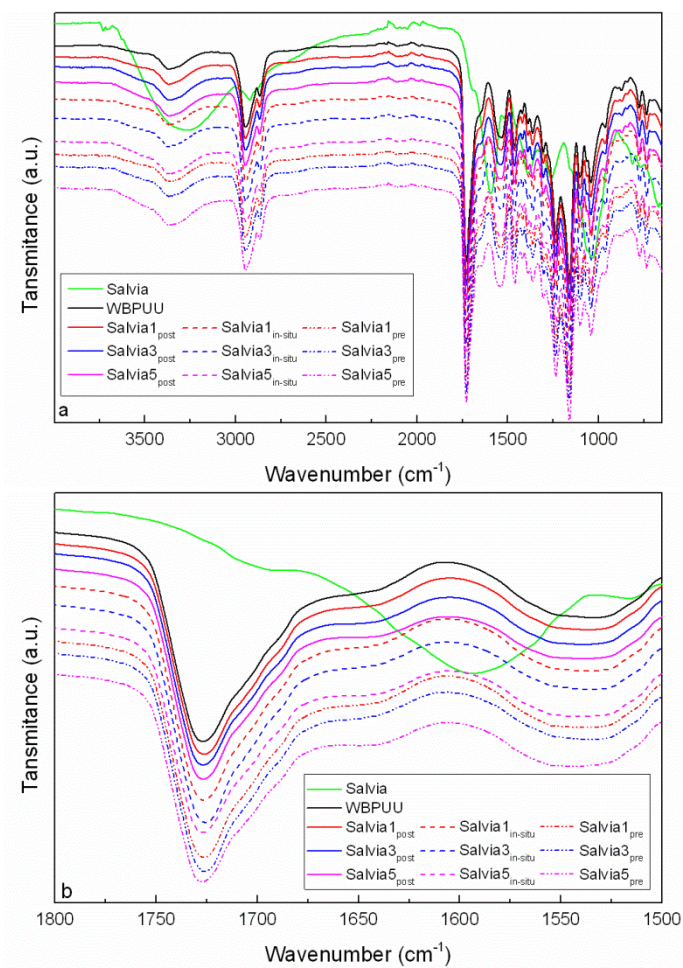
Figure 9.8 *a) FTIR spectra of Salvia, base WBPUU and WBPUU containing Salvia extracts bioactive films b) an amplification of carbonyl spectral region*
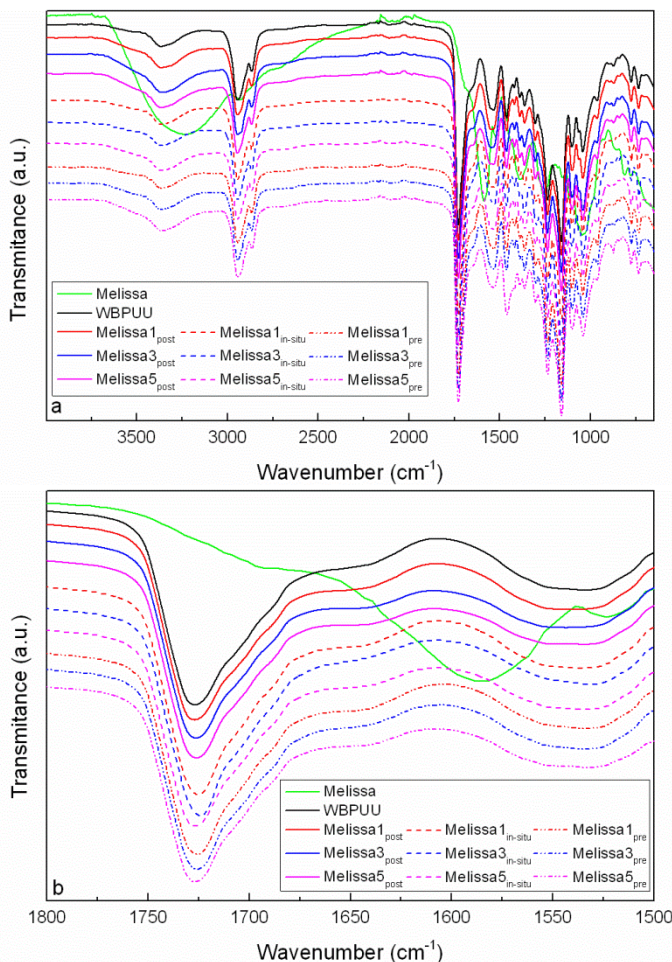
Figure 9.9 *a) FTIR spectra of Melissa, base WBPUU and WBPUU containing Melissa extracts bioactive films b) an amplification of carbonyl spectral region*

As previously observed, polyurethane-ureas showed two main regions in the ranges 3500-3100 cm^{-1} [12] and 1600-1800 cm^{-1} [13], related with the N-H and C=O of urethane and urea groups, respectively. In the case of Salvia and Melissa, a broad peak between 3700 and 3000 cm^{-1} was observed, related with the hydroxyl groups of the bioactive compounds presented in the extract, such as phenolic compounds [2]. Moreover, the broad band around 1700 cm^{-1} attributed

to the C=O of carboxylic groups of phenolic compounds and an intense peak around 1590 cm^{-1} related with the C=C of aromatic rings can be observed [14].

Analyzing spectra in the N-H region, in base WBPUU film a unique peak about 3350 cm^{-1} was observed, indicating that the N-H of both urethane and urea groups were involved in hydrogen bonds [15]. In the case of Salvia- and Melissa-based WBPUU films, an analogous peak was observed, which increased slightly with extract content, but overlapping with their hydroxyl groups peak.

With the purpose of studying the region related with carbonyl group stretching region, an amplification of this region is shown in **Figure 9.8b** and **Figure 9.9b**. In the case of the base WBPUU film, a peak at 1726 cm^{-1} was detected, attributed to the PCL and free C=O of urethane groups, and a band about 1640 cm^{-1} related with the hydrogen bonded C=O of urea groups [16,17]. The principal peak about 1726 cm^{-1} was also observed in the Salvia- and Melissa-based WBPUU films. In the case of post-method, variations were not noticeable in comparison with base WBPUU sample. Instead, by *in-situ* and pre-methods, some differences were observed. For 3 wt% extract content, with both incorporation routes, the peak was shifted towards lower wavenumbers (around 1723 cm^{-1}), indicating an intensification of the hydrogen bonding, in comparison with the base WBPUU. By contrast, for 5 wt% extract content, the peak shifted to higher wavenumbers (about 1728 cm^{-1}), suggesting the tendency towards the occurrence of free C=O groups. Nevertheless, a slight increase of the shoulder about 1640 cm^{-1} was also appreciated, implying a greater amount of hydrogen bonded C=O of urea groups

9.3.2.3 Thermal properties

The thermal behavior of base WBPUU and WBPUU containing Salvia and Melissa extracts bioactive films was analyzed by DSC, and thermograms are shown in **Figure 9.10**.
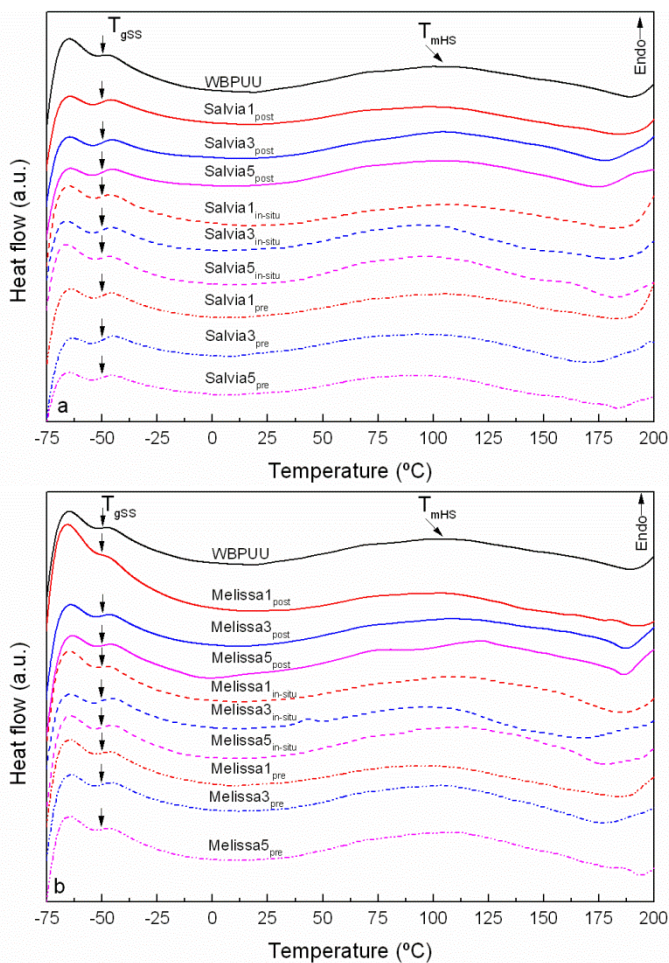
Figure 9.10 *DSC thermograms of base WBPUU and WBPUU containing a) Salvia and b) Melissa extracts bioactive films*

The glass transition temperature, as well as the hard domain melting temperature and enthalpy, obtained from the thermograms of the Salvia- and

Melissa-based WBPUU films, are shown in **Table 9.7** and **Table 9.8**, respectively. Additionally, thermal properties of the base WBPUU film are also shown in both tables.

Table 9.7 *Thermal properties of base WBPUU and WBPUU containing Salvia extracts*

Sample	T_{gSS} (°C)	T_{mHS} (°C)	ΔH_{mHS} (J g^{-1})
WBPUU	-49.8	99.2	32.1
Salvia1$_{post}$	-50.0	97.4	23.2
Salvia3$_{post}$	-50.0	103.7	27.7
Salvia5$_{post}$	-50.0	101.8	27.0
Salvia1$_{in\text{-}situ}$	-50.0	104.9	22.8
Salvia3$_{in\text{-}situ}$	-50.0	92.5	27.6
Salvia5$_{in\text{-}situ}$	-50.0	93.2	37.2
Salvia1$_{pre}$	-50.0	105.1	25.7
Salvia3$_{pre}$	-50.0	96.1	27.0
Salvia5$_{pre}$	-50.0	91.7	28.2

Analyzing the base WBPUU film, it was appreciated that the polyurethane-urea film presented a T_{gSS} around -50 °C, which remained similar in the bioactive films series. Furthermore, a broad transition related with the long range order of hard segment domains [18] was observed. In general, it was observed that Melissa extract incorporation favored the ordering of hard segment domains in a greater extent, comparatively with their homologues containing Salvia extract, thus resulting in higher enthalpy values. In the case of post-method, the extract content increase led to the increase of T_{mHS} and ΔH_{mHS}, which resulted more

discernible in the case Melissa based films. By this incorporation route, it was proposed that the extract would be intercalated between polyurethane-urea nanoparticles, which would facilitate the interactions among them, favoring the occurrence of hard segment order domains.

Table 9.8 *Thermal properties of base WBPUU and WBPUU containing Melissa extracts*

Sample	T_{gSS} (°C)	T_{mHS} (°C)	ΔH_{mHS} (J g^{-1})
WBPUU	-49.8	99.2	32.1
Melissa1$_{post}$	-50.0	102.4	25.5
Melissa3$_{post}$	-50.0	109.2	35.0
Melissa5$_{post}$	-50.0	122.7	41.3
Melissa1$_{in-situ}$	-50.0	105.2	34.7
Melissa3$_{in-situ}$	-50.1	95.5	24.0
Melissa5$_{in-situ}$	-50.1	114.2	37.2
Melissa1$_{pre}$	-50.0	98.3	27.0
Melissa3$_{pre}$	-50.1	104.0	33.0
Melissa5$_{pre}$	-50.1	110.7	41.3

By contrast, by *in-situ* and pre-methods, it was supposed that bioactive compounds could remain either inside or around nanoparticles. In this way, in the case of Salvia extract, it was observed a decrease in ΔH_{mHS} at low extract content (1 wt%). This could be promoted by the high ordered hard domains, as reflected by the significant increase in T_{mHS} value. Then, at higher extract content (3 and 5 wt%), in general, a decrease in T_{mHS} and an increase in ΔH_{mHS} were observed with Salvia-based films. This could be related with the extract

homogeneity, both inside and outside the nanoparticles that interfered in the formation of crystals with higher T_{mHS} but favored the interactions, leading to an increase in enthalpy. In the case of Melissa-based films, in general, the addition of extract favored the arrangement of hard order domains, resulting in a progressive increase of both, T_{mHS} and ΔH_{mHS} values, except in Melissa3$_{in-situ}$ sample. It is thought that in this case different interactions were developed, thus resulting in such elevated pH and viscosity values, as previously discussed. It is worth noting that, in general, Melissa extract incorporation favored the ordering of hard segment domains in a greater extent, in comparison with their homologues containing Salvia extract.

9.3.2.4 Mechanical properties

Mechanical behavior of the Salvia- and Melissa-based WBPUU films is shown in **Figure 9.11**. Also, the comparison with the base WBPUU film is shown.

Mechanical properties obtained from stress-strain curves of base WBPU and Salvia- and Melissa-based films are summarized in **Table 9.9** and **Table 9.10**, respectively.

Analyzing mechanical properties, it was observed that Melissa extract conferred higher stiffness to the bioactive films, in comparison with the Salvia extract. This could be related with the previously discussed higher enthalpy values obtained by DSC.
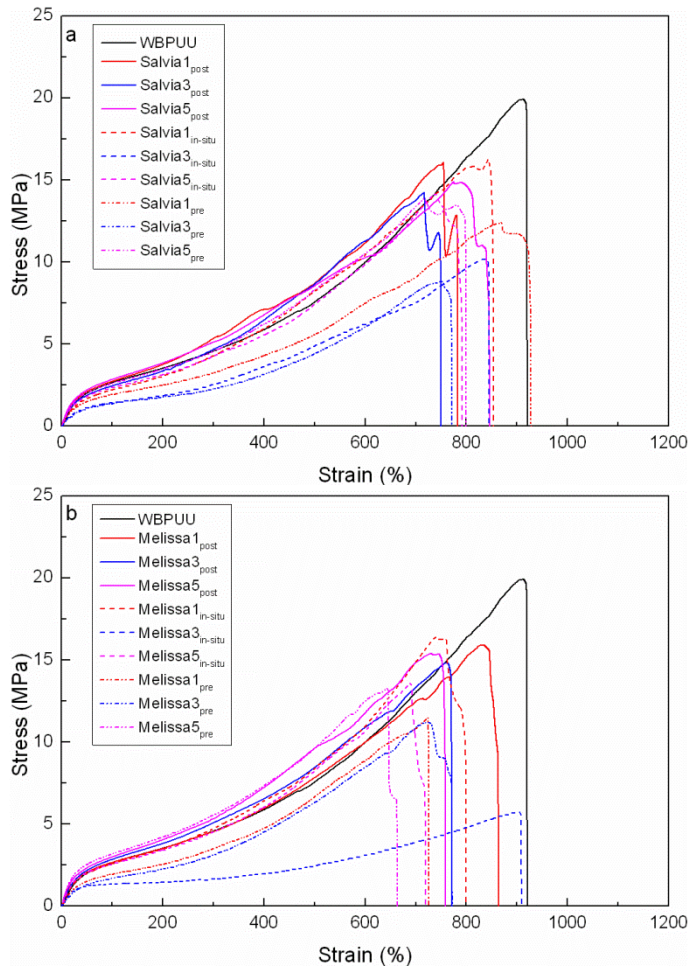
Figure 9.11 *Stress–strain curves of base WBPUU and WBPUU containing a) Salvia and b) Melissa extracts bioactive films*

Table 9.9 *Mechanical properties of base WBPUU and WBPUU containing Salvia extract bioactive films*

Sample	σ_y (MPa)	σ_b (MPa)	E (MPa)	ε_b (%)
WBPUU	3.0 ± 0.1	18.4 ± 1.3	6.4 ± 0.4	891 ± 51
Salvia1$_{post}$	2.4 ± 0.1	15.9 ± 0.3	8.5 ± 0.2	738 ± 45
Salvia3$_{post}$	2.4 ± 0.1	14.3 ± 1.7	8.1 ± 0.4	699 ± 52
Salvia5$_{post}$	2.5 ± 0.1	15.0 ± 1.0	8.1 ± 0.8	777 ± 65
Salvia1$_{in\text{-}itu}$	1.8 ± 0.1	16.4 ± 2.2	6.0 ± 0.4	878 ± 47
Salvia3$_{in\text{-}itu}$	1.3 ± 0.1	9.3 ± 1.6	4.5 ± 0.2	847 ± 53
Salvia5$_{in\text{-}itu}$	2.2 ± 0.2	13.3 ± 0.8	6.5 ± 0.4	728 ± 30
Salvia1$_{pre}$	1.9 ± 0.1	12.3 ± 1.1	5.5 ± 0.3	826 ± 58
Salvia3$_{pre}$	1.5 ± 0.0	9.3 ± 0.7	3.7 ± 0.2	796 ± 60
Salvia5$_{pre}$	2.6 ± 0.0	13.8 ± 0.7	7.8 ± 0.2	716 ± 26

Regarding the post-method, it was observed that bioactive films prepared by Salvia extract, resulted in lower σ_y values comparing with the base WBPUU film, which could be attributed to the decrease in ΔH_{mHS} values, as previously discussed. However, in the case of using Melissa extract, slightly higher σ_y values were obtained, attributable to the greater ordering ability of hard segment domains. Nevertheless, a stiffening effect was observed for both series, which presented slightly higher E values and lower σ_b and ε_b values. Otherwise, in the case of *in-situ* and pre-method, and considering the improved connection of Salvia extract with nanoparticles inside and surrounding them, it is thought that a greater effect in the formation and cohesion process occurred. Thus, more

variations were observed comparatively with post-method and base WBPUU samples.

Table 9.10 *Mechanical properties of WBPUU and WBPUU containing Melissa extract bioactive films*

Sample	σ_y (MPa)	σ_b (MPa)	E (MPa)	ε_b (%)
WBPUU	3.0 ± 0.1	18.4 ± 1.3	6.4 ± 0.4	891 ± 51
Melissa1$_{post}$	3.2 ± 0.3	16.4 ± 1.9	8.3 ± 1.1	848 ± 67
Melissa3$_{post}$	3.3 ± 0.2	15.3 ± 3.0	8.6 ± 0.6	741 ± 70
Melissa5$_{post}$	3.2 ± 0.1	14.9 ± 1.1	9.8 ± 0.3	740 ± 53
Melissa1$_{in-itu}$	2.9 ± 0.1	16.0 ± 2.0	7.3 ± 0.2	766 ± 25
Melissa3$_{in-itu}$	1.4 ± 0.1	5.4 ± 0.7	4.8 ± 0.2	883 ± 27
Melissa5$_{in-itu}$	2.5 ± 0.2	14.7 ± 1.6	7.2 ± 0.2	723 ± 27
Melissa1$_{pre}$	2.0 ± 0.1	10.6 ± 1.2	5.0 ± 0.2	710 ± 16
Melissa3$_{pre}$	1.8 ± 0.1	10.9 ± 1.3	4.1 ± 0.2	769 ± 47
Melissa5$_{pre}$	2.9 ± 0.2	12.9 ± 0.9	10.0 ± 0.0	668 ± 47

In this way, at low Salvia extract contents (1 wt%), lower σ_y and E values were appreciated comparing with base WBPUU films; but in general, increased at high extract contents (5 wt%). In comparison, considering Melissa extract, low extract contents resulted in higher σ_y and E values, which maintained or increased by *in-situ* and pre-methods, respectively, at high extract contents (5 wt%). These results can be related with DSC results, where enthalpy values corroborated film stiffness. It is worth noting that in the case of the use of 3 wt% content, in both methods, the films behavior changed. It is thought that at this

percentage, greater extract quantity would result embedded inside nanoparticles, conferring flexibility to the system.

9.3.2.5 Thermomechanical properties

The thermomechanical properties of the Salvia- and Melissa-based WBPUU films were analyzed by DMA, and E' and Tanδ curves are shown in **Figure 9.12**. For comparison purposes, the analysis of the base WBPUU film was also included.

At low temperatures, in the glassy state, it was observed that in both series, all bioactive films showed higher E' values comparing with base WBPUU sample. At higher temperatures, starting from -50 °C, a decrease in E' curves was observed, being reflected in Tanδ curves as a peak, which was related with the T_{gss} of WBPUU bioactive films. The peak temperature resulted similar in all samples, but it was appreciated an increase in the intensity of the peak in samples prepared by *in-situ* and pre-method for films containing an extract content of 1 and 3 wt%. This fact could be attributed to the greater amount of polyurethane-urea chains involved in the transition [19]. As the temperature increased, i.e. as the polyurethane-urea chains acquired mobility, it was observed for the post-method, that E' curves were maintained above the one of the base WBPUU sample, probably due to the stiffening effect of films observed in mechanical properties results.
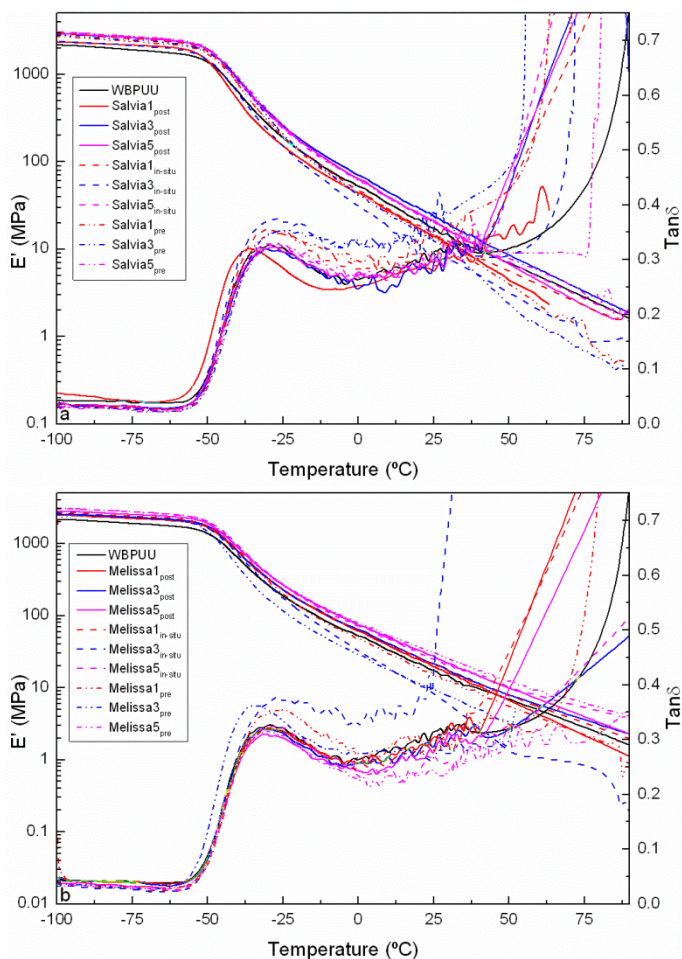
Figure 9.12 *Storage modulus and Tanδ curves of base WBPUU and WBPUU containing a) Salvia and b) Melissa extracts*

An exception was observed with the sample Salvia1$_{post}$, where the produced film showed a lower E' value previously to flow.

Instead, in the case of *in-situ* and pre-methods, once T$_{gSS}$ transition was exceeded, only the film icontaining 5 wt% of Salvia extract maintained higher E' curves in comparison with the base WBPUU film. However, in the case of Melissa extract, E' curves showed higher values than the base WBPUU films, with the exception of the ones containing 3 wt% extract. This fact would be

attributed to the lower stiffness of those films, as discussed previously in mechanical properties section.

9.3.2.6 Morphology

The morphology of the base WBPUU and Salvia- and Melissa-based WBPUU films was analyzed by AFM. Height and phase images of the Salvia series are shown in **Figure 9.13** whereas the images of Melissa series are shown in **Figure 9.14**.

Analyzing the AFM images, it was observed that the base WBPUU films showed bright and dark regions attributed to the hard and soft domains reflecting the microphase morphology of the polyurethane-urea [20]. Considering the image of the WBPUU samples containing an extract content of 3 wt%, although it was not possible to discern the bioactive compounds, some variations were observed in the morphology of the base polyurethane-urea material. The spherical morphology observed in the base WBPUU film was also appreciated in the case of the ones containing the extracts; nevertheless these samples presented a more spherical defined microstructure. This fact can be attributed to polyurethane-urea nanoparticles constituting the dispersion, suggesting the suitable cohesiveness during film formation. It is worth noting that in the case of *in-situ* method, for both extracts, the morphology was more discernible in comparison with other methods, and in the case of Melissa-films, it seemed even to be appreciated the connectivity among some nanoparticles. The analyzed microstructures would support the idea that the extract could act as a surfactant facilitating the formation of the polyurethane-urea nanoparticles.
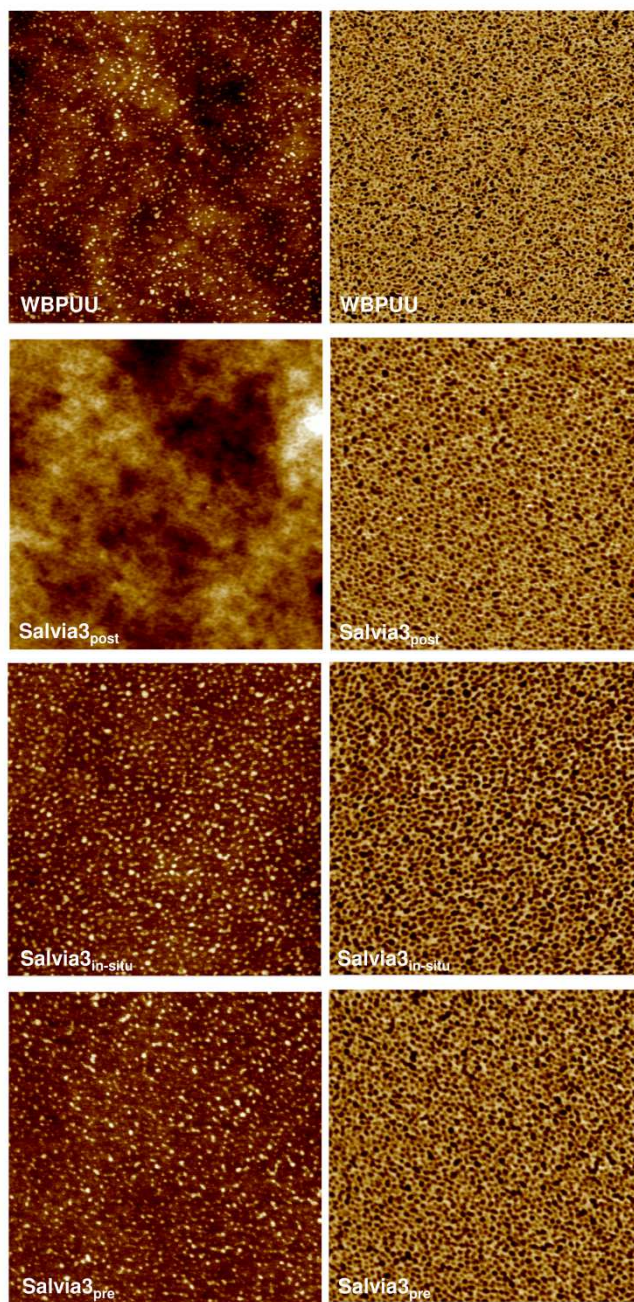
Figure 9.13 *AFM height (left) and phase (right) images of base WBPUU and WBPUU containing 3 wt% of Salvia extract (size: 3x3 μm²)*
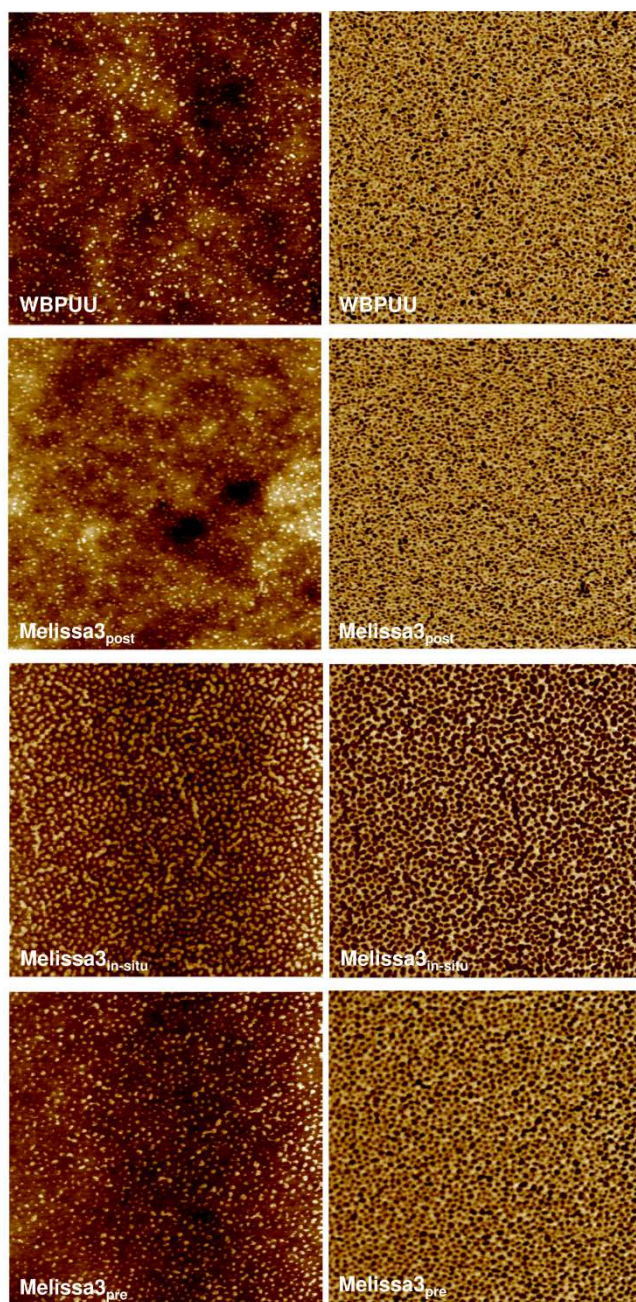
Figure 9.14 *AFM height (left) and phase (right) images of base WBPUU and WBPUU containing 3 wt% of Melissa extract (size: 3x3 μm²)*

9.3.2.7 Antimicrobial properties

The antimicrobial properties of the Salvia- and Melissa-based WBPUU films were analyzed against Gram positive bacteria *Staphylococcus aureus* ATCC 19213 and Gram negative *Escherichia coli* ATCC 10536 and *Pseudomonas aeruginosa* ATCC 9027 as test microorganisms. The results for the incubation at 37 °C, during 1 and 4 days, are summarized in **Table 9.11** and **Table 9.12**, respectively for Salvia- and Melissa- based films.

Table 9.11 *Antibacterial properties of base WBPUU and WBPUU containing Salvia extracts*

Sample	1 day			4 days		
	S. aureus	E. coli	P. aeruginosa	S. aureus	E. coli	P. aeruginosa
PUUD	✓	✓	✓	✿	✿	✿
Salvia1$_{post}$	✓	✓	✓	✿	✓	✿
Salvia3$_{post}$	✓	✓	✓	✿	✓	✿
Salvia5$_{post}$	✓	✓	✓	✿	✓	✿
Salvia1$_{in-itu}$	✓	✓	✓	✿	✿	✿
Salvia3$_{in-itu}$	✓	✓	✓	✓	✓	✓
Salvia5$_{in-itu}$	✓	✓	✓	✓	✓	✓
Salvia1$_{pre}$	✓	✓	✓	✿	✿	✿
Salvia3$_{pre}$	✓	✓	✓	✿	✓	✓
Salvia5$_{pre}$	✓	✓	✓	✿	✓	✓

✓ There was not bacteria growth on the surface or behind the film

✿ There was bacteria growth on the surface or behind the film

Table 9.12 *Antibacterial properties of base WBPUU and WBPUU containing Melissa extracts*

Sample	1 day			4 days		
	S. aureus	E. coli	P. aeruginosa	S. aureus	E. coli	P. aeruginosa
PUUD	✓	✓	✓	● (growth)	● (growth)	● (growth)
Melissa1$_{post}$	✓	✓	✓	✓	✓	● (growth)
Melissa3$_{post}$	✓	✓	✓	✓	✓	✓
Melissa5$_{post}$	✓	✓	✓	✓	✓	✓
Melissa1$_{in\text{-}itu}$	✓	✓	✓	✓	✓	● (growth)
Melissa3$_{in\text{-}itu}$	✓	✓	✓	✓	✓	✓
Melissa5$_{in\text{-}itu}$	✓	✓	✓	✓	✓	✓
Melissa1$_{pre}$	✓	✓	✓	✓	● (growth)	● (growth)
Melissa3$_{pre}$	✓	✓	✓	✓	● (growth)	● (growth)
Melissa5$_{pre}$	✓	✓	✓	✓	✓	● (growth)

✓ There was not bacteria growth on the surface or behind the film

● There was bacteria growth on the surface or behind the film

Analyzing the results, it was observed that after 1 day of incubation, the base WBPUU film presented bacteriostaic properties against the three bacteria, hindering their growth on the film. Nevertheless, none of the samples showed an inhibition zone. Furthermore, Salvia- and Melissa-based WBPUU films, presented also bacteriostatic effect against bacteria. **Figure 9.15**, **Figure 9.16** and **Figure 9.17** show the incubated plates of the base WBPUU and the Salvia-based WBPUU films.
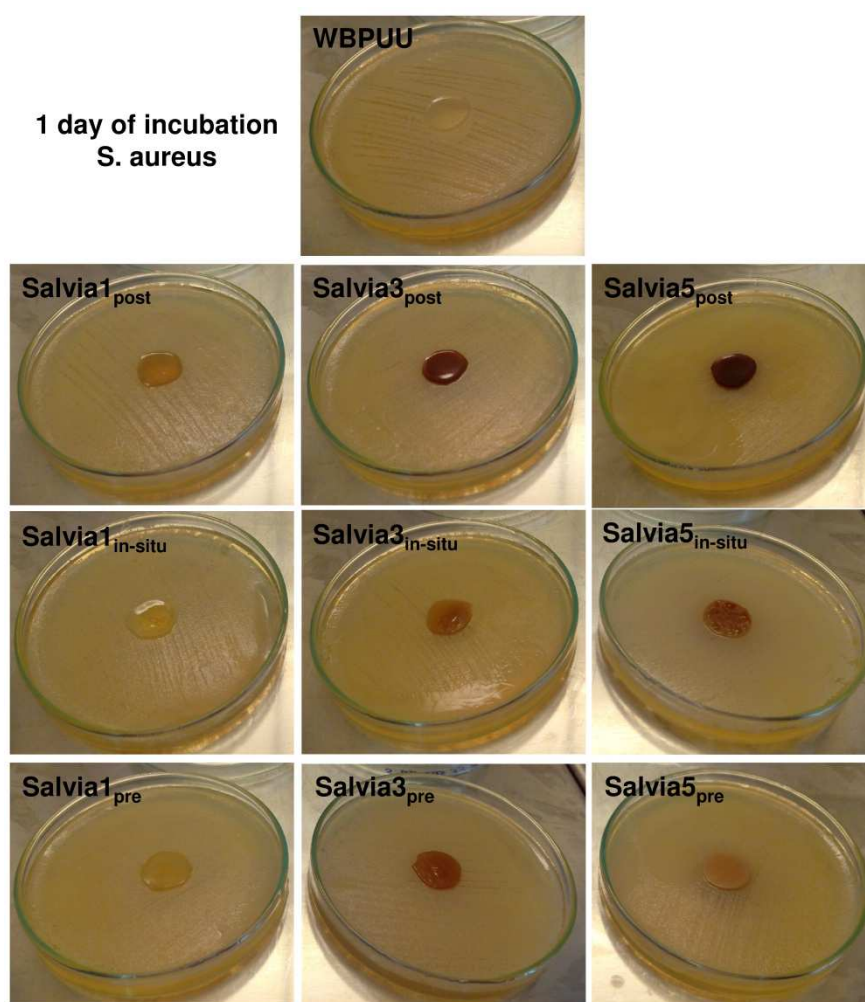
Figure 9.15 *Antimicrobial tests of base WBPUU and WBPUU containing Salvia extract against S. aureus after 1 day of incubation at 37 ℃*
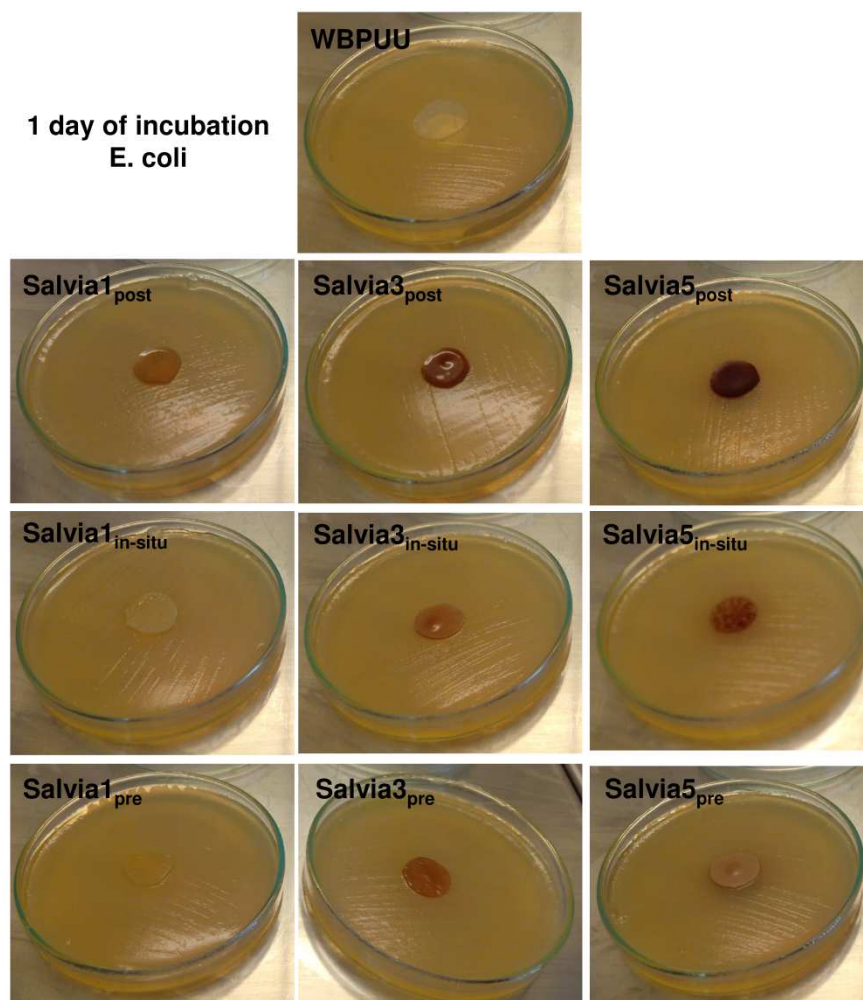
Figure 9.16 *Antimicrobial tests of base WBPUU and WBPUU containing Salvia extract against E. coli after 1 day of incubation at 37 ℃*
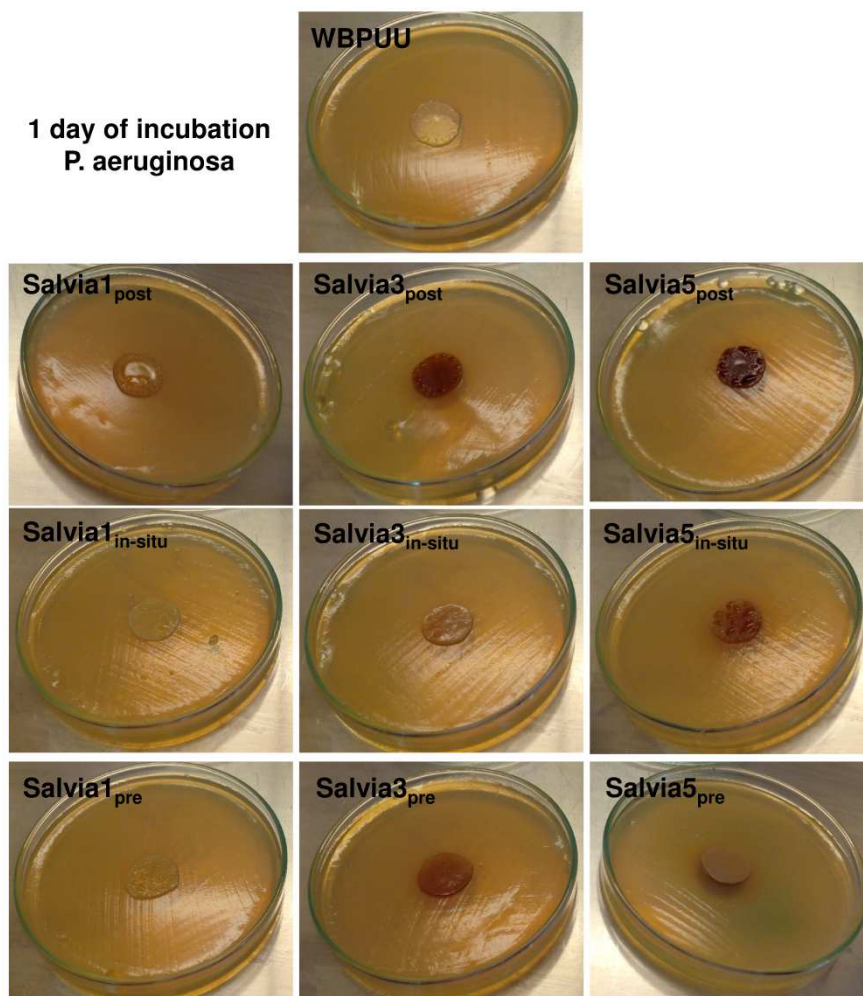
Figure 9.17 *Antimicrobial tests of base WBPUU and WBPUU containing Salvia extract against P. aeruginosa after 1 day of incubation at 37 ℃*

However, it was observed that after 4 days of incubation the base WBPUU sample did not show inhibitory power against none of the assayed bacteria, whereas the addition of the extracts, as well as the incorporation route, resulted in different behaviors, as observed in **Figure 9.18**, **Figure 9.19** and **Figure 9.20** for Salvia extract and **Figure 9.21**, **Figure 9.22** and **Figure 9.23** for Melissa extract.
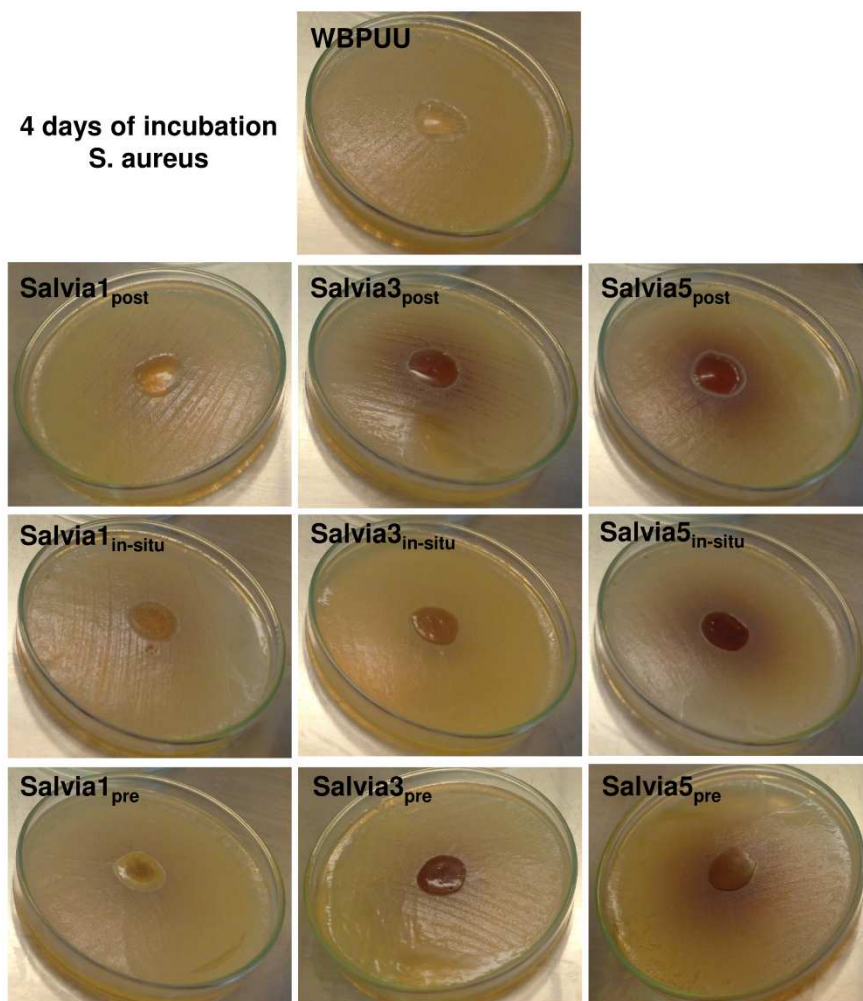
Figure 9.18 *Antimicrobial tests of base WBPUU and WBPUU containing Salvia extract against S. aureus after 4 days of incubation at 37 °C*
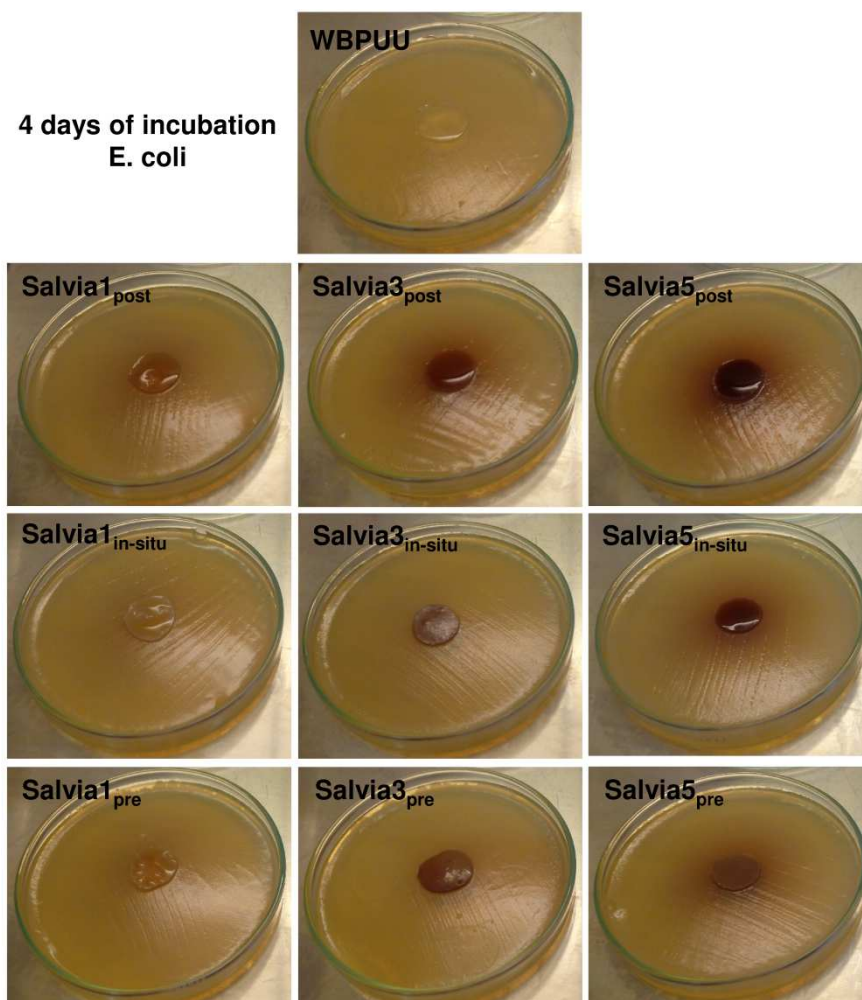
Figure 9.19 *Antimicrobial tests of base WBPUU and WBPUU containing Salvia extract against E. coli after 4 days of incubation at 37 °C*
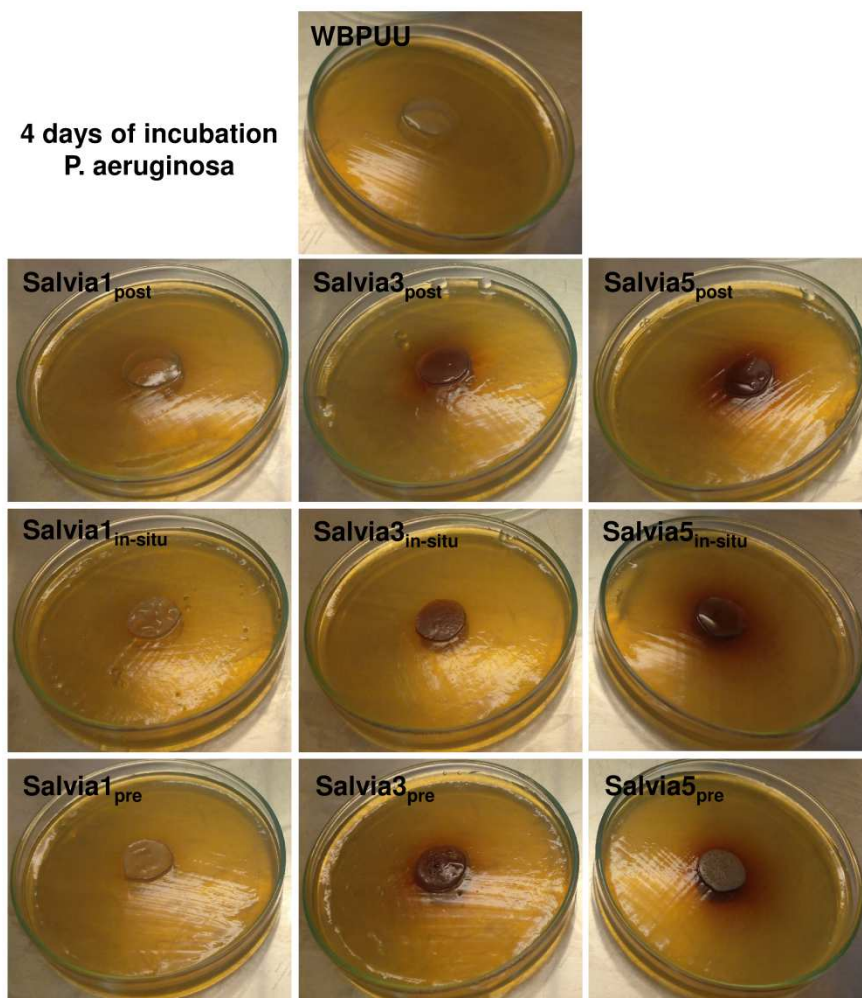
Figure 9.20 *Antimicrobial tests of base WBPUU and WBPUU containing Salvia extract against P. aeruginosa after 4 days of incubation at 37 °C*
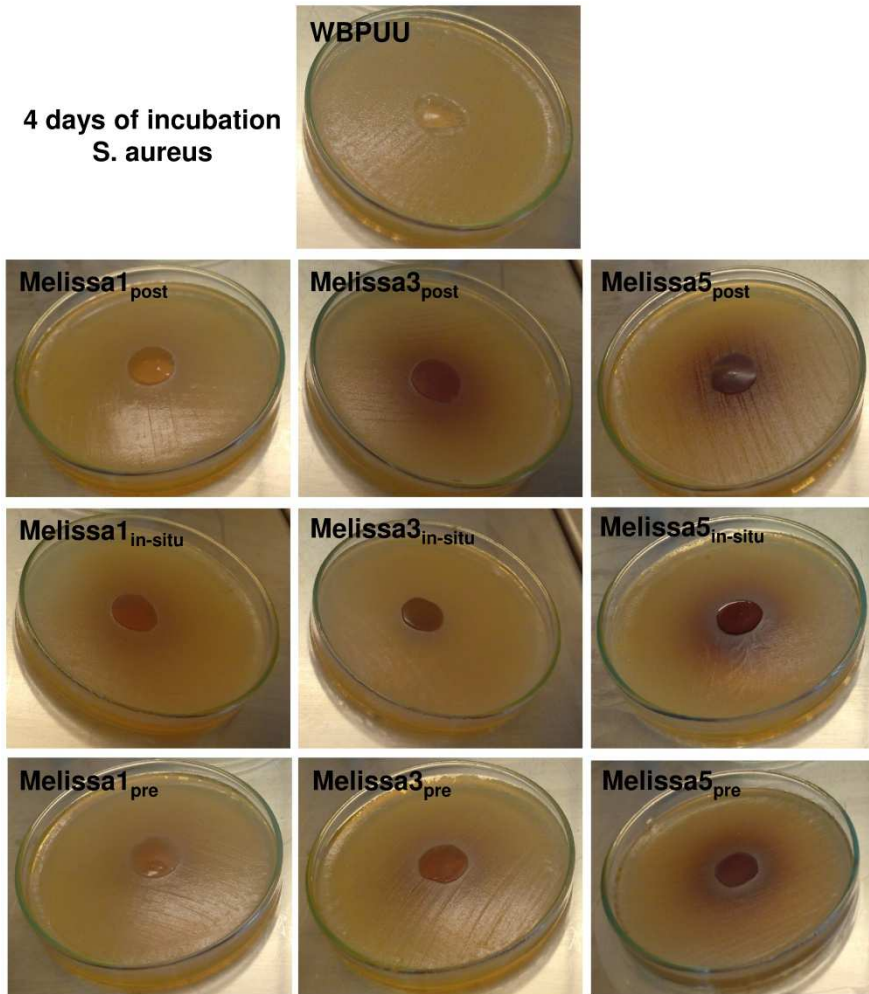
Figure 9.21 *Antimicrobial tests of base WBPUU and WBPUU containing Melissa extract against S. aureus after 4 days of incubation at 37 °C*
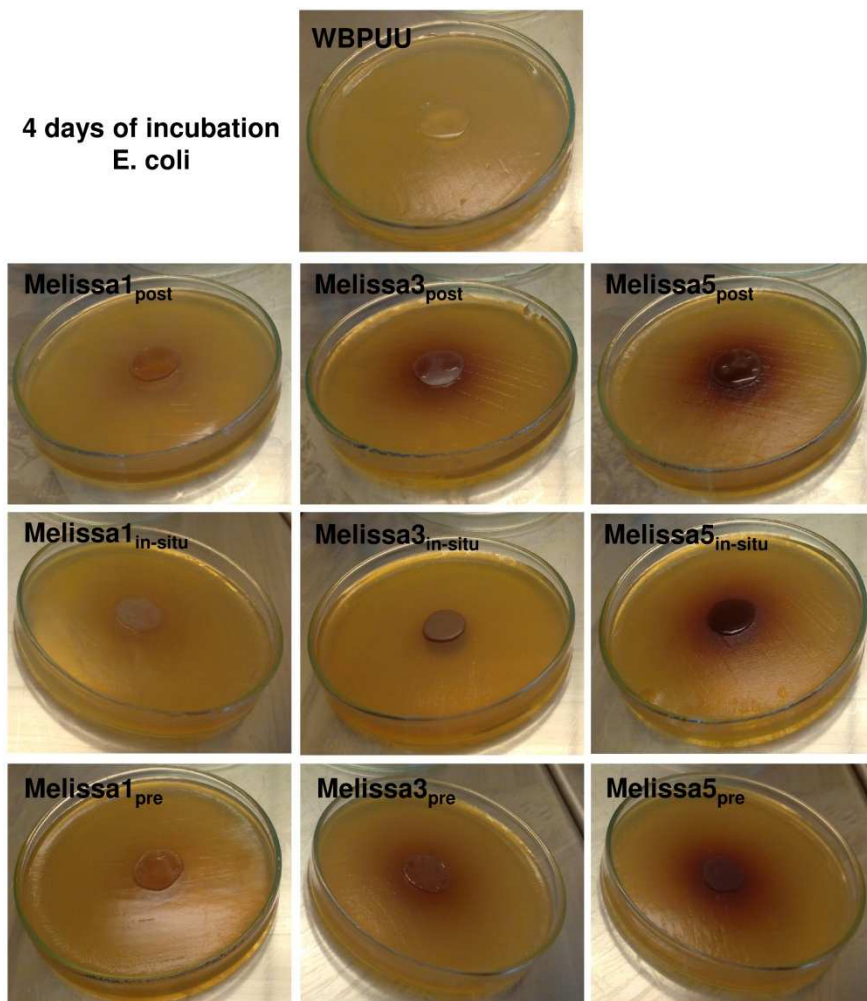
Figure 9.22 *Antimicrobial tests of base WBPUU and WBPUU containing Melissa extract against E. coli after 4 days of incubation at 37 °C*
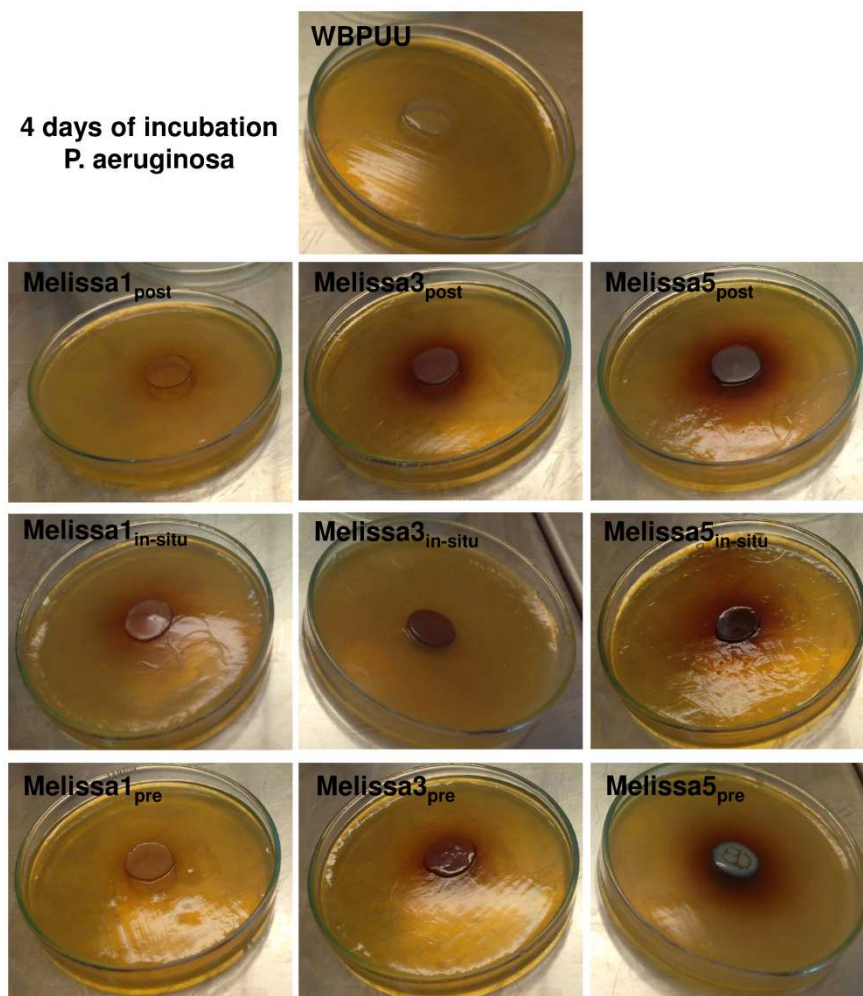
Figure 9.23 *Antimicrobial tests of base WBPUU and WBPUU containing Melissa extract against P. aeruginosa after 4 days of incubation at 37 °C*

Regarding Gram positive S. aureus, it was observed that the inhibitory effect caused by the incorporation of Salvia extract was only effective in the case of *in-situ* method, and at high extract contents (3 and 5 wt%), whereas in the case of Melissa extract the bacteriostatic effect was maintained in all the series. This fact could be related with the bioactive components constituting the extract. For example, some tannin and phenolic compounds would be able to disintegrate

bacterial colonies attributable to their interference in the bacterial cell wall synthesis process by their adsorption to cell membranes [21]. In this way, the amphipatic character of flavonoids promotes their interaction with cell membranes presenting relevance from biological and medical point of view [22]. Nevertheless, it has to be worth noting that the origin of the plant, as well as the extraction process, leads to different extract compositions. Indeed, starting from the same raw material, it was reported that the solvent chosen for extraction can influence the antibacterial ability since different metabolite compositions can be attained [23,24]. In general, in the case of Salvia, the aqueous extract did not result in a significant effect against S. aureus. Only by using *in-situ* method, which promotes the extract to remain more embedded, especially at high extract contents, the bacteriostatic character of bioactive films continued after 4 days of incubation.

Instead, in the case of E. coli, other tendencies were observed. For Salvia extract, the bacteria growth was inhibited in the bioactive films indicating the effectiveness of this extract against E. coli bacteria, except in the films containing 1 wt% incorporated by *in-situ* and pre-methods. In these cases, considering the low content of extract, and the fact that it could have remained embedded, the inhibition effect was hindered. The same tendency was observed against P. aeruginosa. Furthermore, taking into account that P. aeruginosa result more resistant, if comparing with E. coli (being both Gram negative bacteria), post-method did not result effective, probably influenced by the lixiviation effect with time.

Regarding Melissa extract, the bacteriostatic effect against E. coli was maintained in all the series, except for 1 and 3 wt% of extract incorporated by the pre-method. However, at low extract content (1 wt%) the bacteriostatic

effect against P. aeruginosa was not effective, probably due to the low content of bioactive compounds in order to inhibit P. aeruginosa bacteria growth. At higher contents, by the post- and *in-situ* methods, the inhibition effect was achieved after 4 days of incubation, whereas in the case of the pre-method, it was not possible even at high extract contents. These results suggested that pre-method was not very appropriate in the case of Melissa extract incorporation against these Gram negative bacteria. Moreover, as it is shown in **Figure 9.23**, P. aeruginosa bacteria was able to form a biofilm in Melissa5$_{pre}$ sample after 4 days of incubation.

9.4 Conclusions

In this chapter polyurethane-urea dispersions were synthesized, with and without added extracts from *Salvia officinalis L.* and *Melissa officinalis L.*, aiming at preparing bioactive (antimicrobial) films. In this way, 1, 3 and 5 wt% of the extracts were incorporated into the polyurethane-urea dispersions by using three different incorporation routes: post-method, *in-situ* method and pre-method. It was observed that the extract content, as well as the incorporation route, influenced the final properties of the prepared films.

In general, it was observed that the WBPUU dispersions become more viscous with the increase of the extract content. Furthermore, particle size results revealed that the WBPUU particle size distributions broaden to lower values, which was related to the surfactant effect attributed to the used extracts. Regarding thermal properties of the films, it was appreciated that Melissa extract favored, at a greater extent, the ordering ability of hard domains when compared with their homologues prepared with Salvia extract, being the effect more discernible in samples prepared by the post-method. Considering that

extracts could result embedded by the WBPUU particles, when the *in-situ* and pre-methods were followed, it resulted more difficult the increase of ΔH_{mHS} values in some of the samples. This fact influenced the mechanical properties of the films, where it was observed a stiffening effect in samples prepared by the post-method. In the case of *in-situ* and the pre-method (with 3 wt% of extract), films became more flexible, which was related with the distribution mechanism of the extract within the polyurethane-urea nanoparticles. In this way, in thermomechanical analysis, these samples showed lower E' values comparing with the base WBPUU sample. The morphology of WBPUU samples containing extracts at 3 wt%, as analyzed by AFM, revealed that the spherical morphology observed in the base WBPUU sample, resulted more discernible in the presence of extract, suggesting their surfactant effect in the dispersion formation. Antibacterial tests revealed that after 1 day of incubation, all base WBPUU and Salvia- and Melissa-based WBPUU series, showed bacteriostatic effect against the analyzed S. aureus, E. coli and P. aeruginosa bacteria. After 4 days of incubation, only some samples containing Salvia or Melissa extract, presented bacteriostatic effect, being the magnitude of the effect dependent on the extract content and incorporation route. This effect can be attributed, either to the extracts composition in terms of bioactive compounds or to their distribution in the WBPUU system.

9.5 References

[1]   O. Stefanović, L. Comic, Synergistic antibacterial interaction between Melissa officinalis extracts and antibiotics, J. Appl. Pharm. Sci. 2 (2012) 1–5.

[2]   N. Martins, L. Barros, C. Santos-Buelga, M. Henriques, S. Silva, I.C.F.R. Ferreira, Evaluation of bioactive properties and phenolic compounds in different extracts prepared from Salvia officinalis L., Food Chem. 170 (2015) 378–385.

[3]   M. Carocho, L. Barros, R.C. Calhelha, A. Ćirić, M. Soković, C. Santos-Buelga, P. Morales, I.C.F.R. Ferreira, Melissa officinalis L. decoctions as functional beverages: A bioactive approach and chemical characterization, Food Funct. 6 (2015) 2240–2248.

[4]   V.D. Athawale, M.A. Kulkarni, Effect of dicarboxylic acids on the performance properties of polyurethane dispersions, J. Appl. Polym. Sci. 117 (2010) 572–580.

[5]   V. García-Pacios, Y. Iwata, M. Colera, J.M. Martín-Martínez, Influence of the solids content on the properties of waterborne polyurethane dispersions obtained with polycarbonate of hexanediol, Int. J. Adhes. Adhes. 31 (2011) 787–794.

[6]   C.H. Tsou, H.T. Lee, W.S. Hung, M. De Guzman, S.T. Chen, M.C. Suen, S.T. Wicaksono, Effects of different metals on the synthesis and

properties of waterborne polyurethane composites containing pyridyl units, Polym. Bull. (2016). doi:10.1007/s00289-016-1767-3.

[7]   T. Sharma, G.S. Kumar, B.H. Chon, J.S. Sangwai, Viscosity of the oil-in-water pickering emulsion stabilized by surfactant-polymer and nanoparticle-surfactant-polymer system, Korea-Australia Rheol. J. 26 (2014) 377–387.

[8]   A.K. Nanda, D.A. Wicks, S.A. Madbouly, J.U. Otaigbe, Effect of ionic content, solid content, degree of neutralization, and chain extension on aqueous polyurethane dispersions prepared by prepolymer method, J. Appl. Polym. Sci. 98 (2005) 2514–2520.

[9]   L. Tmáková, S. Sekretár, Š. Schmidt, Plant-derived surfactants as an alternative to synthetic surfactants: Surface and antioxidant activities, Chem. Pap. 70 (2016) 188-196.

[10]   K. Holmberg, Natural surfactants, Curr. Opin. Colloid Interf. Sci. 6 (2001) 148–159.

[11]   S. Salati, G. Papa, F. Adani, Perspective on the use of humic acids from biomass as natural surfactants for industrial applications, Biotechnol. Adv. 29 (2011) 913–922.

[12]   A.K. Mishra, D.K. Chattopadhyay, B. Sreedhar, K.V.S.N. Raju, FT-IR and XPS studies of polyurethane-urea-imide coatings, Prog. Org. Coat. 55

(2006) 231–243.

[13]   Y. Shi, X. Zhan, Z. Luo, Q. Zhang, F. Chen, Quantitative IR characterization of urea groups in waterborne polyurethanes, J. Polym. Sci. Part A 46 (2008) 2433–2444.

[14]   Z. Rafiee, M. Barzegar, M.A. Sahari, B. Maherani, Nanoliposomal carriers for improvement the bioavailability of high - valued phenolic compounds of pistachio green hull extract, Food Chem. 220 (2017) 115–122.

[15]   I. Yilgör, E. Yilgör, G.L. Wilkes, Critical parameters in designing segmented polyurethanes and their effect on morphology and properties: A comprehensive review, Polymer 58 (2015) A1–A36.

[16]   M.A. Pérez-Limiñana, F. Arán-Aís, A.M. Torró-Palau, C. Orgilés-Barcel, J.M. Martín-Martínez, Influence of the hard-to-soft segment ratio on the adhesion of water-borne polyurethane adhesive, J. Adhes. Sci. Technol. 21 (2007) 755–773.

[17]   J.T. Garrett, R. Xu, J. Cho, J. Runt, Phase separation of diamine chain-extended poly(urethane) copolymers: FTIR spectroscopy and phase transitions, Polymer 44 (2003) 2711–2719.

[18]   C. Fang, X. Zhou, Q. Yu, S. Liu, D. Guo, R. Yu, J. Hu, Synthesis and characterization of low crystalline waterborne polyurethane for potential application in water-based ink binder, Prog. Org. Coat. 77 (2014) 61–71.

[19]   M.L. Auad, V.S. Contos, S. Nutt, M.I. Aranguren, N.E. Marcovich, Characterization of nanocellulose-reinforced shape memory polyurethanes, Polym. Int. 57 (2008) 651–659.

[20]   S. Das, P. Pandey, S. Mohanty, S.K. Nayak, Influence of NCO/OH and transesterified castor oil on the structure and properties of polyurethane: Synthesis and characterization, Mater. Express 5 (2015) 377–389.

[21]   H.H. Elkamali, S.E. Mahjoob, Evaluation of antibacterial activity of some medicinal plants used in sudanese folk medicine for treatment of gastrointestinal tract Infections, Am. J. Life Sci. 3 (2015) 230–237.

[22]   B. Pawlikowska-Pawlęga, L.E. Misiak, B. Zarzyka, R. Paduch, A. Gawron, W.I. Gruszecki, FTIR, ^{1}H NMR and EPR spectroscopy studies on the interaction of flavone apigenin with dipalmitoylphosphatidylcholine liposomes, Biochim. Biophys. Acta 1828 (2013) 518–527.

[23]   M.I. Okeke, C.U. Iroegbu, E.N. Eze, A.S. Okoli, C.O. Esimone, Evaluation of extracts of the root of Landolphia owerrience for antibacterial activity, J. Ethnopharmacol. 78 (2001) 119–127.

[24]   D. Chamundeeswari, J. Vasantha, S. Gopalakrishnan, E. Sukumar, Antibacterial and antifungal activities of *Trewia polycarpa* roots, Fitoterapia 75 (2004) 85–88.

CHAPTER 10

General conclusions, future works and

publications

10. GENERAL CONCLUSIONS, FUTURE WORKS AND PUBLICATIONS

10.1 General conclusions

The aim of this work was the design of eco-friendly green routes in order to prepare waterborne polyurethane and polyurethane-urea dispersions. Furthermore, dispersions were used for the preparation of films by solvent-casting.

In this way, WBPU with different molar compositions were synthesized in order to analyze the effect of these variables in the final particle size and distribution of dispersions and final properties of films. In general, dispersions with small particle size and narrow distribution were obtained, resulting in films with several mechanical behaviors. In this way, the films presenting low soft segment enthalpies led to strain induced crystallization. Furthermore, it was analyzed the evolution of films properties after 5 months of annealing at room temperature, where the non-annealed films with lower crystallinty, evolved in a great extent to more crystalline systems.

In addition, different WBPUU were synthesized, varying diamine chain extender contents as well as the addition procedure (in homogeneous or heterogeneous medium). In this way, homogeneous medium led to unimodal distribution with lower particle sizes, while in the case of heterogeneous medium broader distributions with bigger particle sizes were observed weakening the cohesiveness between nanoparticles for film forming ability. Thereby, stiffer films were prepared from dispersions synthesized in homogeneous medium, resulting in enhanced thermomechanical stability.

Moreover, focusing on the environmental awareness, cellulose nanocrystals were isolated for their incorporation to WBPU and WBPUU as a renewable reinforcements. Thus, different cellulose nanocrystals reinforced nanocomposites were prepared analyzing different variables: CNC content, CNC incorporation route and dispersion nature (WBPU and WBPUU), as well as the microstructure adopted by the matrix. In general, an effective reinforcement effect was observed with the addition of CNC, which acted as SS crystallinity inhibitor or nucleating agent of the HS short and long order range regions, depending on the microstructure of the matrix. Furthermore, the CNC addition routes designed for the incorporation of the CNC resulted in different dispositions, leading to variations in the final properties of the films. The tailorable structure and properties of WBPU with enhanced properties by CNC incorporation, presented the innovative opportunity of modulating the properties of the final material. Moreover, in terms of applicability, some of the WBPU-CNC dispersions were selected for the preparation of electrospun mats, assisted by PEO as polymer template, which was successfully removed after the process, obtaining mats just composed by WBPU and CNC. The morphology and surface properties of mats were analyzed before and after PEO extraction, where it was observed the different properties obtained comparing the respective systems, opening the opportunity of focusing towards diverse applications.

Following with the quality of eco-friendly character of the systems, two different plants (*Salvia officinalis L.* and *Melissa officinalis L.*) were employed for the extraction of bioactive compounds for the preparation of bioactive WBPUU films. In this way, three incorporation pathways were designed for the incorporation of different extract percentages (1, 3 and 5 wt%) to a WBPUU. It was observed that both, the disposition of the extracts in the WBPUU,

modulated by the incorporation route, and the plant extract content, influenced the final properties of the films. In addition, antibacterial tests were carried out against S. aureus, E. coli and P. aeruginosa bacteria, where the enhancement of the bacteriostatic effect was observed after 4 days of incubation for some of the films containing the extracts.

10.2 Future works

Based on this work and with the aim of following with the research in this field, different challenges are proposed, which would complete this work and would provide suitable outlines for future frameworks:

The study of rheological properties of dispersions, base WBPU and WBPUU and their nanocomposites as well as a further analysis of the variation of different parameters such as pH or temperature.

The use of renewable raw materials for the synthesis of new WBPU and WBPUU compositions, for enhancing the eco-friendly character of these types of materials.

An identification of Salvia and Melissa extracts composition in order to comprehend their influence in the final properties of the films and their antibacterial effect. Furthermore, hydrophilicity measurements and release tests are proposed. In this way, it would be possible to analyze the bioactive compounds disposition in the WBPUU and release behavior considering the extract content and incorporation route.

The preparation of WBPU and or WBPUU dispersions reinforced with CNC and the addition of extracts in order to study the effect of both components together

in the matrix. The preparation of mats by electrospinning these dispersions, would result a suitable via for studying also the extract release behavior and their effect in the antibacterial and antioxidant properties of the mats.

The use of plant extracts as green reducing agents for the preparation of antibacterial nanoentities such as silver nanoparticles, and thus, the study of the antibacterial properties by their incorporation to WBPUU-plant extracts systems.

The preparation of WBPU and WBPUU scaffolds reinforced with CNC and or containing extract and their characterization in terms of physicochemical, thermal mechanical and morphological properties as well as hydrophilicity and extract release measurements is also suggested.

10.3 List of publications and communications

10.3.1 List of publications

Authors	Arantzazu Santamaria-Echart, Isabel Fernandes, Filomena Barreiro, Maria Angeles Corcuera, Arantxa Eceiza
Title	Bacteriostatic properties of waterborne polyurethane-urea films containing bioactive plant extracts by different incorporation routes
Journal	Industrial Crops and Products (In preparation)
Year	2016
Impact factor	3.449 (JCR 2015)
Rank	2/14 Agricultural Engineering (JCR 2015)
	6/83 Agronomy (JCR 2015)

Authors   Arantzazu Santamaria-Echart, Lorena Ugarte, Kizkitza Gonzalez, Loli Martin, Lourdes Irusta, Alba Gonzalez, Maria Angeles Corcuera, Arantxa Eceiza

Title   The role of cellulose nanocrystals incorporation route in waterborne polyurethane for preparation of electrospun nanocomposites mats

Journal   Carbohydrate Polymers (Under review)

Year   2016

Impact factor   4.219 (JCR 2015)

Rank   9/85 Polymer Science (JCR 2015)

                5/72 Chemistry, Applied (JCR 2015)

                11/59 Chemistry, Organic (JCR 2015)

Authors   Arantzazu Santamaria-Echart, Lorena Ugarte, Aitor Arbelaiz, Filomena Barreiro, Maria Angeles Corcuera, Arantxa Eceiza

Title   Modulating the microstructure of waterborne polyurethanes for the preparation of environmentally-friendly nanocomposites by cellulose nanocrystals incorporation

Journal   Cellulose (DOI:10.1007/s10570-016-1158-9)

Year   2016

Impact factor   3.195 (JCR 2015)

Rank   15/85 Polymer Science (JCR 2015)

                2/23 Materials Science, Textiles (JCR 2015)

                1/21 Materials Science, Paper & Wood (JCR 2015)

Authors	Arantzazu Santamaria-Echart, Lorena Ugarte, Clara García-Astrain, Aitor Arbelaiz, Maria Angeles Corcuera, Arantxa Eceiza
Title	Cellulose nanocrystals reinforced environmentally-friendly waterborne polyurethane nanocomposites
Journal	Carbohydrate Polymers 151, 1203–1209
Year	2016
Impact factor	4.219 (JCR 2015)
Rank	9/85 Polymer Science (JCR 2015)
	5/72 Chemistry, Applied (JCR 2015)
	11/59 Chemistry, Organic (JCR 2015)

Authors	Arantzazu Santamaria-Echart, Isabel Fernandes, Ainara Saralegi, Mário Rui P.F.N. Costa, Filomena Barreiro, Maria Angeles Corcuera, Arantxa Eceiza
Title	Synthesis of waterborne polyurethane-urea dispersions with chain extension step in homogeneous and heterogeneous media
Journal	Journal of Colloid and Interface Science 476, 184–192
Year	2016
Impact factor	3.782
Rank	41/144 (Chemistry, physical) (JCR 2015)

Authors	Arantzazu Santamaria-Echart, Lorena Ugarte, Aitor Arbelaiz, Nagore Gabilondo, Maria Angeles Corcuera, Arantxa Eceiza

Title	Two different incorporation routes of cellulose nanocrystals in waterborne polyurethane nanocomposites
Journal	European Polymer Journal 76, 99–109
Year	2016
Impact factor	3.485 (JCR 2015)
Rank	13/85 (Polymer Science) (JCR 2015)

Authors	Arantzazu Santamaria-Echart, Aitor Arbelaiz, Ainara Saralegi, B. Fernández-d'Arlas, Arantxa Eceiza, Maria Angeles Corcuera
Title	Relationship between reagents molar ratio and dispersion stability and film properties of waterborne polyurethanes
Journal	Colloids and Surfaces A: Physicochemical Engineering Aspects 482, 554–561
Year	2015
Impact factor	2.760 (JCR 2015)
Rank	56/144 (Chemistry, physical) (JCR 2015)

10.3.2 List of communications

Authors	Arantzazu Santamaria-Echart, Lourdes Irusta, Alba González, Maria Angeles Corcuera, Arantxa Eceiza
Title	Two different incorporation routes of cellulose nanocrystals in electrospun waterborne polyurethane nanocomposites
Congress	Nature Inspires Creative Emgineers (N.I.C.E. 2016)
Participation	Poster

Year	2016
Place	Nice, France

Authors	Arantzazu Santamaria-Echart, Lorena Ugarte, Aitor Arbelaiz, Nagore Gabilondo, Maria Angeles Corcuera, Arantxa Eceiza
Title	Poliuretano ur-dispertsioetan zelulosa nanokristalak gehitzeko bi metodo ezberdinen azterketa
Congress	Materialen Zientzia eta Teknologia III. Kongresua
Participation	Poster
Year	2016
Place	Markina-Xemein, Spain

Authors	Arantzazu Santamaria-Echart, Tamara Calvo-Correas, Lorena Ugarte, Aitor Arbelaiz, Maria Angeles Corcuera, Arantxa Eceiza
Title	Synthesis of waterborne polyurethane dispersions and cellulose nanocrystals isolation for nanocomposites preparation
Congress	5th International Conference on Biobased and Biodegradable Polymers
Participation	Poster
Year	2015
Place	Donostia-San Sebastian, Spain

Authors	Arantzazu Santamaria-Echart, Ainara Saralegi, Loli Martin, Maria Angeles Corcuera, Arantxa Eceiza
Title	Waterborne polyurethane-cellulose nanocrystals nanocomposites
Congress	6th Workshop on Green Chemistry and Nanotechnologies in Polymer Chemistry
Participation	Oral
Year	2015
Place	Bragança, Portugal

Authors	Arantzazu Santamaria-Echart, Sandra Gómez-Fernández, Aitor Arbelaiz, Maria Angeles Corcuera, Arantxa Eceiza
Title	Different routes of cellulose nanocrystals incorporation in waterborne polyurethanes
Congress	Eurofillers Polymer Blends 2015
Participation	Poster
Year	2015
Place	Montpellier, Francia

Authors	Aarantzazu Santamaria-Echart, Aitor Arbelaiz, Ainara Saralegi, Arantxa Eceiza, Maria Angeles Corcuera
Title	Synthesis and characterization of waterborne polyurethane dispersions and films properties
Congress	5th Workshop Green Chemistry and Nanotechnologies in Polymer Chemistry, ECLIPSE Workshop, BIOPURFIL

	Workshop
Participation	Poster
Year	2014
Place	Donostia-San Sebastian, Spain
Authors	Aarantzazu Santamria-Echart, Aitor Arbelaiz, Arantxa Eceiza, Maria Angeles Corcuera
Title	Ur-dispertsioan oinarritutako poliuretanoen sintesi eta karakterizazioa
Congress	Materialen zientzia eta teknologia II kongresua
Participation	Poster
Year	2014
Place	Donostia-San Sebastian, Spain

ANNEXES

ANNEXES

List of Tables

Chapter 7: Waterborne polyurethane-ureas cellulose nanocrystals nanocomposites

Chapter 9: Different incorporation routes of bioactive plant extracts in waterborne polyurethane-urea dispersions

List of Figures

Chapter 7: Waterborne polyurethane-ureas cellulose nanocrystals nanocomposites

Chapter 8: Electrospinning waterborne polyurethane nanocomposites loaded with cellulose nanocrystals by two incorporation routes

Chapter 9: Different incorporation routes of bioactive plant extracts in waterborne polyurethane-urea dispersions

List of abbreviations

WBPU	Waterborne polyurethanes
WBPUU	Waterborne polyurethane-ureas
CNC	Cellulose nanocrystals
SS	Soft segment
HS	Hard segment
TDI	2,4- or 2,6-Toluene diisocyanate
MDI	4,4'-Diphenyl methane diisocyanate
IPDI	5-Isocyanate-1-(isocyanate methyl)-1,3,3-trimethyl cyclohexane
$H_{12}MDI$	4,4'-Dicyclohexyl methane diisocyanate
HDI	1,6-Hexamethylene diisocyanate
DMPA	2,2-Bis(hydroxymethyl) propionic acid
DMBA	2,2-Bis(hydroxymethyl)butyric acid
MDEA	N-methyldiethanolamine
DABCO	1,4-Diazabicyclo octane
TEA	Tryehylamine
DBTDL	Dibutyltin dilaurate
SnOc	Stannous octoate
NCO/OH	Isocyanate/hydroxyl
MCC	Microcrystalline cellulose
PEO	Poly(ethylene oxide)
PVA	Poly(vinyl alcohol)
S. aureus	Staphylococcus aureus
E. coli	Escherichia coli

P. aeruginosa	Pseudomonas aeruginosa
PCL	Poly(ε-caprolactone) diol
BD	1,4-Butanediol
THF	Tetrahydrofuran
EDA	Ethylenediamine
DLS	Dynamic light scattering
^{1}H NMR	Proton nuclear magnetic resonance
^{13}C NMR	Carbon nuclear magnetic resonance
IP	Polydispersity index
GPC	Gel permeation chromatography
FTIR	Fourier transform infrared spectroscopy
EA	Elemental analysis
DSC	Differential scanning calorimetry
TGA	Thermogravimetric analysis
DTG	Derivative thermogravimetric curves
DMA	Dynamic mechanical analysis
SWCA	Static water contact angles
DWCA	Dynamic contact angles
WA	Water absorption
AFM	Atomic force microscopy
SEM	Scanning electron microscope
DBA	Dibutylamine
PCL/DMPA	Macrodiol/emulsifier
(IPDI/(PCL+DMPA))	Diisocyanate/(macrodiol+emulsifier)

List of symbols

L/D	Length/diameter
η	Viscosity
λ	Wavelength
$\bar{M}_w$	Weight average molecular weight
ΔC_p	Heat capacity change
T_g	Glass transition temperature
T_m	Melting temperature
ΔH_m	Melting enthalpy
T_i	Initial degradation temperature
T_m	Maximum degradation temperature
E	Modulus
σ_y	Yield stress
σ_b	Stress at break
ε_b	Strain at break
E'	Storage modulus
E''	Loss modulus
Tanδ	Tangent of phase angle
θ	Contact angle
θ_a	Advancing contact angles
θ_r	Receding contact angles
W_t	Weitgh of film at time t
W_0	Weitgh of film at time 0
$COOH_{tot}$	Total acid groups content
$DMPA_{tot}$	Total emulsifier content

T_{gSS}	Soft segment glass transition temperature
T_{mSS}	Soft segment melting temperature
ΔH_{mSS}	Soft segment melting enthalpy
$\Delta_{\Delta H_{mSS}}$	Increase of melting enthalpy value after the annealing
T_{mHS1}	Hard segment short range order temperature
T_{mHS2}	Hard segment long range order temperature
ΔH_{mHS1}	Hard segment short range order enthalpy
ΔH_{mHS2}	Hard segment long range order enthalpy
T_{mHS}	Hard segment melting temperature
ΔH_{mHS}	Hard segment melting enthalpy
χ_{cSS}	Relative soft segment crystallinity
ΔH_{100}	Melting enthalpy of the neat WBPU in the nanocomposites
ω	Weight fraction of WBPU in the nanocomposite
V_{Rc}	Theoretical volume fraction of CNC
T_s	Temperature of the shoulder
v_s/V	Physical crosslinking density
A	Constant
E_a	Apparent activation energy of hydrogen bonding dissociation
R	Gas constant
T	Absolute temperature

θ_e	Equilibrium contact angle
χ_{cHS}	Hard segment crystallinity
W_i	Initial plant weight
W_f	Weight of the plant extract
D_{10}	Particle sizes for 10 % of the number of nanoparticles
D_{50}	Particle sizes for 50 % of the number of nanoparticles
D_{90}	Particle sizes for 90 % of the number of nanoparticles